Karlsruher Institut für Technologie

Development and Implementation of an Adaptive Human-Machine Interface based on Ear Muscle Signals

Zur Erlangung des akademischen Grades
Doktor der Ingenieurwissenschaften
der Fakultät für Maschinenbau
Karlsruher Institut für Technologie (KIT)

genehmigte
Dissertation
von

Dipl.-Ing. Michele René Tuga

Tag der mündlichen Prüfung:	22. November 2016
Hauptreferent:	apl. Prof. Dr.-Ing. Ralf Mikut
Korreferent:	Prof. Dr.-Ing. Barbara Deml
Korreferent:	Prof. Dr. med. David Liebetanz

Zusammenfassung

Mensch-Maschine-Schnittstellen fungieren als bidirektionale Interpretierer in der Mensch-Maschine-Kommunikation. Efferente Interpretierer empfangen vom Menschen erzeugte Signale, erzeugen daraus Steuersignale und übermitteln diese an virtuelle oder physikalische Endgeräte. Mit Hilfe von Mensch-Maschine-Schnittstellen können körperlich beeinträchtigte Menschen ihren Handlungsspielraum vergrößern.

Diese Arbeit beschäftigt sich mit dem Bedarf von Tetraplegikern – Personen deren untere und obere Gliedmaßen infolge einer Querschnittläsion gelähmt sind aber deren Kopfbeweglichkeit erhalten ist – Endgeräte zu bedienen wie beispielsweise Elektrorollstühle. Eine "nur-kopfangesteuerte" Mensch-Maschine-Schnittstelle wird vorgestellt, die myoelektrische Signale – Muskelaktivität darstellende Signale – von den äußeren Ohrmuskeln empfängt und verarbeitet.

Da jeder Mensch einzigartig ist, ist die vorgestellte Mensch-Maschine-Schnittstelle derart adaptiv ausgestaltet, dass inter-individuelle Unterschiede physiologischer oder verhaltensbezogener Natur kompensierbar sind. Zu diesem Zweck sind mehrere Ansätze zur effizienten Benutzerspezifizierung berücksichtigt. Die Wichtigkeit von effizientem Training und Benutzermotivation sind erkannt worden. Daher wurde ein Trainingskonzept für ungeübte Benutzer entwickelt.

Verschiedene Aspekte der adaptiven Mensch-Maschine-Schnittstellen sind entwickelt und untersucht worden. Sowohl körperlich gesunde als auch körperlich beeinträchtigte Personen konnten die virtuellen Simulationen und einen Elektrorollstuhl mit Hilfe der in dieser Arbeit entwickelten Mensch-Maschine-Schnittstelle erfolgreich bedienen.

Abstract

Human-machine interfaces act as bidirectional interpreters in human-to-machine communication. Efferent interpreters receive human-generated signals, generate control signals and transfer these to virtual or physical executing devices. With the aid of human-machine interfaces, physically handicapped people are able to augment their range of actions.

This work addresses the need of people living with tetraplegia – people unable to move lower and upper extremities due to a spinal cord injury but able to move their head – for operating executing devices such as an electric-powered wheelchair. An head-only human-machine interface receiving and processing myoelectric signals – that is, signals representing muscle activity – taken from the extrinsic ear muscles is introduced.

As each person is unique, the proposed human-machine interface is designed being adaptive to compensate for inter-individual differences in physiology and behavior. To this end, multiple approaches aiming towards efficient user individualization are incorporated. The importance of efficient training and motivation of the user has been recognized. Therefore, a training concept for unpracticed users is developed.

Diverse aspects of the adaptive human-machine interface have been developed and evaluated. Able-bodied as well as physically handicapped persons successfully operated virtual simulations and an electric-powered wheelchair with the aid of the proposed human-machine interface.

Acknowledgements

This doctoral dissertation would not have been possible without the valuable support of my precious supervisors, colleagues and friends.

First and foremost, I would like to express my sincere gratitude to Prof. Prof. E.h. Dr. Dr. E.h. mult. Georg Bretthauer who made this work possible in the first place and encouraged me in doing research. I would like to thank my advisors Prof. Dr. Ralf Mikut and Dr. Markus Reischl for countless instructive and open-heart meetings. These sessions always yielded overwhelmingly helpful contributions to my work and continuously encouraged me to get on with my research. I am very grateful to Prof. Dr. Barbara Deml for rendering this work possible.

It is essential to sincerely acknowledge with gratitude the TELMYOS-project team, namely Prof. Dr. David Liebetanz, Dr. Rüdiger Rupp, Leonie Schmalfuß, Manuel Hewitt, Ute Eck and Andreas Kogut for numerous in-depth discussions and for fostering ideas. I truly enjoyed each and every meeting in Göttingen, Heidelberg and Karlsruhe.

Furthermore, I am grateful for the valuable contributions of Eduard Hübner, Lena Meister, Eduardt Alberg and Derek Lamont, who I was able to supervise academically. I honestly appreciated being the teacher and student at the same time.

For both contributing open-minded discussions and "sweetening the pill" of academic research I would like to say a big thanks to my fellow PhD students Johannes Stegmaier, Arif ul Maula Khan, Simon Waczowicz, Wolfgang Doneit and Benjamin Schott.

Last but most certainly not least, I would like to warmly thank my beloved parents, Claus and Erika, as well as my sweet sisters Nicole, Denise and Janine as well as my precious Maren for their emotional support!

Contents

List of Figures

List of Tables

List of Acronyms

ACh	Acetylcholine
ADAS	Advanced Driver-Assistance System
ADC	Analog-to-Digital Converter
ADLs	Activities of Daily Living
AIDE	Adaptive Integrated Driver-Vehicle Interface
AIS	ASIA Impairment Scale
ALS	Amyotrophic Lateral Sclerosis
AMG	Acoustic Myography
AP	Access Point
ASCII	American Standard Code for Information Interchange
ASIA	American Spinal Injury Association
ASR	Automatic Speech Recognition
ATD-PA	Assistive Technology Device Predisposition Assessment
ATP	Adenosine Triphosphate
BCI	Brain-Computer Interface
BMBF	German Federal Ministry of Education and Research
BMI	Brain-Machine Interface
BP	Band Power
CNS	Central Nervous System
CPU	Central Processing Unit
CT	Computed Tomography
CVA	Cerebrovascular Accident
DAC	Digital-to-Analog Converter
DC	Direct Current
DESTATIS	Federal Statistical Office of Germany
DgFS	Device-generated Feedback Signal
DNI	Direct Neural Interface
DOF	Degree of Freedom
ECG	Electrocardiography
ECoG	Electrocorticography

ED	End Device
EEG	Electroencephalography
EMA	Electromagnetic Articulography
EMG	Electromyography
EOG	Electrooculography
EPW	Electric-Powered Wheelchair
ERD	Event-Related Desynchronization
ERP	Event-Related Brain Potential
ERS	Event-Related Synchronization
FES	Functional Electrical Stimulation
FSM	Finite State Machine
fwEMG	Fine-Wire EMG
GSR	Galvanic Skin Response
GUI	Graphical User Interface
H2H	Human-to-Human
H2M	Human-to-Machine
HgIS	Human-generated Indication Signal
HRQoL	Health-Related Quality of Life
HMI	Human-Machine Interface
IC	Integrated Circuit
ICF	International Classification of Functioning, Disability and Health
IDE	Integrated Development Environment
iEEG	Intracranial EEG
IgFS	Interface-generated Feedback Signal
IgCS	Interface-generated Control Signal
IIR	Infinite Impulse Response
LDA	Linear Discriminant Analysis
LED	Light-Emitting Diode
LIDAR	Light Detection And Ranging
LIS	Locked-In Syndrome
MAP	Muscle Action Potential
MAV	Mean Absolute Value
MC	Microcontroller
MCU	Microcontroller Unit
MD	Muscular Dystrophy
MEG	Magnetoencephalography
MES	Myoelectric Signal

MHG	Marple-Hovart and Gilbey
MMI	Mind-Machine Interface
MRT	Magnetic Resonance Tomography
MS	Multiple Sclerosis
MU	Motor Unit
MUAP	Motor Unit Action Potential
NASA-TLX	NASA Task Load Index
NLI	Neurological Level of Injury
NSCISC	National Spinal Cord Injury Statistical Center
OS	Operating System
PC	Personal Computer
PMES	Processed Myoelectric Signal
PMG	Phonomyography
PNS	Peripheral Nervous System
QoL	Quality of Life
RF	Radio Frequency
RISC	Reduced Instruction Set Computing
RL	Reinforcement Learning
RMS	Root Mean Square
RT	Real Time
SCI	Spinal Cord Injury
SCP	Slow-Cortical Potential
sEMG	Surface EMG
SMA	Spinal Muscular Atrophy
SMR	Sensorimotor Rhythm
SNP	Sip-and-Puff
SSI	Silent Speech Interface
SSVEP	Steady-State Visually Evoked Potential
STE	Short-Term Energy
STI	Synthetic Telepathy Interface
STT	Speech-to-Text
SVM	Support Vector Machine
TELMYOS	Telemetric and Myoelectric Ear Muscle Sensing System
TMEP	Tongue Movement Ear Pressure
TMR	Targeted Muscle Reinnervation
TMS	Transcranial Magnetic Stimulation
UDP	User Datagram Protocol
USB	Universal Serial Bus

VEP	Visual-Evoked Potential
VR	Virtual Reality
WHO	World Health Organization
WL	Waveform Length
ZC	Zero Crossing

List of Symbols

Latin Symbols

a_i	Trade-off parameter for IIR filtering
$c[k]$	Car position
$c_{d,u,e,t}$	Control ability
$\bar{c}_d^{u,e,t}$	Average control ability
d	Index of days
e	Index of environments
E_d	Default value of the executing device
E_l	Lower limit of the executing device's control signal range
E_u	Upper limit of the executing device's control signal range
$\tilde{E}$	Total number of environments
f	Frequency in Hz
g_i	Gain constant for signal rectification
i	Index of input modalities
$\tilde{I}$	Total number of input modalities
k	Index of discrete instants of time
$\tilde{K}$	Total number of discrete time instants
$\tilde{K}_p$	Total number of discrete time instants of p-th time series
$\tilde{K}_{h,p}$	Total number of discrete time instants of p-th time series for high-level activation
$\tilde{K}_{l,p}$	Total number of discrete time instants of p-th time series for low-level activation
l_f	Index of complete signal activations and deactivations
$\tilde{L}_\mathrm{f}$	Total number of complete signal activations and deactivations
l_rr	Index of time periods (signal within valid signal range)
$\tilde{L}_\mathrm{rr}$	Total number of time periods (signal within valid signal range)
m_i	Window width parameter for RMS filtering

$m[k]$	Middle line position
n	ADC signal resolution in bits
$\mathbf{p}_{\mathrm{H}}$	Parameter vector characterizing the human
$\mathbf{p}_{\mathrm{HMI}}$	Parameter vector characterizing the human-machine interface
$\mathbf{p}_{\mathrm{TE}}$	Parameter vector characterizing the training environment
$\mathbf{p}_{\mathrm{opt}}$	Parameter vector characterizing the human-machine interface and the training environment assumed to be optimal
p	Index of calibration iterations
$\tilde{P}$	Total number of calibration iterations
q	Quantile
Q	User performance estimate
r	Index of runs (i.e., non-simulated trials)
$r_{\mathrm{b},i,j}$	Bilateral paradigm's portion of isolated signal activation with respect to the input modality of interest i versus the reference input modality j
s	Index of simulations (i.e., simulated trials)
$\tilde{S}$	Total number of simulated trials
t_{b1}	Bilateral paradigm's constant time from paradigm start to stimulus appearance
t_{b2}	Bilateral paradigm's constant time of stimulus display
t_{b3}	Bilateral paradigm's constant time from stimulus disappearance to paradigm end
t_{dm}	Duration of maximum activity paradigm's total time
t_{f}	Frequency paradigm's total time
t_{r1}	Response time paradigm's constant time from paradigm start to earliest possible stimulus appearance
t_{r2}	Response time paradigm's additive random time of stimulus appearance
t_{r3}	Response time paradigm's constant time of stimulus display
t_{r4}	Response time paradigm's constant time from stimulus disappearance to paradigm end
t_{sr}	Subrange paradigm's total time
t	Index of trials
$\tilde{T}$	Total number of trials
T	Absolute completion time
T_{emp}	Empirical completion time
T_{invar}	Normalized completion time
u	Index of users

$\tilde{U}$	Total number of users
$x_i(t)$	Physical signal
$x_i[k]$	Digital preprocessed signal
$x_{\mathrm{r},i}[k]$	Digital rectified signal
$x_{\mathrm{f},i}[k]$	Digital filtered signal
$x_{\mathrm{f},i,p}[k]$	Digital, finite signal of sensor calibration
$x^{\mathrm{ord}}_{\mathrm{f},i,p}[\zeta]$	Digital, finite signal of sensor calibration (ordered by decreasing numerical value)
$x_{\mathrm{n},i}[k]$	Digital normalized signal (activity signal)
$x_{\mathrm{n},i,p}[k]$	Digital, finite signal of bimodal calibration
$x^{\mathrm{ord}}_{\mathrm{n},i,p}[\zeta]$	Digital, finite signal of bimodal calibration (ordered by decreasing numerical value)
$x_{\mathrm{n},\Delta 12}[k]$	Bimodal differential signal
$x^{\mathrm{comp}}_{\mathrm{n},\Delta 12}[k]$	Bimodal differential signal (crosstalk compensated)
$x_{\mathrm{n},1\chi T2}$	Crosstalk activity in $i = 2$
$x_{\mathrm{n},2\chi T1}$	Crosstalk activity in $i = 1$
$x_{\mathrm{n},1\chi T2,p}$	Crosstalk activity in $i = 2$ (p-th iteration)
$x_{\mathrm{n},2\chi T1,p}$	Crosstalk activity in $i = 1$ (p-th iteration)
$x_{\mathrm{f,glvl},i}$	Ground level parameter
$x_{\mathrm{f,max},i}$	Maximum parameter
$x^{*}_{\mathrm{f,max},i}$	Constant maximum parameter
$x^{*}_{\mathrm{f,max},t,i}$	Constant maximum parameter of Trial t
$x_{\mathrm{f,min},i}$	Minimum parameter
$x^{*}_{\mathrm{f,min},i}$	Constant minimum parameter
$x^{*}_{\mathrm{f,min},t,i}$	Constant minimum parameter of Trial t
$x_{\mathrm{f,bot},i,p}$	Bottom-end value of p-th iteration of calibration signal
$x_{\mathrm{f,med},i,p}$	Medium-end value of p-th iteration of calibration signal
$x_{\mathrm{f,top},i,p}$	Top-end value of p-th iteration of calibration signal
$\boldsymbol{X}_{\chi T}$	Transformation matrix of crosstalk compensation
$y_{\mathrm{act}}[k]$	Actual, unidimensional position
$y_{\mathrm{des}}[k]$	Desired (ideal), unidimensional position
w	Increment factor
$\mathbf{w}$	Weighting vector consisting of algorithm control options

Greek Symbols

α_{xTi}	Model parameter of crosstalk compensation
$\boldsymbol{\alpha}_{xT}$	Coefficient vector of crosstalk compensation
γ	Supporting factor
γ_T	Scaling parameter of T
γ_Δ	Scaling parameter of Δ
$\chi[k]$	Actual-to-desired relation
δ_{dm}	Maximum duration of maximum activity
$\delta_{\mathrm{dr},l_{\mathrm{rr}}}$	l_{rr}-th time period (signal within valid signal range)
δ_{ra}	Minimum response time of input signal activation
δ_{rd}	Minimum response time of input signal deactivation
Δ_{dr}	Sum of time periods (signal within valid signal range)
Δ	Absolute path error
Δ_{emp}	Empirical path error
Δ_{invar}	Normalized path error
ΔQ	Acute trend of user performance
$\epsilon[k]$	Tolerance range
ϵ_{r}	Dead band of rotational control signal
ϵ_{t}	Dead band of translational control signal
θ_{dml}	Duration of maximum activity paradigm's lower activity threshold
θ_{dmu}	Duration of maximum activity paradigm's upper activity threshold
θ_{fl}	Frequency paradigm's lower activity threshold
θ_{fu}	Frequency paradigm's upper activity threshold
θ_{rl}	Response time paradigm's lower activity threshold
θ_{ru}	Response time paradigm's upper activity threshold
θ_{srl}	Subrange paradigm's lower activity threshold
θ_{sru}	Subrange paradigm's upper activity threshold
ρ	Control range
$\sigma_t^{\tilde{U}}$	Standard deviation
$\bar{\sigma}^{\tilde{U},\tilde{T}}$	Standard deviation mean
υ	V4-Algorithm-specific threshold parameter
Υ	V4-Algorithm-specific term
ω_{l}	Lower bound of the differential signal
ω_{u}	Upper bound of the differential signal

$\boldsymbol{\omega}_{xT}$	Outcome vector containing the desired values of the crosstalk compensation
$\boldsymbol{\xi}[k]$	Vector of preprocessed biosignals
$\boldsymbol{\psi}[k]$	Vector of control signals
ζ	Index of discrete, ordered instants of time
$\tilde{Z}$	Total number of discrete, ordered instants of time

1 Introduction

1.1 Motivation

Disabled persons encounter severe difficulties in several fields of daily life, such as accessing health care services, education, transport and employment [225]. In addition, the poverty rate of disabled persons is higher than those without disabilities [230]. In the broad sense, disability is a result of several concurrent causes that are of both a biological and social nature [204]. According to the international classification of functioning, disability and health (ICF) issued by the World Health Organization the umbrella term "disability" encompasses impairments in bodily functions, activity limitations and participation restrictions. Due to the aging population worldwide the prevalence of disability is expected to grow, as indicated in Appendix A.1.

In order to support people with disabilities, a wide range of assistive technologies addressing the shortcomings of handicapped persons were developed. Specialized assistive and rehabilitative devices that compensate for the deficits were invented. For instance, cochlear implants help deaf people by providing a sense of sound. These devices are prosthetic replacements for the inner ear that are implanted surgically [141]. Moreover, artificial upper limbs are prostheses designated for arm and hand amputees respectively to help them partially reacquire range of motion [17, 184, 185]. Persons incapable of moving the upper body caused by, for example, highly located spinal cord injuries (SCIs) are in need of the help of others throughout life. The development of assistive technologies helps the handicapped to regain autonomy and sovereignty in their lives.

The WHO estimates the annual global incidence of spinal cord injuries at 40 to 80 cases per million population [50]. According to the federal statistical office of Germany (DESTATIS) nearly 17,000 people suffered

from a spinal cord injury in Germany in 2011 [108]. People suffering a spinal cord injury are strongly limited in their actions and mobility. Spinal cord injuries can be induced by either sudden trauma or gradually deteriorating health conditions like diseases. Typically, spinal cord injured persons are confined to a wheelchair. In everyday life they move by sitting passively in a wheelchair that is pushed by able-bodied care attendants or relatives. This imposes a strong dependence on personnel support that results in high costs. Therefore, assistive technologies designed to help disabled persons regain their independence could reduce personnel costs.

In 2011 about 64,000 people suffered from the loss or partial loss of limbs in Germany, according to the federal statistical office of Germany (DESTATIS). In the same year the total number of persons living with spinal cord injuries amounted to 17,000 [108]. According to [48] the total number of new (treated) cases of paraplegia reached 33,974 and the total number of readmissions resulting from prevention and treatment of complications was 77,203 in Germany since the national database began. In Europe the total number of persons with spinal cord injuries is estimated at 300,000 [54]. The national spinal cord injury statistical center (NSCISC) provides an elaborate database about spinal cord injuries in the United States [203], where about 250,000 persons suffer from SCIs [80].

Severely disabled persons typically suffer from both a physical disability and depression in the wake of the physical disability [71]. Authors with disabilities made their handicaps the subjects of their own writing as exemplarily addressed in Appendix A.2. As a sequela the quality of life (QoL) – a general term for the well-being of individuals – tends to decline. This in turn affects the person's physical and mental state negatively, leading to unfortunate self-reinforcing effects.

As a viable option, spinal cord injured persons may navigate electric-powered wheelchairs (EPWs) and thus reduce the dependence on other persons. However, EPWs are usually hand-joystick controlled – thus, not accessible by persons unable to move upper extremities. This has motivated researchers to develop specialized technological systems referred to as head-only human-machine interfaces, enabling people with paralyzed upper limbs to steer EPWs autonomously. Depending on the user's degree of disability, different operating principles for steering EPWs can be applied. The EPW can be controlled, for example, by a chin controller located in front of

the user's face. Theoretical physicist Stephen W. Hawking (who is almost completely paralyzed resulting from amyotrophic lateral sclerosis (ALS)) uses a chin controller. Deliberate tongue movements that are detected by an invasively implanted magnetic tracer provide another way to control EPWs [83]. Yet another means of controlling powered wheelchairs is by monitoring the user's eye movements [12]. However, these systems rely on bodily functions that are usually preoccupied with social interaction or information acquisition. With respect to the aforementioned controls grounded on head, tongue and eye movements, users will not be able to turn their head, talk, eat or look around while steering the EPW.

Generally speaking, there are two approaches to support disabled persons: The medical and the technological approach. For example, to someone who lost an extremity the medical approach implies transplantation of a deceased person's limb. However, to date limb transplants are far from being clinically routine. Moreover, patients are permanently required to take immunosuppressive drugs which suppress the immune system that otherwise would naturally reject the transplanted limb and therefore lead to complete failure. Unfortunately, those drugs typically cause undesired, adverse side effects. As for the care of spinal cord injured persons, the surgical focus lies on the prevention of consequential secondary impairments, such as the increase of height of the spinal cord lesion caused by an unstable vertebral column [205].

On the other hand, following the technological approach, an artificial surrogate limb is used as a substitute for the lost one. These limb prostheses are classified into cosmetic prostheses (passive rehabilitation devices), body-powered prostheses and EMG-controlled prostheses (active rehabilitation devices) [157]. The dexterity of prostheses is determined by two factors, namely the mechanical construction like the shape, dimensions, number of DOF and the bio-signal control ability [228].

1.2 Muscle Physiology

1.2.1 Types of muscles

The human body comprises three major types of muscles, namely skeletal muscles, cardiac muscles and smooth muscles. Table 1.1 provides an overview of the major muscle types. As the term indicates, skeletal muscles control the skeletal and locomotor system. Most of them originate at bones anchored by tendons and couple bones together. Skeletal muscles represent the majority of all muscles and make up approximately 40 % of the body's mass. Oftentimes they are referred to as voluntary muscles as the muscle contraction and relaxation is controlled by will. Cardiac muscles are solely present in the heart. They maintain the circulatory system. Histologically, both skeletal and cardiac muscles are striated muscle tissues. Smooth muscles are found within organ walls. They embrace internal organs as well as blood vessels. They manage bodily functions such as respiration and digestion. These muscle tissues are not striated. Cardiac as well as smooth muscles are labeled involuntary muscles [121].

Muscle Type	Skeletal	Cardiac	Smooth
Occurrence	Bones all over the body	Heart	Internal organs all over the body
Function	Postural control and locomotion	Heart contraction	Diverse bodily functions
Consciousness	Voluntary	Involuntary	Involuntary
Appearance	Striated	Striated	Not striated

Table 1.1: Overview of the three major types of muscles

1.2.2 Skeletal muscles

The main function of skeletal muscles is to attach bones together and to constitute a mechanical linkage as schematically illustrated in Figure 1.1a. Skeletal muscles consist of numerous muscle fascicles as well as connective tissue, blood vessels and nerves as depicted in Figure 1.1b.

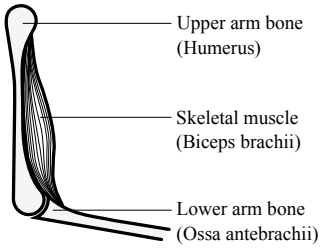

(a) Gross anatomy of biceps brachii flexing the forearm

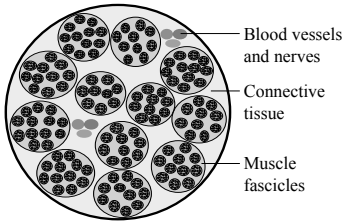

(b) Sectional drawing of a skeletal muscle

Figure 1.1: Simplified models of the skeletal muscle and its components (modified from [190])

Muscle fascicles are bundles of large amounts of long and tubular muscle cells as shown in Figure 1.2a. According to the muscle-specific terminology muscle cells are named muscle fibers or myocytes. As every living cell the muscle fiber contains cytoplasm (muscle-specific term "'sarcoplasm"') which is the gelatinous substance holding the cell organelles in place. The muscle fiber is covered by the cell membrane (muscle-specific term "'sarcolemma"'). Figure 1.2b shows the section of a muscle fiber.

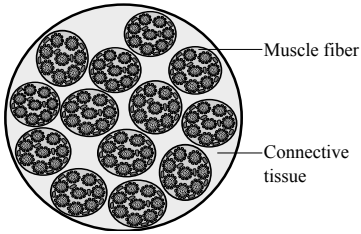

(a) Sectional drawing of a muscle fascicle

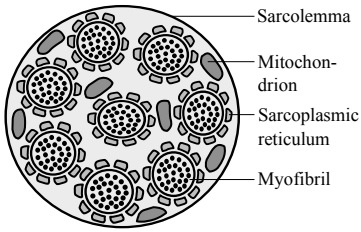

(b) Sectional drawing of a muscle fiber

Figure 1.2: Simplified models of the muscle fascicle and its macroscopic and microscopic components (modified from [190])

Viewed under the optical microscope, the sarcolemma of muscle fibers exhibits regular cross-striations due to dark and light segments called A-bands (anisotropic) and I-bands (isotropic), respectively, illustrated in Figure 1.3. Muscle fibers are multi-nucleated and non-branched.

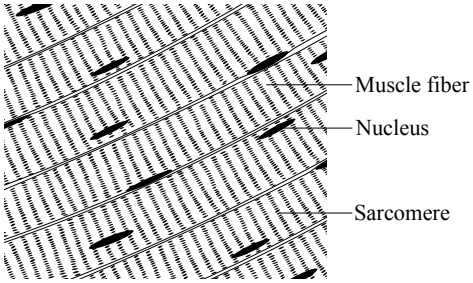

Figure 1.3: Muscle fibers with cross-striations composed by sarcomeres (modified from [190])

The essential organelles of a muscle fiber are mitochondria, myofibrils, transverse tubules and sarcoplasmic reticulum. The mitochondria produce the chemical adenosine triphosphate (ATP) that serve the muscle fiber as chemical energy. The rod-like myofibrils basically perform the muscle contraction and relaxation. One muscle cell contains about 1,000 myofibrils. They are made up of proteins such as troponin, actin, tropomyosin, myosin as well as titin and nebulin. The contractile proteins actin and myosin constitute the thin filaments and thick filaments, respectively. These filaments let the muscle contract or relax by sliding along each other. Sections of overlapping thick and thin filaments along the length of the myofibril are termed sarcomeres. Ranging from one z-disk to another they are about 2 nm long [138]. The transverse tubules (T-tubules) are tunnel-like extensions from the sarcolemma that traverse the muscle fiber from one side to the other. They rapidly convey electrical nerve impulses (muscle action potentials (MAPs)) from the neuromuscular junction, linkage between the nervous system and the muscular system, into the muscle fiber. The sarcoplasmic reticulum is a longitudinal structure (L-tubules) wrapped around the myofibrils. It stores calcium ions (Ca^{2+}) that are needed for the chemical process of muscle contraction.

Since voluntary skeletal muscles are found throughout the human body including the upper body and the face, they are generally qualified for being a source of non-verbal communication.

1.2.3 Contraction of skeletal muscles

Physiologically, two major types of muscle contraction are to be distinguished: The isotonic and the isometric muscle contraction. First, the isotonic muscle contraction is concentric or eccentric. The concentric contraction shortens the muscle, such as when pulling up an external load. This type of contraction matches the common linguistic usage of muscle contraction. The eccentric contraction lets the muscle lengthen – for instance, lowering down an external load. Second, the isometric contraction preserves the muscle length – like holding an external load [193].

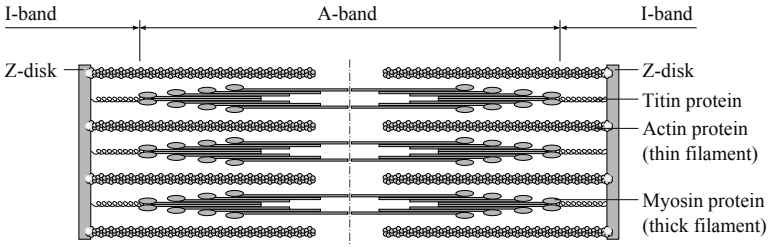

(a) Relaxation phase

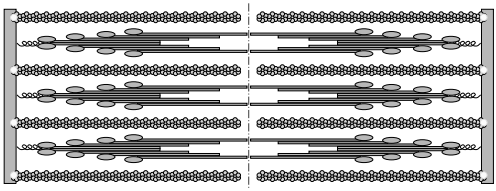

(b) Contraction phase

Figure 1.4: Schematic illustration of a sarcomere with sliding thin and thick filaments in relaxation and contraction phases[1]

[1] modified from `http://en.wikipedia.org/wiki/Muscle_contraction`

Figures 1.4a and 1.4b show schematic illustrations of sliding filaments in relaxation and contraction phases, respectively. The process of sliding filaments leads to an increase of muscle tension referred to as muscle contraction. The sliding filament theory characterizes the process of thin filaments sliding synchronously over thick filaments while remaining at constant length [84, 85].

Action potentials are short-lasting electrical impulses (events) that occur in excitable cells, such as nerve cells and muscle cells. During an action potential the cell's electrical membrane potential quickly increases and decreases again at a regular trajectory. In nerve cells, action potentials serve the inter-cell communication. They are received by the nerve cell's dendrites, move along the axon and eventually emit another action potential that is received by another nerve cell. In muscle cells, action potentials induce intra-cell processes leading to muscle contraction.

Depending on the stimulus strength, muscle fibers either contract at the maximum or not at all. This is termed the all-or-none law [193].

Muscle fibers are innervated by motor neurons that are efferent nerves originating in the motor cortex. The number of muscle fibers innervated by a single motor neuron depends on the type of motion. The linkage between the muscle fibers and the motor neuron is named neuromuscular junction (end-plate). A motor unit (MU) consists of a motor neuron and its affiliated muscle fibers – that being the muscle fibers innervated by the motor neuron. If a MU is activated an electrical potential termed motor unit action potential (MUAP) can be measured.

As skeletal muscle contraction is controlled by one's will, the basic electrical impulse arises from the brain and is propagated via the nervous system to the muscular system, where it causes the muscle to contract. The electrical impulse moves from the brain to the alpha motor nerve cell – also known as alpha motor neuron – at the spinal cord, that in turn sends another electrical impulse down its axon. When reaching the neuromuscular junction, the electrical impulse stimulates voltage-gated calcium channels allowing calcium ions to enter the neuron. The calcium ion influx then causes the neurotransmitter acetylcholine (ACh) to diffuse across the synapse at ACh receptors yielding again an electrical impulse. The electrical impulse gets transmitted via the muscle fiber's T-tubules network.

This depolarizes the muscle fiber and triggers a repetitive biochemical process of binding, releasing myosin and actin. As long as the chemical energy ATP is available, myosin proteins (thin filaments) slide over actin proteins (thick filaments), increasing the muscle tension.

1.2.4 Anatomy and innervation of human ear muscles

The external (outer) ear – also known as auricula or pinna – is the part of the ear that is visible from outside. Its main objective is to focus and redirect the arriving sound pressure waves to the eardrum via the ear canal. To provide an overall view, Figure 1.5 shows the human head and neck, revealing the corresponding muscles. The auricula holds nine muscles in total, classified into three extrinsic and six intrinsic muscles.

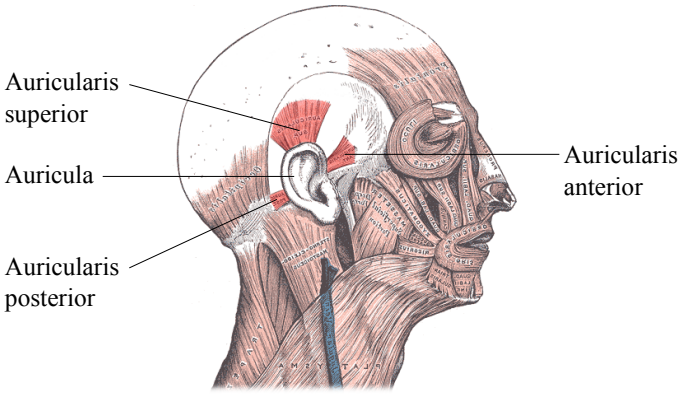

Figure 1.5: Right lateral view showing the extrinsic ear muscles (red highlighted) in the context of neck and head muscles (modified from [65])

The intrinsic muscles of the human auricula form and stabilize it, as highlighted in yellow in Figure 1.6. These muscles are named helicis major, helicis minor, tragicus, antitragicus, transversus auriculae and obliquus auriculae.

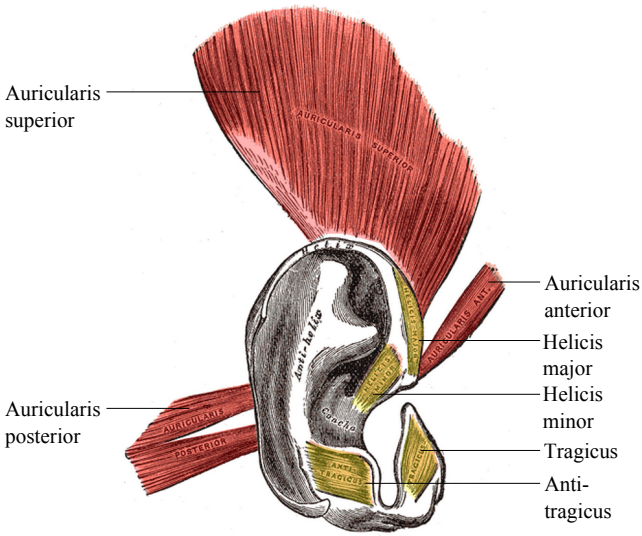

Figure 1.6: Right lateral detail view showing extrinsic muscles (red highlighted) and intrinsic muscles (yellow highlighted) of the human auricula (modified from [65])

The extrinsic ear muscles – auricularis anterior, auricularis superior and auricularis posterior – connect the external ear with the scalp and slightly move it en bloc, as highlighted in red in Figures 1.5 and 1.6. The thin and fan-shaped auricularis anterior is the smallest extrinsic ear muscle, drawing the external ear forward and upward. The auricularis superior is the largest of the three extrinsic ear muscles and is also thin and fan-shaped, drawing the auricula upward. Finally, the auricularis posterior is composed of two fleshy fasciculi and draws the auricula backward.

Both extrinsic ear muscles, auricularis anterior, and the auricularis superior are supplied by the temporal (frontal) branch of the facial nerve – the cranial nerve VII. The auricularis posterior is supplied by the posterior auricular branch of the same nerve [65]. Figure 1.7 illustrates the bilateral facial nerves.

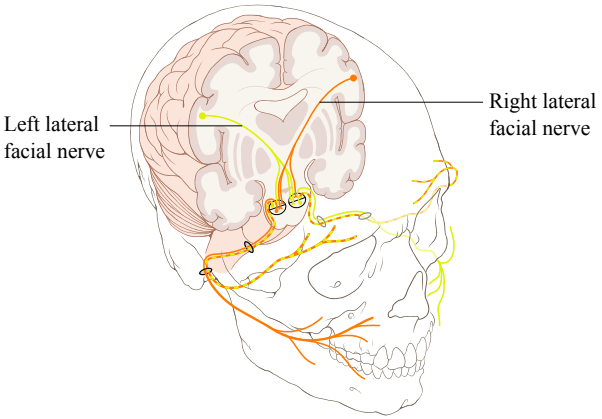

Figure 1.7: Innervation of facial muscles and the external ear muscles[2]

Charles R. Darwin, naturalist and significant contributor to the Theory of Evolution, stated that auricula movements – that is, the extrinsic-ear-muscle-actuated orientation of the auricular which is partly decoupled from the orientation of the head – could have been utilized for sound localization. Furthermore, according to Darwin that function of the extrinsic ear muscles could have been lost during evolution in certain species (including humans) [36]. Some mammalian animals make use of auricula movements. As the oculomotor range – or the range of eye movements – of the cat is rather limited, cats use auricula movements of a certain range for locating sound [158, 233].

Humans feature – if any – only minimal ranges of auricula movement by means of the voluntary activation of the extrinsic ear muscles. In humans the extrinsic ear muscles exist rudimentarily. From the biological point of view, humans are capable of moving the auricula through extrinsic ear muscle activation, since those muscles are certainly innervated. However, the majority of people cannot willfully activate these muscles. Publications regarding the voluntary activation of the extrinsic ear muscles in humans provide inconsistent results [16, 187]. On the other hand, it is commonly

[2]modified from `http://en.wikipedia.org/wiki/Facial_nerve`

known that some people are able to learn the intentional activation of the extrinsic ear muscles to some extent over time, with trial and error.

When a high-intensity acoustic stimulus occurs, a protective reflex termed acoustic stapedius reflex, instantaneously and involuntarily prompts the stapedius muscle in the middle ear to contract. As a consequence of stapedius muscle contraction, the sound pressure representing the high-intensity sound is dampened before passing it on to the inner ear. The acoustic reflex protects the inner ear against sounds that are too loud and can potentially hurt it [2].

1.2.5 Myoelectric signals

Electromyography (EMG) is a method for measuring electrical muscle activity produced by muscle cells when getting activated neurologically when contracting. The electrical muscle activity over time is also said to be the myoelectric signal (MES). The MESs of the three major muscle types (cf. Section 1.2.1) differ from each other. Electrical impulses cause the sarcolemma of the muscle fiber to depolarize, and repolarize again after a certain time. The characteristics of the MES depend on physiological aspects such as muscle size, the contraction strength and the tissue. On the other hand, technological aspects like the electrode type also affect the signal [138].

In general, EMG electrodes do not detect isolated MUAPs induced by a single motor unit, but instead they detect superimposed MUAPs from the motor units within detection range. In other words, the MES is the summation of several MUAPs.

Depending on the type of electrodes this method is either non-invasive or invasive. The muscle activity is measured non-invasively by surface EMG (sEMG) electrodes. They provide low spatial resolution since the detection range is rather wide. Fat tissue effects the signal quality of sEMG. Subcutaneous (intramuscular) EMG electrodes, said to be fine-wire EMG (fwEMG) or needle EMG electrodes, measure muscle activity invasively. The fwEMG electrodes are directly inserted into the muscle tissue. Since the detection range is rather narrow, they provide a high spatial resolution. However, due to skin penetration, fwEMG implies a

certain infection risk. Typical fwEMG electrodes are 50 mm long with an outside diameter of 0.45 mm. Ahead of fwEMG electrode insertion the skin is usually cleaned with an alcohol pad.

Myoelectric signals acquired from the extrinsic ear muscles usually are accessible for persons with tetraplegia as the facial nerves innervating the ear muscles are above the neurological level of injury (NLI). Since the extrinsic ear muscles are skeletal muscles, the contraction and relaxation are controlled voluntarily and hence the myoelectric signals from the extrinsic ear muscles are coherent signals. On the other hand, humans are not used to activating the extrinsic ear muscles because there is no function associated with it. Furthermore, drug-induced, partial spasticity potentially corrupt the myoelectric signals.

1.3 Nervous System

1.3.1 Structure and function

The human nervous system comprises the central nervous system (CNS) and the peripheral nervous system (PNS). The CNS encompasses the brain and the spinal cord, while the PNS refers to the cranial and spinal nerves. Cranial nerves, also known as cerebral nerves, emanate from the brain and the brainstem. Spinal nerves originate from the spinal cord.

Nerves are cable-like bundles of axons (nerve fibers) and constitute the pathways for transmitting the electrochemical nerve impulses (action potentials). The event of nerve cells emitting an action potential is referred to as “firing”.

The spinal cord connects the brain with the extremities and torso. It resides in the spinal canal of the vertebral column that serves as the bone housing and physical protection, as depicted in Figure 1.8. The spinal cord’s three major functions are the transmission of motor information from the CNS to the PNS (efferent direction), the transmission of sensory information from the PNS to the CNS (afferent direction) and the coordination of specific reflexes [123].

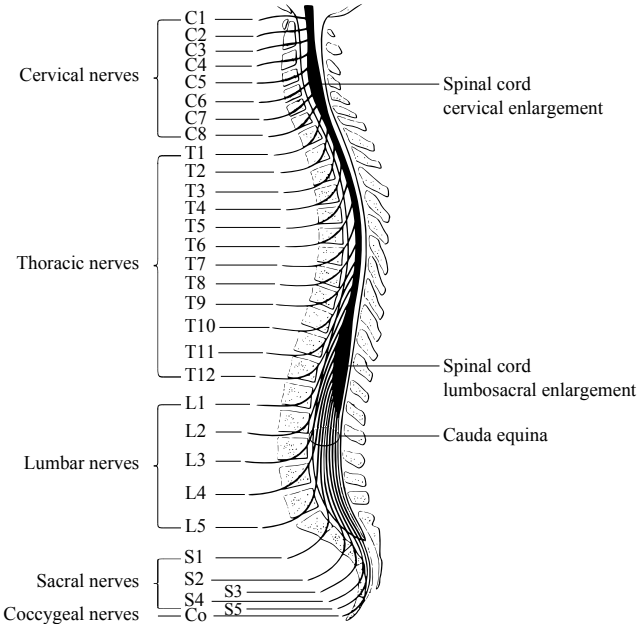

Figure 1.8: Vertebral column housing the spinal cord and spinal nerves (modified from [44])

There are 31 pairs of spinal nerves originating from the spinal cord. Each pair of nerves symmetrically innervates both the left and right side of the body. Along the vertebral column, from top to bottom, the nerves are segmented into regions. There are eight pairs of cervical spinal nerves (C1-C8), twelve pairs of thoracic spinal nerves (T1-T12), five pairs of lumbar spinal nerves (L1-L5), five pairs of sacral spinal nerves (S1-S5) and one pair of coccygeal spinal nerve (Co). The human vertebral column consists of 33 bones referred to as vertebrae that are separated by intervertebral discs – except for five bones that together form the sacrum.

1.3.2 Functional neurological deficits

Spinal cord injuries (SCIs) refer to lesions of the spinal cord. These lesions cause paralysis as the nerve impulses cannot be transmitted by the spinal cord anymore. Paralysis is the partial or total impairment in the body's sensory and motor function, leading to loss of sensation and the control of limbs and torso. SCIs are caused either by traumas, like traffic or sport accidents, by diseases such as multiple sclerosis (MS), poliomyelitis amyotrophic lateral sclerosis (ALS) or by congenital disorders like muscular dystrophy (MD). The progress of non-traumatic SCIs can be gradual.

Other diseases also lead to movement restrictions but are not directly related to the spinal cord. The locked-in syndrome (LIS) implies undamaged sensation but complete loss of muscle control. Locked-in patients are conscious and alert but cannot move: They are "locked-in" their own bodies.

Spinal muscular atrophy (SMA) causes progressive muscle wasting. This genetically-caused disease severely affects the motor functions. Symptoms of SMA are, for example, difficulties in swallowing, tongue muscle fasciculation and muscle weakness. Currently a cure does not exist, but there is palliative care, such as respiratory systems. Depending on the SMA type, life expectancy ranges from a few years to a near-normal life span.

Paralysis may also be induced by strokes – also known as cerebrovascular accidents (CVAs). Different forms of paralysis can be classified as monoplegia, hemiplegia, paraplegia and tetraplegia. Monoplegia refers to a condition where one limb is paralyzed. If the extremities and torso on the same body side are affected by paralysis, then the term is hemiplegia. Paraplegia means the paralysis affecting the lower extremities. Tetraplegia, also known as quadriplegia, refers to the paralysis of both the lower and upper extremities.

The location of the SCI is of prime importance with respect to the person's scheduled medical treatment and rehabilitative aid equipment. The NLI, also known as level of injury, refers to where the spinal cord lesion is located. In general, the higher the lesion, the more sensory and motor functions are lost. The evaluation of the lesion height is carried out either radiographically by means of imaging methods such as X-rays,

magnetic resonance tomography (MRT), computed tomography (CT), or neurologically with the aid of sensory or reflex testing.

Persons with tetraplegia are incapable of moving the lower or upper extremities. Depending on the exact localization of the spinal cord lesion – that is to say the neurological level of injury (NLI) – residual bodily functions vary inter-individually. Figure 1.9 depicts the distribution of tetraplegia with respect to the NLI. Persons living with tetraplegia typically merely have control of head-only activities – for instance, intentional activation of neck, head or facial muscles.

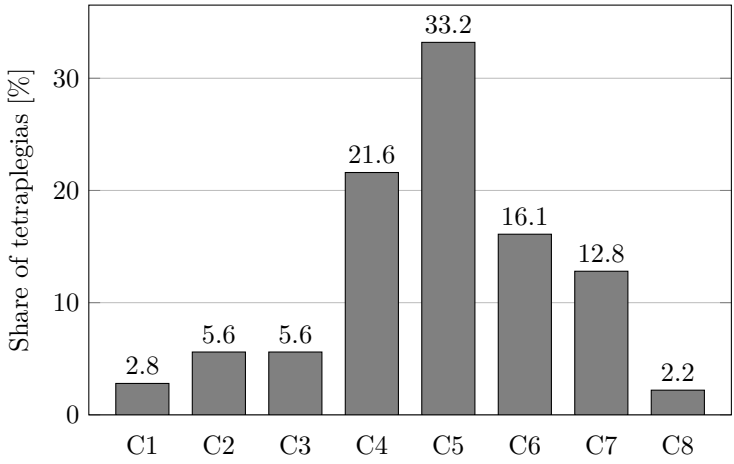

Figure 1.9: Distribution of tetraplegias with respect to the neurological level of injury (NLI) (modified from [54])

Except for the cervical spinal nerve pair C1 and the coccygeal spinal nerve pair Co, all the spinal nerves innervate a specific area of skin termed dermatome, as depicted in Figure 1.10. From evaluating dermatomes at the key sensory points with coldness, touch or pinprick sensations neurologists determine the lesion height.

Depending on the location of the spinal cord's lesion different levels of injuries can be classified. Typically, lesions above or at the spinal nerves C4

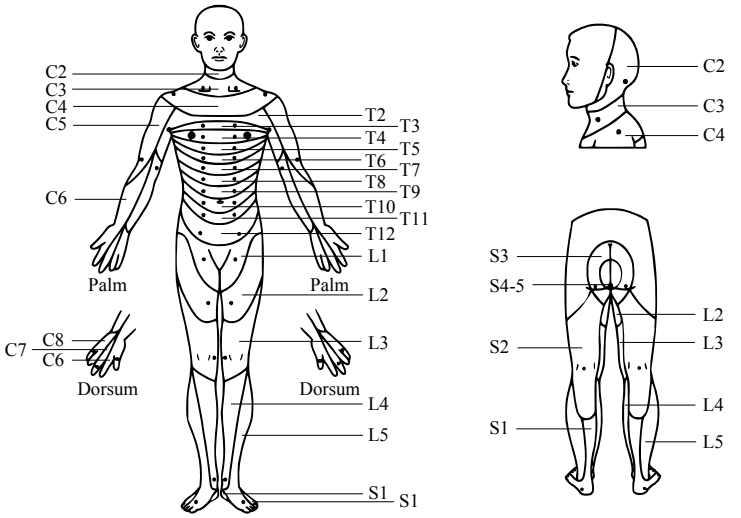

Figure 1.10: Dermatomes with key sensory points (modified from [99])

are acutely life-threatening, since these innervate the thoracic diaphragm via the phrenic nerve. These severe lesions make abdominal (diaphragmatic) breathing impossible. Artificially induced respiration is absolutely necessary in these cases.

Spinal cord injuries are categorized according to the five grades of the ASIA impairment scale (AIS) by the American spinal injury association (ASIA), as shown in Table 1.2. Persons without a SCI do not receive an AIS grade at all [99]. In order to determine the AIS grade the strength of a number of specific muscles need to be evaluated. These muscles – referred to as key muscles – control ten motor functions (key movements) both on the left and right side of the body. Key movements include, for example, shoulder shrug, elbow flexion or wrist extension. In total, twenty key movements are assessed for the AIS grade determination. They receive a muscle strength grade as detailed in Table 1.3 [23]. The ASIA form is provided in Figures A.11 and A.12 in the Appendix.

As SCIs are incurable to date, spinal cord injured persons are permanently reliant on technological rehabilitation aids that aim at improving their

Grade	Status	Criteria
AIS A	Complete SCI	No preserved sensory or motor functions below the NLI including sacral spinal nerves S4-S5.
AIS B	S. incomplete SCI	Preserved sensory functions below the NLI including sacral spinal nerves S4-S5. No preserved motor functions. Typically a transient phase leading to AIS C or D.
AIS C	M. incomplete SCI	Preserved sensory and motor functions below the NLI. At least half of key movements reach muscle strength grades M0-M2.
AIS D	M. incomplete SCI	Preserved sensory and motor functions below the NLI. At least half of key movements reach muscle strength grades M3-M5.
AIS E	Normal	Normal sensory and motor functions but neurological deficits.

Table 1.2: ASIA Impairment Scale (AIS) for grading SCIs [99]

living conditions [64, 215]. Providing windows of communication is key, and the main goal is to enable the patients to perform activities of daily living (ADLs). These refer to a set of skills that constitute essential abilities to care for oneself and meet basic needs.

The ADLs are generally viewed hierarchically from the most basic human skill (i.e., the ability to feed oneself) to somewhat higher abilities (i.e., the ability to dress oneself) [56].

Grade	Criteria
M0	No contraction and no active movement
M1	Visible contraction, but no active movement
M2	Active movement, but not against gravity
M3	Active movement against gravity, but not against additive external load
M4	Active movement against external load, but less than normal
M5	Normal muscle strength

Table 1.3: Muscle strength grading [23]

1.3.3 Treatment approaches to spinal cord injuries

In general, two approaches in SCI treatment can be identified: The medical and the technological approach. Although these approaches follow different philosophies, these are not necessarily mutually exclusive, but rather may be used complementarily for the benefit of the person with a spinal cord injury.

As for the medical approach, the key idea is to promote motor and sensory recovery. Experimental cell therapies are typically tested in animal models. For example, spinal cord injured rats were treated with incubated autologous white blood cells. The cells were injected near the lesion, and some of the rats recovered motor and sensory function [100]. A human embryonic stem cell therapy trial in its early stages was dropped due to financial constraints [57]. Apart from cell injection, transplantation of tissues both in rats and humans is also an object of research [87, 112].

The technological approach encompasses diverse ideas aiming at improving the afflicted person's condition. One idea is bridging the areas of spinal cord injury and the promotion of axonal regeneration by means of artificial scaffolds, such as self-assembling nanofibers [25, 214]. Functional electrical stimulation (FES) – also known as neuromuscular electrical stimulation – is a rehabilitation method that activates nerves through electrical currents. It is used in therapy to restore motor functions. A reciprocal control of an elbow extension was demonstrated based on EMG signals from the upper arm's biceps and the triceps [62]. Actuated technological ortheses, also known as exo-skeletons, guide the user to stand upright and to accomplish certain movements [131, 197]. Human-machine interfaces (HMIs) interpret human-generated signals, link the user with technological executing devices and thereby provide windows of communication for spinal cord injured persons.

The medical approach and its diverse directions show great potential. However, in current stages cell injections and tissue transplantations are rather experimental and far away from becoming clinical routine. On the other hand, bridging the areas of spinal cord injury presents promising reproducible results without the need of immunosuppressive medication. Exo-skeletons are accessible to persons with paraplegia but not those with tetraplegia. Both exo-skeletons and HMIs do not restore the natural motor

or sensory functions, but rather accept the spinal cord injured person's physical disability and aim for technological compensation.

1.4 Human-Machine Interfaces (HMIs)

1.4.1 Human-to-machine communication

The operating principle of human-machine interfaces (HMIs) is based on the concept of human-to-machine (H2M) communication that is depicted in Figure 1.11. In general, as the arrows in the diagram imply, the H2M communication works bidirectionally. HMIs are technological systems receiving (efferent) human-generated indication signals (HgISs) and interpreting these signals in accordance with a predefined processing scheme. In turn, interface-generated control signals (IgCSs) are sent to the executing device, where a corresponding action is executed eventually. In the opposite direction, sensors implemented in the HMI receive (executing) device-generated feedback signals (DgFSs). Afferent interface-generated feedback signals (IgFSs) are produced through stimulation. Typically, the human user observes the executing device and therefore is provided with direct feedback from it.

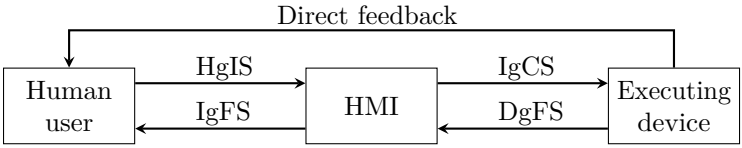

Figure 1.11: Bidirectional human-to-machine communication (modified from [133])

HMIs potentially enable disabled individuals to perform ADLs. The fundamental idea of HMIs is capturing the patient's residual bodily functions. By means of HMIs users like disabled – and able-bodied – persons are able to utilize technical devices such as limb prostheses, powered wheelchairs or word processors.

Human-generated signals may be categorized with respect to both the level of deliberation and the level of endogeneity. Table 1.4 provides an overview. Humans can directly influence intentional (deliberate) signals at will, whereas unintentional signals reflect human body processes that cannot be influenced. For example, electrocardiography (ECG) signals reflect the electrical activity of the heart that is a barely uninfluenceable, bodily process. Another example for uninfluenceable or hardly influenceable signals are the galvanic skin response (GSR) signals that are the electrical conductance of the skin, which varies with its moisture level. As the sweat glands activity is controlled by the sympathetic nervous system the GSR can be utilized as an indication of psychological or physiological arousal. In the field of affective wearables this is potentially helpful [152]. As intentional signals are repeatable at one's desire they are qualified to be utilized as HMI input signals.

Furthermore, endogenous signals, often referred to as biosignals, represent somatic functions while exogenous signals (non-biosignals) stand for non-bodily functions such as key presses, computer mouse clicks, joystick positions or lever positions. Peripheral input devices commonly used for personal computers (PCs) such as computer mice or keyboards can be regarded as the widest spread HMIs to date. This work focuses on HMIs receiving intentional and endogenous signals.

Various fields of research and development are concerned with the innovation and improvement of HMIs such as the fields of assistive technology and the rehabilitation engineering. Also, the relevance of HMIs for the entertainment industry is increasing, as demonstrated through popular game

Deliberation	Intentional		Unintentional	
Endogeneity	Endogenous	Exogenous	Endogenous	Exogenous
	Electromyography (EMG), electrooculography (EOG), tongue movement	Key press, mouse click, joystick position, lever position	Electrocardiography (ECG), galvanic skin response (GSR)	n/a

Table 1.4: Categorization of examples of human-generated signals with respect to deliberation and endogeneity

platforms like Nintendo's Wii Balance Board, Sony's Playstation Move and Microsoft's Xbox Kinect [4, 167, 224].

If the HMI receives one single human-generated signal it is referred to as an unimodal HMI. On the other hand, multimodal HMIs receive two or more human-generated signals. As compared to unimodal HMIs, multimodal HMIs either increase the number of degrees of freedom (DOFs) – such as head movements specifying the EPW's navigation direction and voice commands invoke certain actions – or improve information redundancy – like a certain head movement together with a designated voice command call for a specific action.

Human-to-human (H2H) interaction also relies on multimodal communication. It improves the information redundancy. For example, if people talk to each other there is speaking and gesticulating on the one side and hearing and seeing on the other. Multimodal HMIs are also superior to unimodal HMIs from the mathematical point of view since the information redundancy increases the quality of classification – in other words, the user intention interpretation [189].

The development of HMIs in rehabilitation engineering mainly aims for the improvement of the disabled person's QoL. Especially in the context of healthcare, it is referred to as health-related quality of life (HRQoL) that is effected by diseases and disabilities [45, 70]. The HRQoL is assessed using patient questionnaires to take account of the individual's point of view. An individual places their actual situation in relation to their personal expectation. The personal expectation may change over time due to external influences – for instance, severity of illness and family support [89]. HMIs potentially enhancing the impaired person's QoL, personal independence and competitiveness in the employment market [171].

For able-bodied persons HMIs provide additional communication channels. In that context, sometimes the terms "hands-free control" or "third-hand control" are used. In possible applications ranging from simple, single-shot actions (e.g., tack welding when both hands are busy) to complex action augmentation (e.g., robotic arm control) HMIs contribute helpful support. With certain restrictions HMI technology may also be applied in the field of attentiveness surveillance systems. This applies particularly to eye-based HMIs [24]. Another area of HMI application is the remote-controlled (telemetric) salvage robotics [235].

Human-to-human (H2H) communication is restricted to receiving and transmitting signals based on human sensory perception (esthesia) – seeing (visual perception), hearing (auditory perception), smelling (olfactory perception), tasting (gustatory perception) and feeling (haptic perception). The technological implementation of the human senses – that being the technological imitation of the sensory organs – is a challenging task. On the other hand, the H2M interaction is not restricted to the human sensory perception but rather makes use of additional communication channels like the interpretation of tongue movements or muscle activity.

1.4.2 Learning and training of HMI control

Humans learn constantly as they adapt themselves to varying circumstances. The variation of circumstances may be caused, for instance, by environmental changes or by injuries. Apart from the adaptation to external influences, humans are also capable of changing their behavior and learning purposely to improve physical or mental skills. From the neuroscientific point of view, the ability to learn is due to the neuroplasticity of the brain, also known as brain plasticity. Neuroplasticity can be seen as the adaptability of the CNS [11]. It implies synaptic plasticity (i.e., the strengthening or weakening of synapses) as well as non-synaptic plasticity (i.e., the ion channel function modification in the neuron). Neuroplastic mechanisms not only apply to the brains of children and adolescents, but are also inherent to the adult brain. In other words, humans are able to learn irrespective of how old they are. Neuroplasticity takes place in learning processes of undamaged brains as well as in the recovery of damaged brains [160].

In the spinal cord injured person's brain neurons which formerly took care about the below lesion areas lie idle after the SCI happens. Based on the knowledge about the brain's neuroplasticity, it may be assumed that plenty of these idle neurons of the motor cortex take over the deliberate activation of areas that are still innervated but used to be under-represented in the cortex. In the long term these cortex areas will be overrepresented in the spinal cord injured patient's brain in comparison to that of the non-injured patient.

Figure 1.12 illustrates the cortical homunculi of both the somatosensory cortex and the motor cortex. The primary somatosensory cortex is located at the post-central gyrus, where the human brain processes touch sensations. The primary motor cortex processing voluntary movements is situated at the pre-central gyrus. Areas in the human brain are neurologically connected to their corresponding anatomical regions. This cortical representation is not fixed but may change over time (neuroplasticity).

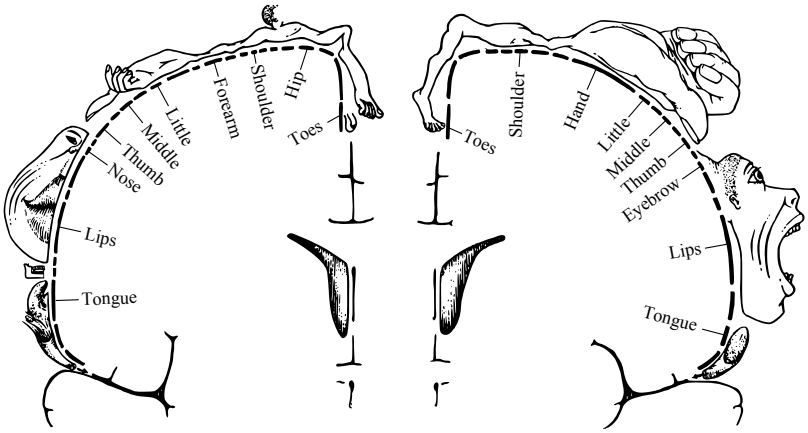

(a) Somatosensory cortex **(b)** Motor cortex

Figure 1.12: Cortical homunculi of the human brain (modified from [194])

Users improve HMI handling through training. The effect of training is the result of the adaptability of humans, that is, in turn, based on the neuroplasticity. Typically, the more intuitive the HMI control is the higher the user's acceptance is. In addition, the more intuitive the HMI is the less learning effort and training time is needed.

The NASA task load index (NASA-TLX) captures the subjective workload of the user while occupying oneself with a given task. It assesses the subjective workload in six aspects, namely the mental (cognitive) demand, the physical demand, the temporal demand of the task as well as the levels of performance, effort and frustration. The NASA-TLX is administered either using printed or computerized questionnaires [76].

The assistive technology device predisposition assessment (ATD-PA) accounts for the subjective perception of the user of a given assistive technology device. It examines the expected advantage of the addressed device from the user's point of view [178].

Transcranial magnetic stimulation (TMS) is a non-invasive method to cause depolarization or hyperpolarization in the neurons of the brain (motor cortex). The stimulation causes the corresponding muscle to move. This method is utilized in therapies for persons suffering from paralysis, depression and tinnitus aiming at changing for the better [192, 221].

The neuroplasticity of human brains makes the development of HMIs, that change their characteristics over time (adaptive HMIs), challenging. In that case, two learning systems are affiliated with each other. Consequently, these two systems influence each other: The user's behavior affects the adaptive HMI's behavior and vice versa. If the design of the adaptive HMI is not diligent enough or does not take the human user's neuroplasticity into account the HMI might not work properly, over or underreacting. This potentially leads to unstable states of the HMI.

1.4.3 Head-only HMIs

As a subclass of HMIs, head-only HMIs receive biosignals exclusively generated by parts of the head. These HMIs can be categorized according to both the sort of biosignals acquired or the part of the head the biosignals are generated by. This section provides a brief overview of these HMIs categorized with respect to the latter, that being the biosignal generating part of the head. A more in-depth literature review is given in Appendix A.4.

Table 1.5 provides an overview of the applicability of different types of head-only HMI controls (cf. Sections A.4.2 - A.4.9) with respect to the user's health constitution. Able-bodied users are capable of controlling every kind of the listed HMI controls. On the other hand, disabled users with certain movement restrictions (e.g., paralysis, spasticity) are not capable to operate particular HMI controls. Input devices for personal computers (PCs) are listed for the sake of completeness since these are not head-only HMIs. Check marks and crosses indicate whether the HMI control is suited for the user of the given health constitution.

User's health constitution	Chin control	Tongue control	Speech control	Airflow control	Facial expression control	Imagination control	Eye control	Muscle control	Input devices for PCs
cf. Appendix	A.4.2	A.4.3	A.4.4	A.4.5	A.4.6	A.4.7	A.4.8	A.4.9	
Able-bodied	●	●	●	●	●	●	●	●	●
Paraplegic	●	●	●	●	●	●	●	❍	●
Tetraplegic	●	●	●	❍	●	●	●	❍	×
Cerebrovascular Accident (CVA)	●	●	❍	❍	❍	●	●	❍	❍
Spinal Muscular Atrophy (SMA)	●	●	●	●	●	●	●	×	×
Locked-In Syndrome (LIS)	×	×	×	×	×	×	×	×	×

Table 1.5: Overview of head-only HMI controls and their applicability with respect to the user's health constitution ranging from good applicability (●), to limited applicability (❍), to no applicability (×)

1.5 User Individualization of HMIs

1.5.1 Adaptive HMIs

Traditional HMIs do not alter their characteristics, but act rather the same – notwithstanding the individual current human user.

As people have different characteristics and behavior the supply of a wide range of users with tailor-made systems necessitates HMI individualization. Therefore, calibration procedures have been developed executed offline ahead of normal operation [113]. However, due to non-stationary signal components – such as muscle fatigue in case of muscle controlled HMIs – offline calibration procedures have to be repeated periodically to ensure proper system functioning. To address that issue researchers seek to develop procedures that recalibrate the system permanently to match with the current user state. But most of these systems deal with readjustments of the pattern recognition [124].

Commonly, human users learn how to handle interfaces and adjust themselves over time to improve performance. That means human users are adaptive systems by default (cf. Section 1.4.2). Examples are activities that require a certain level of dexterity, such as playing video games or typewriting. However, in the context of biosignal-based HMIs it is of prime importance that the interface adjusts to the user in order to improve performance. These interfaces are said to be adaptive HMIs.

The term co-adaptive learning refers to at least two coupled adaptive systems effecting one another. Therefore, co-adaptive learning is given if human users (adaptive systems by default) operate adaptive HMIs.

At the time of Microsoft's disk operating system (MS-DOS) based on command line interaction, early works aiming at adaptive HMIs mainly considered interface computer software to be adaptive. While that definition is still valid, nowadays it has been extended to a larger context. Not merely the interface computer software but each technological subsystem within the H2M communication may be designed, thereby altering its behavior. Nevertheless, Norcio and Stanley stated the most fundamental principle of adaptive HMIs: The interface adapts to the individual

user [142]. In other words, the interface changes its behavior depending on external influences such as the user's behavior. As a consequence, two adaptive systems, namely the human user and the interface, are involved. The collaboration of two or more adaptive systems is referred to as co-adaptation.

In the following collection of research works the focus lies on adaptive HMIs irrespective of the manner of adaptation, the sort of biosignal or which part of the human body the biosignal emanates from. Table 1.6 gives an overview of applications of adaptive HMIs.

An adaptive prosthetic hand was developed in [92]. It was tested with two able-bodied subjects and one amputee. The four-channel sEMG signal was acquired from the right, lower arm. Signal features were extracted and as a result of clustering classification eight hand motions were performed by the prosthesis. An online and supervised learning method was proposed that adapted the mapping between sEMG signal features and clustering output classes.

In [144], an adaptive 5-class driving simulator was evaluated with five able-bodied subjects. The four-channel sEMG signal was taken from the lower arm. Time domain signal features such as mean absolute value (MAV), waveform length (WL) and zero crossings (ZCs) were extracted and exposed to a classifier. The support vector machine (SVM)-based classifier outputs five classes for the driving task – go forward, backward, right, left and stop – corresponding to five hand motions, specifically hand flexion, extension, abduction, adduction and keeping straight. Both supervised and unsupervised learning was performed. As for online supervised learning, an additional goniometry sensor was implemented that assessed the current hand state. The goniometrical information was used to label the sEMG features online.

An adaptive two DOFs robotic arm simulator was demonstrated in [154] with one able-bodied subject. From the left side's wrist and both the lower and upper arm a four-channel sEMG signal was acquired. An online reinforcement learning (RL) method based on either system-generated or human-generated reward signals (key presses) was utilized.

An adaptive HMI was presented in [163] to operate a hand prosthesis that extracts sEMG signal features to identify different hand grip types.

Depending on the contracting muscle group and the amplitude of the MES, the hand prosthesis opens or closes at a specific speed.

Research on neurally-controlled systems revealed preliminary but promising results. [130] showed an adaptive EEG-based two-class driving simulator that was tested with six able-bodied subjects. The subjects were asked to imagine left or right hand movements in order to let the car move to the left or right side. From the EEG signal the logarithmic band power (BP) as well as the MAV were extracted and exposed to the linear discriminant analysis (LDA) classifier. [60] conducted a study with six Long-Evans rats. They presented an adaptive 16-channel ECoG-based HMI. The rats were requested to operate a one-dimensional auditory center-out cursor to match a predefined frequency (reaching task). By providing a food pellet as an incentive, the rats associatively learned the task. The characteristics of the decoding Kalman filter was adapted after each trial (inter-trial). Neurally-controlled robotic or prosthetic systems that incorporate adaptive interfaces were also developed in [67, 98, 179]. A detailed review of adaptive HMIs in the context of assistive technologies is provided in Appendix A.8.

In case of EMG-based systems, preprocessed MESs are barely comprehensible. In contrast to MESs, activity signals are open to interpretation and therefore activity signals need to be generated. A well-known algorithm to transform MESs into activity signals contains the subsequent steps of signal rectification, low-pass filtering and normalization. Appendix A.5 provides the mathematical details of the digital signal normalization.

Reference	Application	Subjects	Signal	Generator	Algorithm	Output	Learning
Kato et al., 2006 [92]	Prosthetic hand	2 able-bodied, 1 amputee	4-channel sEMG	Lower arm	Cluster	8 hand movements	Supervised, online
Oskoei et al., 2009 [144]	5-class driving simulator	5 able-bodied	4-channel sEMG	Lower arm	SVM	5 car states	Un-/Supervised, online
Pilarski et al., 2011 [154]	Robotic arm simulator	1 able-bodied	4-channel sEMG	Lower and upper arm	RL	5 joint velocities	Supervised, online
Mend et al., 2012 [130]	2-class driving simulator	6 able-bodied	EEG	Brain	LDA	2 car states	Supervised, online
Cai et al., 2014 [26]	Electric-powered wheelchair	12 able-bodied	1-channel sEMG	Jaw	SVM	2 types of jaw clenching	Supervised, online
Tervo et al., 2014 [202]	Trolley crane simulator	4 able-bodied	Lever motion	Manual input	Skill Adaptive Control (SAC)	Trolley crane 1-DOF position	Supervised, offline

Table 1.6: Applications of adaptive human-machine interfaces

1.5.2 Intelligent vehicles

In the field of automotive engineering adaptive management systems changing behaviors depending on the driver's state and current traffic situation are of great interest. Advanced driver-assistance systems (ADASs) support the driver and mitigate potentially dangerous traffic situations [111]. For example, the adaptive integrated driver-vehicle interface (AIDE) aims at avoiding driver overload by unfiltered information flow [7, 8]. It provides adaptive management functions for drivers. That way the road safety is to be increased because the driver gets to know only the essential information rather than being distracted by meaningless data in stressful situations.

Also, incoming telephone calls are automatically redirected to the telephone mailbox if the driver's workload estimate exceeds a certain threshold [153].

Moreover, an aircraft cockpit's display changes its configuration depending on the situation. In order to support the pilot in establishing and maintaining situation awareness the adaptive interface is able to present the right information in the right format at the right time [1].

1.5.3 Criticisms and merits

Adaptive HMIs are not free from controversy. Critics reproach higher complexity of implementation and therefore higher development costs as compared to non-adaptive HMIs [142]. Moreover, because the adaptive interface changes its behavior permanently and automatically the user might encounter difficulties to create a cognitive model of the interface [66]. Some users might perceive the adaptation of the HMI as a loss of control over the technology [220].

In addition to the mentioned criticisms, adaptive HMIs potentially provide beneficial aspects. If they are carefully designed, adaptive interfaces make the system more useful to a larger number of people. Both novices and experts can use an adaptive system with equal ease, since the system is capable of serving both [142].

1.6 Open Problems

In consideration of state-of-the-art HMI concepts described in the previous section, there are still open problems and unsolved challenges in the field of HMI development. Some of those are outlined hereinafter.

1. **Lack of specific design methodologies** Developers hitting on an idea of a HMI have to follow guidelines concerning general product engineering. There is no design methodology that covers the specifics of HMI design.
2. **Few biosignals accessible for head-only activities** Severely disabled persons capable of activating merely the head muscles are limited to very few biosignals to operate HMIs. Therefore, additional biosignals for head-only activities are needed.
3. **Aesthetic impairment through excessive apparatus** The technological realization of HMIs requires biosignal acquiring metrology at the site of biosignal generation. However, an overly salient apparatus in the face of the user should to be avoided. An unobtrusive outward appearance is of importance.
4. **Double occupancy of bodily functions** The functional overlapping with bodily functions such as breathing, speaking, eating and seeing causes the loss of functionality. Human-generated signals not interfering with other bodily functions are therefore preferable.
5. **Poor biosignal controllability in the early stages** Inexperienced users – such as those who only recently lost upper extremities – may encounter difficulties in HMI control in the early stages. This typically is caused by the user's poor biosignal controllability. Therefore, a systematical training concept leading to full HMI control step-by-step for inexperienced users is highly desired.
6. **Time-variant biosignal drifts** Over time, biosignals tend to drift gradually due to various reasons – like physiological response, mental fatigue – and as a consequence HMI control becomes more challenging. Hence, an adaptation scheme coping with time-variant biosignal drifts is to be developed.

1.7 Proposal and Structure

The overall objective of this work is to provide a wide range of persons with an easy-to-use HMI. Taking the aforementioned open problems into account, this work aims at the evaluation of novel biosignals that are accessible for severely handicapped persons without interfering with remaining bodily functions. Furthermore, this work proposes developing a new training scheme facilitating HMI control.

This doctoral dissertation is organized into six chapters. Figure 1.13 provides a graphic overview of the structure of this work and displays the relationships among the chapters.

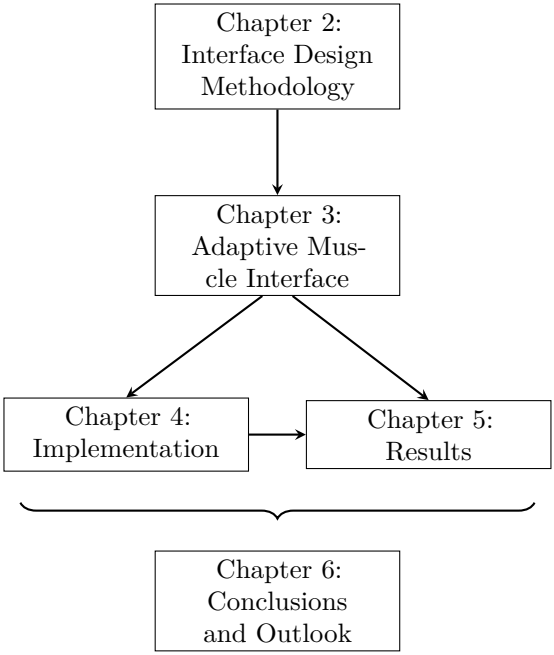

Figure 1.13: Graphical overview of this doctoral dissertation

The subsequent chapters are briefly outlined as follows.

Chapter 2 introduces a novel design methodology for HMIs based on uncharted biosignals. In Chapter 3 the realization of the adaptive HMI dedicated to MESs acquired from the outer ear muscles is presented. The individualization of the interface allows users with different physiological and habitual attributes to manage the robust and fail-safe control. Chapter 4 portrays the implementation of the novel concept including both hardware and software details. In Chapter 5 results are presented. Chapter 6 summarizes this work, gives a conclusion and provides an outlook for further research.

2 Interface Design Methodology

2.1 Generic Framework

Whenever developers intend to come up with concepts of HMIs, fundamental questions regarding the technological and economic feasibility arise – especially if the HMI applies uncharted biosignals. Due to human-generated signals that are challenging to process and not commonly used by researchers, developers usually approach the realization in an unstructured manner resulting from the lack of guidance in the literature. In scientific literature, traditional design tools and design processes concerning general product engineering can be found [72, 145].

Literature addressing the challenges of interface design often emphasize the intuitiveness and psychological involvement of interactive systems, such as computer software, electronic books or virtual reality devices [29, 109, 191].

However, none of these methodologies cover the specifics of HMI designs in this work's understanding: The choice of human-generated biosignals, the metrological acquisition of the biosignals and the algorithmic interpretation of the biosignals. Generally, the traditional design guidelines do not reflect upon the necessity of the human-to-machine communication and its improvement. The traditional approaches imply the selection of one solution out of a pool of possible solutions on the basis of stationary processes. Inspired by developments in the field of precision engineering and power transmission engineering, they focus on the best possible solution in terms of mechanics and electronics. The design of HMIs should be user-centric and improve user experience.

The generic framework for designing HMIs proposed here is a stepwise development approach from the idea of a HMI to its realization. The steps

are illustrated in Figure 2.1. It focuses on the establishment of a HMI that allows for well functioning human-to-machine communication. To begin with, the *target group analysis* needs to be undertaken where the target group of people, that the development is mainly intended for, is to be identified. Subsequently, the *scope statement analysis* needs to be performed where technological objectives and design decisions (e.g., tethered or wireless inter-subsystem communication) as well as user-centered objectives and design decisions (e.g., aesthetic design of the apparatus) are defined. The scope statement analysis eventually yields a *set of requirements* that is referred to by each of the subsequent steps of the generic design framework. In other words, the set of requirements has direct repercussions on the other steps.

Next, the *signal specification and assessment* of both the acquired biosignals and the processed control signals is necessary. The exact utilization of the various signals is to be clarified. The quality criteria need to be defined in order to assess the biosignal control ability numerically. Furthermore, techniques of *biosignal control ability improvement* are of prime interest when developing a HMI. If users encounter difficulties controlling the executing device for some time the motivation will most likely drop. Next, the *biosignal interpretation* is to be characterized. The signal-to-meaning mapping [67] matches the incoming biosignal with the outgoing control signal. Finally, the *technical implementation* of the HMI concept in terms of hardware and software components completes the framework.

As a meta-strategy of technical system design, simplicity is to be preferred to complexity in all aspects. This idea is represented, for instance, by the MAYA principle that reads “Most advanced yet acceptable” [78].

The guidance provided by the generic framework aims at covering the specifics of HMI designs. However, as the field of HMI design is overly wide, the lists presented hereinafter make no claim of completeness.

2.2 Target Group Analysis

The target group analysis aims at clarifying the fundamental cornerstones of the development and helps to focus the endeavors.

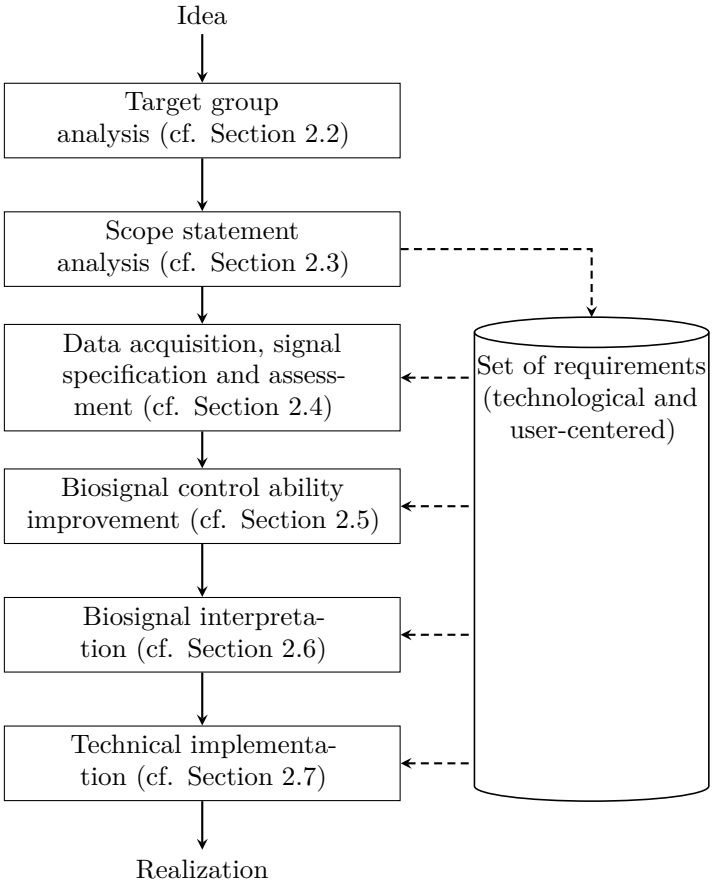

Figure 2.1: Generic framework for designing human-machine interfaces from the idea to its realization

The analysis should result in documents that are referred to by the developers throughout the development process. They constitute the basis for the scope statement analysis. The considerations of the target group analysis are:

- Intended target group of people: The group of human users to whom the development is mainly dedicated. For instance, "third-hand" applications for welding in the industrial context may be dedicated to workers of a specific body height. HMIs based on gesture interpretation in video games predominantly are dedicated to players of a certain age range. In rehabilitation engineering, HMIs compensating disability induced shortcomings are dedicated to a particular type of patients.
- Minimum and maximum number of the target group of people: The estimation of the target group size yields the approximate numbers for the economic weighing of interests. For instance, in case the maximum number exceeds a threshold (depending on the involved developers) it does not make good economic sense to develop many subsystems in-house, but rather to purchase them from other vendors.
- Characteristics of the target group individuals: The knowledge of the typical skills and shortcomings of the individuals affiliated with the target group plays an important role in designing the HMI. The HMI ideally compensates for shortcomings while emphasizing the skills of the users. For example, HMIs dedicated to below-knee amputees do not rely on biosignals acquired from the calf, but rather make use of other parts of the body for biosignal acquisition.
- Potential windows of communication for target group individuals: The identification of various biosignals that are under intentional control of the target group individuals is significant information for the developers. The interpretation (extraction of the underlying meaning) of the identified biosignals establishes various windows of communication.

2.3 Scope Statement Analysis

After clarifying to whom the endeavors of the HMI development relate, the scope statement analysis needs to be conducted. This is of prime importance as it is supposed to result in a set of requirements. The

set of requirements contains the technological and user-centered (non-technological) objectives and design decisions of the HMI that is to be developed.

Depending on the preferences of the developers the set of requirements can be embodied by simple documents or spreadsheets as well as by complex project management software tools like Redbooth[1], Smartsheet[2] or Basecamp[3].

The set of requirements encompasses hard factors like technological considerations, such as:

- System partitioning: The overall system needs to be partitioned into logical and physical subsystems, meaning the subsystem boundaries are to be defined.
- Inter-subsystem communication: The transmission of information between the subsystems is either mechanical, hydraulic, pneumatic, electric or hybrid combinations therein. As for electric information transmission, developers need to opt for a tethered design if cables can be tolerated or a wireless design to implement telemetric inter-subsystem communication. In addition, communication protocols should be defined.
- Input signals: The type of input signals is to be characterized. Human-generated input signals are, for example, EMG, EOG or EEG signals.
- Signal acquisition: The techniques of acquiring the input signals needs to be decided, such as invasive or non-invasive signal acquisition methods. The part of the body generating the signal should be readily accessible.
- Signal processing: Digital or analog signal processing methodologies and algorithms need to be selected.
- Scope of information provision and visualization: It needs to be decided whether information (e.g., numeric intermediate or end

[1] `http://www.redbooth.com`
[2] `http://www.smartsheet.com`
[3] `http://www.basecamp.com`

results) and visualizations (e.g., signal graphs) are intended to be for supervisors only, for users only, for none or for both.

On the other hand, soft factors are user-centric considerations especially factoring in the user acceptance and the approval of the social environment, such as:

- Signal coherence: To avoid user frustration the human-generated signals need to reflect the intention of the user. To this end, user individualization of the HMI is of prime importance to realize accessibility for an as wide as possible range of users with different behavioral and physiological characteristics.
- Aesthetic impairment: The aesthetic impact of the apparatus on the overall visual appearance of the user is to be taken into account. Obtrusive equipment and apparatus potentially causes a negative response from people and social stigmatization. Therefore, subtle cosmetics and minimum aesthetic interference are desirable. For instance, large and obtrusive technical devices prominently placed in front of the head might have a negative aesthetic impact.
- Health risks: Developers also should think about possible endangerments of the health of the user. The HMI should have the lowest possible injury risk for the user. Precautionary measures are needed to minimize health risks like inflammations caused by invasive data acquisition methods.
- Ergonomic efforts: The ergonomic design of the HMI is another crucial aspect when it comes to user acceptance. Uncomfortable stances or postures are to be avoided.
- Mental efforts: In order to facilitate the overall usage of the HMI, the developers would be well served by contemplating how to keep down the essential mental efforts during operation. An intuitive and easy-to-use control requiring minimum mental effort is preferred. Moreover, it would be appreciated turning HMI operation into a subconscious routine in the long term. As a consequence, the HMI needs to feature motivating methods yielding minimum training time.

- Fault tolerance: Since system-inherent errors and user-induced errors cannot be ruled out, the HMI requires being robust against incorrect operation. The system is supposed to be fail-safe.
- Commercial availability: The majority of current HMIs are experimental systems that are developed for research purposes. They are solely available for a small group of subjects participating in the corresponding research study. Oftentimes, the handicapped study participants are not supplied with the HMI for their everyday life after the research study.
- Low costs: Disabled persons often have large financial expenses on realizing a comfortable everyday life due to high costs of rehabilitation aids. In that context, the HMI is preferably as inexpensive as possible. To this end, the enhancement of the in-place system by means of the incorporation of standard parts (add-ons) is useful.

The set of requirements is utilized for quality management throughout the entire development process. If needed, the set can be complemented during the development process.

2.4 Data Acquisition, Signal Specification and Assessment

2.4.1 Data acquisition

Depending on the desired type of input signals and the desired signal source, the electrodes for the data acquisition need to be selected.

Considering the type of input signals, various electrode types might be available. For instance, EEG signals can be acquired by means of surface or implanted electrodes. As for EMG signals, surface, fine-wire or implanted electrodes are conceivable.

The signal source that is desired also affects the type of electrodes. In case of EMG signals, the spatial resolution is an important aspect. Surface electrodes provide a lower spatial resolution as compared to fine-wire electrodes. If the muscle that is selected as the EMG signal source is

small, fine-wire electrodes typically are more eligible because they are more precise and require less installation space than surface electrodes. Generally speaking, the decision regarding the electrodes should carefully consider two counterparts, namely health risks for the user and signal quality.

The frequency of data acquisition needs to be decided once the type of input signals and the signal source are selected. Ideally the sampling frequency is set such that it covers all the essential information of the biosignal. On the one hand, if the frequency is set too high it includes all the information of the biosignal, but also creates an overhead of signal processing and hence energy. On the other, if the frequency is set too low it saves energy but does not include all the information.

2.4.2 Biosignal digitalization

The total number of input modalities (biosignals) $\tilde{I}$ intended to be interpreted by the HMI is to be determined. This partly constitutes a design decision and partly is restricted by the skills and shortcomings of the users.

The index of input modalities is termed $i \in \{1, ..., \tilde{I}\}$. The biosignals should not affect each other, but rather be independent. The more independent input modalities are available, the more degrees of freedom (DOFs) for HMI control are available. In turn, the higher the number of DOFs, the more diversified and complex HMI control can be realized, since each input modality potentially controls a separate DOF simultaneously instead of sequentially. Deploying the maximum number of acquirable biosignals is desirable. On the other hand, to a degree, this deteriorates the usability of the HMI as the mental effort increases.

Digital signal processing (e.g., bit operations) is easier to bring about as compared to analog signal processing (e.g., electric circuits). By default, the physical (analog) biosignal is defined in the time and value-continuous domain

$$x_i(t) \in \mathbb{R}, t \in \mathbb{R}_{\geq 0}. \tag{2.1}$$

In order to deploy digital signal processing, the biosignal needs to be digitized. The quantization resolution (in bits) of the analog-to-digital converter (ADC) is referred to as n. The sampling rate or frequency (in Hz) is termed f. This leads to time-discrete and value-discrete biosignal

$$x_i[k] \in [0, 2^n - 1], k \in \{0, ..., \tilde{K}\}, \tag{2.2}$$

where the time point of the k-th sample is

$$t = \frac{k}{f}. \tag{2.3}$$

The last sample index is termed $\tilde{K}$. Figure 2.2 illustrates the analog-to-digital conversion process.

The digitized biosignal $x_i[k]$ ranges from 0 to $2^n - 1$ and reflect the original, physical biosignal $x_i(t)$. Hence, $x_i[k]$ contains an unknown bias together with an unknown signal-to-noise ratio. These signal distortions are to be compensated before utilizing the biosignals for any HMI control purposes. The digital signal process compensating the signal distortions should eventually yield a digital, normalized biosignal in the range of 0 to 1, since this meets the intuitive understanding of gradual activity between 0 % and 100 %.

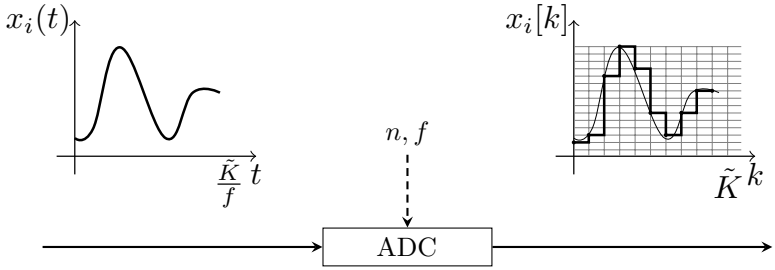

Figure 2.2: Analog-to-digital converter (ADC) digitizing an analog signal with respect to the quantization resolution n and the sampling rate f

2.4.3 Biosignal assessment paradigms

In the scientific literature two types of biosignal assessment paradigms exist. The first category focuses on the physiological interpretation of the biosignal. As for EMG signals, results are indicative of dysfunctioning muscles [5, 38] or muscle fatigue [207]. Regarding EEG signals, assessment paradigms make mental fatigue of the user evident [91]. The second type of biosignal assessment paradigms evaluates the aptitude for HMI operation of the biosignal rather than appraising the biosignal itself. Commonly these paradigms assess the features or subsets of features regarding the aptitude for HMI operation [22].

The following assessment paradigms count among the second category. They are purely based on the amplitude of the preprocessed biosignal (e.g., normalized biosignal) and without the extraction of biosignal features the assessment paradigms evaluate the aptitude for HMI operation. They quantitatively capture the diverse abilities of the user to modify the biosignal. To this end, they allow for inter as well as intra-individual comparison on a numerical basis. Table 2.1 provides an overview of the assessment paradigms with respect to the biosignal quality criteria and with respect to the demands of the HMI control.

Biosignal Assessment paradigm	Biosignal quality criteria	Control demand
Duration of activity	Endurance of activation	Isotonicity
Rate of range activity	Fine-granularity of activation	Sensitivity
Response time of activation	Promptness of activation	Spontaneity
Response time of deactivation	Promptness of deactivation	Spontaneity
Frequency of alternation	Rate of significant activation changes	Spontaneity

Table 2.1: Assessment paradigms with respect to biosignal quality criteria and control demands

In case of an isotonic HMI control, the user is required to keep up the biosignal activation for an extended time period. Therefore, the endurance of biosignal activation is an essential quality criterion. On the other hand,

if the HMI control needs to be sensitive – for instance, the range of the biosignal amplitude is by design broken up into many countable or infinite subranges affecting distinct consequences – then the fine-granularity of biosignal activation is the crucial quality criterion. Moreover, if the HMI control is promptness-critical requiring a certain degree of spontaneity – like when the biosignal amplitude needs to be changed rapidly in certain situations – then quality criteria such the promptness of biosignal activation and deactivation as well as the rate of significant activation changes are of prime interest.

Response time assessment

The minimum response time of input signal activation numerically captures how quickly the biosignal $x(t)$ raises, for instance, positive signal edge, caused by the response of the human user covering a predefined magnitude (difference of two distinct signal levels). This quality criterion is of importance for HMI control if the time span of input signal activation matters. The assessment paradigm is depicted schematically in Figure 2.3.

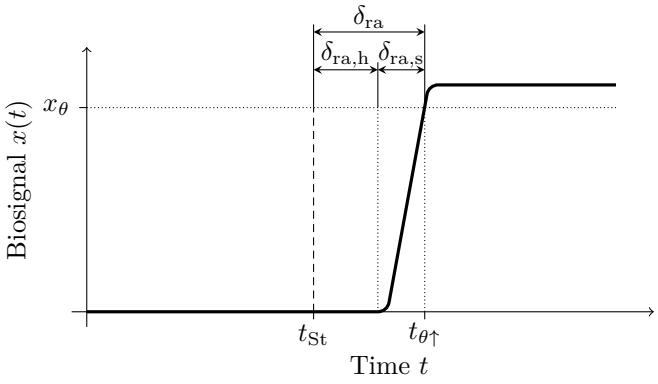

Figure 2.3: Response time assessment of activation with exemplary signal (——) and stimulus (- - -)

It determines the total response time of input signal activation like muscle contraction, termed δ_{ra}. This characteristic value is represented by time in milliseconds. It is defined as

$$\delta_{\mathrm{ra}} = t_{\theta\uparrow} - t_{\mathrm{St}}, \tag{2.4}$$

where t_{St} is a stipulated point in time triggering a stimulus and $t_{\theta\uparrow}$ is a subsequent point in time indicating that the biosignal exceeds the predefined upper threshold x_θ. The total response time consists of the response time of the human user $\delta_{\mathrm{ra,h}}$ and the response time of the system $\delta_{\mathrm{ra,s}}$ according to

$$\delta_{\mathrm{ra}} = \delta_{\mathrm{ra,h}} + \delta_{\mathrm{ra,s}}. \tag{2.5}$$

The point in time $t_{\theta\uparrow}$ is dependent on the actual biosignal following the definition

$$t_{\theta\uparrow} = \min\left\{t > t_{\mathrm{St}} | x(t) \geq x_\theta\right\}. \tag{2.6}$$

Analogous, the minimum response time of input signal deactivation characterizes how quickly the biosignal – the negative signal edge, caused by the response of the human user covering a predefined magnitude (difference of two distinct signal levels) – drops. In cases where the promptness of input signal deactivation makes a difference, this quality criterion is an important indicator. The assessment paradigm is presented in Figure 2.4.

It finds the total response time of input signal deactivation, such as muscle relaxation (referred to as δ_{rd}) represented by time in milliseconds. Its definition reads

$$\delta_{\mathrm{rd}} = t_{\bar{\theta}\downarrow} - t_{\overline{\mathrm{St}}}, \tag{2.7}$$

where $t_{\overline{\mathrm{St}}}$ denotes the point in time disappearing the stimulus and $t_{\bar{\theta}\downarrow}$ is another point in time when the biosignal falls below the preset lower threshold $x_{\bar{\theta}}$. The total response time is made up of the response time of the human user $\delta_{\mathrm{rd,h}}$ together with the response time of the system $\delta_{\mathrm{rd,s}}$ according to

$$\delta_{\mathrm{rd}} = \delta_{\mathrm{rd,h}} + \delta_{\mathrm{rd,s}}. \tag{2.8}$$

The point in time falling below the lower threshold is defined as

$$t_{\bar{\theta}\downarrow} = \min\left\{t > t_{\mathrm{St}} | x(t) \leq x_{\bar{\theta}}\right\}. \tag{2.9}$$

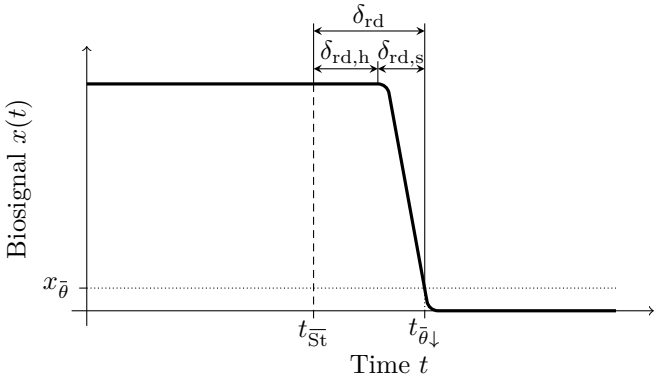

Figure 2.4: Response time assessment of deactivation with exemplary signal (—) and stimulus (---)

Frequency of alternation assessment

The maximum frequency of activations and deactivations of the input signal determines how quickly the biosignal alternates the sign of the signal edge while covering a predefined magnitude – for instance, the difference of two distinct signal levels. If the rapidness of changes in the sign of the signal edge matters, then this criterion is insightful. The frequency of alternation assessment paradigm is shown in Figure 2.5.

As the characteristic value of interest, this assessment identifies the maximum frequency of input signal activations and deactivations defined as

$$f_{\mathrm{f}} = \frac{\tilde{L}_{\mathrm{f}}}{t_{\mathrm{end}}}, \tag{2.10}$$

where $\tilde{L}_{\mathrm{f}}$ is the total number of complete input signal activations and deactivations (e.g., muscle contractions and relaxations), and t_{end} is a predefined time.

The ongoing index $l_{\mathrm{f}} \in \{1, ..., \tilde{L}_{\mathrm{f}}\}$ represents the consecutive events of complete input signal activations and deactivations.

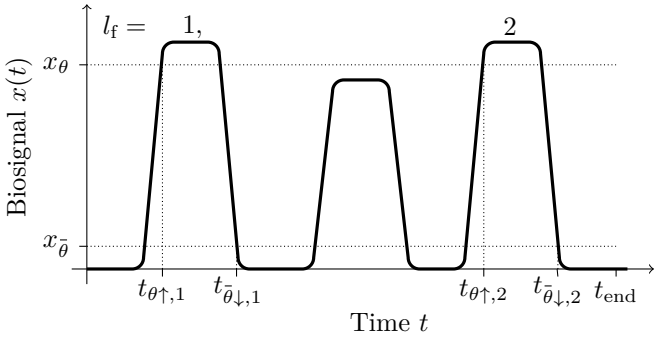

Figure 2.5: Frequency of alternation assessment with exemplary signal (—) and ongoing index l counting only the complete signal activations and deactivations

It is important to note that the input signal (originating from below $x_{\bar{\theta}}$) needs to exceed the upper threshold x_θ and then fall below the lower threshold $x_{\bar{\theta}}$ again in order to be counted as a complete activation and deactivation.

Duration of activity assessment

The duration of activity assessment quantifies how long the biosignal activation lasts while being beyond a predefined signal level. This value is informative for isotonic controls requiring full activation for a long period of time. Figure 2.6 illustrates the scheme of the duration of activity assessment paradigm.

This paradigm determines the maximum duration of the input signal activity, termed δ_dm. The characteristic value is represented by time in milliseconds. It is defined as

$$\delta_\mathrm{dm} = t_{\bar{\theta}\downarrow} - t_{\theta\uparrow}, \tag{2.11}$$

where $t_{\theta\uparrow}$ and $t_{\bar{\theta}\downarrow}$ are defined by (2.6) and (2.9), respectively.

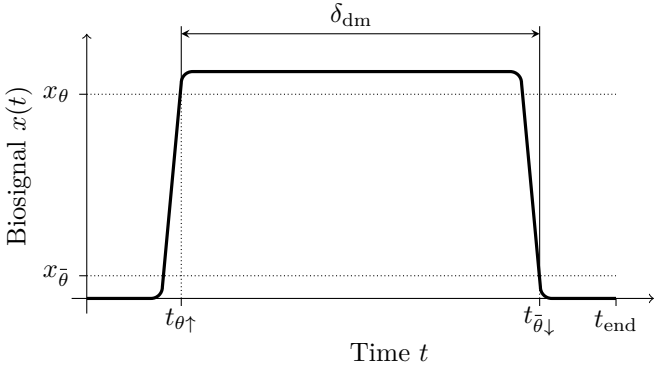

Figure 2.6: Duration of activity assessment with exemplary signal (—)

Rate of range activity assessment

The rate of range activity assessment characterizes how long the biosignal activation matches a predefined signal level subdomain as compared to the total duration. This is of prime importance considering controls where subdomains of the signal level carry distinct information. The paradigm is shown with an exemplary signal in Figure 2.7.

As the characteristic value of interest, this paradigm determines the relative duration of the input signal activity τ being within the (valid) range between the lower threshold $x_{\bar{\theta}}$ and the upper threshold x_θ with respect to the total paradigm time. It is defined as

$$\tau = \frac{\Delta_{\mathrm{dr}}}{t_{\mathrm{end}}}, \tag{2.12}$$

where t_{end} is the total time of the paradigm and Δ_{dr} is the sum of durations of range activity, defined as

$$\Delta_{\mathrm{dr}} = \sum_{l_{\mathrm{rr}}=1}^{\tilde{L}_{\mathrm{rr}}} \delta_{\mathrm{dr},l_{\mathrm{rr}}}. \tag{2.13}$$

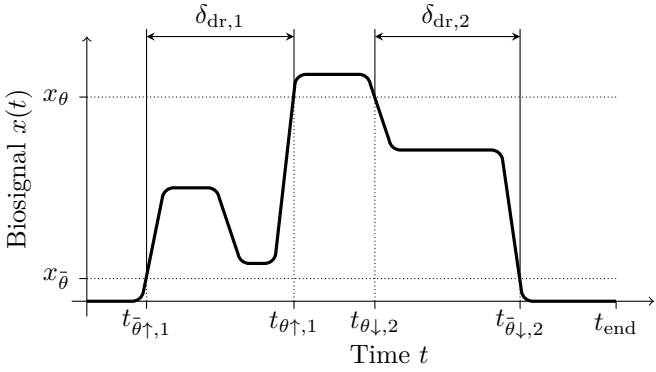

Figure 2.7: Rate of range activity assessment with exemplary signal (—)

The durations $\delta_{\mathrm{dr},l_{\mathrm{rr}}}$ are the l_{rr}-th time periods when the signal is within the valid range, $l_{\mathrm{rr}} \in \{1, ..., \tilde{L}_{\mathrm{rr}}\}$. They are defined as

$$\delta_{\mathrm{dr},l_{\mathrm{rr}}} = t_{\mathrm{out},l_{\mathrm{rr}}} - t_{\mathrm{in},l_{\mathrm{rr}}}, \tag{2.14}$$

where $t_{\mathrm{in},l_{\mathrm{rr}}}$ and $t_{\mathrm{out},l_{\mathrm{rr}}}$ stand for the points in time when the signal goes into and out of the valid signal range, respectively. The possibility of both rising signals and falling signals at the upper and lower thresholds is covered by the case differentiation

$$t_{\mathrm{in},l_{\mathrm{rr}}} = \min\left\{t_{\bar{\theta}\uparrow,l_{\mathrm{rr}}}, t_{\theta\downarrow,l_{\mathrm{rr}}}\right\}, \tag{2.15}$$

$$t_{\mathrm{out},l_{\mathrm{rr}}} = \min\left\{t_{\theta\uparrow,l_{\mathrm{rr}}}, t_{\bar{\theta}\downarrow,l_{\mathrm{rr}}}\right\}. \tag{2.16}$$

The point in time of exceeding the lower threshold $t_{\bar{\theta}\uparrow,l_{\mathrm{rr}}}$, the point in time of falling below the upper threshold $t_{\theta\downarrow,l_{\mathrm{rr}}}$, the point in time of exceeding

the upper threshold $t_{\theta\uparrow,l_{\mathrm{rr}}}$ and the point in time of falling below the lower threshold $t_{\bar{\theta}\downarrow,l_{\mathrm{rr}}}$ correspond with

$$t_{\bar{\theta}\uparrow,l_{\mathrm{rr}}} = \min\left\{t|x(t-\Delta t) < x_{\bar{\theta}} \wedge x(t) \geq x_{\bar{\theta}}\right\}, \tag{2.17}$$

$$t_{\theta\uparrow,l_{\mathrm{rr}}} = \min\left\{t|x(t-\Delta t) < x_{\theta} \wedge x(t) \geq x_{\theta}\right\}, \tag{2.18}$$

$$t_{\theta\downarrow,l_{\mathrm{rr}}} = \min\left\{t|x(t-\Delta t) > x_{\theta} \wedge x(t) \leq x_{\theta}\right\} \text{and} \tag{2.19}$$

$$t_{\bar{\theta}\downarrow,l_{\mathrm{rr}}} = \min\left\{t|x(t-\Delta t) > x_{\bar{\theta}} \wedge x(t) \leq x_{\bar{\theta}}\right\}. \tag{2.20}$$

Bimodal assessment

Given a bimodal HMI (i.e., receiving two input signals) if isolated activation of only one signal at the same time is desired, this signal is typically termed signal of interest, while the other is the reference signal. In case of isolated biosignal activation, the biosignal of interest ideally is at its maximum while the activation of the reference biosignal is at its minimum.

The bimodal assessment captures the portion of isolated signal activation with respect to the biosignal of interest versus the reference biosignal. This value represents the quality of signal isolation that is of prime interest considering bimodal controls. The bimodal paradigm is illustrated in Figure 2.8.

This paradigm identifies the portion of isolated signal activation with respect to the input modality of interest versus the reference input modality, termed $r_{\mathrm{b},i,j}$, defined as

$$r_{\mathrm{b},i,j} = \int_{t_{\mathrm{St}}}^{t_{\overline{\mathrm{St}}}} \frac{x_i(t) - x_j(t)}{x_{\mathrm{b,des}}(t)} dt. \tag{2.21}$$

2.5 Biosignal Control Ability Improvement

2.5.1 Biosignal feedback

The user operating an executing device via a HMI typically perceives the impact of one's own acts on the executing device (late-stage feedback).

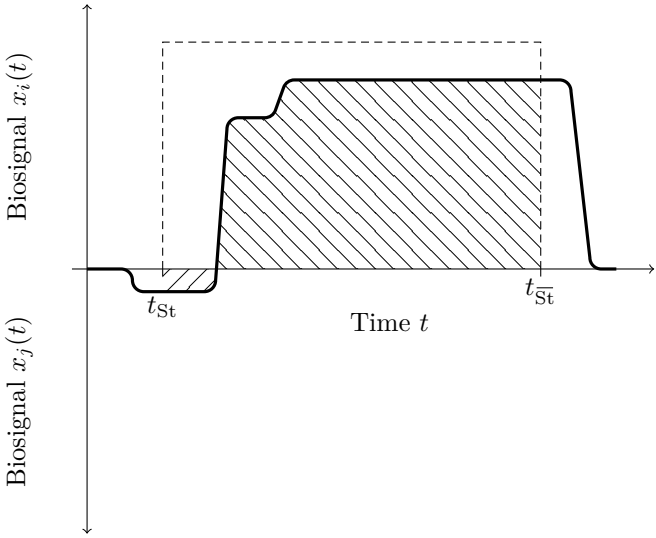

Figure 2.8: Bimodal assessment with exemplary signal (—) and desired ideal signal $x_{\mathrm{b,des}}(t)$ (- - -). The sum of activity of the biosignal of interest $\int x_i(t)dt$ (\\\\) and the sum of activity of the reference biosignal $\int x_j(t)dt$ (////).

The biosignal feedback (early-stage feedback) provides information being the fundamental basis of the actions of the executing device.

The feedback of the user's "own" biosignal involve a considerable potential for the biosignal control ability improvement. Without knowing the correlation between the action of the user in hopes of the resulting biosignal and the actual biosignal (cause-and-effect) the user is, per se, incapable of improving the biosignal control ability. The confrontation with the biosignal establishes that correlation. Feedback mechanisms that are easily understandable to the user (intuitive feedback mechanisms) are to be preferred over less intuitive feedback mechanisms. In addition, the feedback mechanisms should be direct and prompt.

Biosignal feedback in the context of HMIs can be visual, like signal representatives visualized and displayed by computer monitors or LEDs. The

amplitude of the biosignal can be represented by the increasing number of flashing LEDs. Auditory biosignal feedback is another option. The frequency of the generated feedback sound stands for the amplitude of the biosignal.

Both the visual and the auditory feedback can be realized with the aid of computer programs, such as graphical user interfaces (GUIs). For example, GUIs have been implemented for playing Tetris with hand gestures [163], gait analysis feedback [177], tongue-controlled EPW navigation [83] and EMG-controlled robotic arms [37]. These computer programs need to be specifically designed and parameterized in order to meet both the task's as well as its user's requirements.

2.5.2 Adaptation

The adaptation of the HMI refers to the idea that the HMI changes its characteristics by modifying the inherent parameters. The objective is to enhance the biosignals' coherence of the user. In other words, HMI adaptation methods aim at changing the signal-to-meaning mapping for the better. The adaptation of the HMI allows for user individualization leading to less frustration and more motivation.

Generally, user individualization applies to both inter and intra-individual diversity. Inter-individual diversity is caused by variant physiological, neurological or habitual attributes. For instance, the contraction of the identical muscle but performed by different individuals typically yield distinct signal patterns. The reasons are manifold, due to the complexity of the human organism.

Intra-individual diversity denotes variations in signal patterns that occur when measuring the biosignal from the same person and the same biosignal generator but at different times. This is caused by non-stationarities – time-variations – in the biosignal. Intra-individual diversity also appears when measuring the biosignal from the same person but from distinct biosignal generators (e.g., different muscles).

Three types of parameter adaptation methods are identified, namely

1. open-loop offline adaptation,

2. closed-loop offline adaptation, and
3. closed-loop online adaptation.

Open-loop offline adaptation methods are applied once a session, depicted in Figure 2.9. The adaptation takes place ahead of the application in order to determine suitable parameter values for the human user. The user is guided through a fixed procedure to identify the parameter values automatically once started by the human supervisor. During the *application* the user operates the HMI applying these settings. Once set in the adaptation, it is not possible to modify the settings during the application, meaning the adaptation is open-loop. The application itself is referred to as being an *online* process. On the other hand, as the adaptation is performed when the actual application is inactive or paused, the adaptation is considered being an *offline* process. The open-loop offline adaptation poses the risk of determining inapt parameters that are applied throughout the sessions.

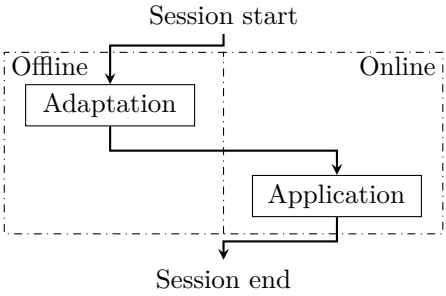

Figure 2.9: Course of events from session start to open-loop offline adaptation to online application to session end

Closed-loop offline adaptation methods, as pictured in Figure 2.10, feedback user-specific information extracted from the application that is utilized for the calculation of new, suitable parameter values for the human user. In order to process that information the application needs to be paused. Closed-loop offline adaptation is of particular interest for time-variant signals and non-stationary processes. On the other hand, closed-loop

adaptation methods potentially pose the risk of confusing the human user since making an appropriate mental model of the (ever-changing) HMI becomes more difficult.

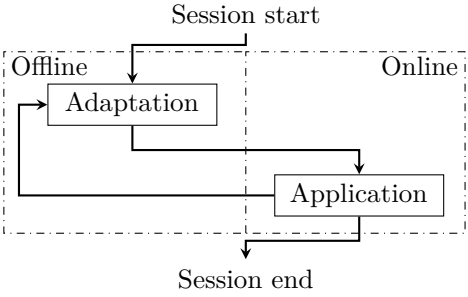

Figure 2.10: Course of events from session start to closed-loop offline adaptation to online application to session end

The closed-loop online adaptation methods, as shown in Figure 2.11, constantly extract the user-specific information during the application in order to recalculate optimal parameter values "on the fly" and instantly apply those. These methods necessitate criteria for assessing the quality of signal coherence. As an option, the offline adaptation can be performed before the application phase begins.

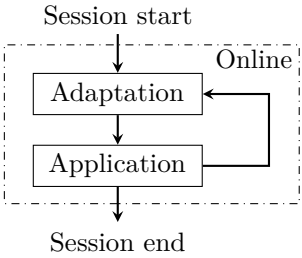

Figure 2.11: Course of events from session start to closed-loop online adaptation to online application to session end

2.5.3 Gamification

Maintaining the motivation of the user as high as possible for a long period of time plays a key role when it comes to improving the biosignal control ability. In the fourth step, developers need to come up with methods to encourage the users so that they are willing to practice and to improve the biosignal control ability in order to master the HMI control. To this end, the gamification of HMIs is an useful technique.

The umbrella term "gamification" refers to the general idea of utilizing elements and mechanisms that are typical in video, card and board games in a non-game contexts [40]. Those game elements and mechanics in non-game contexts serve the purpose of engaging the users and enabling the users to solve problems [237]. Gamification does not mean the user plays a fully-fledged game. Rather, gamification merely modifies single aspects of an application that can be virtual (computer application) or physical (tangible device). These modifications affect the application that probably is considered dull or tedious in a positive manner so the user obtains pleasure dealing with it. Such applications are referred to as gamified applications [41].

The concept of gamification can be applied in various non-game fields such as education or physical exercising. One of the main intentions of applying gamification in non-game fields is to improve user engagement, performance and experience [41].

Figure 2.12 visualizes the principle of gamification. Gamification enhances the *application* with *motivational affordances*, meaning game elements and mechanisms. The gamified applications invoke psychological experiences for the user similar to those found in games. As a consequence, the motivational affordances cause certain *psychological outcomes* which, in turn, effect distinct *behavioral outcomes* [75]. These outcomes are what the HMI developers strive for.

In the context of HMI development, the idea of designing interfaces that are more delightful to use dates back some centuries [120]. Various HMIs associated with diverse gamification were developed – like playing Tetris – by means of hand gestures [163].

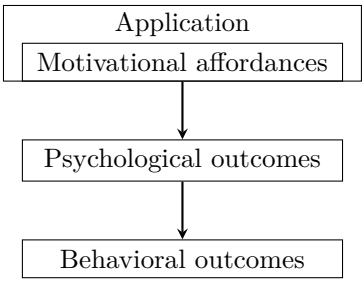

Figure 2.12: Principle of gamification (modified from [75])

In [75] various empirical studies on gamification were reviewed. The majority of these studies reported positive effects due to the gamification implementation. On the other hand, it was assumed that the positive implications are caused by a novelty effect that most likely does not work long-term [52, 74]. Moreover, it was assumed that removing gamification implementation after adding it in the first place affects the results negatively [206].

When gamifying applications developers need to consider two major aspects, namely

- how to motivate the users to keep practicing HMI control for the long term (i.e., how to gamify the HMI), and
- which skills are most appropriate to be practiced by the gamified HMI for accurate control.

2.5.4 Training

It is also feasible to improve the biosignal control ability through training in the traditional understanding (repetitions over time). The training ideally

- is geared to the needs of the specific HMI,
- is structured in a way that is unambiguous and lucid to the user,

- provides the user with a sufficient amount of time for practicing,
- provides the supervising persons with means to quantify the user's skill,
- is customizable to some extend meeting the needs of the user, and
- is entertaining as well as enjoyable for the user (through gamification, cf. Section 2.5.3).

The improvement of the control ability is measurable. The average control ability $\bar{c}_d^{u,e,t}$ over all users (index $u = 1, ..., \tilde{U}$), over all environments (index $e = 1, ..., \tilde{E}$) and over all trials (index $t = 1, ..., \tilde{T}$) per day is defined as

$$\bar{c}_d^{u,e,t} = \frac{1}{\tilde{U}} \cdot \sum_{u=1}^{\tilde{U}} \left(\frac{1}{\tilde{E}} \cdot \sum_{e=1}^{\tilde{E}} \left(\frac{1}{\tilde{T}} \cdot \sum_{t=1}^{\tilde{T}} c_{d,u,e,t} \right) \right), \tag{2.22}$$

where $c_{d,u,e,t}$ denotes the result of User u within the Environment e at the Trial t on Day d.

2.6 Biosignal Interpretation

Developers of HMIs need to take the biosignal interpretation into consideration. Generally, the *control signal generator* works as an interpreter converting (human-generated) biosignals that are unintelligible for the executing device into signals that are. In other words, it receives one or several *preprocessed biosignals* and outputs one or several *control signals*, as shown in Figure 2.13. The generation of the control signals is based on the algorithmic interpretation of the preprocessed biosignals.

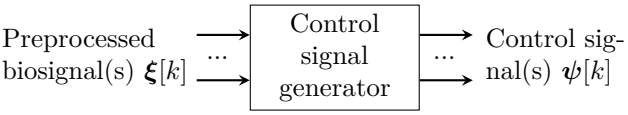

Figure 2.13: Control signal generator converting preprocessed biosignals into control signals

The main objective of the control signal generator is meeting the specifications of the human-generated signal as well as meeting the specifications of the expected input signals of the executing device and converting these. To accomplish that, there are numerous algorithmic conversions between input signals and output signals feasible.

In general, the control signal generator can be seen as a function mapping one or multiple input signals $\boldsymbol{\xi}[k]$ onto one or multiple output signals $\boldsymbol{\psi}[k]$ according to

$$\boldsymbol{\xi}[k] \rightarrow \boldsymbol{\psi}[k]. \tag{2.23}$$

The control signals necessarily meet the specifications of the expected input signals of the executing device. Each executing device requires distinct control signals.

Providing an example, navigation applications – like steering an electric-powered wheelchair – necessitate two control signals for both translation (propulsion) and rotation (steer angle). On the other hand, abstract game applications such as Tetris require control signals covering the left and right shift as well as the spin. Virtual and physical executing devices typically expect different control signals.

With respect to the biosignals, the individual abilities and shortcomings of the users vary. This is due to personal preferences and distinct personal skills. As for persons with disabilities, the residual bodily functions may vary, depending on the exact disability. Therefore, both the number and the characteristics of the available biosignals vary inter-individually.

2.7 Technical Implementation

Eventually, the developers need to realize the HMI. The technical implementation of a HMI includes both, the hardware and the software implementation.

As for the hardware implementation, a number of design decisions need to be made:

- Platform: The operating system MS Windows and Unix are mutually exclusive, whereas MS Windows is more widespread. Cross-platform developments combine platforms that are natively complementary but are typically more complex to develop. Another option is to develop for mobile platforms.
- Topology: The logical and physical topologies of the subsystem network are, for instance, ring, star, tree or line.
- Inter-subsystem communication: As for electrical inter-subsystem communication, the design options are, for example, tethered or wireless.
- Intelligent subsystems: The usage of microcontrollers as intelligent subsystems allows the developers to design a subsystem network that is decentralized from the signal processing point of view.
- Electronics development: Developers either make use of development kits by commercial electronics vendors or make their own electronics in-house.

Regarding the software implementation, further design decisions are required to be made:

- Programming paradigm: The software can follow diverse paradigms like procedural programming, object-oriented programming or symbolic programming.
- Programming language: Depending on the preferences of the developers, the software can be written in a lot of different programming languages, some of which are C, C++, Java, Matlab or LISP.
- Architectural patterns: The software architectural patterns for diverse main tasks of the software are, for instance, presentation-abstraction control, model-view controller or model-view presenter.

2.8 Contribution of the Interface Design Methodology

The interface design methodology covers Item 1 in the list of open problems as formulated in Section 1.6.

It addresses the lack of specific design methodologies that are dedicated to the development of HMIs. It provides a guidance for developers seeking to establish HMIs. As opposed to traditional design tools aiming mostly at general product engineering and in contrast to user interface design tools emphasizing psychological aspects, this novel interface design methodology concerns the development of HMIs that receive biosignals generated by human users and output control signals for the executing devices. It covers subjects that are specific to HMIs and relevant for the developers, such as target group and scope state analyses, data acquisition and signal assessments, biosignal control ability improvement and biosignal interpretation.

3 Adaptive Muscle Interface

3.1 Applying Interface Design Methodology for the Adaptive Muscle Interface

In this chapter a novel HMI based on the interpretation of two independent muscle signals (EMG signals) is proposed. As opposed to brain-computer interfaces (BCIs) dealing with EEG signals, EMG signals are more robust and provide higher information transfer rates [172]. The experimental platforms of this HMI are firstly, virtual environments visualized on computer displays and secondly, an electric-powered wheelchair. This HMI is first and foremost developed for people living with tetraplegia.

The muscle interface is about to be

- adaptive, in order to meet the characteristics of the individual user,
- easy-to-learn, allowing the user to accomplish a decent level of control accuracy within an acceptable period of time, and
- multipurpose, to be applicable for a variety of scenarios.

The development of this HMI follows the steps of the proposed design methodology (cf. Chapter 2).

Figure 3.1 illustrates the specific instantiation of the interface design methodology, as introduced in Figure 2.1, for the adaptive muscle interface. The key requirements include that the development should aim at persons living with tetraplegia, EMG signals from the ears should be the biosignal generator, the aesthetical impairment caused by the HMI should be minimal, distinct user and base station sites should coexist while the inter-subsystem communication should be wireless.

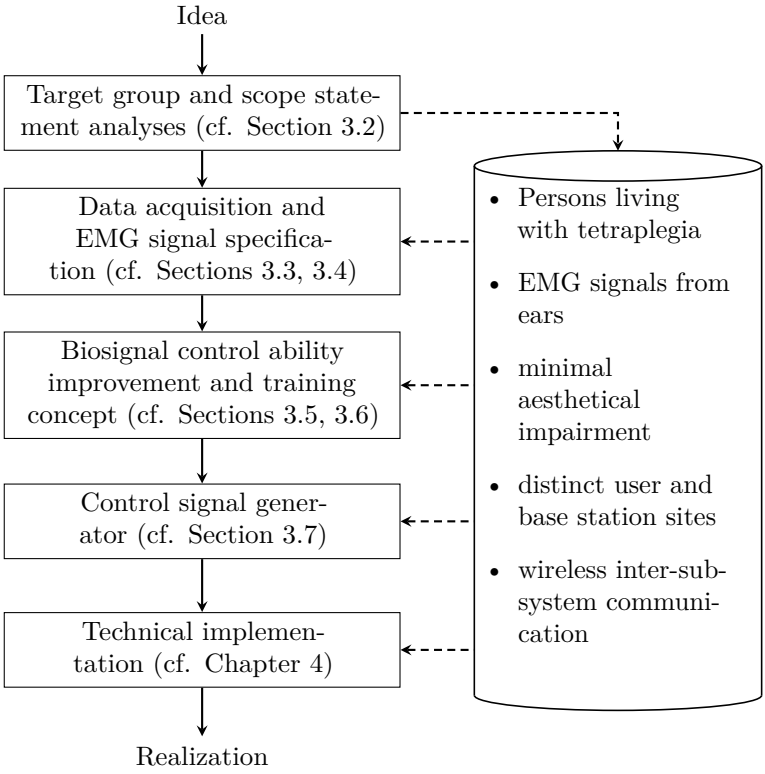

Figure 3.1: Development process of the adaptive muscle interface with representative characteristics as the set of requirements

3.2 Target Group and Scope Statement Analyses

The intended target group contains both persons with physical handicaps as well as able-bodied persons. Examples of persons with physical handicaps include those living with tetraplegia, persons suffering from paraplegia with difficulties moving upper extremities due to spasticities, persons with

limbs amputated. As for the able-bodied persons, “hand-free control” or “third-hand control” applications are of particular interest. However, the focus of development lies on persons with highly located SCIs and with tetraplegia, since it is assumed that able-bodied persons are capable of operating HMIs that were developed especially for and dedicated to persons of this target group.

Persons with tetraplegia have potential access to windows of communication based on facial muscles like eyebrows and lids, forehead, and tongue. Apart from these, head movements (induced by neck muscle activity), oral sounds, speech and brain activity signals can serve as windows of communication. In research studies, experimental system implementations of the aforementioned windows of communication were tested [82, 227]. A standardized patient care for persons with tetraplegia allowing for an active participation in social life by means of HMIs does not exist to date.

Figure 3.2 portrays the system partitioning and the signal flow of the proposed HMI. At the *user site* it includes two sensors, *EMG sensor 1* and *EMG sensor 2*, acquiring the human-generated biosignals as well as a microcontroller unit (MCU) termed *end-device (MCU-ED)*. The *base station site* contains the *access-point (MCU-AP)* and the *graphical user interface (GUI)*. These components constitute the *human-machine interface* by which the *human user* is enabled to operate *virtual executive devices* and *physical executive devices*.

The input signals are myoelectric signals (MESs) – that being signals originating from electromyography (EMG). In this work the extrinsic ear muscles as well as the forearm muscles are acquired. The technique of signal acquisition can be both invasive – by means of fine-wire EMG (fwEMG) – or non-invasive – with the aid of surface EMG (sEMG). The signals are digitized by the MCU-ED and digitally processed by a GUI. The GUI also provides means to set up the scope of information provision and visualization. Usually the supervisor is provided with the full range of information while the user is exposed to certain relevant information. To achieve a high level of signal coherence the GUI implements user individualization methods.

The aesthetic impairment of the HMI on the user should be as small as possible in order to avoid social stigmatization.

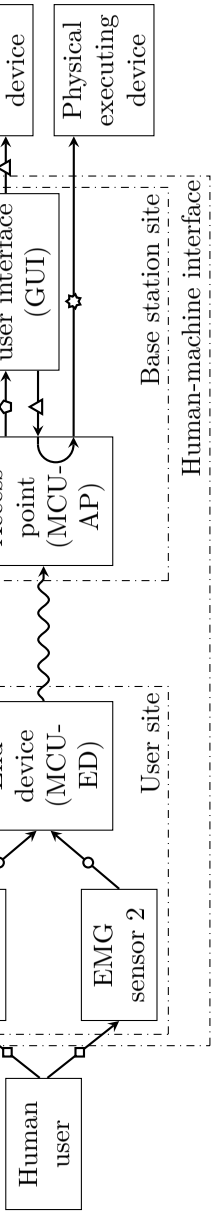

Figure 3.2: System partitioning and signal flow of the proposed HMI with human-generated muscle signals (⊣□⊢), analog representations of muscle signals (⊣○⊢), wireless digital representations of muscle signals (⊣∿⊢), digital representations of muscle signals (⊣○⊢), digital control signals (⊣△⊢) and analog control signals (⊣☼⊢)

The communication between the user site and the base station site is wireless. This provides the user with a high degree of flexibility. The design enables the user to operate the executing device telemetrically.

3.3 Data Acquisition

3.3.1 Levels of system integration

The proposed HMI is generally applicable with

- surface electrodes,
- fine-wire electrodes, and
- implants.

The use of surface electrodes is the safest way to acquire data since the health risk to the user is practically zero. The electrodes merely touch the skin without penetrating it. However, the quality of the biosignals potentially suffers from displacements of the electrodes or skin perspiration. In addition, surface electrodes acquire the sum of a lot of muscle fascicles covered by the area of the electrode and therefore provide only minor spatial resolution. The system integration making use of surface electrodes from the bilateral forearm muscles is approved in this work.

On the contrary, the use of fine-wire electrodes implies the minimally invasive penetration of the skin (subcutaneous) and thus poses a potential health risk to the user. There is a certain risk of local inflammation of the skin but it can be reduced to a minimum via hygiene standards. Advantageously, it yields high-quality biosignals without taking the risk of electrode displacements or skin perspiration. The fine-wire electrodes warrant a higher spatial resolution compared to the surface electrodes. In this work fine-wire electrodes are tested for the bilateral extrinsic ear muscles.

Implants need to be surgically inserted into the human body. For instance, during or after the surgical operation complications may appear. They pose the highest potential risk for the human user, but on the other

hand potentially yield the highest quality biosignals. This level of system integration is not tested in the scope of this work.

3.3.2 Forearm muscle signals

Figure 3.3 shows the acquisition of MESs from the forearm muscles. These muscles are rather large, so good quality biosignals are acquirable even through sEMG electrodes. In order to reduce signal artifacts caused by electrode displacements the sEMG electrodes are fastened by means of cuffs. The skin is wet locally at the position of the electrodes to warrant decent electric conductivity [209].

In case the upper extremities of the human user are in working order the sEMG electrodes can be placed at the extensor digitorum muscle together with the extensor carpi ulnaris muscle at the dorsal side.

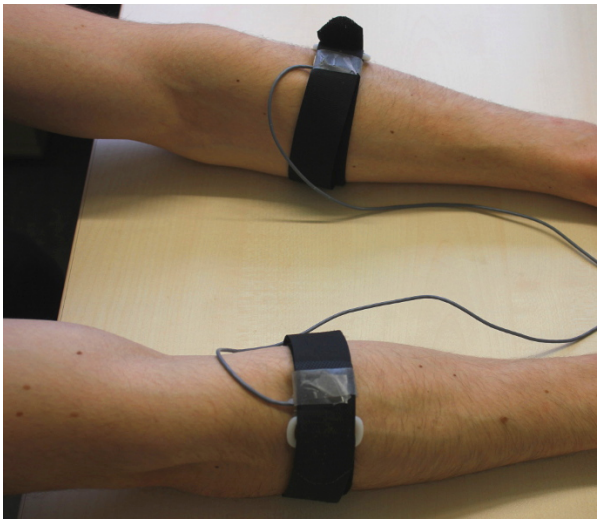

Figure 3.3: Surface EMG electrodes placed at the dorsal side of the user's forearms and fastened through cuffs [209]

If the user is incapable of activating one forearm – due to stroke, hemiplegia, spasticity or amputation – the two sEMG electrodes can be placed at the dorsal and ventral sides of the other forearm respectively. The flexor carpi radialis muscle and the pronator teres muscle at the ventral side as well as the extensor digitorum muscle and the extensor carpi ulnaris muscle at the dorsal side serve as muscle signal generators.

3.3.3 External ear muscle signals

The external ear muscles (cf. Section 1.2.4) are well suited to serve as sources for the EMG-based HMI since they are voluntarily controllable even in individuals with high-level tetraplegia. In addition, the minimal interference with other activities and the easy accessibility represent major advantages as compared to other HMIs dedicated to persons with tetraplegia [172].

As both the length and the cross-sectional area of the posterior auricular muscle are significantly smaller as compared to major muscles like forearm muscles, the muscle force is smaller and needs to be acquired with the aid of fwEMG electrodes. Moreover, the shortage of space behind the ear exacerbates the application of sEMG electrodes. Figure 3.4 shows the backside of the right ear with inserted fine-wires.

Each fwEMG electrode system consists of two fine-wire electrodes, one sEMG electrode and the housing containing the electronics such as the signal amplifier. The fine-wire electrodes are of 6 cm length and 50 µm diameter. In order to place the fine-wire electrodes beneath the skin (subcutaneously), a hollow needle, referred to as canula, carrying the fine-wire electrode pierces the skin as depicted in Figure 3.4a. The primary fine-wire electrode is positioned right at the posterior auricular muscle.

The secondary fine-wire electrode is positioned at the backside of the external ear (retroauricularly) as presented in Figure 3.4b. The non-invasive sEMG electrode is placed at the earlobe to determine the electrical ground as reference. The pigtails of the fine-wire electrodes are electrically connected to the fwEMG electrode system with small metal springs.

(a) Canula pierces the skin to position the primary fine-wire electrode

(b) Primary and secondary fire-wire electrodes

Figure 3.4: Positioning of fine-wire EMG electrodes behind the ear[1]

The muscle action potential is defined as the difference between the primary and the secondary fine-wire electrode. Both fwEMG electrode systems are attached to goggles on both sides.

The goggles are worn by the user during the application, as shown in Figure 3.5. The aesthetic impairment of the HMI on the user is reduced to a minimum. The EMG sensors and metrological apparatuses that pick up extrinsic ear muscle signals are covered by the ears. There is no obtrusive equipment needed in the face of the human user.

[1] Courtesy of D. Liebetanz, University Medical Center Göttingen

Figure 3.5: Right lateral fwEMG electrode system attached to goggles[2]

3.4 Biosignals of EMG Control

The total number of input modalities for the proposed HMI is limited to $\tilde{I} = 2$ as humans have two ears and two forearms. By definition, these input modalities are

$$i = \begin{cases} 1 & \text{, muscle activity of left flank} \\ 2 & \text{, muscle activity of right flank} \end{cases} . \tag{3.1}$$

At either flanks, the differential EMG signal (between primary and secondary fine-wire electrodes) get amplified (gain = 1.000), band-pass filtered

[2]Courtesy of D. Liebetanz, University Medical Center Göttingen

(4th order Butterworth filter, 20-1.000 Hz), digitized (sampling frequency 2.000 Hz) and digitally down-sampled to 125 Hz [172]. These preprocessed, digitized biosignals of both the left and the right muscle are $x_i[k]$ (cf. (2.2)) with the quantization resolution $n = 10$. The signals $x_i[k]$ are processed in real time by the consecutive operations rectification, filtering and normalization, depicted in Figure 3.6.

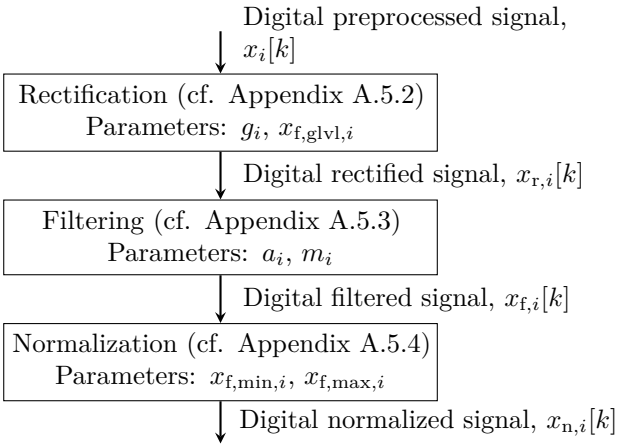

Figure 3.6: Work flow diagram of digital signal normalization showing the processing stages and the processed digital signals

Each processing stage is characterized by distinct parameters. The gain constant g_i and the ground level parameter $x_{\mathrm{f,glvl},i}$ specify the rectification. The trade-off parameter for IIR-filtering a_i as well as the window width parameter m_i describe the filtering. Eventually, both the minimum parameter $x_{\mathrm{f,min},i}$ and the maximum parameter $x_{\mathrm{f,max},i}$ characterize the normalization.

The filtered signal is defined as

$$x_{\mathrm{f},i}[k]=a_i\cdot x_{\mathrm{f},i}[k-1]+(1-a_i)\cdot\sqrt{\frac{1}{m_i+1}\cdot\sum_{l=0}^{m_i}\left(g_i\cdot\left|x_i[k-l]-x_{\mathrm{f,glvl},i}\right|\right)^2}, \quad (3.2)$$

and the normalized signal reads

$$x_{\mathrm{n},i}[k] = \begin{cases} 1 & , \text{if } x_{\mathrm{f},i}[k] \in (x_{\mathrm{f,max},i}, 2^n - 1] \\ \frac{x_{\mathrm{f},i}[k] - x_{\mathrm{f,min},i}}{\rho} & , \text{if } x_{\mathrm{f},i}[k] \in [x_{\mathrm{f,min},i}, x_{\mathrm{f,max},i}] \\ 0 & , \text{if } x_{\mathrm{f},i}[k] \in [0, x_{\mathrm{f,min},i}) \end{cases}, \tag{3.3}$$

where the control range ρ is defined as

$$\rho = x_{\mathrm{f,max},i} - x_{\mathrm{f,min},i}. \tag{3.4}$$

Treating g_i, a_i, m_i and $x_{\mathrm{f,glvl},i}$ as system-specific constants, the normalized signal depends on the preprocessed signal as well as the user-specific parameters $x_{\mathrm{f,max},i}$ and $x_{\mathrm{f,min},i}$ according to

$$x_{\mathrm{n},i}[k] = f(x_i[k], x_{\mathrm{f,max},i}, x_{\mathrm{f,min},i}). \tag{3.5}$$

The digital signal processing is described in detail in the Appendix A.5.

The proposed HMI is supposed to feature an isotonic (cf. Section 1.2.3), multi-level signal amplitude and promptness-critical control (cf. Section 2.4.3).

3.5 Biosignal Control Ability Improvement

3.5.1 Open-Loop unimodal calibration

The sensor calibration method is executed for each sensor – that is, left and right flank ($i \in \{1, 2\}$) – separately. This is required since the left and right flank muscles are not perfectly balanced by nature because of anatomical and neurological imperfections. The method compensates this natural imbalance. It finds user-individual parameters, essential for the digital signal normalization (cf. Appendix A.5), namely

- $x_{\mathrm{f,min},i}$ (minimum parameter), responsible for canceling out user-individual base levels of muscle tension,

- $x_{\mathrm{f,max},i}$ (maximum parameter), standing for the user-individual, maximum possible muscle tension, and
- $x_{\mathrm{f,glvl},i}$ (ground level parameter), representing the system-inherent base levels of the acquired signal.

The user generates low-level (index symbol ℓ) – that is, muscle relaxation – and high-level (index symbol $\hbar$) – that is, muscle contraction – activities successively producing the finite calibration signal $x_{\mathrm{f},i,p}[k]$ where $p \in \{1, ..., \tilde{P}\}$ is the index of low-level-high-level iterations and $\tilde{P}$ is the total number of these iterations. It is set to $\tilde{P} = 3$ to have a crisp procedure. The finite calibration signal $x_{\mathrm{f},i,p}[k]$ holds $\tilde{K}_p$ samples in total. $\tilde{K}_p$ is defined as a sum according to

$$\tilde{K}_p = \tilde{K}_{\ell,p} + \tilde{K}_{\hbar,p}, \tag{3.6}$$

it is the endmost discrete time index of $x_{\mathrm{f},i,p}[k]$. The endmost discrete time indices of the low-level and high-level activities are $\tilde{K}_{\ell,p}$ and $\tilde{K}_{\hbar,p}$, respectively.

Figure 3.7 shows an exemplary finite calibration signal that is idealized for the sake of clear depiction. For better understanding, the signals $x_{\mathrm{f},i,1}[k]$, $x_{\mathrm{f},i,2}[k]$ and $x_{\mathrm{f},i,3}[k]$ are illustrated with rising edges and in ascending order. This way, the top-end values $x_{\mathrm{f,top},i,p}$ are unambiguously depicted. The top-end values are essential for the determination of the sought-for maximum parameters $x_{\mathrm{f,max},i}$.

As for this simplified example, the medium-end values as well as the bottom-end values equal zero. That is, they are not explicitly depicted in Figure 3.7.

The user is urged by the supervisor to perform moderate high-level activities that are not at the physiological maximum. If the user performed high-level activities at the physiological maximum they will be required to generate such high-level signals in the application phase as well. Repeatedly high-level signals involve the risk of early exhaustion and fatigue – hence, it is not desired.

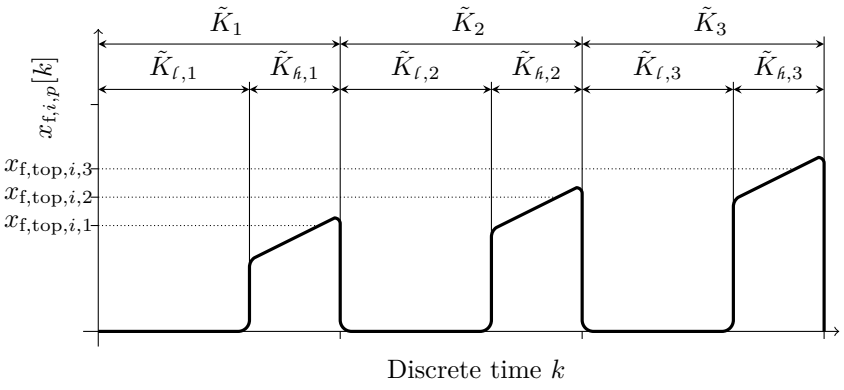

Figure 3.7: Sensor calibration with exemplary calibration signal $x_{\mathrm{f},i,p}[k]$ (——) and resulting top-end values $x_{\mathrm{f,top},i,p}$ (quantile 1-q)

Each of the finite calibration signals $x_{\mathrm{f},i,p}[k]$ (i.e., the values of the p-th time series) are ordered by decreasing numerical value according to

$$x^{\mathrm{ord}}_{\mathrm{f},i,p}[\zeta] = x_{\mathrm{f},i,p}[k_\zeta], \text{ with} \tag{3.7}$$

$$x_{\mathrm{f},i,p}[k_\zeta] \geq x_{\mathrm{f},i,p}[k_{\zeta+1}], \text{ and} \tag{3.8}$$

$$\{k_1, ..., k_{\tilde{Z}}\} = \{1, ..., \tilde{K}_p\}, \tag{3.9}$$

where $\zeta \in \{k_1, ..., k_{\tilde{Z}}\}$ represents the index of the ordered finite calibration signal. The index of the largest numerical value is k_1 while $k_{\tilde{Z}}$ is the index of the smallest numerical value.

The medium-end $x_{\mathrm{f,med},i,p}$ of the p-th finite calibration signal equals the median of the ordered, finite calibration signal $x^{\mathrm{ord}}_{\mathrm{f},i,p}[\zeta]$. As for the determination of the medium-end value with the aid of the median, it is essential to meet the condition

$$\tilde{K}_{\hbar,p} < \frac{1}{2}\tilde{K}_p. \tag{3.10}$$

The p-th bottom-end value $x_{\mathrm{f,bot},i,p}$ is defined as quantile q of the ordered, finite calibration signal. Likewise, the p-th top-end value $x_{\mathrm{f,top},i,p}$ is determined as quantile $1-q$. It is $q \in [0, 0.5)$. The median and the

quantiles are known as robust statistics, meaning they are not overly effected by outliers within the signals. When it comes to outliers, the robust statistics outperform the arithmetic mean and the sample minimum and sample maximum, respectively. The parameter values are set according to the definitions

$$x_{\mathrm{f,top},i,p} = x^{\mathrm{ord}}_{\mathrm{f},i,p}[k^*_{1-q}], \tag{3.11}$$

$$x_{\mathrm{f,med},i,p} = x^{\mathrm{ord}}_{\mathrm{f},i,p}[k^*_{0.5}], \text{ and} \tag{3.12}$$

$$x_{\mathrm{f,bot},i,p} = x^{\mathrm{ord}}_{\mathrm{f},i,p}[k^*_{q}], \tag{3.13}$$

where k^*_{1-q}, $k^*_{0.5}$ and k^*_q denote the indices of the ordered, finite calibration signal. They are defined as

$$k^*_{1-q} = \left\lfloor (\tilde{K}_p - 1) \cdot (1-q) \right\rceil, \tag{3.14}$$

$$k^*_{0.5} = \left\lfloor (\tilde{K}_p - 1) \cdot 0.5 \right\rceil, \text{ and} \tag{3.15}$$

$$k^*_{q} = \left\lfloor (\tilde{K}_p - 1) \cdot q \right\rceil. \tag{3.16}$$

The operators $\lfloor . \rceil$ stand for the numerical rounding off. The indices allow for the computation of the median and quantiles, notwithstanding the parity of the finite signal, whether $\tilde{K}_p$ is odd or even.

The parameter values are averaged with

$$x_{\mathrm{f,max},i} = \frac{1}{\tilde{P}} \cdot \sum_{p=1}^{\tilde{P}} x_{\mathrm{f,top},i,p}, \tag{3.17}$$

$$x_{\mathrm{f,glvl},i} = \frac{1}{\tilde{P}} \cdot \sum_{p=1}^{\tilde{P}} x_{\mathrm{f,med},i,p}, \text{ and} \tag{3.18}$$

$$x_{\mathrm{f,min},i} = \frac{1}{\tilde{P}} \cdot \sum_{p=1}^{\tilde{P}} x_{\mathrm{f,bot},i,p}. \tag{3.19}$$

3.5.2 Open-loop bimodal calibration with linearization

In case of bimodal biosignal control, beside the activity of the intended input modality there is oftentimes a certain activity level in the other

input modality that does not correspond to the intention of the user. This phenomenon of unintended interference between acquired signals is referred to as crosstalk (index symbol xT).

Providing an example, if persons attempt to activate only the left extrinsic ear muscle the right extrinsic ear muscle most likely also will be activated unintentionally. In particular, inexperienced users have difficulties activating facial muscles independently due to the presence of crosstalk.

The two-dimensional, linear regression stipulates the two outcome values. Given the user-individual amplitudes of the input modalities, the sought-for regression parameter values match the input values with the output values.

The following user-individual regression parameters that are crucial for the crosstalk compensation (i.e., improving differential control quality) are determined

- α_{xT1} (first crosstalk compensation parameter), representing the factor amplifying the first biosignal, and
- α_{xT2} (second crosstalk compensation parameter), standing for the second biosignal amplifier.

Differential control is based on the difference of activity signals of two input modalities such as

$$x_{\mathrm{n},\Delta 12}[k] = x_{\mathrm{n},1}[k] - x_{\mathrm{n},2}[k] \in [\omega_{\mathrm{l}}, \omega_{\mathrm{u}}], \tag{3.20}$$

where $x_{\mathrm{n},\Delta 12}[k]$ is the bimodal differential signal, ω_{l} and ω_{u} stand for the lower and upper bounds of the differential signal (i.e., denoting the range of the differential signal). Bimodal calibration is executed for both input modalities.

Ideally, both input modalities are independent and uncorrelated. In that case it is

$$\omega_{\mathrm{l}} = -1, \tag{3.21}$$

$$\omega_{\mathrm{u}} = 1. \tag{3.22}$$

Formally, given two input modalities, the unintended crosstalk in $i = 2$ when only the activity in $i = 1$ is intended is referred to as $x_{\mathrm{n},1xT2}$. On

the other hand, the unintended crosstalk in $i = 1$ when only the activity in $i = 2$ is intended is denoted as $x_{\mathrm{n},2\mathit{xT}1}$ in the remainder of this work. In other words, the intended input modality is the first-mentioned while the unintended input modality is the second-mentioned. The two scalar values, $x_{\mathrm{n},1\mathit{xT}2}$ and $x_{\mathrm{n},2\mathit{xT}1}$, are found by the bimodal calibration as intermediate results for the calculation of $\alpha_{\mathit{xT}1}$ and $\alpha_{\mathit{xT}2}$.

The more prominent the crosstalk is, the more aggravated the differential control becomes. If crosstalk is present, the quality of the differential signal typically deteriorates because the range of the differential signal is reduced and the lower and upper bounds are

$$-1 < \omega_{\mathrm{l}} < \omega_{\mathrm{u}} < 1. \tag{3.23}$$

The compensation for crosstalk aims at restoring the full range of the difference signal (i.e., $\omega_{\mathrm{l}} = -1$ and $\omega_{\mathrm{u}} = 1$). The crosstalk compensation for two input modalities is based on the two-dimensional, linear regression model defined as

$$\boldsymbol{\omega}_{\mathit{xT}} = \boldsymbol{X}_{\mathit{xT}}\, \boldsymbol{\alpha}_{\mathit{xT}}. \tag{3.24}$$

The desired outcome vector $\boldsymbol{\omega}_{\mathit{xT}}$ holds the target output values ω_{l} and ω_{u} and is defined as

$$\boldsymbol{\omega}_{\mathit{xT}} = \begin{pmatrix} \omega_{\mathrm{l}} \\ \omega_{\mathrm{u}} \end{pmatrix} = \begin{pmatrix} -1 \\ 1 \end{pmatrix}, \tag{3.25}$$

the transformation matrix $\boldsymbol{X}_{\mathit{xT}}$ contains the measured crosstalk activities for both input modalities and is written as

$$\boldsymbol{X}_{\mathit{xT}} = \begin{pmatrix} 1 & x_{\mathrm{n},1\mathit{xT}2} \\ x_{\mathrm{n},2\mathit{xT}1} & 1 \end{pmatrix}. \tag{3.26}$$

The coefficient vector $\boldsymbol{\alpha}_{\mathit{xT}}$ holds the unknown coefficients that are to be determined

$$\boldsymbol{\alpha}_{\mathit{xT}} = \begin{pmatrix} \alpha_{\mathit{xT}1} \\ \alpha_{\mathit{xT}2} \end{pmatrix}. \tag{3.27}$$

As opposed to the sensor calibration, the bimodal calibration considers the interference between both input modalities. First, the user is prompted to generate high-level activity in $i = 1$ while generating low-level activity in $i = 2$. Second, the user is asked to generate high-level activity in $i = 2$

and generating low-level activity in $i = 1$ at the same time. The user guidance of the bimodal calibration is identical with the user guidance of the open-loop sensor calibration (cf. Section 3.5.1), that is, $\tilde{P} = 3$, yielding the finite calibration signal $x_{\mathrm{n},i,p}[k]$. Figure 3.8 illustrates the simplified and idealized calibration signals of the bimodal calibration.

Analogous to the sensor calibration, the finite calibration signal $x_{\mathrm{n},i,p}[k]$ gets ordered by decreasing numerical value (cf. (3.7), (3.8) and (3.9)). This leads to the ordered, finite calibration signal $x^{\mathrm{ord}}_{\mathrm{n},i,p}[\zeta]$.

The unintended crosstalks of the p-th iteration are

$$x_{\mathrm{n},1\text{x}T2,p} = x^{\mathrm{ord}}_{\mathrm{n},2,p}[k^*_{1-q}], \text{ and} \tag{3.28}$$

$$x_{\mathrm{n},2\text{x}T1,p} = x^{\mathrm{ord}}_{\mathrm{n},1,p}[k^*_{1-q}]. \tag{3.29}$$

Averaging over $\tilde{P}$ yields

$$x_{\mathrm{n},1\text{x}T2} = \frac{1}{\tilde{P}} \cdot \sum_{p=1}^{\tilde{P}} x_{\mathrm{n},1\text{x}T2,p}, \text{ and} \tag{3.30}$$

$$x_{\mathrm{n},2\text{x}T1} = \frac{1}{\tilde{P}} \cdot \sum_{p=1}^{\tilde{P}} x_{\mathrm{n},2\text{x}T1,p}. \tag{3.31}$$

Solving (3.24), the model coefficients are calculated following the formulas

$$\alpha_{\text{x}T1} = -\frac{1 + x_{\mathrm{n},1\text{x}T2}}{1 - x_{\mathrm{n},1\text{x}T2} \cdot x_{\mathrm{n},2\text{x}T1}}, \text{and} \tag{3.32}$$

$$\alpha_{\text{x}T2} = \frac{1 + x_{\mathrm{n},2\text{x}T1}}{1 - x_{\mathrm{n},1\text{x}T2} \cdot x_{\mathrm{n},2\text{x}T1}}. \tag{3.33}$$

The detailed procedure of solution is presented in the Appendix A.6. In the application phase, crosstalk compensation for a bimodal differential signal (cf. (3.20)) is accomplished by applying the equation for crosstalk compensation according to

$$x^{\mathrm{comp}}_{\mathrm{n},\Delta 12}[k] = \alpha_{\text{x}T1} \cdot x_{\mathrm{n},1}[k] + \alpha_{\text{x}T2} \cdot x_{\mathrm{n},2}[k] \in [-1, 1]. \tag{3.34}$$

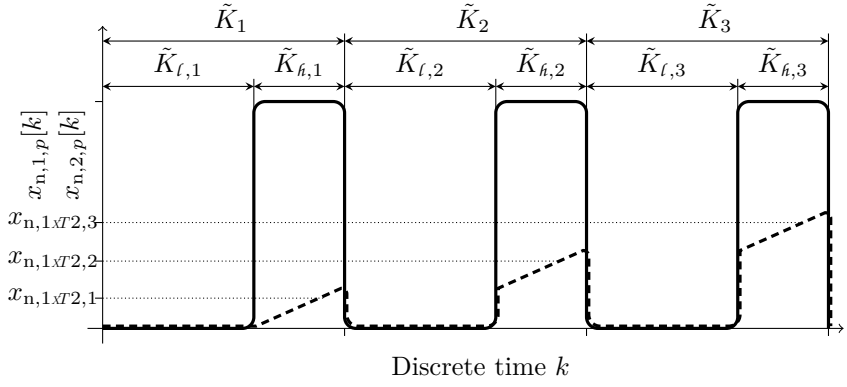

Figure 3.8: Bimodal calibration with exemplary calibration signals $x_{\mathrm{n},1,p}[k]$ (intended, ——) and $x_{\mathrm{n},2,p}[k]$ (unintended, - - -) and resulting parameters $x_{\mathrm{n},1\mathit{x}T2,p}$ (unintended crosstalk in $i = 2$)

The model coefficients $\alpha_{\mathit{x}T1}$ and $\alpha_{\mathit{x}T2}$ are to be determined in the calibration phase. The signal is equal to -1 if the user intentionally activates $i = 1$ and unintentionally activates $i = 2$ to the extent of $x_{\mathrm{n},1\mathit{x}T2}$. Vice versa, it is equal to $+1$ if the user intentionally activates $i = 2$ and unintentionally activates muscle $i = 1$ to the extent of $x_{\mathrm{n},2\mathit{x}T1}$.

The compensated difference signal is coherent and matches the intention of the user by design. It gradually ranges from its lower limit -1 to its upper limit +1, so it is suitable for representing bends of different degrees for electric-powered wheelchairs.

On the other hand, if the crosstalk drifts over time, the compensated difference signal may exceed the limits -1 and +1, respectively. Therefore, the crosstalk compensation needs to be performed repeatedly. Moreover, the compensated difference signal basically results from the linear regression (cf. (3.24)). Hence, it is incapable of embodying non-linear characteristics some user might reveal in bimodal biosignal control. The high dimensional approach of the bimodal calibration is presented in [43].

3.5.3 Open-loop bimodal calibration without linearization

Difference models result in signals that are based on two normalized input signals. The objective is to compensate for the user-individual crosstalk for as many scenarios as possible. Those scenarios generally include all types of different combinations of the two normalized input signals and different degrees of crosstalk.

While pursuing the mentioned objective, the difference signal should feature the desired characteristics smoothness, flatness at value zero, coverage of the full range of values and boundary by values -1 and +1. Various models without linear regression were developed presented in this section.

For the better legibility the following short forms are introduced

$$x_{\mathrm{n},1}[k] \text{ short “}n_1\text{”, and} \tag{3.35}$$

$$x_{\mathrm{n},2}[k] \text{ short “}n_2\text{”.} \tag{3.36}$$

The main idea of model V1 is to have a model that is simple, user-individual and feature the desired characteristics at the same time. The difference signal is defined as

$$x^{\mathrm{V1}}_{\mathrm{n},\Delta 12}[k] = 2 \cdot \frac{x_{\mathrm{n},\Delta 12}[k] - x^{[101,\ldots,200]}_{\mathrm{min},\Delta 12}}{x^{[1,\ldots,100]}_{\mathrm{max},\Delta 12} - x^{[101,\ldots,200]}_{\mathrm{min},\Delta 12}} - 1, \tag{3.37}$$

where the signal $x_{\mathrm{n},\Delta 12}[k]$ was defined earlier (cf. (3.20)). The user-individual, scalar parameters $x^{[101,\ldots,200]}_{\mathrm{min},\Delta 12}$ resp. $x^{[1,\ldots,100]}_{\mathrm{max},\Delta 12}$ are the minimum resp. maximum values of the difference between the signals $x_{\mathrm{n},1}$ and $x_{\mathrm{n},2}$ in specific time sections $k = 101, ..., 200$ resp. $k = 1, ..., 100$. Consequently, they follow the definitions

$$x^{[101,\ldots,200]}_{\mathrm{min},\Delta 12} = \min\left\{x_{\mathrm{n},1}[101, ..., 200] - x_{\mathrm{n},2}[101, ..., 200]\right\}, \text{ and} \tag{3.38}$$

$$x^{[1,\ldots,100]}_{\mathrm{max},\Delta 12} = \max\left\{x_{\mathrm{n},1}[1, ..., 100] - x_{\mathrm{n},2}[1, ..., 100]\right\}. \tag{3.39}$$

Model V2 makes use of three cases in order to handle the different scenarios. The usage of cases depends on the signal value of $x_{\mathrm{n},\Delta 12}[k]$. A threshold value of 10 % was fixed as an indicator for a slight difference between the

two normalized input signals. Its difference signal follows the definition given by

$$x_{\mathrm{n},\Delta 12}^{\mathrm{V2}}[k] = \begin{cases} \frac{1}{x_{\mathrm{max},\Delta 12}^{[1,\ldots,100]}} \cdot x_{\mathrm{n},\Delta 12}[k] & ,\text{if } x_{\mathrm{n},\Delta 12}[k] > 0.1 \\ -\frac{1}{x_{\mathrm{min},\Delta 12}^{[101,\ldots,200]}} \cdot x_{\mathrm{n},\Delta 12}[k] & ,\text{if } x_{\mathrm{n},\Delta 12}[k] < -0.1 \\ x_{\mathrm{n},\Delta 12}[k] & ,\text{else} \end{cases} . \tag{3.40}$$

As a version, in model V2A the usage of cases depends on the value of the larger of the two signals. The corresponding signal is defined as

$$x_{\mathrm{n},\Delta 12}^{\mathrm{V2A}}[k] = \begin{cases} \frac{1}{x_{\mathrm{max},\Delta 12}^{[1,\ldots,100]}} \cdot x_{\mathrm{n},\Delta 12}[k] & ,\text{if } \max\{n_1, n_2\} > 0.1 \\ -\frac{1}{x_{\mathrm{min},\Delta 12}^{[101,\ldots,200]}} \cdot x_{\mathrm{n},\Delta 12}[k] & ,\text{if } \max\{n_1, n_2\} < -0.1 \\ x_{\mathrm{n},\Delta 12}[k] & ,\text{else} \end{cases} . \tag{3.41}$$

Difference model V3 defines two cases. The use of cases depends on $x_{\mathrm{n},\Delta 12}^{\mathrm{V1}}[k]$. The difference signal is

$$x_{\mathrm{n},\Delta 12}^{\mathrm{V3}}[k] = \begin{cases} \sqrt{x_{\mathrm{n},\Delta 12}^{\mathrm{V1}}[k] \cdot \max\{n_1, n_2\}} & ,\text{if } x_{\mathrm{n},\Delta 12}^{\mathrm{V1}}[k] \geq 0 \\ -\sqrt{\left|x_{\mathrm{n},\Delta 12}^{\mathrm{V1}}[k]\right| \cdot \max\{n_1, n_2\}} & ,\text{if } x_{\mathrm{n},\Delta 12}^{\mathrm{V1}}[k] < 0 \end{cases} . \tag{3.42}$$

Model V3B is consistent with model V3 but with a superordinated case. The definition of the difference signal reads

$$x_{\mathrm{n},\Delta 12}^{\mathrm{V3B}}[k] = \begin{cases} x_{\mathrm{n},\Delta 12}^{\mathrm{V3}}[k] & ,\text{if } n_1 + n_2 \geq 0 \\ 0 & ,\text{else} \end{cases} . \tag{3.43}$$

The difference model V4 defines seven cases seeking to cover the scenarios as well as possible. The difference signal is

$$x^{\mathrm{V4}}_{\mathrm{n},\Delta 12}[k] = \begin{cases} x^{\mathrm{V2}}_{\mathrm{n},\Delta 12}[k] & , \text{if } n_1 > n_2 \wedge x^{[101,\ldots,200]}_{\mathrm{min},\Delta 12} < -\upsilon \\ \Upsilon_1 \cdot x^{\mathrm{V3}}_{\mathrm{n},\Delta 12}[k] & , \text{if } n_1 > n_2 \wedge x^{[101,\ldots,200]}_{\mathrm{max},\Delta 12} > \upsilon \wedge n_2 > \Upsilon_2 \\ x^{\mathrm{V2}}_{\mathrm{n},\Delta 12}[k] & , \text{if } n_1 > n_2 \wedge x^{[101,\ldots,200]}_{\mathrm{max},\Delta 12} > \upsilon \wedge n_2 \leq \Upsilon_2 \\ x^{\mathrm{V3}}_{\mathrm{n},\Delta 12}[k] & , \text{if } n_1 < n_2 \wedge x^{[1,\ldots,100]}_{\mathrm{max},\Delta 12} > \upsilon \\ \Upsilon_3 \cdot x^{\mathrm{V3}}_{\mathrm{n},\Delta 12}[k] & , \text{if } n_1 < n_2 \wedge x^{[1,\ldots,100]}_{\mathrm{min},\Delta 12} < -\upsilon \wedge n_1 > \Upsilon_4 \\ x^{\mathrm{V3}}_{\mathrm{n},\Delta 12}[k] & , \text{if } n_1 < n_2 \wedge x^{[1,\ldots,100]}_{\mathrm{min},\Delta 12} < -\upsilon \wedge n_1 \leq \Upsilon_4 \\ x^{\mathrm{V3}}_{\mathrm{n},\Delta 12}[k] & , \text{else} \end{cases}, \tag{3.44}$$

where the threshold υ is a predefined parameter and the terms of Υ read

$$\Upsilon_1 = 1 + x^{[101,\ldots,200]}_{\mathrm{max},\Delta 12}, \tag{3.45}$$

$$\Upsilon_2 = 1 - x^{[1,\ldots,100]}_{\mathrm{max},\Delta 12}, \tag{3.46}$$

$$\Upsilon_3 = 1 - x^{[1,\ldots,100]}_{\mathrm{min},\Delta 12} \text{ and} \tag{3.47}$$

$$\Upsilon_4 = 1 + x^{[101,\ldots,200]}_{\mathrm{min},\Delta 12}. \tag{3.48}$$

3.5.4 Closed-loop offline parameter adaptation

The open-loop methods presented in Sections 3.5.1, 3.5.2, 3.5.3 can be executed repeatedly whenever the application is paused. However, there is no feedback information from the application. Therefore, the only way of coping with drifts (i.e., non-stationarities) in the signal is to repeat the parameter adaptation. Closed-loop adaptation methods make use of feedback information and aim at obviating the need for repeated parameter adaptation steps. Instead these methods want to re-adapt "on-the-fly".

In [210], the idea of the closed-loop offline adaptation was proposed and refined in [211], as illustrated in Figure 3.9. The *EMG signals* of the human user are acquired and transmitted to the *HMI*. In turn, it computes *control signals* and sends those to the *task* where *features* are extracted standing for the degree of fulfillment of the task. The extracted features

are forwarded to the adaptation of the HMI (*Adapt. HMI*) that adjusts the behavior of the HMI represented by the parameter vector defined as

$$\mathbf{p}_{\mathrm{HMI}}^{T} = (a_i, m_i, x_{\mathrm{f,min},i}, x_{\mathrm{f,max},i}), \tag{3.49}$$

where the contained parameters are defined previously (cf. Section 3.4). In [210], $x_{\mathrm{f,glvl},i}$ was not changed by the closed-loop parameter adaptation.

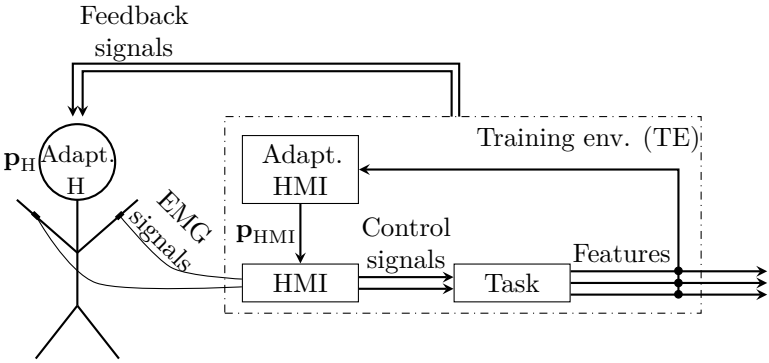

Figure 3.9: Co-adaptive training environment for closed-loop offline adaptation (modified from [211])

In addition, the features could be forwarded to the adaptation of the *training environment (TE)*. The training environment, represented by the parameter vector $\mathbf{p}_{\mathrm{TE}}$, contains meta-descriptions like task settings and difficulty level.

The training environment generates multimodal *feedback signals* and sends those to the human user who makes up a mental model of both the HMI and the training environment represented by $\mathbf{p}_{\mathrm{H}}$. The human user, as an adaptive system by default, constantly (subconsciously or consciously) changes the mental model (*Adapt. H*) in one's mind.

Parameters get adapted offline in a closed-loop scheme based on multiple features by a single-objective optimization. Features such as the completion time and the path error are extracted from the task – for instance, an

obstacle course with a predefined ideal trajectory – and a scalar-valued evaluation score is computed. The single-objective optimization problem is formulated as

$$\mathbf{p}_{\text{opt}} = \underset{\mathbf{p}_{\text{HMI}},\mathbf{p}_{\text{TE}}}{\arg\max}\, Q(\mathbf{p}_{\text{HMI}}, \mathbf{p}_{\text{TE}}, \mathbf{p}_{\text{H}}), \tag{3.50}$$

where Q is the scalar-valued user performance estimate (evaluation number) for the current trial.

The optimization problem (cf. (3.50)) cannot be solved directly but candidate values for optimal parameters can be found by varying parameter values between trials. Hence, Q is to be maximized by altering the parameter values. The user performs the subsequent trial applying the newly determined parameter values $\mathbf{p}_{\text{opt}}$. Only parameter sets $\mathbf{p}_{\text{HMI}}$ and $\mathbf{p}_{\text{TE}}$ can be varied while $\mathbf{p}_{\text{H}}$ cannot be affected. The scalar-valued user performance estimate for each trial is calculated according to

$$Q(\mathbf{p}_{\text{HMI}}, \mathbf{p}_{\text{TE}}, \mathbf{p}_{\text{H}}) = \mathbf{w}^T\mathbf{g}, \tag{3.51}$$

where $\mathbf{w}$ denotes the algorithm control vector containing the weights associated with the extracted features $\mathbf{g}$ according to

$$\mathbf{w}^T = (w_{T_{\text{invar}}}, w_{\Delta_{\text{invar}}}), \text{ and} \tag{3.52}$$

$$\mathbf{g}^T = (T_{\text{invar}}, \Delta_{\text{invar}}), \tag{3.53}$$

where $T_{\text{invar}} \in [0, 1]$ is the normalized completion time and $\Delta_{\text{invar}} \in [0, 1]$ is the normalized path error. For the sake of simplicity, the number of extracted features was reduced in [211] as compared to [210].

In order to assess the fulfillment of a navigation task, the completion time and the path error are well-suited features. They reflect the ability of the user to navigate in a fast and accurate manner.

The calculus in (3.51) enables to quantify the user performance when operating an EMG-based HMI. It allows for adaptation of certain parameters depending on the current user performance in a given task.

Extreme values in g_i should have only a little effect on $g_{i,\text{invar}}$. Therefore, the limits are desired to be

$$\lim_{g_i \to +\infty} \nu_i(g_i) = 0 \text{ , and} \tag{3.54}$$

$$\lim_{g_i \to -\infty} \nu_i(g_i) = 1. \tag{3.55}$$

The feature normalization is accomplished by means of the arc tangent functions defined as

$$\nu_T(T) = T_{\text{invar}} = \frac{\frac{\pi}{2} - \arctan(\gamma_T \cdot (T - T_{\text{emp}}) \cdot T_{\text{emp}}^{-1})}{\pi} \text{ , and} \tag{3.56}$$

$$\nu_\Delta(\Delta) = \Delta_{\text{invar}} = \frac{\frac{\pi}{2} - \arctan(\gamma_\Delta \cdot (\Delta - \Delta_{\text{emp}}) \cdot \Delta_{\text{emp}}^{-1})}{\pi} \text{ ,} \tag{3.57}$$

where T and Δ denote the unnormalized features together with T_{emp} and Δ_{emp} representing empirical values for either features. The scaling parameters γ_T and γ_Δ can be set individually as required. The functions are depicted in Figure 3.10.

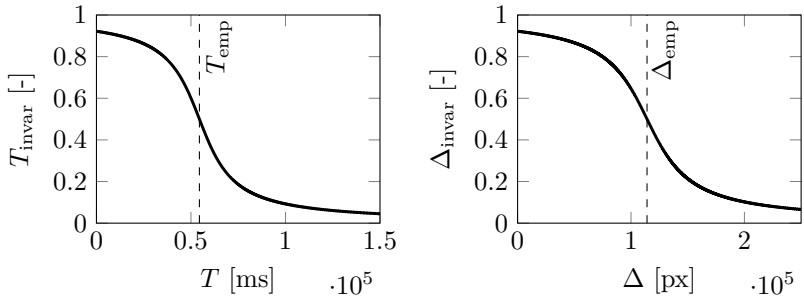

(a) $\nu_T(T)$ with T_{emp} and $\gamma_T = 4$ **(b)** $\nu_\Delta(\Delta)$ with Δ_{emp} and $\gamma_\Delta = 4$

Figure 3.10: Feature normalization functions (—) with corresponding empirical values (- - -) (modified from [211])

As an approach to solve the optimization problem (cf. (3.50)) the heuristic algorithm depicted in Figure 3.11 was developed. It determines candidate

values for optimal parameters in iterations of simulated trials (index $s \in \{1, ..., \tilde{S}\}$) where the parameter values $\mathbf{p}_{\mathrm{HMI},r,s}$ are algorithmically varied with $\tilde{S}$ being the maximum number of simulations. In other words, the algorithm looks for parameter values that would have yielded better user performance Q if applied to the same EMG signals.

The user performs a run (index r), that is, an actual trial, a non-simulated trial, applying the parameters $\mathbf{p}_{\mathrm{HMI},r}$. The resulting user performance $Q_r(\mathbf{p}_{\mathrm{HMI},r})$ is computed. Then another trial based on the exact EMG signals of the run that was recorded applying the parameter values $\mathbf{p}_{\mathrm{HMI},r,s}$ is simulated by an offline algorithm. The resulting user performance $Q_{r,s}(\mathbf{p}_{\mathrm{HMI},r,s})$ of the simulated trial is calculated. Unless neither the first termination criterion, that is, maximal number of iterations was reached ($s \geq \tilde{S}$) nor the second termination criterion, that is, user performance improved to a certain extent ($\Delta Q = Q_{r,s} - Q_r \geq \Delta Q^*$) is met the next iteration of simulated trials applying new algorithmically varied parameters $\mathbf{p}_{\mathrm{HMI},r,s+1}$ is executed.

The algorithmic parameter variation determines parameter values in accordance with

$$\mathrm{p}_{i,r,s+1} = \mathrm{p}_{i,r,s} \cdot (1 + d \cdot \rho \cdot \theta), \tag{3.58}$$

where $d \in \{-1, 1\}$ denotes the direction of optimization, $\rho \in (0, 1)$ represents the normalized randomness factor and $\theta \in (0, 1)$ stands for the maximal, relative increment. The parameter value of the subsequent simulation $\mathrm{p}_{i,r,s+1}$ conforms with the previous parameter value $\mathrm{p}_{i,r,s}$ except for the modification given by the product of d, ρ and θ.

After termination of the algorithm the offline parameter optimization with respect to the previous run is completed. In case the user performance improved in simulation as compared to the user performance of the run, meaning $Q_{r,s} > Q_r$, the corresponding parameter values get applied in the subsequent run (i.e., $\mathbf{p}_{\mathrm{HMI},r+1} = \mathbf{p}_{\mathrm{HMI},r,s}$).

In this way, $\mathbf{w}_1^T = (1, 0)$ finds parameter values ensuring minimal completion time and $\mathbf{w}_2^T = (0, 1)$ determines parameter values warranting minimal path error (cf. (3.52)).

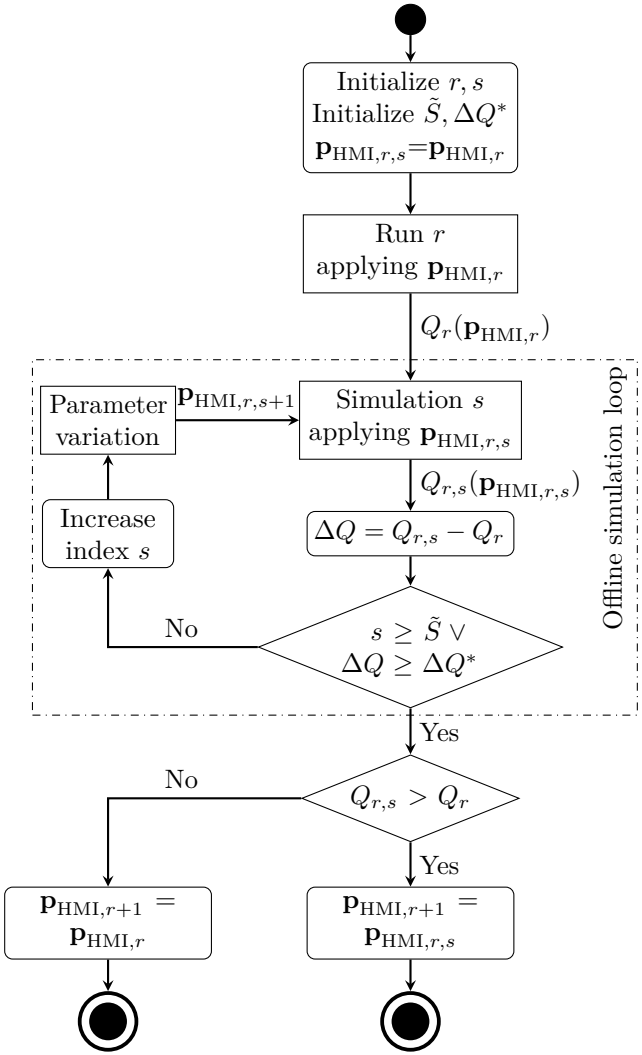

Figure 3.11: Heuristic algorithm to solve the single-objective optimization problem (modified from [211])

3.5.5 Closed-loop online parameter adaptation

Offline calibration determines tailor-made parameter values for each user. However, the optimal values may vary over time due to physical or mental fatigue on the one hand as well as improving personal skills (human learning) on the other. To cope with those non-stationarities in the biosignals, a strategy is needed that dynamically matches the parameter values with the current physical and mental states of the user. The parameter values need to be adapted dynamically.

Pseudo-stationarity of parameters can be assumed to be true only if the time span between parameter determination and parameter application is short, and in cases where the application phase does not last too long.

In [209] an online parameter adaptation scheme was proposed. In general, the actual value $y_{\mathrm{act}}[k]$ depends on the bimodal differential signal according to

$$y_{\mathrm{act}}[k] = x_{\mathrm{n},1}[k] - x_{\mathrm{n},2}[k] \in [0, 1]. \tag{3.59}$$

As for the specific case of providing 100 discrete and equidistant positions, the actual value reads

$$y^*_{\mathrm{act}}[k] = 50 - (x_{\mathrm{n},1}[k] - x_{\mathrm{n},2}[k]) \cdot 50 \in [1, 100]. \tag{3.60}$$

The difference between the actual and the desired value $y_{\mathrm{des}}[k] \in [0, 1]$ makes up the general form of the user performance $Q[k]$ in accordance with

$$Q[k] = 1 - |y_{\mathrm{des}}[k] - y_{\mathrm{act}}[k]| \in (0, 1]. \tag{3.61}$$

Regarding the aforementioned case together with the specific, desired value $y^*_{\mathrm{des}}[k] \in [1, 100]$ the user performance reads

$$Q^*[k] = 1 - \frac{|y^*_{\mathrm{des}}[k] - y^*_{\mathrm{act}}[k]|}{100} \in (0, 1], \tag{3.62}$$

where the absolute value of the difference needs to get normalized with the division by 100, that is, the maximum range between actual and desired value.

Values of $Q[k]$ resp. $Q^*[k]$ close to one represent decent user performance while values close to zero relate to poor user performance. Therefore, $Q[k]$ resp. $Q^*[k]$ is to be maximized by parameter adaptation of the HMI. Based on $Q[k]$ resp. $Q^*[k]$, the parameter adaptation is performed incrementally (i.e., every instant of time k).

In the remainder of this section the general forms $y_{\text{act}}[k]$, $y_{\text{des}}[k]$ and $Q[k]$ are used as synonyms for the specific forms $y^*_{\text{act}}[k]$, $y^*_{\text{des}}[k]$ and $Q^*[k]$.

The parameter that is to be adapted in order to maximize $Q[k]$ is $x_{\text{f,max},i}[k]$. This parameter directly affects the digital signal normalization (cf. Appendix A.5). The incremental adaptation follows

$$x_{\text{f,max},i}[k] = x_{\text{f,max},i}[k-1] \cdot (1 + \chi[k] \cdot w \cdot (1 - \frac{1}{Q[k]})^2), \tag{3.63}$$

where $\chi[k]$ denotes the actual-to-desired relation that is defined as

$$\chi[k] = \begin{cases} 1 & \text{, if } y_{\text{act}}[k] < y_{\text{des}}[k] - \epsilon[k] \wedge y_{\text{des}}[k] \leq y_{\text{des}}[k-1] \quad \text{I} \\ 1 & \text{, if } y_{\text{act}}[k] > y_{\text{des}}[k] + \epsilon[k] \wedge y_{\text{des}}[k] \geq y_{\text{des}}[k-1] \quad \text{II} \\ 0 & \text{, if } y_{\text{des}}[k] - \epsilon[k] \leq y_{\text{act}}[k] \leq y_{\text{des}}[k] + \epsilon[k] \quad \text{III} \\ -1 & \text{, if } y_{\text{act}}[k] > y_{\text{des}}[k] + \epsilon[k] \wedge y_{\text{des}}[k] \leq y_{\text{des}}[k-1] \quad \text{IV} \\ -1 & \text{, if } y_{\text{act}}[k] < y_{\text{des}}[k] - \epsilon[k] \wedge y_{\text{des}}[k] \geq y_{\text{des}}[k-1] \quad \text{V} \end{cases} . \tag{3.64}$$

The constant increment factor w determines the maximum numerical change of the parameter. The tolerance range (i.e., the acceptable deviation from the desired value) is termed $\epsilon[k]$.

If the actual value is out of the tolerance range, the parameter adaptation is enabled. Two major conditions of falling out of tolerance can occur, firstly, falling below the lower threshold $y_{\text{act}}[k] < y_{\text{des}}[k] - \epsilon[k]$ (cf. I and V in (3.64)), secondly, exceeding the upper threshold $y_{\text{act}}[k] > y_{\text{des}}[k] + \epsilon[k]$ (cf. II and IV in (3.64)).

A further distinction is made. As for the first major condition, if the signal value of $y_{\text{des}}[k]$ is decreasing between time points k and $k+1$, $\chi[k]$ equals 1 (cf. I in (3.64)). If $y_{\text{des}}[k]$ is increasing within that time span, $\chi[k]$ equals -1 (cf. V in (3.64)). As for the second major condition, it is $\chi[k] = 1$ (cf. II in (3.64)) and $\chi[k] = -1$ (cf. IV in (3.64)).

Otherwise, if the actual value is within the tolerance range, the parameter adaptation is disabled ($\chi[k] = 0$) (cf. III in (3.64)).

It should be noted that $\chi[k] = 1$ implies incremental increase of the parameter value $x_{\mathrm{f,max},i}[k]$ while $\chi[k] = -1$ leads to incremental decrease of $x_{\mathrm{f,max},i}[k]$.

Under academic supervision in the scope of a bachelor's thesis, a variation of the incremental adaptation was proposed [128]. It features a supporting factor for the user. Its definition reads

$$x_{\mathrm{f,max},i}[k] = x_{\mathrm{f,max},i}[k-1] \cdot ((-\operatorname{sign}(\Delta Q) \cdot w \cdot (1 - \frac{1}{Q[k]})^2) \cdot \gamma), \quad (3.65)$$

where $\gamma \in [0, 1]$ denotes the supporting factor. Low values represent little support by the incremental parameter adaptation while high values stand for significant support. By supporting the user significantly in the beginning and gradually diminishing γ over the trials less frustrating trials possibly happen.

The acute trend of user performance ΔQ is defined as

$$\Delta Q = Q[k] - Q[k-1]. \quad (3.66)$$

In the scope of a further bachelor's thesis under academic supervision, this adaptation method was applied and analyzed [129].

As for evaluation purposes, average user performances are defined. The user performance standing for one trial that is performed by a single user reads

$$\bar{Q}_{u,t} = \frac{1}{K} \cdot \sum_{k=1}^{K} Q[k], \quad (3.67)$$

where $u = 1, ..., \tilde{U}$ denotes the index of users and $\tilde{U}$ is the total number of users [213]. K is the total number of discrete time points of the trial [213].

Moreover, the two-way average user performance reflecting one trial performed by one plurality of users reads

$$\bar{\bar{Q}}_t^{\tilde{U}} = \frac{1}{\tilde{U}} \cdot \sum_{u=1}^{\tilde{U}} \bar{Q}_{u,t}. \quad (3.68)$$

The standard deviation of the two-way average user performance is defined as [213]

$$\sigma_t^{\tilde{U}} = \sqrt{\frac{1}{\tilde{U}-1} \cdot \sum_{u=1}^{\tilde{U}} (\bar{Q}_{u,t} - \bar{\bar{Q}}_t^{\tilde{U}})^2}. \tag{3.69}$$

The mean of standard deviations is

$$\bar{\sigma}^{\tilde{U},\tilde{T}} = \frac{1}{\tilde{T}} \cdot \sum_{t=1}^{\tilde{T}} \sigma_t^{\tilde{U}}, \tag{3.70}$$

where $\tilde{T}$ is the total number of trials.

3.5.6 Gamified interface

As for isotonic HMI controls, it is advisable to provide the user with gamified virtual environments (cf. Section 2.5.3) encouraging to keep the biosignal at a high-level for a long period of time. In case the user succeeds in this a considerable score is achieved.

By definition, motivational affordances aim at motivating the user to proceed using the application. Different motivational affordances may serve distinct purposes. The following list illustrates various motivational affordances that are utilized in the adaptive muscle interface in order to achieve certain results.

- Reward together with penalty points: The instantaneous reward and penalization in distinct situations are useful to direct the behavior of the user in certain ways. The user perceives the instantaneous reward and penalization as direct feedback depending on the behavior and thus can extract the information of tendency. On the other hand, accumulated reward and penalization still serve as feedback for the user but do not imply the information of tendency.
- Leaderboards or highscore tables: Accumulated points achieved by the user during completing a task are used for both inter and intra-individual comparison.

- 3D computer graphics: For the virtual simulation of physical devices three-dimensional computer graphics are well suited. The users can immerse themselves in the situation of applying the physical device. Variations of controlling the physical device can be tested in risk-free simulation. The user is provided with a virtual environment for training and improving confidence in controlling the physical device.
- Difficulty levels: User-individual adjustments of the difficulty level ensure that the individual performance level is met and potentially avoids frustration.
- Story mode or progress visualization: In order to achieve intra-individual motivation from session to session, telling an engaging story in form of texts, graphics or videos is helpful. In addition, the progress could be visualized, like a progress bar, or indicated as a percentage.
- Trophies or badges: As a form of visualization of special achievements and as an extraordinarily noticeable motivation trophies as well as badges can be introduced. Those trophies or badges could optionally be published for inter-individual comparison.

3.6 Training Concept for Unpracticed Users

Apart from parameter adaptation on the HMI side, the human user also adapts the internal mental model, representing the circumstances, in order to improve the performance over time. That is, humans learn by doing [232].

On the other hand, it is unknown to what extent the HMI control via the external ear muscles is learnable at all.

To provide the best support to the human user towards mastering the HMI control – to maximize the learning effect for the user – a new training concept was developed in this work. This training concept especially aims at unpracticed users, such as human users that do not have any experience in operating the HMI. For instance, it is applicable to persons that were just injured at the spinal cord in an accident. The training concept for

unpracticed users essentially is a composition of methods addressed earlier in this work. It encompasses five main steps described as follows.

1. **Biosignal feedback** Feedback information (cf. Section 2.5.1) about the current quality of HMI control enables the user to act accordingly, leading to an improvement in HMI control quality. This step is crucial as the human user is instantaneously confronted with the biosignal generation. The mere feedback of the "own" biosignal is the very first step of improving the HMI control. The user consciously or unconsciously begins to reflect the own behavior. In general, the biosignal is fed back multimodally to the user by the HMI, auditorily and visually.

2. **User individualization** The open-loop adaptation methods, namely the sensor calibration for each biosignal (cf. Section 3.5.1) and the bimodal calibration (cf. Section 3.5.2), help to generate normalized biosignals and a crosstalk compensated bimodal difference signal. The user individualization is helpful in terms of avoiding situations of frustration in favor of situations of motivation.

3. **User skill quantification** The assessment paradigm methods (cf. Section 2.4.3) allow for the numerical rating of the user skill ahead of and after the user individualization. Those methods are employed to rate the initial skill as well as to rate the progress of the skill and documentation of the learning process. Both unimodal and bimodal biosignal skills are rated.

4. **Virtual reality training with gamified environments** The users perform diverse trainings in virtual reality. Those virtual realities are gamified (cf. Section 3.5.6), meaning, they are designed incorporating game elements and mechanics to improve user engagement. Within the virtual realities the user controls avatars using the same skills that are needed for controlling real executing devices like the electric-powered wheelchair. In the long term, virtual reality training aims at reducing the mental effort for operating the HMI, converting the conscious control of the HMI into a more subconscious control.

5. **Real executing device training** After the period of virtual reality training the optimal control scheme (cf. Section 3.7), the preferred scheme for controlling, for example, the electric-powered wheelchair that

meets the individual skills and deficiencies of the human user the best will be identified. Eventually, that control scheme is utilized to control the actual executing device.

3.7 Control Signal Generator

The control signal generator realizes the biosignal interpretation (cf. Section 2.6). It outputs at least one control signal indicating the executing device what to do.

Various control signal generators covering diverse purposes are feasible. Table 3.1 shows examples of control signal generators for the purpose of electric-powered wheelchair (EPW) navigation. They receive either one or two input signals and provide various options to navigate the EPW ranging from simplistic to complex controls.

Control signal generator	$x_{\mathrm{n},1}[k]$	$x_{\mathrm{n},2}[k]$	Navigation options
One-Signal Morse (cf. Appendix A.7.1)	✓	×	↑ ↻ ↺
One-Signal Morse Proportional (cf. Appendix A.7.2)	✓	×	↑ ↻ ↖ ↺ ↗
Two-Signal Threshold (cf. Appendix A.7.3)	✓	✓	↑ ↻ ↺
Two-Signal Proportional (incl. r/t-generator, r/t-converter)	✓	✓	↑ ↻ ↖ ↺ ↗

Table 3.1: Control signal generators providing navigation options: Straightforward movements (↑), left resp. right curves (↖, ↗) and left resp. right on-the-spot turns (↻, ↺)

The *One-Signal Morse* control signal generator (cf. Appendix A.7.1) receives one input signal and generates straightforward movements as well as double-sided on-the-spot turns. This control signal generator allows disabled persons capable of activating merely one biosignal to navigate

electric-powered wheelchairs without the prerequisite of differential control.

The *One-Signal Morse Proportional* control signal generator (cf. Appendix A.7.2) also receives one biosignal. As opposed to the previous one, this control signal generator allows for left and right curves in addition to on-the-spot turns.

The *Two-Signal Threshold* control signal generator (cf. Appendix A.7.3) poses a more comfortable way of performing navigation tasks. Albeit it requires two input signals and therefore is not applicable for persons generating merely one biosignal.

The *Two-Signal Proportional* control signal generator extends the navigation options provided by the previous control signal generators and allows for left and right curves. Figure 3.12 depicts this control signal generator. It contains the rotational/translational-generator (r/t-generator) and the rotational/translational-converter (r/t-converter).

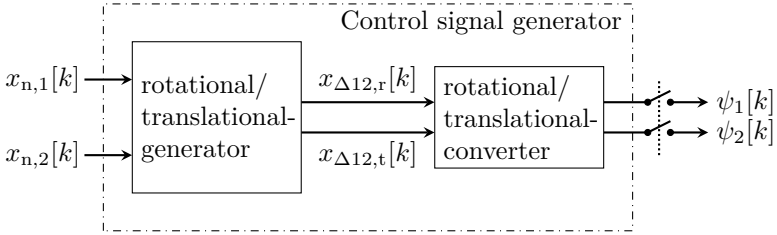

Figure 3.12: Two-signal proportional control signal generator with signal clutch

First, the *r/t-generator* produces the intermediate rotational signal $x_{\Delta 12,\mathrm{r}}[k] \in [-1, 1]$ that equals (3.34). The radii of the curves are proportional to the degree of the signal difference between $x_{\mathrm{n},1}[k]$ and $x_{\mathrm{n},2}[k]$, the characteristic of the bimodal differential signal. The r/t-generator also produces the intermediate translational signal, defined as

$$x_{\Delta 12,\mathrm{t}}[k] = (1 - |x_{\Delta 12,\mathrm{r}}[k]|) \cdot x^*_{\Delta 12,\mathrm{t}}[k] \in [0, 1], \tag{3.71}$$

where $x^*_{\Delta 12,\mathrm{t}}[k] \in [0,1]$, analogous to (3.34), is obtained by the open-loop bimodal calibration with linear regression (cf. Section 3.5.2). The signal $x_{\Delta 12,\mathrm{t}}[k]$ works as a throttle. Only if the rotational signal is low, the translational signal is allowed to be high.

Second, the *r/t-converter* converts these signals into control signals $\boldsymbol{\psi}[k]$ that meet the specifications of the executing device according to

$$\psi_1[k] = \begin{cases} E_\mathrm{d} & , \text{if } \left| x_{\Delta 12,\mathrm{r}}[k] \cdot \frac{E_\mathrm{u} - E_\mathrm{l}}{2} \right| < \epsilon_\mathrm{r} \\ E_\mathrm{d} + x_{\Delta 12,\mathrm{r}}[k] \cdot \frac{E_\mathrm{u} - E_\mathrm{l}}{2} & , \text{else} \end{cases} , \text{ and} \tag{3.72}$$

$$\psi_2[k] = \begin{cases} E_\mathrm{d} & , \text{if } \left| x_{\Delta 12,\mathrm{t}}[k] \cdot \frac{E_\mathrm{u} - E_\mathrm{l}}{2} \right| < \epsilon_\mathrm{t} \\ E_\mathrm{d} + x_{\Delta 12,\mathrm{t}}[k] \cdot \frac{E_\mathrm{u} - E_\mathrm{l}}{2} & , \text{else} \end{cases} . \tag{3.73}$$

The default value of the executing device is defined as

$$E_\mathrm{d} = E_\mathrm{l} + \left(\frac{E_\mathrm{u} - E_\mathrm{l}}{2} \right), \tag{3.74}$$

where E_l and E_u stand for the lower resp. upper limit of the executing device's control signal range.

ϵ_r and ϵ_t denote the dead band parameters of the rotational and translational control signals. Unless the signals exceed the dead band values they continue to be at default value E_d. This way, low disturbing signals are efficiently suppressed.

Moreover, due to the discontinuities in $\psi_1[k]$ and $\psi_2[k]$ caused by the incorporation of the dead bands the electric-powered wheelchair is given a slight jolt as soon as the dead band parameter values are exceeded. This way, the user is notified and gently alerted that the vehicle is about to move in that very moment.

The rotational control signal $\psi_1[k]$ and the translational control signal $\psi_2[k]$, that are digital signals, are sent to the digital-to-analog converter (DAC). Then, the electric-powered wheelchair, as the executing device, interprets the incoming analog control signals and creates corresponding motions.

In our case, the electric-powered wheelchair receives analog control signals (in mV) ranging from $E_{\mathrm{l}} = 1700$ to $E_{\mathrm{u}} = 3300$. Accordingly, the default value is $E_{\mathrm{d}} = 2500$.

On-the-spot turns correspond to a high differential signal and curves coincide with a moderate differential signal. If the differential signal is below a predefined threshold straightforward movements are produced.

The signal clutch, designed as double-pole, single-throw (DPST) switch, connects and disconnects the output of the control signal generator. This clutch permits safety controlling. In case the user is not able to generate appropriate biosignals or the overall system is corrupted and generates incorrect control signals, the clutch allows for quick disconnection of the executing device.

3.8 Contribution of the Adaptive Muscle Interface

The adaptive muscle interface covers Items 2 to 6 in the list of open problems as outlined in Section 1.6.

The proposed interface is accessible via muscle signals acquired from the external ears – that is, head-only activities. At the same time it avoids overly salient apparatus and double occupancy of commonly employed bodily functions. This provides the user with additional windows of communication. Moreover, it holds means available for improving biosignal controllability and coping with biosignal drifts.

4 Implementation

4.1 Levels of Implementation

The implementation of human-machine interfaces (HMIs) can be seen as three hierarchical levels [164]. Figure 4.1 illustrates the levels of implementation. First, the *general implementation* represents the most abstract level and constitutes the basis for any other level of implementation. It defines the communication interfaces of the high-level subsystems. The main objective of the general implementation is to bring the basic communication between the associated high-level subsystems into being. Second, the *application-specific implementation* explicitly narrows down the sort of application, namely the input and output signals. It substantiates the communication interfaces of the low-level subsystems. Third, the *user-specific implementation* specifies the signal-to-meaning mapping between the user individual input signals and the output signals to control the executing device.

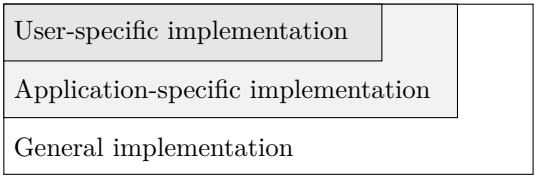

Figure 4.1: Levels of HMI implementation (according to [164])

In the context of this work, the general implementation is illustrated in Figure 1.11. The high-level subsystems are the human user, the HMI as well as the executing device. The human user generates biosignals that are

received by the HMI. In turn, the interface generates control signals based on an algorithmic interpretation of the biosignals and transmits those to the executing device. The executing device performs actions representing the control signals based on the interpretation of the biosignals.

The application-specific implementation of the telemetric and myoelectric ear muscle sensing system (TELMYOS) is illustrated in Figure 4.2. It allows the user to control both physical executing devices and virtual executing devices by means of muscle activity. This level of implementation specifies details of low-level subsystems such as the biosensor, the MCUs end device (ED) and access point (AP) as well as the GUI and describes their objective targets. It also defines the communication between the low-level subsystems.

The biosensor captures muscle activity in the form of electrical potentials. The analog myoelectric signals (MESs) are transmitted to the end device (ED). It incorporates an ADC and sends the digitized MESs to the access point (AP) that, in turn, sends the signals to the GUI. Based on the incoming digital MESs the GUI generates digital control signals. Depending on the application and the type of executing device the digital control signals are of different nature, that is, the control signals designated for physical executing devices and for virtual executing devices differ from each other. The digital control signals are sent either directly to the virtual executing device, displayed on the computer monitor, or via the AP that incorporates a DAC and sends the analog signals to the physical executing device.

The human supervisor sets application-related parameter values – like the sampling rate – in three steps via an integrated development environment (IDE) by modifying the source code of the MCUs, recompiling the modified source code and eventually porting it onto the MCUs. Alternatively, the human supervisor may also modify the application-related settings directly via the GUI. Special transmitting functions of the GUI as well as receiving and transmitting functions of the MCUs allow for bidirectional communication between GUI and MCUs. In other words, the GUI may send messages to both the AP and ED requesting (read functions) or setting (write functions) specific parameter values. This is more comfortable, less error-prone and faster.

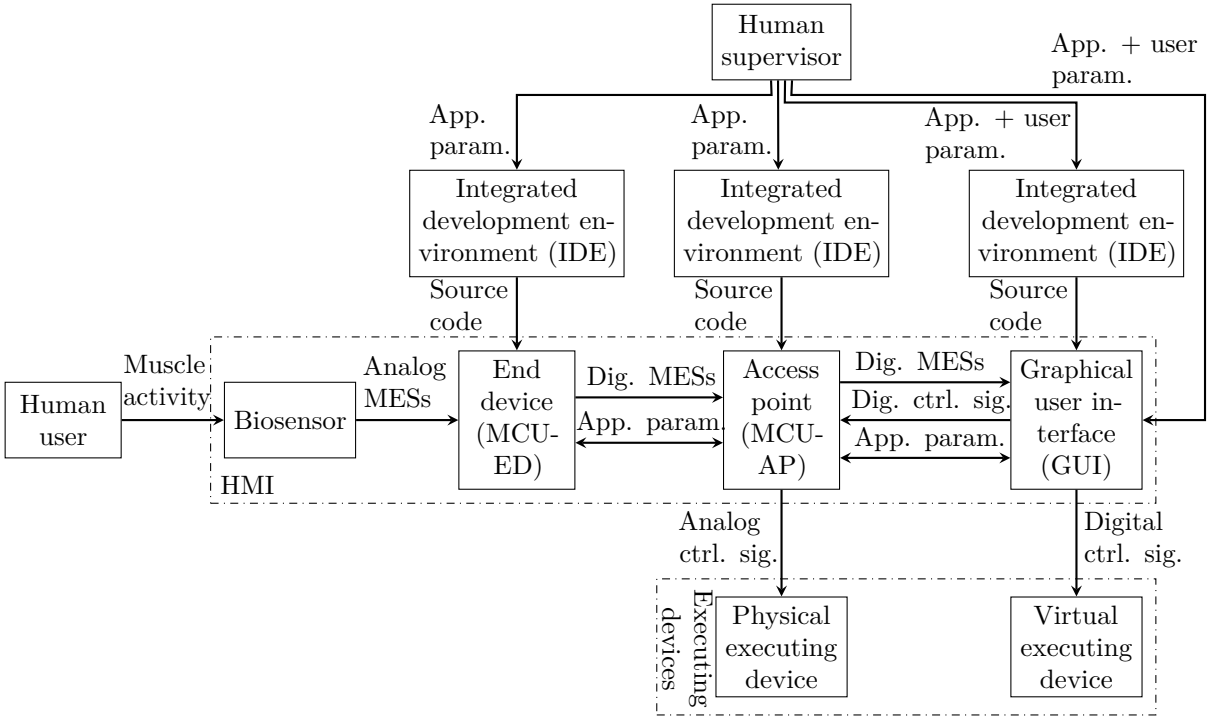

Figure 4.2: Application-specific implementation of TELMYOS (application parameters (app. param.), digital (dig.), control signals (ctrl. sig.))

The human supervisor and the human user may be the same person for testing purposes. However, as editing the source code requires expert know-how the human supervisor usually is a system developer.

The user-specific implementation is detailed in Figure 4.3. Grounded on the application-specific implementation it defines the user individualization of the system that is realized through providing feedback to the user, customizable user-related parameter values and user-specific control schemes. With the aid of feedback mechanisms both, the user and the technological subsystems such as the GUI and the MCUs, are provided with user-related information. The GUI provides various control schemes that can be customized at the preferences of the user. The control scheme calculates digital control signals.

Typically, the human user observes the immediate acting of the executing device and therefore is provided with direct, visual feedback information. In the understanding of the human user (mental model) this feedback interrelates the action of the human user (i.e., muscle activity) and the action of the executing device (i.e., acting of the executing device). In addition, user-related information is extracted from the virtual executing devices (virtual realities (VRs)) and fed back to the GUI. In turn, the GUI uses the feedback for visualization (i.e., feedback to the human user) or for parameterization (i.e., feedback to the HMI).

The human supervisor sets user-related parameter values like affecting the algorithmic interpretation of the biosignal by means of the GUI.

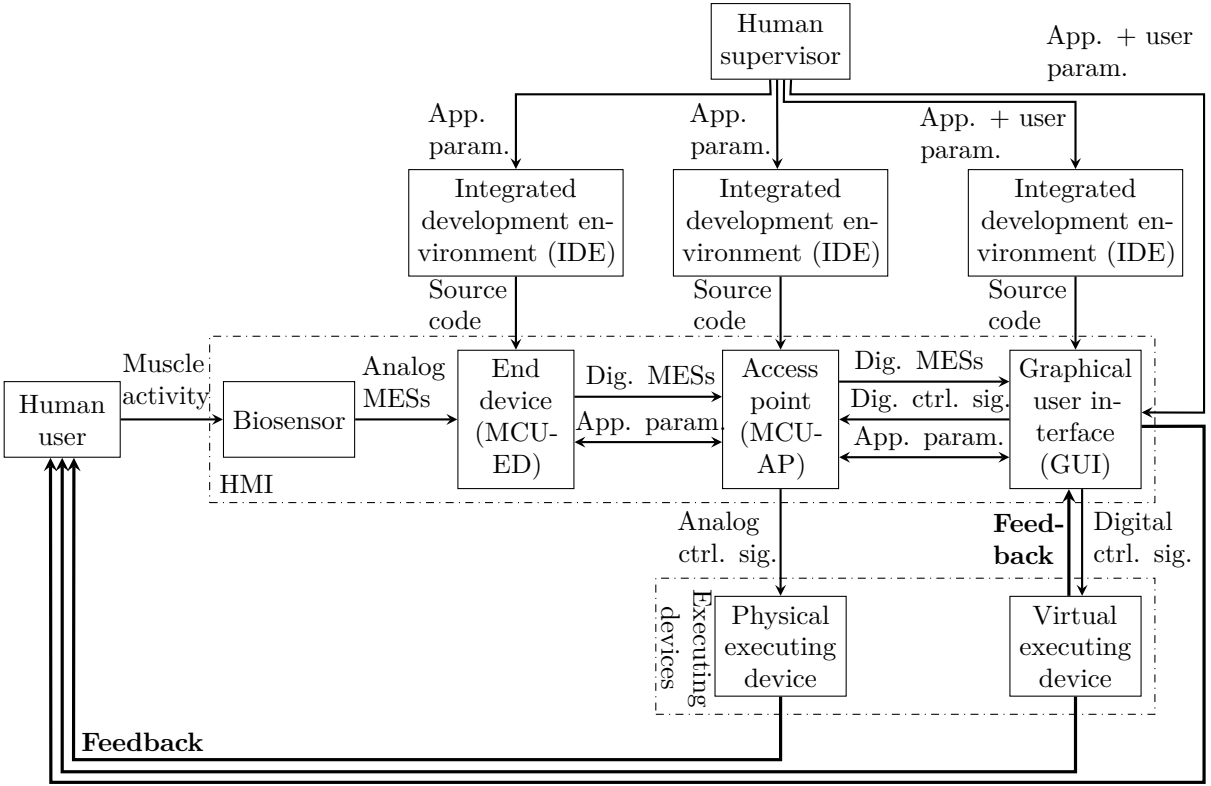

Figure 4.3: User-specific implementation of TELMYOS (application parameters (app. param.), digital (dig.), control signals (ctrl. sig.)) (bold font indicates addendum to Figure 4.2)

4.2 Standard System Setup

The standard setup of the system for controlling both virtual and non-virtual executing devices through myoelectric signals (MESs) follows the user-specific implementation and is detailed in Figure 4.4. An electric-powered wheelchair represents the physical executing device and VRs materialize diverse virtual executing devices. Two electromyography (EMG) electrode systems (EMG sensors 1 and 2) acquire the MESs corresponding to the activity of the muscles.

The topology of the HMI can be subdivided into the user site and the base station site (cf. Section 3.2). The signal transmission between ED at the user site and AP at the base station site is wireless. Therefore, the user is free to move the head and look around while sitting in the wheelchair. Dependent on the constitution of the user, this wireless system design also allows the user to leave the wheelchair. Moreover, the supervisor can set application-related or user-related parameter values telemetrically at the base station site during normal operation.

Generally, the proposed HMI concept is not limited to two electrode systems of a specific kind. However for the sake of simplicity, the standard system setup comprises two electromyography (EMG) electrode systems acquiring the muscle activity (i.e., MESs) of the human user. These are acquired either (minimally) invasively by means of fine-wire electrodes (fwEMG) or non-invasively with the aid of surface electrodes (sEMG).

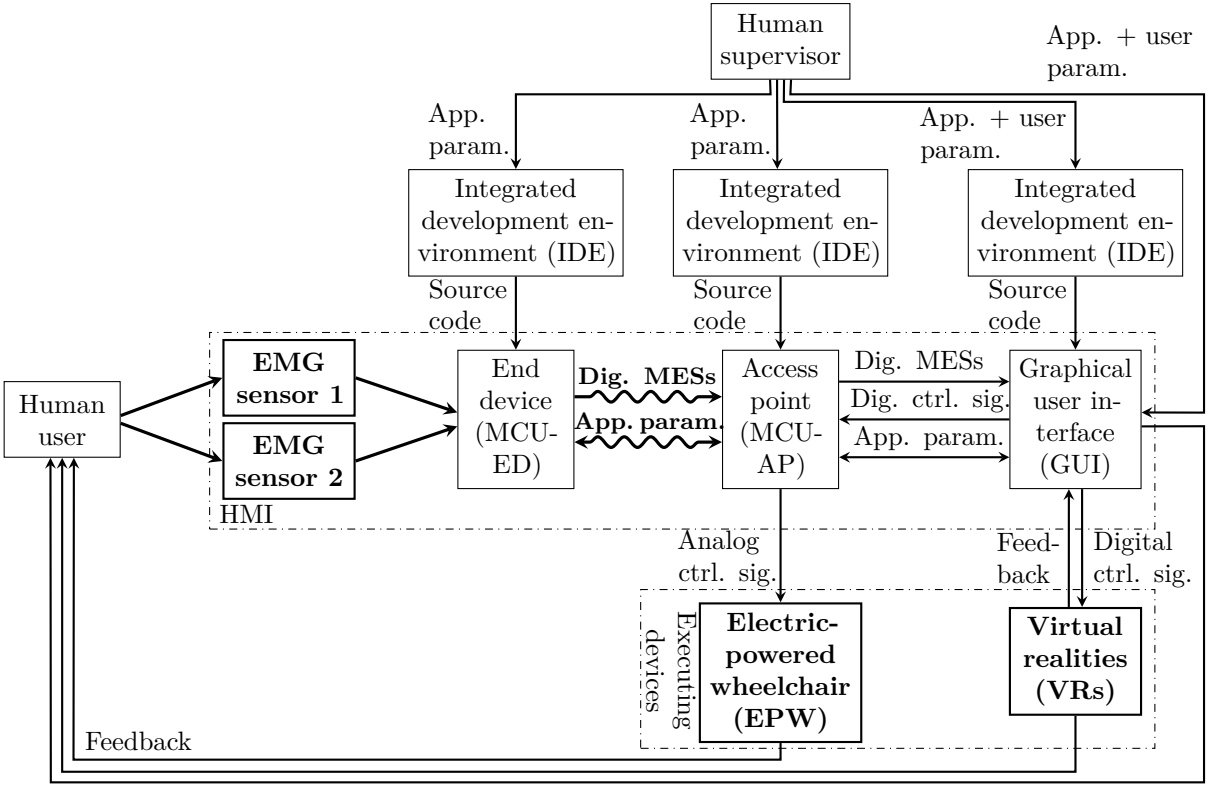

Figure 4.4: Standard system setup for controlling executing devices based on electromyography sensors (EMG sensors 1 and 2) acquiring myoelectric signals (MESs) (application parameters (app. param.), digital (dig.), control signals (ctrl. sig.)) (modified from [211]) (bold font indicates addendum to Figure 4.3)

4.3 Embedded System

In addition to the GUI, the embedded system is also capable of performing the basic signal processing described in Appendix A.5. The advantage of the GUI performing the signal processing is the manifold of feedback tools helping to optimize the experience for the user. If needed, once the user got familiar with the HMI and proper user-specific parameters were found the basic signal processing can be outsourced for the sake of performance enhancement of the overall system. With the aid of special transmission protocols, parameter values used for the signal-processing algorithm are readable and writable.

The embedded system comprises two electronic boards, these are the microcontroller unit (MCU) end device (ED) at the user site and the microcontroller unit (MCU) access point (AP) at the base station site. Both serve different purposes within the context of the overall system. The electronic boards mechanically fasten and electrically connect diverse miniaturized modules. The microcontroller (MC) is the central component of the board. It is a miniaturized computer implemented on an integrated circuit (IC). In addition, various communication modules such as radio frequency (RF) transceiver, chip antenna, push buttons, light-emitting diodes (LEDs) and general-purpose pins are available.

The MCUs MSP430F2274[1] by Texas Instruments are employed. They feature ultralow-power architecture, 16-bit reduced instruction set computing (RISC) central processing unit (CPU) and a flexible clock system [49]. Figure 4.5 depicts the eZ430-RF2500[2] development tool kit by Texas Instruments which is used as the initial design for the wireless communication of the system. While both MCUs are identical regarding their hardware specification, the boards differ from each other with respect to the software programs since they serve different purposes.

The MCU ED, depicted in Figure 4.5a, receives analog signals acquired by the biosignal sensors that are connected to the external input channels and digitizes them with the 10-bit ADC module. The digitized biosignals are sent via the on-board 2.4 GHz RF transceiver CC2500[3] to the MCU AP.

[1] `http://www.ti.com/product/msp430f2274`
[2] `http://www.ti.com/eZ430`
[3] `http://www.ti.com/product/cc2500`

Figure 4.5b depicts the MCU AP. It receives the data, adds header information that is required for the safe communication and sends it to the PC.

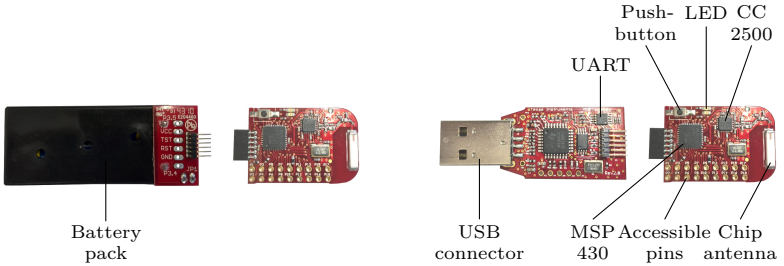

(a) Battery board with MCU ED board **(b)** USB board with MCU AP board

Figure 4.5: Development tool kit eZ430-RF2500

Code Composer Studio software by Texas Instruments is an IDE that is used to edit the C source code, to compile the executable program and to port the executable program onto the MCU. In the Appendix, Figure A.27 shows a screen shot of Code Composer Studio.

There are two main objectives of the embedded system. First, the embedded system constitutes the linkage between hardware and software components through DAC and ADC such as biosignal sensors, PC, EPW – that is, the MCUs communicate with other subsystems. Second, the embedded system wirelessly transmits information between both MCUs. In general, this data transmission is bidirectional.

To realize robust and fast communication between the subsystems – namely ED, AP, GUI and non-virtual executing devices – transmission protocols for various application scenarios need to be deployed.

4.4 Transmission Protocols

4.4.1 Unidirectional two-sensor data transmission

In case of unidirectional, cyclical two-sensor data transmission from ED to GUI the transmission protocol as depicted in Figure 4.6 is utilized. The ED sends sensor data acquired from the biosignal sensor systems via the AP that, in turn, passes it on to the GUI.

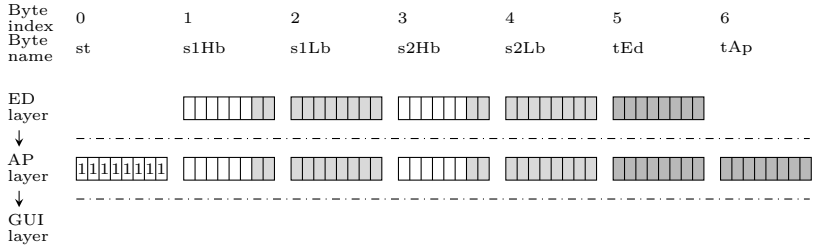

Figure 4.6: Protocol for cyclical two-sensor data transmission from ED to GUI. Sensor values split into high byte (Hb) and low byte (Lb).

The ED software layer is implemented in the ED. It compiles a five-byte array containing two sensor values (bytes s1Hb, s1Lb, s2Hb and s2Lb) as well as the time index of the ED (byte tEd). Each sensor value is represented by a 10-bit binary number, split into two bytes. The high-order bytes (suffix Hb) carry two high-order bits while the low-order bytes (suffix Lb) contain eight low-order bits. The five-byte array is transmitted to the AP via Texas Instruments' RF network protocol SimpliciTI[4].

The AP software layer adds two bytes to the original byte array. The message start (byte st) is prepended to the original byte array and the time index generated by the AP (byte tAp) is appended to the original byte array. By design of the transmission protocol, the fixed value of the message start equals 0b11111111 = 0xFF. It indicates the beginning of a new message. The time indices are counter variables and function as

[4] `http://www.ti.com/simpliciti`

indicators for data loss. The total number of bytes sent by the AP to the GUI amounts to seven.

4.4.2 Unidirectional two-sensor data transmission with accelerometer

The unidirectional two-sensor data transmission with accelerometer adds two aspects as compared to the transmission protocol discussed in Section 4.4.1. The three-dimensional data from two acceleration sensors as well as the supply voltage of the EDs provide supplementary information. The enhanced transmission protocol is illustrated in Figure 4.7.

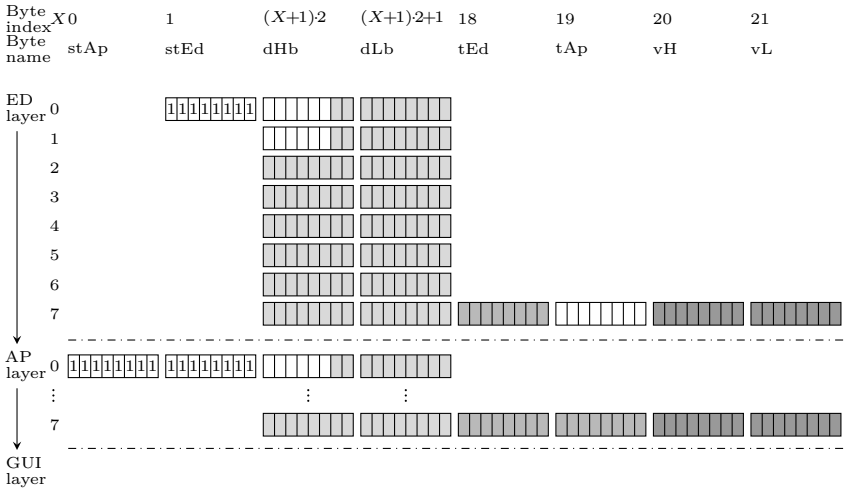

Figure 4.7: Protocol for cyclical two-sensor data transmission from ED to GUI with accelerometer information. Sensor values split into high byte (Hb) and low byte (Lb).

4.4.3 Bidirectional two-sensor data transmission

Typically, altering meta-data of the embedded systems such as the sampling rate of the ED is time-consuming. Setting meta-data requires modifying the C source code of the embedded system, re-compiling the modified source code and eventually porting the newly- generated, executable program onto the embedded system.

Bidirectional communication (i.e., the information flow goes both ways) from the ED to the GUI and vice versa enables altering the parameters of the embedded system during run time without the aforementioned, time-consuming steps. The bidirectional, cyclical two-sensor data with acyclical meta-data transmission protocol was developed under academic supervision in the scope of a Master's thesis [42].

As for cyclical two-sensor transmission with acyclical meta-data transmission in the direction from the ED to the GUI the protocol as shown in Figure 4.8 is applied.

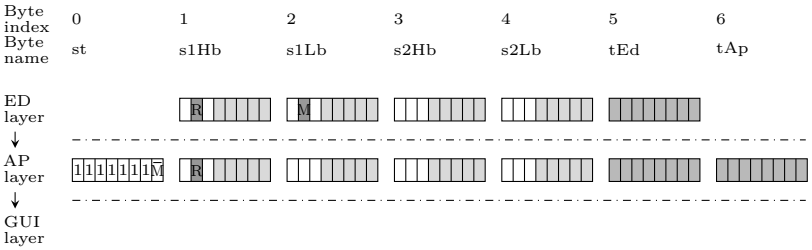

Figure 4.8: Protocol for cyclical two-sensor transmission and acyclical meta-data transmission from ED to GUI. Sensor values split into high byte (Hb) and low byte (Lb) (modified from [42]).

The 10-bit sensor values are split equally into two bytes. Each byte contains five bits sensor information. The low-order bytes (suffix Lb) hold five low-order bits and the high-order bytes (suffix Hb) contain five high-order bits. The ED transmits either sensor data or meta-data (parameters). The second-highest-order bit in the second byte denotes the meta-flag "M". If

this flag is set the ED is transmitting meta-data to the AP. Otherwise it is transmitting sensor data. Setting the second-highest-order bit equals the addition of 64 decimal value. The AP forwards messages coming from the ED to the GUI with the corresponding message start byte. The lowest-order bit of the message start byte is the negated meta-flag. This way, the transmission of sensor data is indicated by the message start byte containing 0b11111111 = 0xFF and the transmission of meta-data is pointed out by 0b11111110 = 0xFE. The second-highest-order bit in the first byte indicates the receive-flag "R". If this flag is set the ED is ready to receive commands coming from the AP.

As the information flow goes the opposite direction, that is, from the GUI to the ED, the transmission protocol as shown in Figure 4.9 is used. The GUI software layer is implemented in the GUI. The message start byte containing 11111110 = 0xFE sent by the GUI tells the AP the beginning of another byte array. The first byte contains an identifier (ID) that is unique to the command intended for either the AP or ED. If the command is intended for the ED, the AP redirects it to the ED. In case of argument carrying commands the bytes two to four contain the corresponding argument values. The message end byte equals 0b11111101 = 0xFD. Table A.2 in the Appendix gives an overview of the commands.

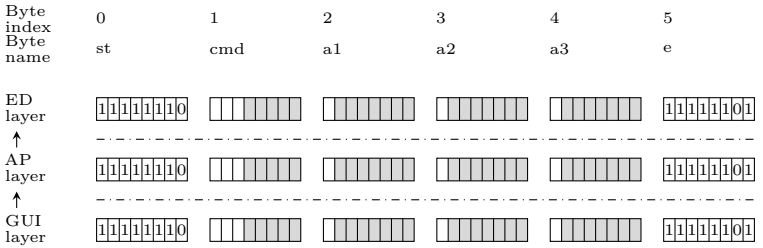

Figure 4.9: Protocol for acyclical parameter requests from GUI to ED (modified from [42]).

4.4.4 Unidirectional eight-sensor data transmission

For the unidirectional, eight-sensor, cyclical data transmission with 16-bit digital signal resolution the protocol as depicted in Figure 4.10 is utilized. The low-power, eight-sensor analog-to-digital converter ADS1298[5] by Texas Instruments is deployed.

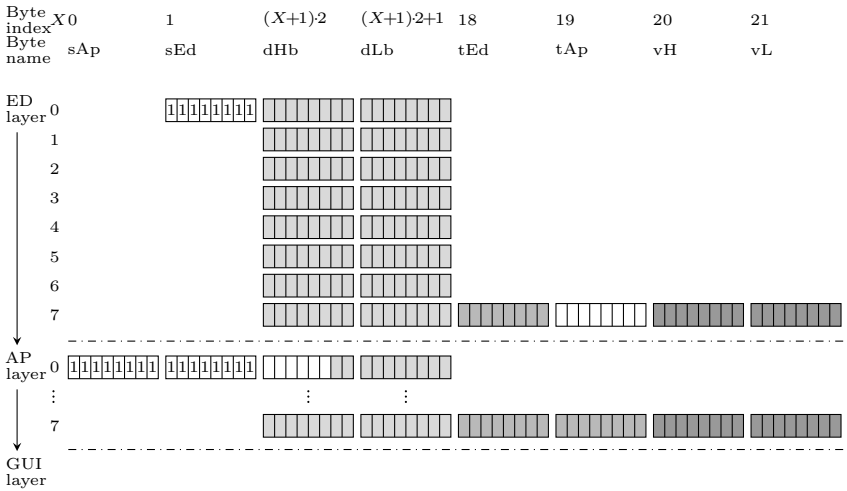

Figure 4.10: Protocol for cyclical eight-sensor data transmission from ED to GUI

4.5 Graphical User Interface

4.5.1 Overview

The graphical user interface (GUI) is implemented with standard C++ utilizing the Qt application framework[6] for the realization of the graphical

[5] http://www.ti.com/product/ads1298
[6] http://www.qt-project.org

widgets. The software is cross-platform, meaning, it is applicable to various operating systems (OSs). The Qt application framework supports Unix OSs, for example, Apple's OS X, Linux OS, and Microsoft's Windows OSs as well as cell phone OSs, for instance, Google's Android, Microsoft's Windows Phone to provide a wide range of platforms with TELMYOS.

The main window of the GUI is shown in Figure 4.11. It is subdivided into four main sections, namely the superordinate menu (A), the tab area (B), the parameter field (C) and the signal graphs (D).

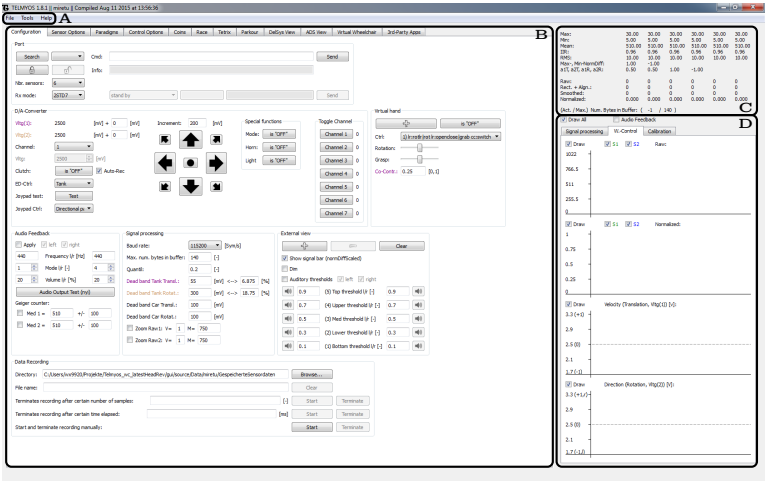

Figure 4.11: Main window of the graphical user interface with the superordinate menu (A), the tab area (B), the parameter field (C) and the signal graphs (D)

Role-dependent views allow for supervisor view (back-end of the GUI) and user view (front-end of the GUI) that can be displayed on separate screens if needed. The supervising person is provided with information about the biosignal of the user in real-time and monitors the full range of results. With the aid of specific user views, the users are enabled to focus on the actual task as solely relevant information is displayed (cf. Section 2.3).

The superordinate menu includes options to change the user, to connect or disconnect the incoming biosignals, to close the GUI, to open or close the user view, to pseudonymize the user names and to show the help information. The menu is accessible at all times by the supervisor.

The tab area contains several tabs. Each tab is dedicated to a specific group of functionalities and features. Figure 4.12 depicts examples of these tabs. The Configuration tab (cf. Figure 4.11) provides the supervisor with general settings.

The Sensor Options tab, as depicted in Figure 4.12a, is dedicated to settings regarding the biosensors. The Paradigms tab, shown in Figure 4.12b, holds the implementations of the biosignal assessment paradigms (cf. Section 2.4.3) available. The Coins tab, the Race tab, as depicted in Figure 4.12c, the Tetris tab, the Parkour tab and the Virtual Wheelchair tab, illustrated in Figure 4.12d, contains the implementations of virtual environments. The ADS View tab, presented in Figure 4.12e, is dedicated to visualization methods of up to 16 biosignals. The 3rd-Party Apps tab provides with interface options to operate third-party applications.

The parameter field concisely provides the supervisor with the most important parameter values as they are currently applied.

The signal graphs visualize the incoming biosignals, the digitally processed signals with intermediate processing steps as well as the control signals for the virtual environments or the electric-powered wheelchair (EPW).

Inter as well as intra-individual user sessions are manageable. Each user is represented via a separate working directory where sessions are administrated. The dialog window for changing the current user is depicted in Figure 4.13. The name of the user is to be specified and optionally the age, gender and handedness can be set. User-related data is saved into designated subfolders of the working directory for offline analysis and documentation. By default, saved data files are automatically labeled with the current system date and time as a distinct file identifier. An unambiguous data structure allows for multi-user management. Previous user sessions can be resumed by reference to the user names (user identifiers).

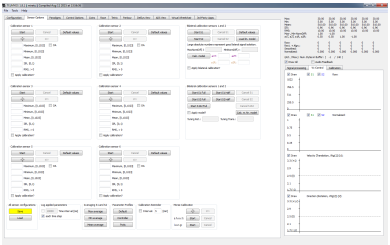

(a) Sensor options tab

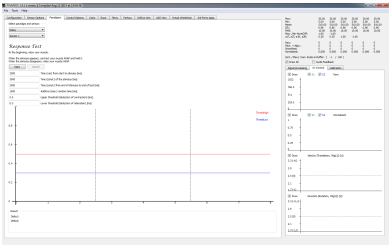

(b) Paradigms tab

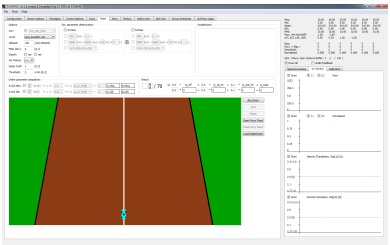

(c) Race tab

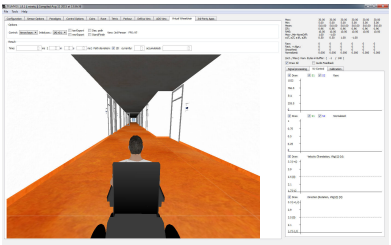

(d) Virtual wheelchair tab

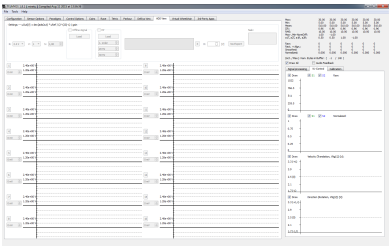

(e) ADS view tab

Figure 4.12: Examples of tabs in supervisor view

If needed, the real name of the user can be pseudonymized in retrospect. The integrated user pseudonymization tool ensures data privacy and data integrity. It replaces every occurrence of the real name by a pseudonymized name in the windows of the software as well as in the saved data files. The user pseudonymization tool is based on a look-up table realized by a American standard code for information interchange (ASCII) text file.

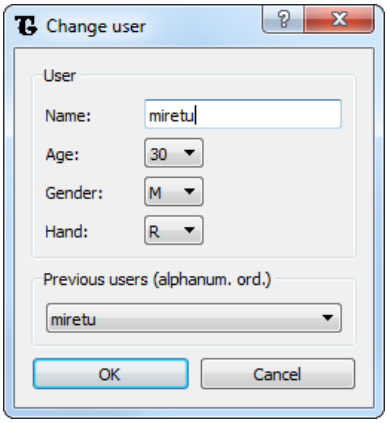

Figure 4.13: Dialog window for user change

The look-up table bidirectionally maps the real name onto a pseudonymized name. Enabling and disabling the user pseudonymization tool causes the pseudonymized name or the real name to appear. The format of the look-up table is `userPSEUDONYMIZED_USER_NAME,REAL_USER_NAME`. Each line of the text file represents the pseudonymization of one user where the supervisor administrates and edits the text file and explicitly sets `REAL_USER_NAME` and its alias `PSEUDONYMIZED_USER_NAME`.

By using user names without any personal relevance from the beginning, user anonymization can be realized. User anonymization allows for the maximum data privacy, but in contrast to user pseudonymization, obstructs multi-session user tests such as training over a number of days.

The online data import is implemented via the standard serial port of the PC (i.e., universal serial bus (USB)), applying Qt's native class QSerialPort. Both, biosignals and non-biosignals (e.g., analog signals from potentiometers) may serve as input data that is acquired in real time (RT). The offline data import functionalities ensure seamless data interchange across local PCs.

Incoming data is processed and feedbacked both visually and auditorily in RT. Auditory signal feedback is realized by including Firelight Technolo-

gies' sound library FMOD Ex[7]. The supervisor sets the auditory signal feedback's frequency and volume.

Figure 4.14 shows the supervisor view for setting user individual parameter values related to the first biosignal. It is a detail view of the sensor options tab (cf. Figure 4.12a). The supervisor has reading and writing access to all relevant parameters, for instance, the maximum parameter $x_{\mathrm{f,max},i}$, the minimum parameter $x_{\mathrm{f,min},i}$, the ground level parameter $x_{\mathrm{f,glvl},i}$, the IIR filtering trade-off parameter a_i and the RMS filtering window width parameter m_i of biosignal i, as well as to its corresponding calibration methods.

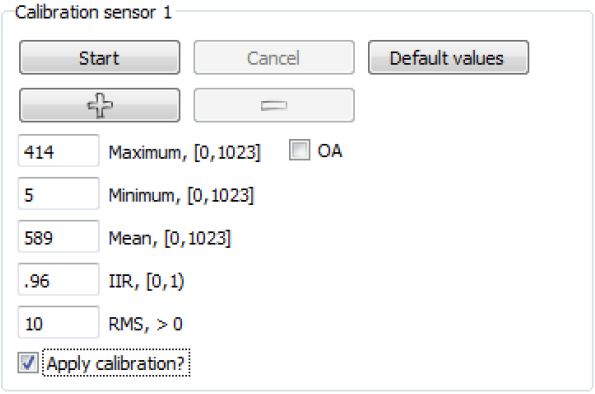

Figure 4.14: Supervisor view for setting user individual parameter values of sensor 1

The GUI was developed by the Karlsruhe Institute of Technology (KIT) as the essential software of the adaptive muscle interface. Currently, it is only available for the developers.

4.5.2 User guidance

The user guidance of the sensor calibration, as depicted in Figure 4.15, consists of six consecutive countdowns. The countdown for the low-level

[7] http://www.fmod.org

activity phase lasts five seconds. During this time the user observes the countdown (bright background color) and is asked to generate a low-level activity signal like relaxing the muscle. The countdown for the high-level activity phase lasts three seconds. The user observes the numbers counting down (green background color) and is instructed to generate high-level activity signal, contracting the muscle moderately. The user guidance eventually terminates after these countdowns (red background color).

The appearance of the user view is dependent on the task. Figure 4.16 shows the user view window during sensor calibration. The user is provided with brief descriptions about the task, gets instantaneous visual signal feedback as well as visual clues or stimuli if needed.

Biosignal quantification paradigms are implemented providing both supervisor and user views. They determine user characteristic values reflecting the biosignal control ability of the user and serve as both intra and inter-individual comparators. In general, any kind of input signal (biosignal or non-biosignal) can be subjected to the quantification paradigms. The implemented paradigms are described closely in Section 2.4.3. If needed, multiple paradigm descriptive parameters such as time spans or threshold values are customizable by the supervisor.

Diverse types of virtual environments are implemented enabling the user to practice and improve biosignal control ability. The user controls virtual devices – like agents, cars and tokens – displayed on the screen by means of the intentional biosignal activation and deactivation. Virtual environments encompass both games and simulated rehabilitation aids.

Games provide diversified options for practicing biosignal control. Both Qt-native games as well as third-party games are supported. The supervisor sets the controls, visualization options and various game-related parameters. Figure 4.17 depicts user views of Qt-native games.

The Coins game, as illustrated in Figure 4.17a, is a two-dimensional animation presenting a simplified avatar from the aerial perspective that features an arrow as the visual indicator for the current forward direction. The avatar navigates freely within the area of bounded horizontal and vertical elongation.

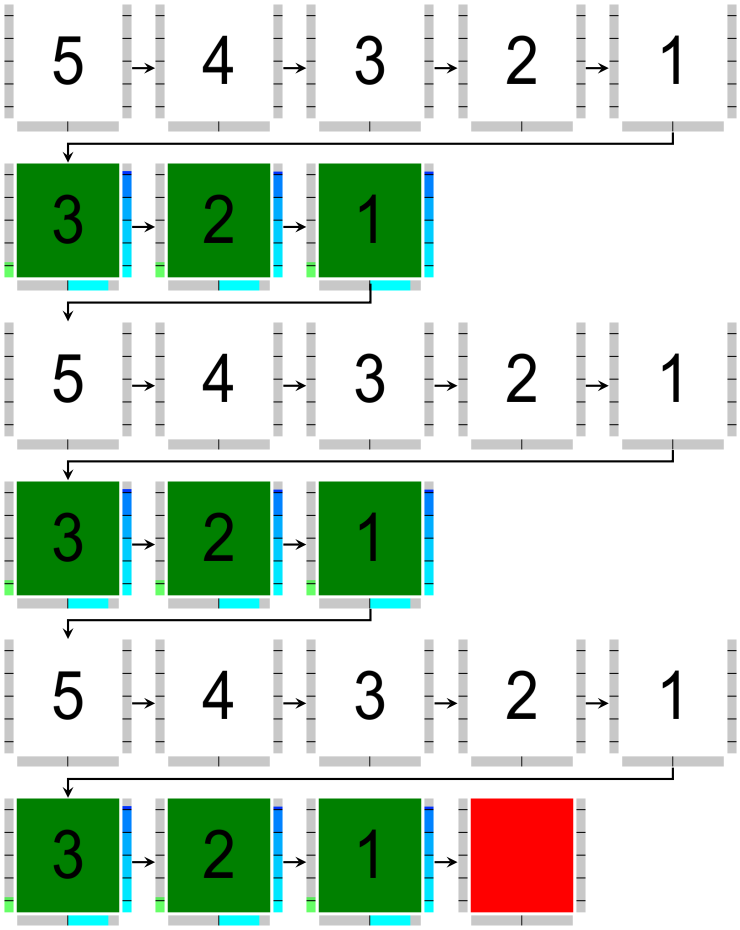

Figure 4.15: User guidance during sensor calibration including low-level activity phases (bright background color), high-level activity phases (green background color) and termination (red background color)

The objective is to reach all coins that are randomly spread across the area as fast as possible. As the avatar reaches one coin, the very next coin that is to be reached appears somewhere in the area.

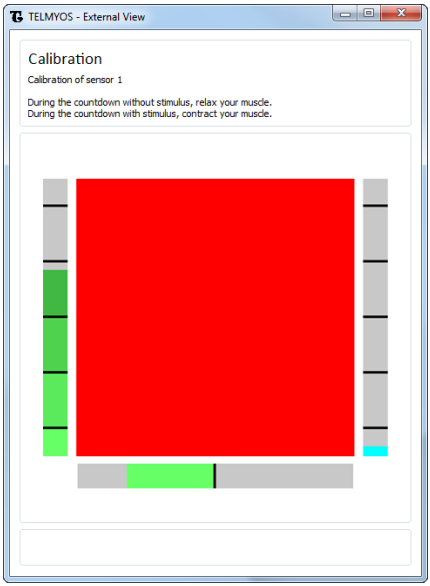

Figure 4.16: User view window during calibration of sensor 1

The Parkour game is depicted in Figure 4.17b. Alike the Coins game, it is a two-dimensional animation with a simplified avatar from the aerial perspective. It is an obstacle course and the objective is to reach the finish area as fast as possible, beginning from the starting area where the avatar spawns. Both, the Coins and the Parkour game demand a decent level of spatial thinking.

Figure 4.17c shows the Race game. A simplified car serves as an avatar. The user is able to control merely the horizontal position of the avatar. The track moves on (vertically from top to bottom) at constant time intervals creating the illusion of driving the car forward. The street is represented with straight lines and arcs of distinct degrees. The street is of varying width. The middle line of the street stands for the ideal path along the track. The objective is to follow the ideal path as close as possible.

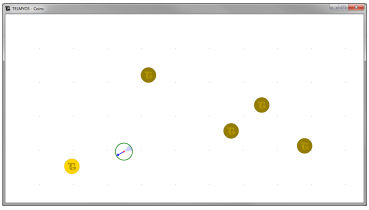

(a) Coins game: Top-view avatar is navigated to reach the next highlighted coin

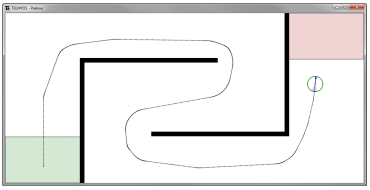

(b) Parkour game: Top-view avatar is navigated through the obstacle course from start area to finish area

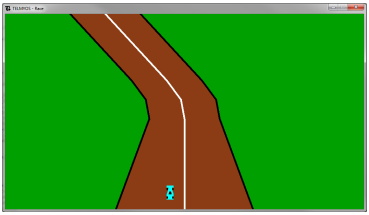

(c) Race game: Avatar is controlled one-dimensionally (left resp. right-hand side) to meet the road's middle line

(d) Tetris game: Descending tokens are controlled in position and orientation to achieve a gapless merging

Figure 4.17: User views of various Qt-native games

The Tetris game, as depicted in Figure 4.17d, follows the game mechanics of classic Tetris. The objective is to achieve an as high as possible accumulated score where each removed line is awarded with points.

The third-party game interface enables the user to play third-party games by means of biosignals normally controlled by peripheral equipment, some of which are keyboards or computer mice. Keyboard presses or mouse clicks are emulated by the GUI as a function of the biosignal input.

Figure 4.18 shows the customizable interface for third-party applications. The emulated key press (e.g., left cursor, space or any other key press) for the single and combined activation of input modalities' i are specified by

the supervisor. Also, the thresholds for detecting the modalities' activation are set. Emulated mouse movements can be restricted either to the vertical or to the horizontal axis and the emulated mouse movement's sensitivity is set. The software clutch that can be engaged or disengaged by the supervisor ensures the acquired biosignals are only translated into control signals and transferred to the third-party game at the supervisor's wish.

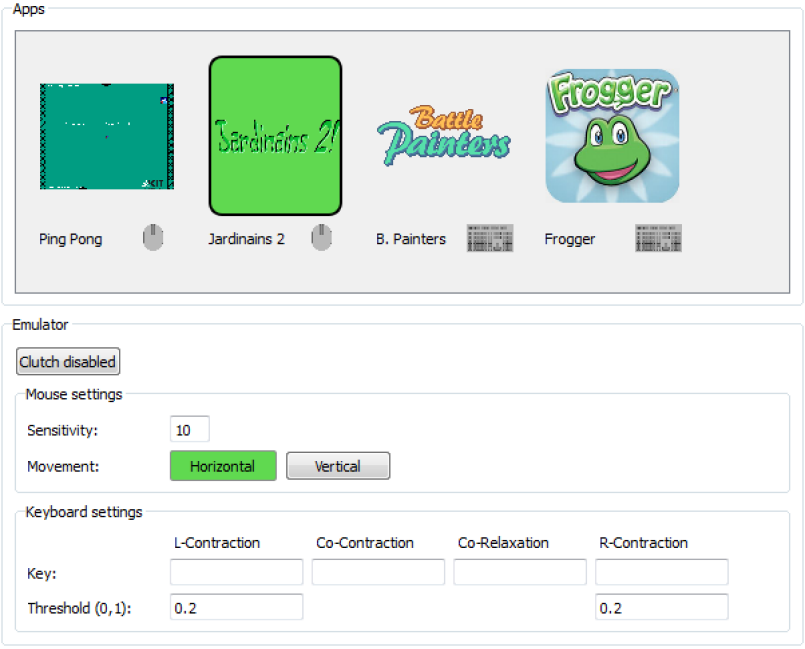

Figure 4.18: Third-party games interface

In general, browser games of any kind are supported. However, in case of mouse-controlled browser games the area of valid mouse positions is not restricted. This could cause problems in game handling. Games based on the application programming interface (API) open graphics library (OpenGL) are generally supported. Microsoft's DirectX including DirectInput is currently not supported.

The three-dimensional simulation of an electric-powered wheelchair (EPW) was developed and implemented under academic supervision in the scope of an internship [3]. The user view is depicted in Figure 4.19a. The physical attributes (e.g., mass, acceleration or deceleration) of the simulated EPW can be specified by the supervisor to match the physical attributes of a real electric-powered wheelchair. The three-dimensional visual appearance together with the simulation of the physical attributes induces a high level of user immersion. The supervisor sets a control signal generator that is suitable of the user and that is preferred by the user. The user navigates the simulated wheelchair freely within the virtual environment. If needed, all acquired biosignals, generated control signals and parameters can be logged for documentation and offline analysis. Obstacle collision detection is also implemented.

The virtual hand prosthesis Michelangelo is a three-dimensional model of a real prosthesis by OttoBock developed by the Department for Neurorehabilitation Engineering at University Medical Center Göttingen. Figure 4.19b shows the user view. The interface for biosignal control was realized with the aid of user datagram protocol (UDP). Based on finite state machine (FSM) implementations, the virtual hand prosthesis performs movements such as hand opening and closing as well as hand rotation.

Both simulations serve as three-dimensional virtual realities (VRs) that help to accustom the user to the real rehabilitation aids.

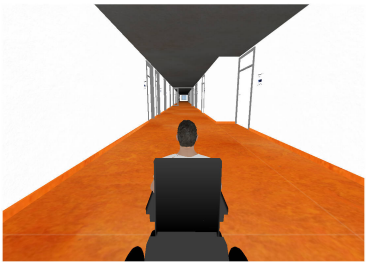

(a) Electric-powered wheelchair simulation

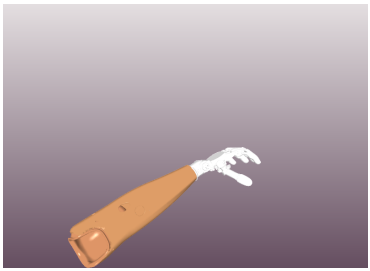

(b) Hand prosthesis simulation Michelangelo

Figure 4.19: Virtual realities of rehabilitation equipment

The user's biosignals and any other kind of signal generated during run time can be recorded and exported as ASCII text files by means of export functionalities. The file extension is *.tss which refers to time series. Exported tss-files are used for offline analysis, such as Mathwork's Matlab, Microsoft's Excel, Gait-CAD[8] [132], or documentation.

Control signals are transmitted to real rehabilitation aids such as EPWs. Real-time data output is realized via the computer's standard serial port USB applying Qt's native class QSerialPort.

The GUI is used by healthcare professionals at the department for Clinical Neurophysiology at University Medical Center Göttingen.

The user assessment paradigms (cf. Section 2.4.3) are implemented in the paradigms tab (cf. Figure 4.12b). The supervisor manually determines settings such as the lower and upper thresholds as well as the time parameters.

The response time assessment paradigm guides the user according to the scheme depicted in Figure 4.20.

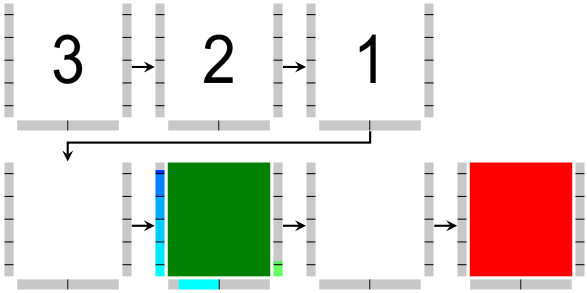

Figure 4.20: User guidance during response time assessment

After counting down three seconds of preparation, the user is prompted to deactivate the biosignal (bright background color) – like relaxing the muscle – for a pseudo-randomized time, composed of a constant time

[8] `http://sourceforge.net/projects/gait-cad`

together with a random time. Then, the user view displays a visual stimulus (green background color) cueing the user to activate the biosignal – like contracting the muscle – as soon as possible. The visual stimulus is displayed for the constant time. Eventually, the visual stimulus is hidden again notifying the user to deactivate the biosignal – such as relaxing the muscle – as soon as possible. Finally, a constant time terminates the paradigm.

After each of the paradigms is completed, its results are presented both to the supervisor and to the user as depicted exemplarily for the response time assessment paradigm in Figure 4.21.

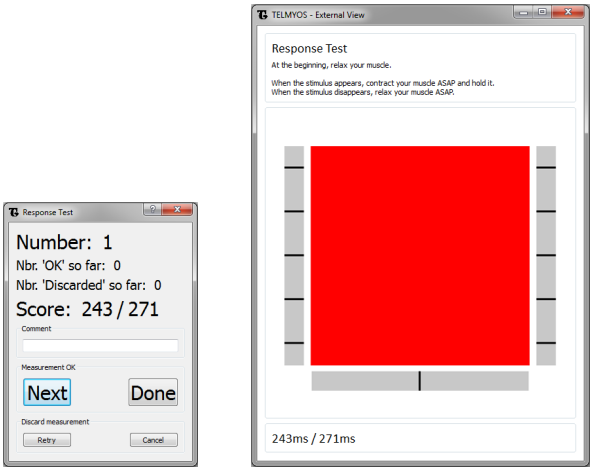

(a) Supervisor view (repeat dialog)

(b) User view

Figure 4.21: Result presentation after completion of the response time assessment paradigm

The results are the response time for activation $\delta_{\mathrm{ra}} = 243$ ms and the response time for deactivation $\delta_{\mathrm{rd}} = 271$ ms. In the repeat dialog, as shown in Figure 4.21a, the supervisor is provided with options to label the recorded tss-file of the trial positively (valid trial) or negatively (invalid trial). One session of the same paradigm may consist of several trials and

can be continued or discontinued by the supervisor. It is also possible to write comments (e.g., documentation of special facts) that are then saved within the tss-file.

The implementations of the supervisor view of the paradigms are depicted in Figures A.22 - A.26 of the Appendix A.11.

Figure 4.22 shows the “navi monitor”, that is, a visualization means of the translational velocity and the rotation angle of a vehicle, for example, a navigation avatar or wheelchair. The length of the arrow represents the translational velocity while the direction (originating in the center) stands for the rotation angle. The navi monitor is useful to get a better understanding of the cause-and-effect relation between the biosignals and the actions performed by navigation avatar or wheelchair.

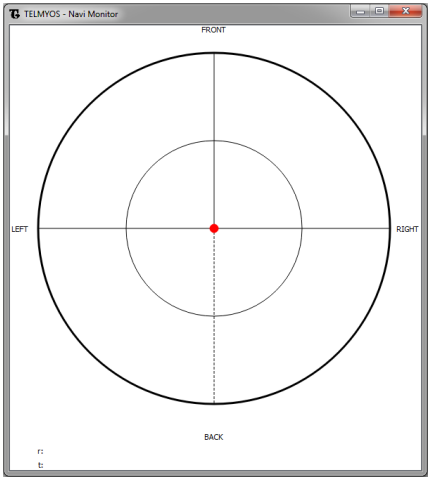

Figure 4.22: Navi monitor in case of idle state (i.e., translational velocity is zero)

4.6 Electric-Powered Wheelchair Interface

The digital-to-analog converter (DAC) (cf. Section 3.7) receives control signals from the GUI and generates corresponding analog signals in compliance with the specifications of the electric-powered wheelchair (EPW). Eventually, these analog signals get interpreted by the wheelchair and lead to actual movements.

In addition, special functions that are natively available by the wheelchair, such as the enabling and disabling of the horn, the headlights and the direction indicators (left and right) were implemented, directly looped through the GUI.

An emergency stop was also realized. The implementation of the emergency stop comprises, firstly, the transmission of an idle-command to the wheelchair with the result that the wheelchair immediately stops and, secondly, the decoupling of GUI and the wheelchair (software clutch). Among others, the supervisor can manually trigger the emergency stop.

5 Results

5.1 Overview

The adaptive human-machine interface based on ear muscle input signals, as introduced in this work, is being assessed. The results are presented in this chapter. The assessments relate to distinct aspects of the HMI. Some do not involve any user while some involve users ranging from able-bodied to physically handicapped.

The assessment of the proposed difference models (cf. Section 3.5.3) is presented in Section 5.2 of this chapter. Criteria for an ideal difference signal are postulated. The difference models receive made-up benchmark signals that reflect real use scenarios. The difference signals are qualitatively examined with regard to the postulated criteria.

The *inter*-trial parameter adaptation (cf. Section 3.5.4) is analyzed in Section 5.3. By means of forearms muscle signals, users complete trials of a virtual task. Between the trials, new parameter values are algorithmically generated. The assessment of this method's quality is carried out in regard to the accomplished time and accuracy.

The examination of the *intra*-trial parameter adaptation (cf. Section 3.5.5) is presented in Section 5.4. With inappropriately preset parameter values, the user performs a virtual task controlled by forearms muscle signals. During task completion, new parameter values are algorithmically generated. The method's ability to adapt the parameter values stepwise towards more suitable values based on the user performance is examined.

Some of the parameter adaptation methods proposed in this work compile different schemes of parameter adaptation. These schemes are compared in a study with 20 subjects in Section 5.5. The subjects perform virtual tasks by means of the forearm muscle signals.

Aiming at the development of a HMI accessible for head-only activities, able-bodied users performed the training of the ear muscles, as presented in Section 5.6. The users performed virtual tasks and navigated an electric-powered wheelchair.

Physically handicapped subjects belong to the target group of this work's development of a HMI (cf. Section 3.2). The training of the ear muscles with the aid of virtual tasks and EPW navigation is presented in Section 5.7.

5.2 Assessment of Difference Models for Crosstalk Compensation with Benchmark Signals

The open-loop bimodal calibration methods (cf. Sections 3.5.2, 3.5.3) aim at compensating for crosstalk and generating an appropriate difference signal.

These methods represent distinct difference models. In the application phase they receive two normalized signals (inputs) acquired from the user and generate one difference signal (output). In the adaptation phase, these difference models need to get calibrated in order to meet the characteristics of the individual user.

The difference models were experimentally assessed with the aid of benchmark signals that were designed using Matlab. These benchmark signals are the calibration signals and input signals.

The difference signal ideally meets the desired properties (des. prop.):

#1) smoothness and homogeneousness,

#2) flatness at value zero (flatline, idle state),

#3) full range coverage $[-1, 1]$ spanned by the two user-specific calibration settings, and

#4) boundary by -1 resp. $+1$ at the two user-specific calibration settings.

The benchmark signals of both the adaptation phase (two calibration signals) and the application phase (two evaluation signals) serve as representatives of the actual biosignals of the users. The conjunction of distinct calibration signals together with various evaluation signals is about to assess how the difference models cope with diverse situations.

Figure 5.1 exemplarily depicts a specific design of the two calibration signals: Normalized signals ($x_{\mathrm{n},1}[k]$ and $x_{\mathrm{n},2}[k]$) for two calibration settings. These normalized signals represent the calibration settings of a notional – exemplary and made-up – user.

l) On the left-hand side, a first calibration setting represents the user intention "navigating sharp left" (time indices 1-100). In the first calibration setting there is no presence of crosstalk, meaning $x_{\mathrm{n},1}[k] = 1 \ \wedge \ x_{\mathrm{n},2}[k] = 0$.

r) On the right-hand side, a second calibration setting stands for the user intention "navigating sharp right" (time indices 101-200). In the second calibration setting crosstalk is apparent, meaning $x_{\mathrm{n},1}[k] = 0.8 \ \wedge \ x_{\mathrm{n},2}[k] = 1$.

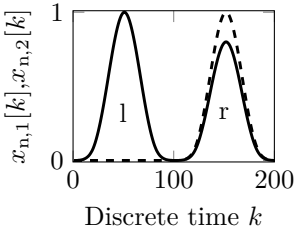

Figure 5.1: Benchmark calibration signals: Exemplary, normalized signals $x_{\mathrm{n},1}[k]$ (——) and $x_{\mathrm{n},2}[k]$ (- - -) making up two calibration settings, namely "navigating sharp left" and "navigating sharp right"

The exemplary benchmark evaluation settings are illustrated in Figure 5.2. They are constituted by two input signals – normalized signals ($x_{\mathrm{n},1}[k]$ and $x_{\mathrm{n},2}[k]$) that are designed with Matlab. Seven combinations of benchmark input signals represent distinct situations (evaluation settings) that are being evaluated. These include

i) $x_{\mathrm{n},1}[k] = 1 \ \wedge \ x_{\mathrm{n},2}[k] = 0$ (time indices 1-100) representing ideal "navigating sharp left" without any crosstalk,

ii) $x_{\mathrm{n},1}[k] = 1 \ \wedge \ x_{\mathrm{n},2}[k] = 0.2$ (time indices 101-200),

iii) $x_{\mathrm{n},1}[k] = 1 \ \wedge \ x_{\mathrm{n},2}[k] = 0.8$ (time indices 201-300),

iv) $x_{\mathrm{n},1}[k] = x_{\mathrm{n},2}[k] = 1$ (time indices 301-400) standing for ideal "straightforward" without crosstalk,

v) $x_{\mathrm{n},1}[k] = 0.8 \ \wedge \ x_{\mathrm{n},2}[k] = 1$ (time indices 401-500),

vi) $x_{\mathrm{n},1}[k] = 0.2 \ \wedge \ x_{\mathrm{n},2}[k] = 1$ (time indices 501-600), and

vii) $x_{\mathrm{n},1}[k] = 0 \ \wedge \ x_{\mathrm{n},2}[k] = 1$ (time indices 601-700) typifying ideal "navigating sharp right" without crosstalk.

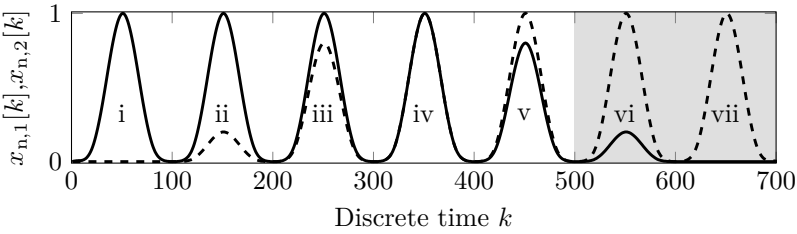

Figure 5.2: Benchmark input signals: Exemplary, normalized signals $x_{\mathrm{n},1}[k]$ (——) and $x_{\mathrm{n},2}[k]$ (- - -) making up seven benchmark evaluation settings. Inaccessible evaluation setting are grayed out.

Considering the benchmark calibration signals of the notional user (cf. Figure 5.1), merely evaluation settings i to v are accessible because of the presence of crosstalk. Thus, the evaluation settings vi and vii are grayed out, insinuating those evaluation settings that remain inaccessible for the notional user. In other words, the notional user is unable to generate input signals for ideal "navigating sharp right" without crosstalk.

For this reason, the optimal difference model is expected to output +1 for evaluation setting i. Due to the presence of crosstalk, the notional user is unable to reach evaluation settings vi and vii. Thus, the ideal "navigating sharp right" without crosstalk is not achievable for the notional

user. Therefore, the optimal difference model is expected to output -1 for evaluation setting v, as that is reachable for the notional user. In between $+1$ at evaluation setting i and -1 at evaluation setting v, for a decent predictability the optimal difference model is expected to generate the value 0 at evaluation setting iii. Moreover, the optimal difference model is expected to yield the value $+0.5$ at evaluation setting ii and -0.5 at evaluation setting iv.

The assessment of the difference models reveals the actual difference signals. They are presented in Figures 5.3 and 5.4. The optimal difference model's output for the accessible evaluation settings i to v is hinted by circle marks. The signals need to be assessed with respect to the aforementioned desired properties of an ideal difference signal.

The difference model V1 generates the difference signal as depicted in Figure 5.3a. It is smooth (des. prop. #1), covers the full range (des. prop. #3) and is bounded (des. prop. #4). However, the flatness is not at value zero. There is an offset along the y-axis. In other words, it does not meet the desired property #2. This difference model outputs a signal suggesting activity when the user actually is idling.

The output signal of difference model V2, illustrated in Figure 5.3b, is flat at value zero (des. prop. #2), covers the full range (des. prop. #3) and is correctly bounded (des. prop. #4). On the downside, the signal is not smooth at time indices 430 and 470. That is, difference model V2 fails regarding the desired property #1. The user will be strongly confused as the generated output around -1 and $+1$ is not homogeneous.

The difference signal of model V2A, presented in Figure 5.3c, is smooth (des. prop. #1), is flat at value zero (des. prop. #2) and respects the desired boundaries (des. prop. #4). Albeit it does not cover the full range, neglecting the desired property #3. This difference model merely generates slight signal amplitude for the fifth evaluation setting (time indices 401-500) and therefore is unable to generate an output standing for "navigating sharp right".

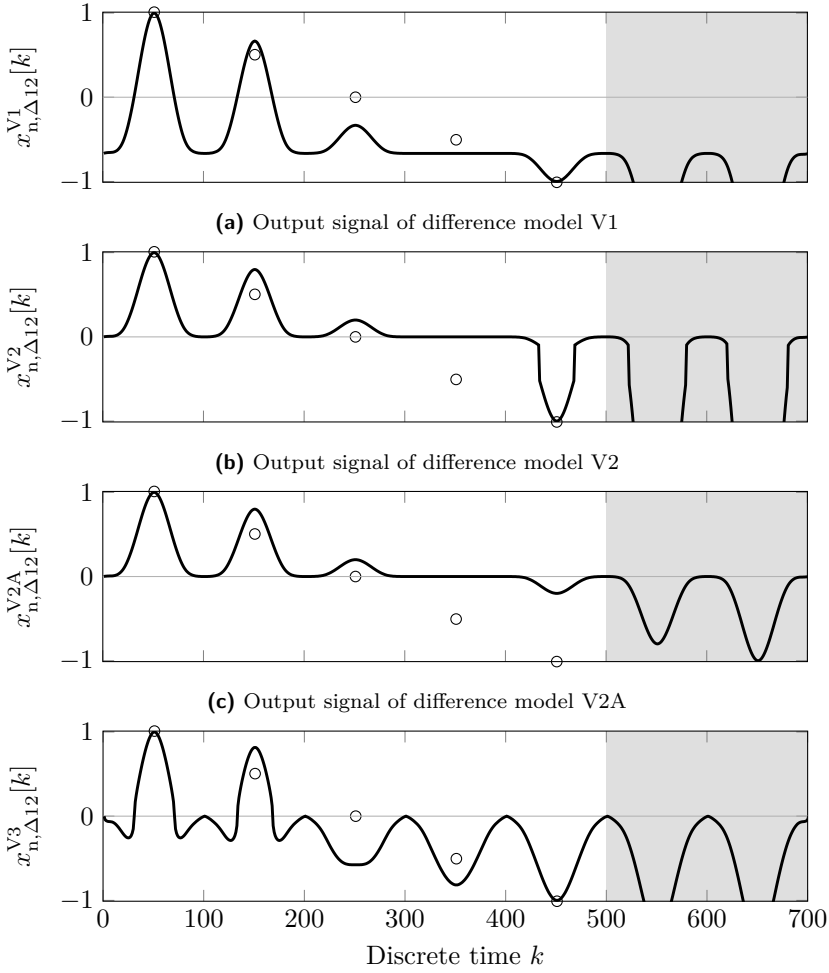

(a) Output signal of difference model V1

(b) Output signal of difference model V2

(c) Output signal of difference model V2A

(d) Output signal of difference model V3

Figure 5.3: Output of models V1, V2, V2A and V3 resulting from evaluation settings i - vii with calibration settings l and r. Inaccessible evaluation settings are grayed out. Optimal output is hinted by circle marks.

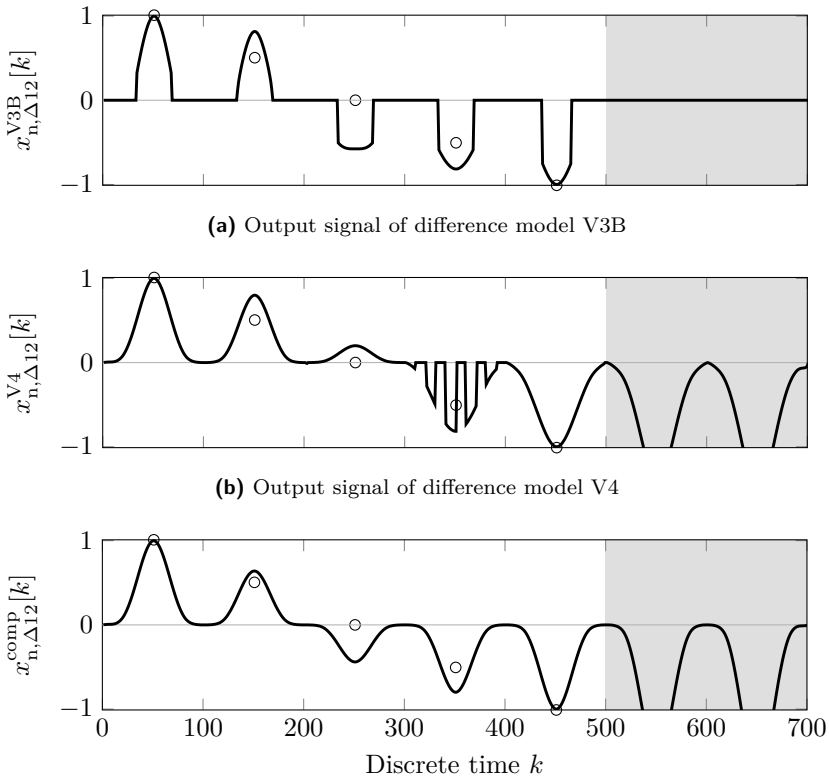

(a) Output signal of difference model V3B

(b) Output signal of difference model V4

(c) Output signal of difference model utilizing linear regression

Figure 5.4: Output of models V3B, V4 and linear regression resulting from evaluation settings i - vii with calibration settings l and r. Inaccessible evaluation settings are grayed out. Optimal output is hinted by circle marks.

The model V3 creates the difference signal, shown in Figure 5.3d. This signal is flat at value zero (des. prop. #2), covers the full range (des. prop. #3) and is correctly bounded (des. prop. #4). But the signal is inhomogeneous: The desired property #1 is neglected. Therefore, it will be challenging for the user to navigate safely.

The difference model V3B yields an output signal, depicted in Figure 5.4a, that is flat at value zero (des. prop. #2), covers the full range (des. prop. #3) and also is bounded as desired (des. prop. #4). However, this signal is not smooth, as it violates the desired property #1. The edges of the signal lead to abrupt changes of the amplitude making the navigation difficult for the user.

The output signal of difference model V4 is shown in Figure 5.4b. It is flat at value zero (des. prop. #2), covers the desired range (des. prop. #3) and is correctly bounded (des. prop. #4). However, it is not smooth and thus does not meet the desired property #1.

Eventually, the model that makes use of linear regression (cf. Section 3.5.2) meets all of the desired properties of an ideal difference signal. That is, the difference signal is smooth and homogeneous, it is flat at value zero, it covers the full range $[-1, 1]$ and it is bounded by -1 resp. $+1$. The optimal output at time index 250 is not reached. This is due to the application of the strictly linear regression to the "asymmetrical" benchmark calibration signals. The signal is illustrated in Figure 5.4c. It is defined in (3.34).

Table 5.1 provides an overview of assessment of the difference models with respect to the desired properties. Only the model with linear regression satisfies all of the properties.

#	Desired Property	V1	V2	V2A	V3	V3B	V4	Linear Regression
1	Smoothness/Homogen.	●	×	●	×	×	×	●
2	Flatness at Zero	×	●	●	●	●	●	●
3	Full Range Coverage	●	●	×	●	●	●	●
4	Boundary	●	●	●	●	●	●	●

Table 5.1: Comparison of difference models with respect to the desired properties ranging from satisfaction (●) to no satisfaction (×)

5.3 Heuristic Inter-Trial Parameter Adaptation with Forearm Muscle Signals

In order to evaluate the heuristic inter-trial parameter adaptation (cf. Section 3.5.4), experiments with two able-bodied subjects (23-year-old male and 28-year-old male) were conducted. The experiments lasted less than one day per subject.

In sequential, non-simulated trials the subjects navigated an avatar within the two-dimensional, virtual Parkour environment (cf. Section 4.5) by means of EMG signals acquired from the left and right forearms with surface electrodes. The subjects sat conveniently on a chair in front of a desktop computer and looked at the monitor where the virtual avatar, controlled by the user's signals, was displayed. The forearms rested conveniently on the table. The subjects were requested to complete specific courses from the start area (bottom left corner) to the finish area (top right corner) by navigating the avatar.

In distinct trials, the subjects needed to fulfill two different tasks representing two constraints. First, the subjects were ought to reach the finish area as fast as possible, as depicted in Figure 5.5. Second, they were requested to reach the finish area while respecting the given, desired trajectory as accurate as possible, as illustrated in Figure 5.6.

After the completion of each run (index r), that is, non-simulated trial, and on the basis of the corresponding recorded EMG signals, the offline heuristic algorithm (cf. Figure 3.11) was executed determining optimal parameter values.

As for the first task with algorithm control option $\mathbf{w}_1^T = (1, 0)$ (cf. (3.52)), that is, looking for the minimal completion time, Figure 5.5 illustrates the setting. Figure 5.5a shows the non-simulated x-y-trajectory of the avatar, meaning, the trajectory that was recorded while the human user was actually navigating the avatar and where the parameters $\mathbf{p}_{\mathrm{HMI},r}$ were utilized. Figure 5.5b depicts the simulated trajectory resulting from the parameter values $\mathbf{p}_{\mathrm{HMI},r,s=3}$, found by the offline heuristic algorithm after three loops of offline simulation, applied to the recorded EMG signals. The parameter values $\mathbf{p}_{\mathrm{HMI},r,s=3}$ are said to be the outcome of the algorithm.

The completion time of the simulated trial is shorter than the completion time of the non-simulated trial. This becomes evident analyzing the simulated trajectory. It ends at the very corner of the finish area instead of at the vertical bound. This indicates that the parameter values found by the offline heuristic algorithm are better suited for achieving optimal trial results. If needed, these parameter values can be applied to the subsequent non-simulated trials.

As for the second task with algorithm control option $\mathbf{w}_2^T = (0, 1)$ (looking for the minimal path deviation) Figure 5.6 shows the setting.

Figure 5.6a presents the recorded trajectory of the non-simulated trial utilizing parameter values $\mathbf{p}_{\mathrm{HMI},r}$. Figure 5.6b shows the simulated x-y-trajectory that is based on the parameters $\mathbf{p}_{\mathrm{HMI},r,s=77}$ determined by the offline heuristic algorithm after 77 simulation loops.

As the iterations of the simulated trials (index $s = 1, ..., \tilde{S}$) proceed, many combinations of parameter values $\mathbf{p}_{\mathrm{HMI},r,s}$ are found and applied to the recorded EMG signals in the distinct simulation loops. For each loop of simulation, the resulting x-y-trajectory is assessed yielding the simulated user performance $Q_{r,s}(\mathbf{p}_{\mathrm{HMI},r,s})$. Some of the combinations of parameter values induce improvements in the simulated user performance while some others yield deteriorations in the simulated user performance.

For the sake of clear and unambiguous depiction, Figure 5.7 does not plot the deteriorated, simulated user performances but rather only the improved, simulated user performances, meaning the envelope of the simulated user performances over all simulations, defined as

$$Q_{\mathrm{impr},r,s} = \max \{Q_{r,s}\} . \tag{5.1}$$

Unless another improved, simulated user performance is achieved by the offline algorithm the previously improved, simulated user performance is conserved and depicted as a horizontal line (cf. Figure 5.7).

As the offline algorithm proceeds with ongoing simulation loops, ever-improving, simulated user performances are achieved.

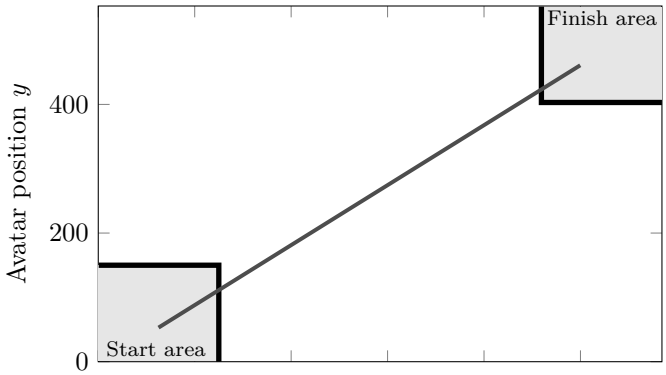

(a) Non-simulated x-y-trajectory based on $\mathbf{p}_{\mathrm{HMI},r}$

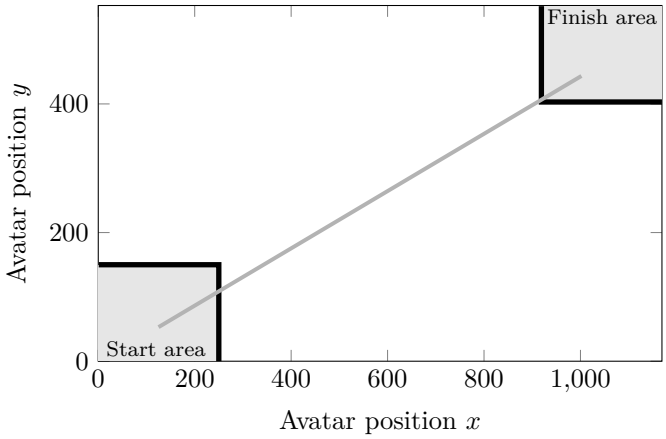

(b) Simulated x-y-trajectory based on $\mathbf{p}_{\mathrm{HMI},r,s=3}$

Figure 5.5: Trial of the Parkour environment with non-simulated (——) and simulated (——) x-y-trajectories of the avatar applying algorithm control option $\mathbf{w}_1^T = (1, 0)$ (i.e., minimal completion time)

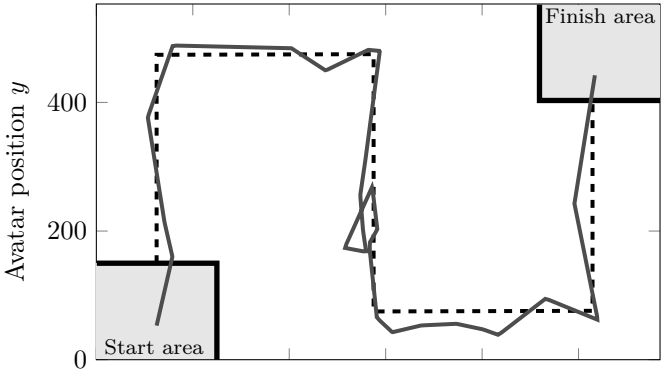

(a) Non-simulated x-y-trajectory based on $\mathbf{p}_{\mathrm{HMI},r}$

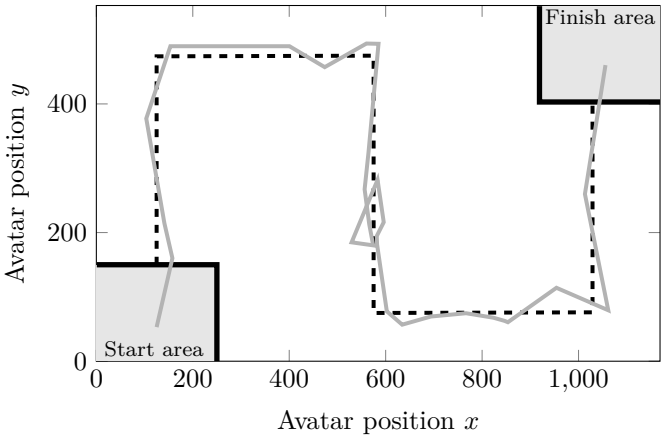

(b) Simulated x-y-trajectory based on $\mathbf{p}_{\mathrm{HMI},r,s=77}$

Figure 5.6: Trial of the Parkour environment with desired (**---**), non-simulated (**——**) and simulated (——) x-y-trajectories of the avatar applying algorithm control option $\mathbf{w}_2^T = (0, 1)$ (i.e., minimal path deviation)

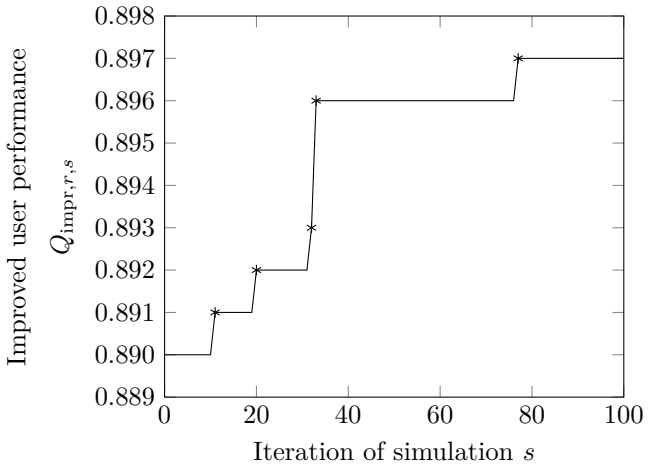

Figure 5.7: Improved simulated user performance over iterations of simulation ($\tilde{S} = 100$)

Starting at the very first simulated user performance $Q_{r,s=1} = 0.890$ that (by design of the algorithm) equals the non-simulated user performance Q_r, the offline algorithm finds step-by-step parameter values leading to improved, simulated user performances.

This reveals that the offline algorithm (cf. Figure 3.11) works as expected. It generates parameter values that in simulation yield better, user performances/results.

Then, the newly determined parameter values were applied to subsequent non-simulated tasks. Significant improvements in the user performances of both subjects could not be found – albeit both subjects mentioned that navigating the avatar within the virtual environment was more comfortable with the newly determined parameter.

5.4 Incremental Intra-Trial Parameter Adaptation with Forearm Muscle Signals

The closed-loop online parameter adaptation (cf. Section 3.5.5) was evaluated in experiments with one able-bodied subject (29 years old male) [209]. Within the Race environment (cf. Section 4.5) the able-bodied subject navigated an avatar by means of forearm EMG signals with surface electrodes. One trial lasted about 30 seconds. The user is called upon to navigate the car that is controlled by the EMG signals as close to the middle line of the road as possible (cf. Figure 4.17c).

In these experiments, inappropriate parameter values were set prior to the trial execution on purpose in order to evaluate the efficacy of the incremental intra-trial parameter adaptation. The aim of this approach was to show the ability of the method to change the parameters from the initial inappropriate values to suitable values step-by-step (i.e., incrementally).

Scenario S1 and Scenario S2 were set up to simulate inappropriate parameter values. In S1 the initial parameter values $x^{\mathrm{S1}}_{\mathrm{f,max},i}[0]$ were set -90% off. That is, they were set too low with respect to those values being considered optimal for the user at that very time determined by the open-loop parameter adaptation $x^{*}_{\mathrm{f,max},i}$ (cf. Section 3.5.1). On the other hand, in S2 the starting parameter values $x^{\mathrm{S2}}_{\mathrm{f,max},i}[0]$ were set +300% off, meaning, too high in regard to $x^{*}_{\mathrm{f,max},i}$. The definitions of the initial parameter values therefore read

$$x^{\mathrm{S1}}_{\mathrm{f,max},i}[0] = 0.1 \cdot x^{*}_{\mathrm{f,max},i}, \text{ and} \tag{5.2}$$

$$x^{\mathrm{S2}}_{\mathrm{f,max},i}[0] = 4 \cdot x^{*}_{\mathrm{f,max},i}. \tag{5.3}$$

In this evaluation, the specific forms (specifically for the Race environment) of the actual value, the desired value and the user performance are applied. The specific actual value, namely $y^{*}_{\mathrm{act}}[k]$ (cf. (3.60)), is represented by the horizontal car position. The horizontal middle line position of the road stands for the specific, desired value $y^{*}_{\mathrm{des}}[k]$. In the specific Race environment context, $\chi[k]$ (cf. (3.64)) is termed car-to-middle-line relation. The specific user performance $Q^{*}[k]$ follows (3.62). The parameter adaptation is carried out incrementally according to (3.63) with the constant increment factor $w = 1.2$.

Figure 5.8 shows the way how the incremental intra-trial adaptation of the parameter $x_{\mathrm{f,max},i}$ works. Starting from the initially and inappropriately set values $x^{\mathrm{S1}}_{\mathrm{f,max},i}[0]$ and $x^{\mathrm{S2}}_{\mathrm{f,max},i}[0]$, respectively, the adaptation determines parameter values better suited to the current situation. The left-hand sides of Figures 5.8a and 5.8b, at discrete time $k = 0$, stand for the settings before the beginning of the trial while the corresponding right-hand sides, at discrete time $k = 3000$, represent the settings after the trial termination. During trial execution (i.e., online), the parameter value gets altered from the inappropriate value towards the desired value. This indicates that the incremental intra-trial parameter adaptation is able to alter user-individual parameter values dynamically coping with non-stationarities in the biosignals.

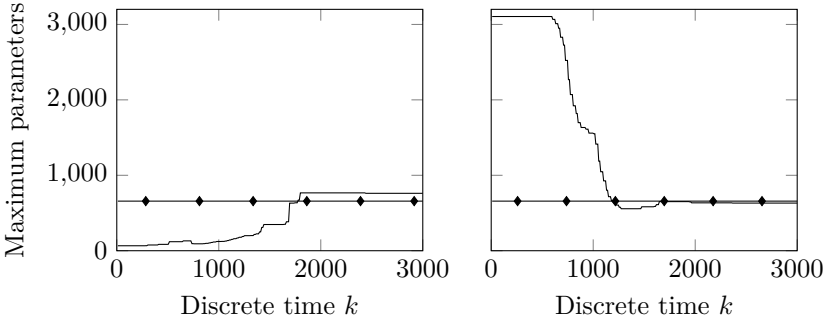

(a) Scenario S1 **(b)** Scenario S2

Figure 5.8: Progression of the incremental parameter adaptation during trial execution with maximum parameters $x^{\mathrm{S1}}_{\mathrm{f,max},i}$ (**(a)**,——) resp. $x^{\mathrm{S2}}_{\mathrm{f,max},i}$ (**(b)**,——) with the corresponding desired values $x^{*}_{\mathrm{f,max},i}$ (–♦–) [209]

In Figure 5.9 the effect of altering $x_{\mathrm{f,max},i}$ on the user performance is demonstrated. Both the current user performance and the average user performance are depicted. The current user performance fluctuates depending on the position of the car with respect to the position of the middle line.

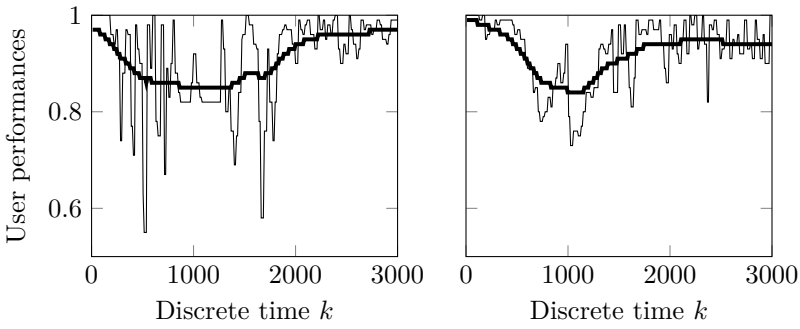

(a) Scenario S1 **(b)** Scenario S2

Figure 5.9: Current user performance $Q[k]$ (——) and average user performance (——) during trial execution [209]

As the car position is initialized at the middle line position the user performance is high at the very beginning of the trial. This must be considered an artifact caused by the initialization of the Race environment. It does not reflect the correct user performance in the initial phase.

The average user performance is determined by zero-phase digital filtering in the forward and reverse direction. Thus, it does not equal one at the very beginning. The average user performance declines after the initial phase since an accurate control using inappropriate parameter values is hard to accomplish. As the user continues the trial execution and the adaptation incrementally alters the parameter values towards appropriate values, the user performance increases gradually.

Figure 5.10 depicts the trajectories of the horizontal car and middle line positions, respectively. In Scenario S1, at first the car overreacts due to the low initial parameter value. Even subtle EMG signals cause heavy control signals and consequently let the car fluctuate a lot.

After a while, the parameter values better suit the user and it becomes easier to navigate the car accurately on the middle line. On the other hand, in Scenario S2 the car reacts too lazy due to the high initial parameter value. Strong EMG signals only result in subtle control signals.

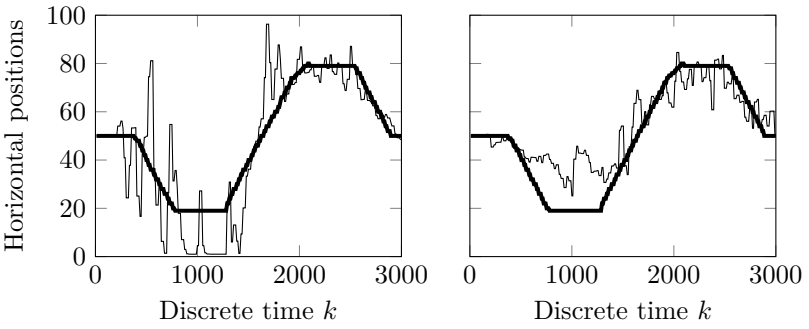

(a) Scenario S1 **(b)** Scenario S2

Figure 5.10: Horizontal car position $y^*_{\text{act}}[k]$ (——) and horizontal middle line position $y^*_{\text{des}}[k]$ (——) during trial execution [209]

The squared and averaged deviation (position error) between the car and middle line positions is depicted in Figure 5.11. The trend of this evaluation measure indicates that in both scenarios the online parameter adaptation makes it easier for the user to steer the car.

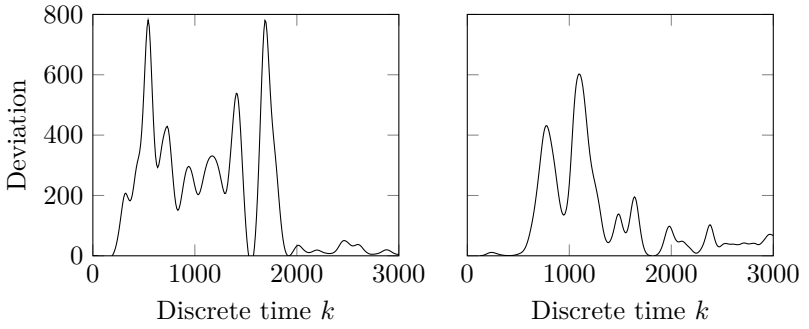

(a) Scenario S1 **(b)** Scenario S2

Figure 5.11: Squared and averaged deviation between car and middle line positions during trial execution [209]

Parameter values that are incorrect or inappropriate due to, for instance, incorrect calibration, can be compensated by this method. It autonomously determines appropriate parameter values meeting the needs of the user. The capability of the incremental intra-trial parameter adaptation to alter user-individual parameter values dynamically was substantiated here with the aid of the Race environment. Generally, this method can be incorporated into diverse environments to provide the users with a variety of experiences. It can be utilized as a more exciting alternative to the open-loop parameter adaptation.

5.5 Empirical Comparison of Parameter Adaptation Methods with Forearm Muscle Signals

A volunteer study was conducted to evaluate the efficacy of the different parameter adaptations developed in this work [166, 213].

Twenty able-bodied subjects participated in the volunteer study. A session of each subject typically lasted a few hours (i.e., less than one day per subject). In the first stage, 12 trials (index $t = 1, ..., 12$) within the Race environment (cf. Section 4.5) were executed by each subject for the actual parameter adaptation. In the second stage, the subjects completed trials within the Virtual Wheelchair environment (cf. Section 4.5) for the subsequent assessment of the parameter adaptation. The virtual avatars in either of the environments were controlled by means of forearm EMG signals with surface electrodes.

Asking for permission to conduct the volunteer study an application for ethical approval was filed [212]. The documents of the application for ethical approval (German language) are provided in Appendix A.10. The Ethical Committee of the Karlsruhe Institute of Technology approved the volunteer study.

The volunteer study's data was statistically evaluated by means of two-sampled Student's t-tests, multiple Student's t-tests with Bonferroni cor-

rection, analyses of variance (ANOVAs) and Pearson product-moment correlation coefficients (PCCs).

In the remainder of this section the significance of p-values is denoted according to [213]

$$p = \begin{cases} p^{***} & \text{, if } p \leq 0.001 \\ p^{**} & \text{, if } p \leq 0.005 \\ p^{*} & \text{, if } p \leq 0.05 \end{cases}. \tag{5.4}$$

Four parameter adaptation methods were compared. The total number of subjects was equally divided over the four adaptation methods. Consequently, four test groups (A, B, C and D) of subjects were acquired, namely

A. one-size-fits-all parameterization group (5 subjects),

B. initial calibration group (5 subjects),

C. inter-trial calibration (offline recalibration) group (5 subjects), and

D. intra-trial calibration (online recalibration) group (5 subjects).

The subjects were briefly informed of the existence of the differing test groups. However, in order to preserve the subjects' unbiased approach the explicit differences between the test groups were not revealed (blinded study design).

As human users naturally can be considered as adaptive systems (cf. Section 1.5.1), the interaction of human users and parameter adaptation in test groups B, C and D are co-adaptive systems.

Test group A (one-size-fits-all parameterization) did not utilize any parameter adaptation and served as a control group. The fixed parameter values were estimated based on prior experience and manually set to

$$x_{\mathrm{f,min},t,i} = 20, \text{ and} \tag{5.5}$$

$$x_{\mathrm{f,max},t,i} = 280. \tag{5.6}$$

Test group B (initial calibration group) made use of the open-loop sensor calibration (cf. Section 3.5.1) once, prior to the first trial execution, yielding

$x^*_{\mathrm{f,min},1,i}$ and $x^*_{\mathrm{f,max},1,i}$. These parameter values were not changed after the initial determination, but rather they were applied as fixed values throughout all trials according to

$$x_{\mathrm{f,min},t,i} = x^*_{\mathrm{f,min},1,i}, \text{ and} \tag{5.7}$$

$$x_{\mathrm{f,max},t,i} = x^*_{\mathrm{f,max},1,i}. \tag{5.8}$$

Test group C (inter-trial calibration group) performed the open-loop sensor calibration (cf. Section 3.5.1) repeatedly, prior to the each trial execution yielding $x^*_{\mathrm{f,min},t,i}$ and $x^*_{\mathrm{f,max},t,i}$. Accordingly the distinct values for the Trials 1 to 12 are defined as

$$x_{\mathrm{f,min},t,i} = x^*_{\mathrm{f,min},t,i}, \text{ and} \tag{5.9}$$

$$x_{\mathrm{f,max},t,i} = x^*_{\mathrm{f,max},t,i}. \tag{5.10}$$

Test group D (intra-trial calibration group) applied the open-loop sensor calibration (cf. Section 3.5.1) once, prior to the first trial execution. In addition, the closed-loop online parameter adaptation (cf. Section 3.5.5) was performed during the trials. The incremental parameter adaptation is defined as

$$x_{\mathrm{f,min},t,i} = x^*_{\mathrm{f,min},1,i}, \text{ together with} \tag{5.11}$$

(3.65) where

$$x_{\mathrm{f,max},i}[k] \equiv x^*_{\mathrm{f,max},1,i}[k], \text{ and} \tag{5.12}$$

$$x_{\mathrm{f,max},i}[k-1] \equiv x^*_{\mathrm{f,max},1,i}[k-1]. \tag{5.13}$$

Table 5.2 provides an overview of the applied parameter values over Trials 1 to 12.

Trial t	Input i	A	B	C	D
1	1	(20,280)	$(x^*_{\text{f,min},1,1}, x^*_{\text{f,max},1,1})$	$(x^*_{\text{f,min},1,1}, x^*_{\text{f,max},1,1})$	$(x^*_{\text{f,min},1,1}, x^{\gamma=1}_{\text{f,max},1,1}[k])$
	2	(20,280)	$(x^*_{\text{f,min},1,2}, x^*_{\text{f,max},1,2})$	$(x^*_{\text{f,min},1,2}, x^*_{\text{f,max},1,2})$	$(x^*_{\text{f,min},1,2}, x^{\gamma=1}_{\text{f,max},1,2}[k])$
2	1	(20,280)	$(x^*_{\text{f,min},1,1}, x^*_{\text{f,max},1,1})$	$(x^*_{\text{f,min},2,1}, x^*_{\text{f,max},2,1})$	$(x^*_{\text{f,min},1,1}, x^{\gamma=.86}_{\text{f,max},1,1}[k])$
	2	(20,280)	$(x^*_{\text{f,min},1,2}, x^*_{\text{f,max},1,2})$	$(x^*_{\text{f,min},2,2}, x^*_{\text{f,max},2,2})$	$(x^*_{\text{f,min},1,2}, x^{\gamma=.86}_{\text{f,max},1,2}[k])$
3	1	(20,280)	$(x^*_{\text{f,min},1,1}, x^*_{\text{f,max},1,1})$	$(x^*_{\text{f,min},3,1}, x^*_{\text{f,max},3,1})$	$(x^*_{\text{f,min},1,1}, x^{\gamma=.72}_{\text{f,max},1,1}[k])$
	2	(20,280)	$(x^*_{\text{f,min},1,2}, x^*_{\text{f,max},1,2})$	$(x^*_{\text{f,min},3,2}, x^*_{\text{f,max},3,2})$	$(x^*_{\text{f,min},1,2}, x^{\gamma=.72}_{\text{f,max},1,2}[k])$
4	1	(20,280)	$(x^*_{\text{f,min},1,1}, x^*_{\text{f,max},1,1})$	$(x^*_{\text{f,min},4,1}, x^*_{\text{f,max},4,1})$	$(x^*_{\text{f,min},1,1}, x^{\gamma=.58}_{\text{f,max},1,1}[k])$
	2	(20,280)	$(x^*_{\text{f,min},1,2}, x^*_{\text{f,max},1,2})$	$(x^*_{\text{f,min},4,2}, x^*_{\text{f,max},4,2})$	$(x^*_{\text{f,min},1,2}, x^{\gamma=.58}_{\text{f,max},1,2}[k])$
5	1	(20,280)	$(x^*_{\text{f,min},1,1}, x^*_{\text{f,max},1,1})$	$(x^*_{\text{f,min},5,1}, x^*_{\text{f,max},5,1})$	$(x^*_{\text{f,min},1,1}, x^{\gamma=.44}_{\text{f,max},1,1}[k])$
	2	(20,280)	$(x^*_{\text{f,min},1,2}, x^*_{\text{f,max},1,2})$	$(x^*_{\text{f,min},5,2}, x^*_{\text{f,max},5,2})$	$(x^*_{\text{f,min},1,2}, x^{\gamma=.44}_{\text{f,max},1,2}[k])$
6	1	(20,280)	$(x^*_{\text{f,min},1,1}, x^*_{\text{f,max},1,1})$	$(x^*_{\text{f,min},6,1}, x^*_{\text{f,max},6,1})$	$(x^*_{\text{f,min},1,1}, x^{\gamma=.30}_{\text{f,max},1,1}[k])$
	2	(20,280)	$(x^*_{\text{f,min},1,2}, x^*_{\text{f,max},1,2})$	$(x^*_{\text{f,min},6,2}, x^*_{\text{f,max},6,2})$	$(x^*_{\text{f,min},1,2}, x^{\gamma=.30}_{\text{f,max},1,2}[k])$
7	1	(20,280)	$(x^*_{\text{f,min},1,1}, x^*_{\text{f,max},1,1})$	$(x^*_{\text{f,min},7,1}, x^*_{\text{f,max},7,1})$	$(x^*_{\text{f,min},1,1}, x^{\gamma=.16}_{\text{f,max},1,1}[k])$
	2	(20,280)	$(x^*_{\text{f,min},1,2}, x^*_{\text{f,max},1,2})$	$(x^*_{\text{f,min},7,2}, x^*_{\text{f,max},7,2})$	$(x^*_{\text{f,min},1,2}, x^{\gamma=.16}_{\text{f,max},1,2}[k])$
8	1	(20,280)	$(x^*_{\text{f,min},1,1}, x^*_{\text{f,max},1,1})$	$(x^*_{\text{f,min},8,1}, x^*_{\text{f,max},8,1})$	$(x^*_{\text{f,min},1,1}, x^{\gamma=0}_{\text{f,max},1,1}[k])$
	2	(20,280)	$(x^*_{\text{f,min},1,2}, x^*_{\text{f,max},1,2})$	$(x^*_{\text{f,min},8,2}, x^*_{\text{f,max},8,2})$	$(x^*_{\text{f,min},1,2}, x^{\gamma=0}_{\text{f,max},1,2}[k])$
9	1	(20,280)	$(x^*_{\text{f,min},1,1}, x^*_{\text{f,max},1,1})$	$(x^*_{\text{f,min},9,1}, x^*_{\text{f,max},9,1})$	$(x^*_{\text{f,min},1,1}, x^{\gamma=0}_{\text{f,max},1,1}[k])$
	2	(20,280)	$(x^*_{\text{f,min},1,2}, x^*_{\text{f,max},1,2})$	$(x^*_{\text{f,min},9,2}, x^*_{\text{f,max},9,2})$	$(x^*_{\text{f,min},1,2}, x^{\gamma=0}_{\text{f,max},1,2}[k])$
10	1	(20,280)	$(x^*_{\text{f,min},1,1}, x^*_{\text{f,max},1,1})$	$(x^*_{\text{f,min},10,1}, x^*_{\text{f,max},10,1})$	$(x^*_{\text{f,min},1,1}, x^{\gamma=0}_{\text{f,max},1,1}[k])$
	2	(20,280)	$(x^*_{\text{f,min},1,2}, x^*_{\text{f,max},1,2})$	$(x^*_{\text{f,min},10,2}, x^*_{\text{f,max},10,2})$	$(x^*_{\text{f,min},1,2}, x^{\gamma=0}_{\text{f,max},1,2}[k])$
11	1	(20,280)	$(x^*_{\text{f,min},1,1}, x^*_{\text{f,max},1,1})$	$(x^*_{\text{f,min},11,1}, x^*_{\text{f,max},11,1})$	$(x^*_{\text{f,min},1,1}, x^{\gamma=0}_{\text{f,max},1,1}[k])$
	2	(20,280)	$(x^*_{\text{f,min},1,2}, x^*_{\text{f,max},1,2})$	$(x^*_{\text{f,min},11,2}, x^*_{\text{f,max},11,2})$	$(x^*_{\text{f,min},1,2}, x^{\gamma=0}_{\text{f,max},1,2}[k])$
12	1	(20,280)	$(x^*_{\text{f,min},1,1}, x^*_{\text{f,max},1,1})$	$(x^*_{\text{f,min},12,1}, x^*_{\text{f,max},12,1})$	$(x^*_{\text{f,min},1,1}, x^{\gamma=0}_{\text{f,max},1,1}[k])$
	2	(20,280)	$(x^*_{\text{f,min},1,2}, x^*_{\text{f,max},1,2})$	$(x^*_{\text{f,min},12,2}, x^*_{\text{f,max},12,2})$	$(x^*_{\text{f,min},1,2}, x^{\gamma=0}_{\text{f,max},1,2}[k])$

Table 5.2: Schedule of the parameter adaptation methods with corresponding parameter values over Trials 1 to 12 (modified from [213])

Figure 5.12 shows the progress of the user performances (cf. (3.68)) over Trials 1 to 12 with corresponding standard deviations (cf. (3.69)).

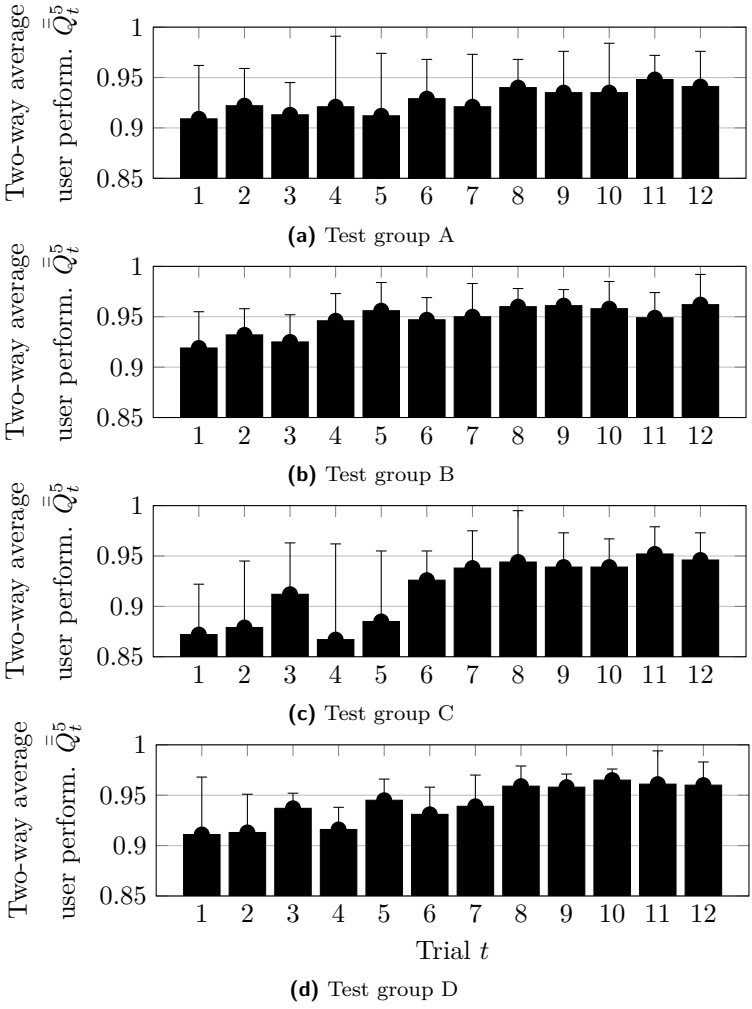

(a) Test group A

(b) Test group B

(c) Test group C

(d) Test group D

Figure 5.12: User performances $\bar{\bar{Q}}_t^5$ with standard deviations σ_t^5 over Trials 1 to 12 of the test groups A to D in Race environment ($\tilde{U} = 5$) [213]

Figure 5.12a illustrates the user performance $\bar{\bar{Q}}_t^5$ of the five subjects belonging to test group A. The very first value reads $\bar{\bar{Q}}_1^5 = 0.909$ while the final value equals $\bar{\bar{Q}}_{12}^5 = 0.941$. Thus, a moderate and linear improvement is visible. The mean of standard deviations is $\bar{\sigma}^{5,12} = 0.044$.

Figure 5.12b shows the progress in $\bar{\bar{Q}}_t^5$ of test group B subjects. The value of Trial 1 equals $\bar{\bar{Q}}_1^5 = 0.919$ and the value of Trail 12 results is $\bar{\bar{Q}}_{12}^5 = 0.962$. A decent improvement in the Trials 1 to 5 but stagnation in the remaining trials is indicated. The standard deviation mean is $\bar{\sigma}^{5,12} = 0.026$. This is less than the standard deviation mean of test group A.

Figure 5.12c presents the result of test group C. The initial trial yields $\bar{\bar{Q}}_1^5 = 0.872$. The final trial's value is $\bar{\bar{Q}}_{12}^5 = 0.946$. The standard deviation mean results in $\bar{\sigma}^{5,12} = 0.047$. Notionally, the user performance values $\bar{\bar{Q}}_1^5$ of test groups B and C are expected to be the same due to the identical initial procedure. In practice, these values are not equal because of user individual variations.

Figure 5.12d depicts the outcome of test group D. Initially, the value equals $\bar{\bar{Q}}_1^5 = 0.911$. After Trial 12 the value reads $\bar{\bar{Q}}_{12}^5 = 0.960$. The mean of the standard deviations is $\bar{\sigma}^{5,12} = 0.026$.

The two-way average user performances $\bar{\bar{Q}}_t^5$ of each of the test groups A to D feature an increasing trend (cf. Figures 5.12a - 5.12d).

The user performances $\bar{\bar{Q}}_t^{20}$ are depicted in Figure 5.13.

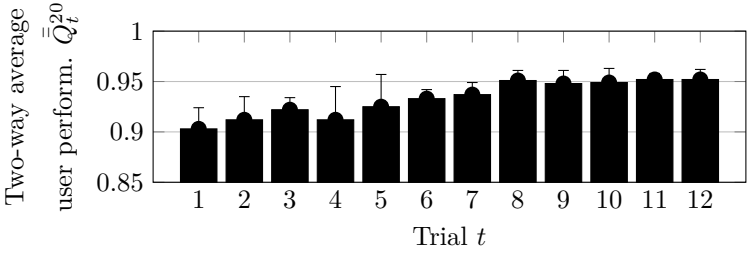

Figure 5.13: User performances $\bar{\bar{Q}}_t^{20}$ with standard deviations σ_t^{20} over Trials 1 to 12 of all test groups in Race environment ($\tilde{U} = 20$) [213]

The two-way average user performance $\bar{\bar{Q}}_t^{20}$ represents the average over all test groups. The initial user performance value is $\bar{\bar{Q}}_1^{20} = 0.903$ and the final value yields $\bar{\bar{Q}}_{12}^{20} = 0.952$. The standard deviation mean is $\bar{\sigma}^{20,12} = 0.016$. An ANOVA test of $\bar{\bar{Q}}_t^{20}$ reveals a p-value of $p = 0.001^{***}$ and a Student's t-test leads to $p = 0.005^{**}$. Thus, the improvement in $\bar{\bar{Q}}_t^{20}$ is statistically significant.

The correlation coefficient is $R = 0.955$ with a p-value of $p = 0.000^{***}$. This result suggests a strong correlation between the number of trials and the user performance. Thus, with increasing experience the user generally improves. This is in turn reflected in increasing user performance [128, 213].

It suggests an overall increasing trend. This emphasizes that training in the virtual Race environment naturally causes positive trends in the user performance.

Figure 5.14 illustrates a comparison between the test groups by means of second-order polynomials fitting the user performances in the least-squares sense.

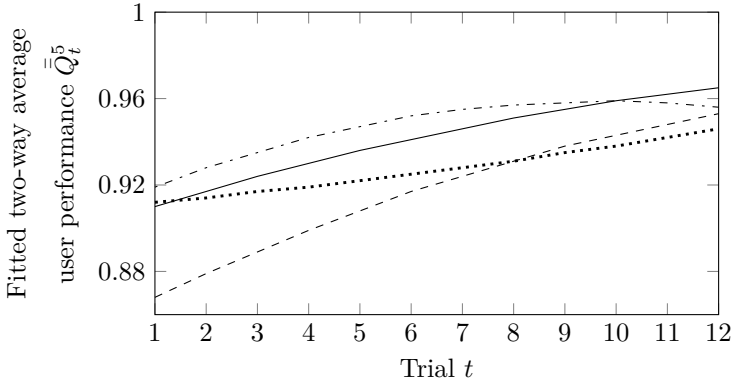

Figure 5.14: Second-order polynomially fitted (least-squares) user performance $\bar{\bar{Q}}_t^5$ over Trials 1 to 12 of test groups A (·····), B (-·-·), C (- - -) and D (——) in Race environment [213]

Initially, the user performances $\bar{\bar{Q}}_t^5$ of the test groups A, B and D were at about the same levels. In contrast, the initial polynomially fitted user performance $\bar{\bar{Q}}_t^5$ of the test group C was considerably lower. The levels at the very beginning strongly depend on the differences between the individual users. Finally, the test group D yielded the highest polynomially fitted user performance $\bar{\bar{Q}}_t^5$. The test groups B and C had final polynomially fitted user performances $\bar{\bar{Q}}_t^5$ of about the same level. The lowest final level was yield by test group A.

Looking at the overall progress from Trial 1 to 12, the test group A accomplished the lowest relative increase. This is probably because the one-size-fits-all parameter values do not meet the individual requirements of the users at the very beginning like the initial calibration (test group B) does. Furthermore, this is likely due to the fact that the one-size-fits-all parameter values does not adapt to the user like the inter-trial calibration (test group C) does, who learns how the handling better over time (i.e., over the trials). Test group C accomplished the highest increase. It is indicated that parameter adaptation positively affects the user performance.

Figure 5.15 shows fitted standard deviation σ_t^5.

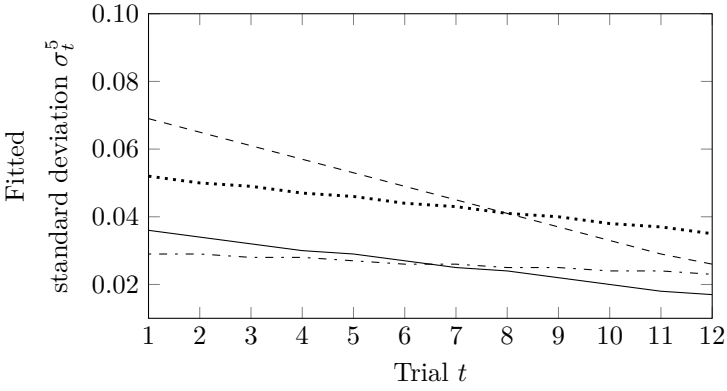

Figure 5.15: Second-order polynomially fitted (least-squares) standard deviations of user performance over Trials 1 to 12 of test groups A (·····), B (-·-·), C (- - -) and D (——) in Race environment [213]

The σ_t^5 is fitted in the least-squares sense with second-order polynomials of the test groups A to D over Trials 1 to 12. Each of the polynomials declines due to the naturally caused training effects (cf. Figure 5.12). The test group D accomplished the best final result $\sigma_{12}^5 = 0.017$ in addition to a substantial improvement given the decent starting level $\sigma_1^5 = 0.036$.

Comparing the standard deviations between the test groups, Student's t-tests together with a Bonferroni correction coefficient $m = 6$ were applied. The comparison of test groups A and B results in $p \cdot m = 0.004^{**}$. As for test groups A and C there is $p \cdot m = 1$. Moreover, test groups A and D results in $p \cdot m = 0.027^{*}$. The comparison of test groups B and C leads to $p \cdot m = 0.020^{*}$. Test groups B and D yield $p \cdot m = 1$ while test groups C and D gives $p \cdot m = 0.046^{*}$ [213].

Figure 5.16 shows a scatter plot of the average user performance $\bar{Q}_{u,t}$ (cf. (3.67)) and the control range ρ (cf. (3.4)) of test group C. The control range, defined as the difference between the maximum parameter and the minimum parameter, insinuates the ability of the user to intentionally establish both high and low values.

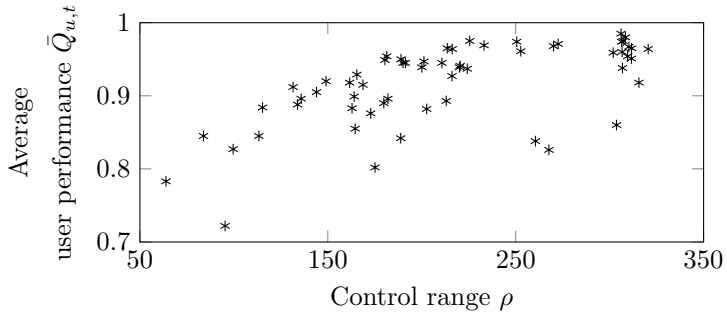

Figure 5.16: User performance $\bar{Q}_{u,t}$ over control range ρ of test group C in Race environment [213]

As test group C consists of five subjects and each subject completed 12 trials, the total number of data points amounts to 60. Each data point represents one control range value ρ that was collected before trial execution

and one average user performance value $\bar{Q}_{u,t}$ that was determined after trial execution. Applying the Student's t-test to the control range ρ of Trials 1 and 12 yields $p = 0.346$. Thus, an influence of the training on the quantity of the control range is likely to be ruled out.

The PCC of correlation between $\bar{Q}_{u,t}$ and ρ is $R = 0.62$ with $p = 0.000^{***}$ [128, 213]. This result gives indication of a moderate correlation between $\bar{Q}_{u,t}$ and ρ. The volunteer study presents a positive correlation between user performance and control range. Users who are well able to establish high and low values tend to achieve higher performance values.

In Figure 5.17 the results of the trials in Virtual Wheelchair environment (second stage) with respect to two different values are depicted.

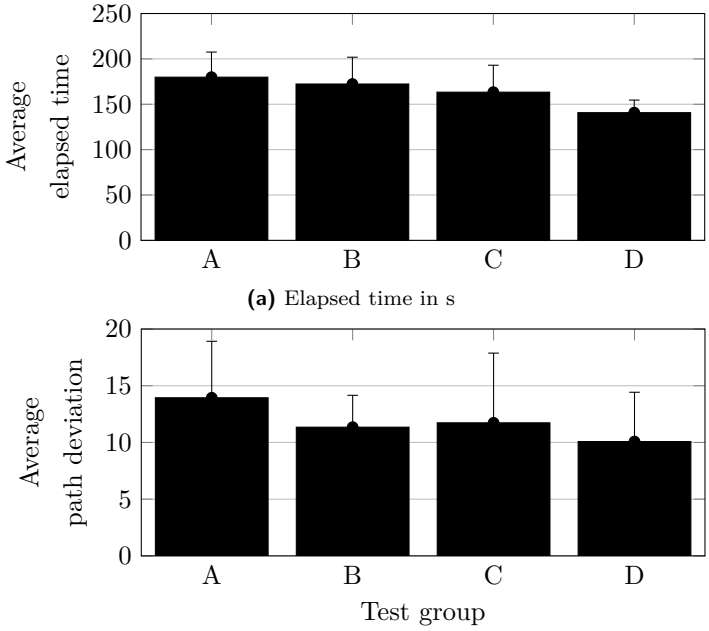

(a) Elapsed time in s

(b) Path deviation in px

Figure 5.17: Elapsed time and path deviation with standard deviations of test groups A to D in Virtual Wheelchair environment [213]

The users were prompted to navigate along a reference path both as fast and accurate as possible. In this assessment none of the parameter adaptations were activated but rather those trials served as comparison of the performance levels of the distinct test groups after the dedicated training and adaptation phase (first stage).

Figure 5.17a presents the average elapsed time. It is the mean value over the subjects belonging to the test groups of the time from leaving the start location to arriving at the designated finish location. The subjects of test group D completed the reference path the fastest (140.8 s). The second fastest results were achieved by the subjects of test group C (163.3 s), followed by those of test group B (172.3 s) and A (179.9 s). This result is promising because the higher-level adaptation methods tend to outperform lower-level adaptation methods. However, the ANOVA test of the average elapsed times results in a p-value of $p = 0.138$. Hence, these results are not significant, and the number of subjects is probably insufficient. Conducting a follow-up study including more participants possibly would clarify this matter.

Figure 5.17b shows the average path deviation. It corresponds to the mean value over the test group's subjects of the accumulated, orthogonal distances between the actual and the reference avatar position. These orthogonal distances are defined as

$$\Delta(y_{\text{ref}}, y_{\text{act}})[k] = \sqrt{(\vec{y}_{\text{ref}}[k] - \vec{y}_{\text{act}}[k])^T \cdot (\vec{y}_{\text{ref}}[k] - \vec{y}_{\text{act}}[k])}, \tag{5.14}$$

where $\vec{y}_{\text{ref}}[k]$ and $\vec{y}_{\text{act}}[k]$ denote the reference and actual avatar positions.

The subjects of test group D reached the best result, meaning the least average accumulated path deviation (10.1 px). The average accumulated path deviations of the subjects belonging to test group B (11.3 px), test group C (11.7 px) and test group A (13.9 px) accomplished not as good results. Albeit, the ANOVA test yields $p = 0.638$. Therefore, significance could not be found. A follow-up study with more subjects could resolve this uncertainty.

Further PCC were calculated by examining the correlations between the results in the Virtual Wheelchair environment and those of the Race environment. The average elapsed time within the Virtual Wheelchair environment and the average user performance within the Race environment

correlate with $R = 0.118$. Therefore, a cross-environment correlation is not evident.

Also, the correlation coefficient between the average path deviation and the average user performance within the Race environment amounts to $R = -0.228$. Hence, a significant correlation is not indicated.

5.6 Training of Ear Muscle Signals for the Able-Bodied

For the first time, the concept of EMG-based human-machine interfaces (HMIs) was expanded by utilizing the extrinsic ear muscles (cf. Section 1.2.4) as EMG-signal sources. The utilization of EMG-signals, acquired from the human extrinsic ear muscles, as HMI input signals denote a completely novel approach. As the extrinsic ear muscles usually are not activated in humans, individualized training was absolutely necessary.

The adaptive muscle interface, as introduced in this work (cf. Chapter 3), was evaluated. The individualized training was conducted with ten able-bodied subjects. They completed the individualized training of the extrinsic ear muscles for unpracticed users (cf. Section 3.6), developed in this work. This training, aiming at enabling the users to activate their ear muscles, lasted five days per subject. The daily training endured about one hour per subject. EMG signals from the extrinsic ear of both the left and the right flank were acquired [181, 209].

To provide the subjects with biosignal feedback, visualization methods of the graphical user interface (GUI) (cf. Section 4.5) were utilized. This enabled the users to establish a cause-and-effect relationship between their own intention and the actual, resulting EMG signals of the extrinsic ear. This was of prime importance as most naive users (i.e., users who never before attempted to activate their extrinsic ear muscles) were incapable of intentional activations of their extrinsic ear muscles.

After that initial phase the users completed diverse virtual tasks. The implementation of the biosignal assessment paradigms (cf. Section 2.4.3)

captured the abilities of the users to modify the EMG signals in specific ways.

Figure 5.18 presents the comparison of trials between Day 1 and Day 5 (i.e., the final day) of the training in the Parkour environment (cf. Section 4.5).

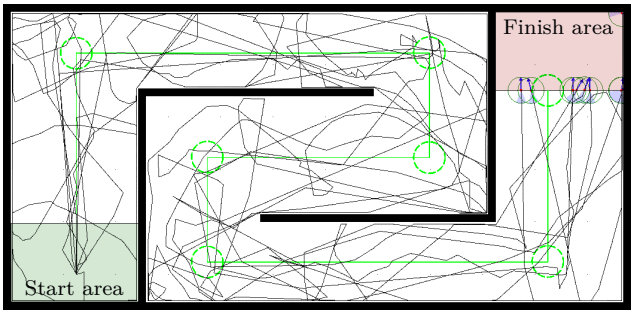

(a) Trials of Day 1 (beginning day)

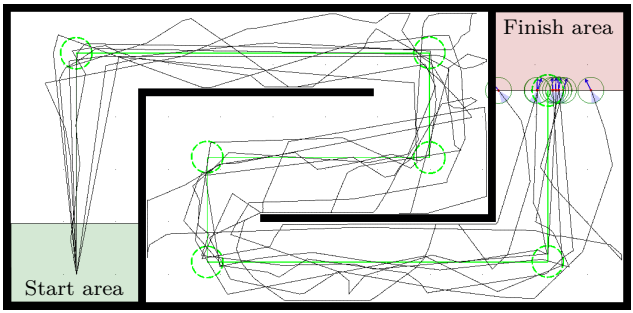

(b) Trials of Day 5 (final day)

Figure 5.18: Actual path trajectories of trials of Parkour environment [181]

Each user was required to complete the obstacle course from the start area to the finish area. Looking at Figures 5.18a and 5.18b, the visual impression indicates an improvement in the user's ability to control the virtual avatar.

The positive visual impression is also reflected in the numerical evidence. The average control ability $\bar{c}_d^{u,e,t}$ (cf. (2.22)) was determined with $\tilde{U} = 10$. Figure 5.19 illustrates the average control ability in percent with corresponding standard errors. The normalization of the average control abilities is in accordance with $\bar{c}_1^{u,e,t} \equiv 100$ %, that is, the results of the Days 2 to 5 were referred to the result of the Day 1.

The average control ability over the training turned out being 112.11 % at Day 2, 142.52 % at Day 3, 159.16 % at Day 4 and 174.09 % at Day 5.

Hereby, an absolutely novel conclusion is indicated. The ability to control the virtual environments by means of EMG signals from the extrinsic ear muscles is trainable. Albeit the promising trend in the data, significance could not be found. Therefore, a follow-up study with more subjects might resolve this uncertainty.

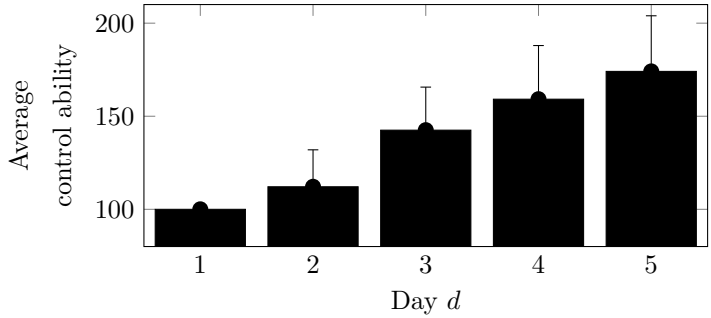

Figure 5.19: Averaged control ability in percent with corresponding standard errors over Days 1 to 5 in Parkour environment [181]

In Figure 5.20, as the final examination, at Day 5 the able-bodied users were asked to navigate a real electric-powered wheelchair (EPW), the B600 by Otto Bock as presented in Appendix A.3, through a real obstacle course by means of the EMG signals from the extrinsic ear muscles. This final examination was geared towards being an incitement and motivation for the users. Thus, quantitative data was not acquired from these real obstacle courses.

For reasons of safety, the subjects were instructed not to release the built-in emergency stop of the electric-powered wheelchair (EPW). Together with

Figure 5.20: Able-bodied user steering the electric-powered wheelchair (EPW) by EMG signals from the extrinsic ear muscles through an obstacle course with hand set to the built-in emergency stop[1]

the implemented emergency stop (cf. Section 4.6) any kind of occurring problems during operation could have been handled by both the users and the supervising staff.

5.7 Training of Ear Muscle Signals for the Physically Handicapped

5.7.1 Tetraplegia

As an absolute novelty, the adaptive muscle interface as introduced in this work (cf. Chapter 3), utilizing the EMG-signals from the extrinsic ear

[1] Courtesy of D. Liebetanz, University Medical Center Göttingen

muscles, was applied in a study with physically handicapped individuals. The participants, who were limited in their mobility due to physical handicaps, freely navigated a real electric-powered wheelchair (EPW).

Two subjects living with tetraplegia, caused by a cervical spinal cord injury (SCI) (cf. Section 1.3.2), participated in the study [172, 182]. Parameter adaptation was applied in order to support the users in controlling the executing device [209]. Furthermore, the biosignal feedback and visualization methods of the graphical user interface (GUI) (cf. Section 4.5), as developed in this work, were applied. The subjects represented particularly the main target group of the adaptive muscle interface (cf. Section 3.2). Subject 1 resp. Subject 2 exhibit neurological levels of injury (NLIs) of C5 resp. C3 with ASIA impairment scale (AIS) of A resp. C.

From the extrinsic ear muscles of both the left and the right flank the EMG signals were acquired bilaterally. Asking the subjects prior to the execution of the training whether they can activate the extrinsic ear muscles on purpose revealed distinct answers. Subject 1 answered in the affirmative, while Subject 2 answered in the negative.

The five-days training consists of virtual training at the computer monitor as described above (cf. Section 5.3) as well as navigation of a real electric-powered wheelchair (EPW), the B600 by Otto Bock as presented in Appendix A.3, through an obstacle course. The real obstacle course was built up in an indoor sports arena. The corridor width of the obstacle course was about 2 m. For the sake of the subjects' safety, the demarcation indicators were not irremovable but rather, in cases the subjects clashed with the demarcation indicators, were easily to push aside. Figure 5.21 presents one subject during the real electric-powered wheelchair (EPW) navigation.

The trajectories of Subject 1 resp. Subject 2 in the virtual Parkour environment resp. in the real obstacle course are portrayed in Figure 5.22 resp. Figure 5.23. The implementation of the virtual Parkour environment (cf. Section 4.5) permitted the collisions in a manner of scraping along the virtual walls. In contrast, in cases of collisions of the real electric-powered wheelchair (EPW) the vehicle was stopped by the supervising staff via an emergency stop as implemented (cf. Section 4.6).

Figure 5.21: Spinal cord injured user steering the electric-powered wheelchair (EPW) through an obstacle course[2]

Then, the supervisors instantaneously positioned the EPW correctly on the obstacle course again so that the subject could continue the course.

As shown in Figure 5.22a, the initial virtual trial of Subject 1 was rather choppy and implicated five collisions with the demarcation walls. Figure 5.22b shows the trace of trial in the real obstacle course of Subject 1. The subject clashed once with the demarcation indicators but could continue immediately after the supervisor repositioned the wheelchair again.

In Figure 5.23a the initial trial in the virtual Parkour environment of Subject 2 reveals two collisions with the demarcation walls while navigating choppily. The same subject completed the real obstacle course with one collision in a smooth fashion, as shown in Figure 5.23b.

[2]Courtesy of U. Eck, Heidelberg University Hospital

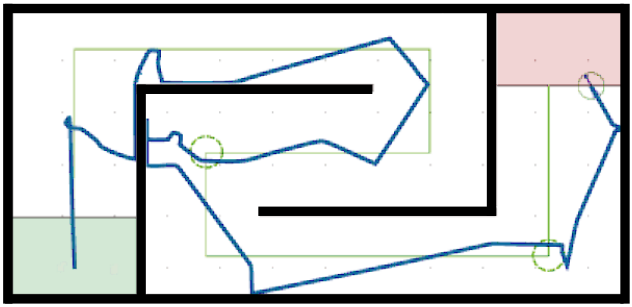

(a) Virtual trial in Parkour environment at Day 1

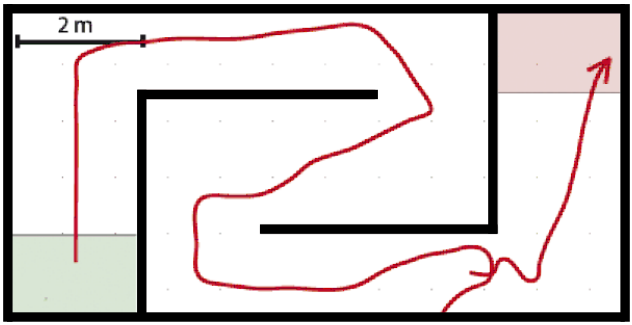

(b) Trace of trial in real obstacle course at Day 5

Figure 5.22: Path trajectories of trials of Subject 1 [182]

The training over five days was reflected positively in the numerical results. The implementations of the biosignal assessment paradigms (cf. Section 2.4.3) showed improvements over the training time. Also, in the virtual Parkour environment the completion time, that is, the elapsed time from leaving the start area to arriving at the finish area, improved. As for Subject 1, the completion time was improved from 91.0 s (at Day 1) to 71.6 s (at Day 5) which corresponds to about 20 s of betterment. Subject 2 managed to improve from 139.5 s (at Day 1) to 104.9 s (at Day 5) measuring up to about 35 s advancement.

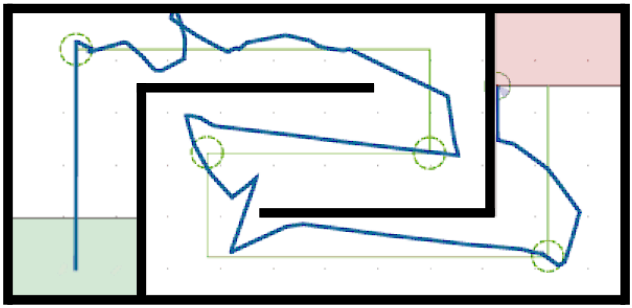

(a) Virtual trial in Parkour environment at Day 1

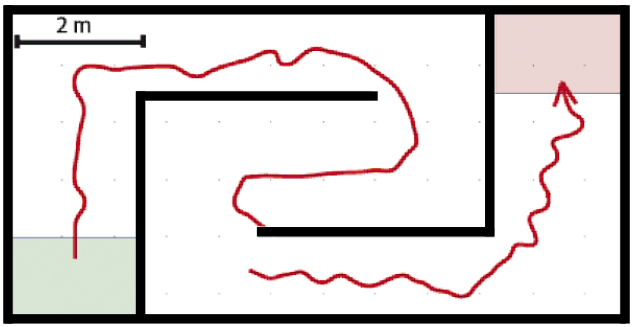

(b) Trace of trial in real obstacle course at Day 5

Figure 5.23: Path trajectories of trials of Subject 2 [182]

After finishing the virtual training phase, at Day 5, both subjects succeeded in completing the real obstacle course. The Subject 1 took 86.0 s while Subject 2 took 201.6 s.

The results suggest that the deliberate activation of the extrinsic ear muscles can be trained over time by persons with highly located SCIs. Moreover, it becomes evident that intuitive navigation of EPWs is possible for persons that typically use to be significantly immobile due to their impairment of motor functions. The NASA-TLX (cf. Section 1.4.2) indicated a low resp. medium subjective workload for T1 resp. T2.

5.7.2 Spinal muscular atrophy

A subject suffering from a severe type of spinal muscular atrophy (SMA) participated in another setting as shown in Figure 5.24.

Figure 5.24: User living with spinal muscular atrophy (SMA) playing the Tetris game by means of the extrinsic ear muscles[3]

Artificial respiration and drip-feed is given to the 13-year-old subject with a short life expectancy as there are only very few remaining motor functions. Numeric data was not explicitly recorded but rather this setting served for testing purposes.

With the adaptive muscle interface (cf. Chapter 3) the severely handicapped subject succeeded in controlling the Tetris environment (cf. Section 4.5) by means of the extrinsic ear muscles. For the first time the subject was able to actually control a computer game. This would have been inconceivable and poses a real asset for the subject.

[3]Courtesy of U. Eck, Heidelberg University Hospital

5.8 Summary

The experimental assessments of the difference models for crosstalk compensation brought to light that the model with linear regression satisfies all of the desired properties. Various parameter adaptation methods were tested and statistically evaluated in experimental studies with subjects. The novel adaptive muscle interface, as introduced in this work (cf. Chapter 3), was also successfully tested where the muscle signals were acquired from the extrinsic ear muscles of the subjects.

Ultimately, the adaptive muscle interface was tested for the first time with physically handicapped individuals. With training for unpracticed users according to the concept of this work (cf. Section 3.6) the handicapped individuals completed the virtual and real navigation tasks with success.

6 Conclusions and Outlook

Persons incapable of moving extremities due to trauma or disease induced disabilities such as spinal cord injuries (SCIs) are highly dependent on other persons' help in everyday life. Human-machine interfaces (HMIs) potentially alleviate the suffering of the disabled persons and change living conditions for the better, for instance, by regaining independence of mobility through navigation of electric-powered wheelchairs (EPWs).

This work addresses the need for HMIs applicable for persons suffering from highly located SCIs. The main aspects of this work are listed below.

- Introduction of a novel HMI concept based on the user's intentional activation of the outer ear muscles (cf. Chapter 2).
- Design of user and supervisor-centered tools (cf. Chapter 3).
- Implementation of the introduced HMI concept (cf. Chapter 4).
- Experimental validation of the implemented system (cf. Chapter 5).

Considering the requirements effecting user acceptance and addressing open problems of state of the art HMI concepts, this work achieved the following main results.

1. Introduction of a new HMI concept named telemetric and myoelectric ear muscle sensing system (TELMYOS). As opposed to state of the art HMI concepts, it enables persons with tetraplegia to control various kinds of technological devices without the loss of remaining bodily functions or major aesthetic impairments. It encompasses biosignal quantification, user-specific calibration and training scheme for unpracticed users.

2. Development of biosignal quantification methods for the numerical assessment of the user's biosignal control ability. These methods allow evaluation of inter-individual variations as well as intra-individual variations over time and provide the basis for user individualization.
3. Invention of novel user-specific parameter calibration methods enabling a wide range of users to accomplish accurate HMI operation despite of inter-individual differences.
4. Design of a training scheme aiming at unpracticed users to promote improvements in control ability. This scheme is highly customizable to meet each user's individual strengths and weaknesses.
5. Demonstrating the evidence of functionality of the HMI concept with both able-bodied and handicapped persons. In studies, participants showed an increase of biosignal control ability (i.e., outer ear muscle activity). Persons with paraplegia accomplished navigating an EPW autonomously through an obstacle course.
6. Examination of co-adaptive learning with respect to parallel and sequential application of user training and parameter adaptation.
7. Analysis of biosignal processing algorithms incorporating user-specific and time-variant parameters to generate activity signals.
8. Analysis of procedures for user-specific parameter adaptation coping with the non-stationary nature of the acquired biosignals.
9. Implementation of development tools featuring both front- and back-end usage of a graphical user interface (GUI) for users and supervisors, respectively.
10. Development of new transmission protocols and implementation of wireless data transmission for subsystems.
11. Analysis of individualized control schemes dependent on the user's bodily functions and the user's preferences.

The open problems outlined in Section 1.6 have been researched. The proposed HMI concept makes use of an additional head-only activity. Moreover, while acquiring facial biosignals it provides an unobtrusive outward appearance and it preserves remaining bodily functions like breathing or speaking. The poor biosignal controllability of users in the early stages has

also been addressed. A supportive training scheme helps users to improve control skills. Finally, by means of an adaptation scheme the proposed HMI concept is able to cope with time-variant biosignal drifts.

Further research is still necessary and the implementation of useful features helps to improve the system:

- Facilitation of EPW navigation
  - Development of non-isotonic controls such as cruise control, to be easy on the user's muscle stamina
  - Improvement of the reverse gear functionality
- Safety functions for the EPW
  - Addition of hardware components like light detection and ranging (LIDAR) sensors for obstacle detection
  - Implementation of stop zones in the front and rear as well as slow down zones to the left and right
- Miniaturization of system components such as the development of a mobile GUI version on cell phones
- Enhancement of the system error management, like adding light-emitting diode (LED) displays at the subsystems
- Tethered inter-subsystem communication
- Extension of types of electrodes for acquiring input signals, for instance, activity signal electrodes (commonly used in prostheses)
- Studies including more subjects for statistical proving of effects of training and adaptation
- Improvement of the immersion of virtual realities (VRs) to provide the user with more realistic simulations
  - Haptic feedback, such as a vibration actuator
  - Head-mounted displays, for instance, Oculus Rift, Google Glass
  - Assessment of the subjective mental and physical workload of the user

A Appendix

A.1 Population Aging and its Consequences

Figure A.1 indicates the prevalence of disability is expected to grow due to the aging populations and the increase in chronic health conditions. The European Commission declared participation, equality and employment among others as areas of action in the European Disability Strategy [47]. In accordance with WHO's estimates about 15 % of the world's population experience disabilities of variant degrees.

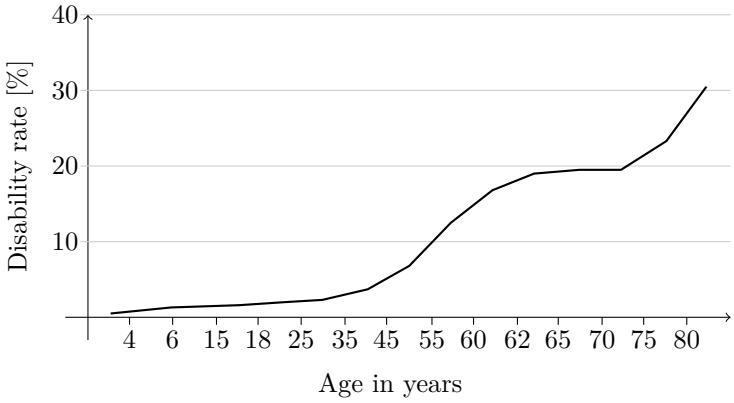

Figure A.1: The prevalence of disabilities increases with the age (modified from [108])

A.2 Disability and Writing

Locked-in patient Jean-Dominique Bauby wrote his autobiographical novel "The Diving Bell and the Butterfly" with the aid of a device interpreting his left eyelid blinking. It was the only remaining bodily function controllable by will [15]. He finalized his novel successfully. The entire book took about 200,000 blinks.

Paraplegic patient Robert Francis Murphy described the gradual deterioration caused by a slow-growing spinal cord tumor in his personal narrative "The Body Silent: The Different World of the Disabled" [136].

A.3 Experimental Wheelchair Platform

The highly versatile, electric-powered wheelchair B600 by Otto Bock is the utilized experimental platform. It is portrayed in Figure A.2a. Users capable of moving at least one upper extremity typically maneuver this EPW via the control panel by hand, as depicted in Figure A.2b.

(a) B600 **(b)** enAble50

Figure A.2: Electric-powered wheelchair B600 and the hand control panel enAble50[1]

[1] Courtesy of Otto Bock HealthCare GmbH

The B600 is designed for indoor and outdoor use. The maximum speed is declared as 10 km/h, the climbing ability amounts to 17 % and the approximate distance range is 35 km. On-the-spot turns are feasible. The main scope of application is the electric mobility for persons with walking impediments or walking inability. The wheelchair is adjustable in many ways to meet the personal requirements of the user. Seating position can be adjusted with the backrest, arm rests, foot rests and the seat cushion. Furthermore, electric motors help adjust the seat height and angle [86].

A.4 Head-only HMIs

A.4.1 Hybrid HMIs

Hybrid HMIs apply two or more operating principles within one system. As a consequence, at least two biosignals of different types are acquired from the human user. The information of these biosignals is eventually merged by algorithmic calculus to gain a rich data representation of the intention of the user. For hybrid HMIs, the categorization is challenging since various operating principles are utilized and each can be categorized according to either of the aforementioned ways. Therefore, in this section some publications appear in several different categories if needed.

A.4.2 Chin Control

An established and well-known head-only HMI is the chin-controlled interface. The user's chin deflects the miniaturized joystick that is situated in front of the user's face to generate control signals. This HMI requires head movements to some extent. Hence, the user needs to have certain control over the neck muscles. The chin-controlled joystick basically works the same way hand-controlled joysticks do. As for EPW control systems, the deflection of the joystick to the front direction causes the wheelchair to drive forward. The joystick deflection is typically proportional to the velocity of the wheelchair [116]. Chin controllers to navigate EPWs are commercially available for example by Otto Bock HealthCare GmbH.

As chin controller systems are simple and intuitive because they resemble hand-controlled joysticks merely moderate training is needed. However, the joystick positioned in front of the user's head implies aesthetic impairment.

A.4.3 Tongue Control

Tongue-controlled HMIs generate control signals depending on the user's tongue movements. Two major classes are distinguished, namely systems relying and not relying on auxiliary means in mouth or throat.

Systems utilizing auxiliary means in mouth or throat provide high information density. These systems are invasive and require surgical interventions to position the auxiliary means. A magnetic field that serves as HMI input can be altered by movements of a magnetic implant or piercing in the user's tongue, termed tracer. The magnetic field is detected by sensors located in a headset or other peripheral structures. Depending on the comparison between the actual tongue movement and a priori recorded tongue movement patterns control signals are generated [82, 83, 97, 117, 176].

Interfaces without auxiliary means in mouth or throat are non-invasive but only provide low information density. Some systems make use of tongue movement ear pressure (TMEP) signals that are detected in the user's ear by pressure sensors incorporated in the earplugs. By tongue clicking the ear pressure alters because the mouth cavity and the ear canal are interconnected. The TMEP signal gets digitized, filtered, segmented and its short-term energy (STE) is calculated. Signal interpretation is accomplished via classification based on a priori generated templates. Researchers conducted a case study with real-time simulation and control of a wheelchair moving through a constrained 2D environment [118, 119]. Different tongue movements yield distinct TMEP signals that can be classified [216]. Another tongue-controlled system without auxiliary means extracts the shape of the tongue from images of an ultrasonic scanner for mapping images of the vocal tract onto a sound output. This is not used as a general HMI but rather as a musical controller [219].

Tongue-controlled HMIs provide advantages such as high agility, high accuracy, intuitive movements and only little muscle fatigue. However,

in some cases the systems imply a certain aesthetic impairment through headset or earplugs. Also, irrespective of the usage of auxiliary means in mouth or throat tongue-controlled HMIs do not allow the user to speak while operating the interface because tongue movements are essential for verbal articulation. In addition, eating also causes artifacts in the control signal as the tongue is used for handling the meal in the oral cavity. Yawning also potentially result in control signal artifacts.

A.4.4 Voice Control

Automatic speech recognition (ASR), also known as speech-to-text (STT), utilizes human language for the H2M communication. Early works are presented in [9, 134]. Overviews of conversational user interfaces can be found in [27, 127]. There are two major classes, namely the speaker- independent approach and the speaker-dependent approach. The speaker-independent approach does not necessitate the system to learn the individual speech of the user [102]. On the other hand, the speaker-dependent approach is based on a training phase where the user reads some text aloud so the system learns how the user speaks [147]. There are diverse techniques realizing silent speech interfaces (SSIs), such as electromagnetic articulography (EMA) [39]. Systems following the speaker-dependent approach usually achieve more accurate transcription results [126, 155].

In order to find voice commands ensuring robust and safe navigation some works conducted experiments where blind subjects were guided by seeing supporters through a course. A minimum number of voice commands is required for safe navigation [102].

Phonetic control focuses on the sounds generated by the vocal tract rather than the human language. By interpreting the pitch and duration of humming sounds it is language-independent and hence multilingual. However, this approach is rather counter-intuitive [73].

Speech-controlled HMIs are extraordinary intuitive as speech is the most natural manner of H2H communication. On the downside, verbal H2H communication and HMI control are largely mutually exclusive – the user cannot talk to people while operating the interface. Moreover, many different voice commands are needed for accurate wheelchair control. As

for speaker dependent systems long training phases are required. Speech control also potentially annoys other people as they inevitably hear the voice commands.

A.4.5 Airflow Control

Some HMIs make use of pressure sensors to measure the nasal airflow. Nasal sniffing and breath inhalation through the mouth is utilized as a communication channel.

In passive sniff controllers, a pump generates a low-flow stream of air into a nasal mask. The mask pressure is measured via the sniff controller. Opening and closing the soft palate (velum palatinum) decreases and increases the pressure, respectively. The pressure signal is independent of respiration as the user can breathe normally during both opened and closed soft palate [156].

The sip-and-puff (SNP) principle relies on the deliberate variation of air pressure in a pneumatic tube. It is also known as suck-and-blow. Both the amplitude and the sign of the airflow may be altered by the user. The user holds the mouthpiece of a pneumatic tube which is connected to the SNP system. If the user inhales (sip) the air pressure in the pneumatic tube decreases, and if the user exhales (puff) it increases, respectively. That way the user generates input signals for the SNP-based HMI.

Typically, four patterns of input signals are differentiated in SNP control, namely high-level sip, high-level puff, low-level sip and low-level puff. A common field of application for SNP-based HMIs is the EPW control. Starting from the stationary state a high-level puff lets the wheelchair move forward (non-stationary state) as long as a high-level sip stops the wheelchair into the stationary state again. This also applies vice versa – starting from the stationary state a high-level sip moves the wheelchair backwards as long as a high-level puff stops the wheelchair. Low-level sips or low-level puffs move the wheelchair to the left or to the right, respectively. The rotation is proportional to the duration of continuous in- or exhaling. A survey of SNP is available in [61]. Commercial SNP-based EPW controllers are available from vendors such as Otto Bock HealthCare GmbH. In [88] the operation of an Apple iPod via SNP remote control is

examined. To prevent unintentional control commands through sneezing or coughing (signal artifacts) the patterns for the control have to be performed repeatedly. However, that scheme complicates the control.

Airflow-controlled HMIs imply aesthetic interferences caused by the prominent nasal sensors and pneumatic tubes in the user's face. In addition, the deliberate control of one's airflow is not always easy to handle and in some cases there are complications with colds or bronchitis. Spinal cord injured persons often encounter difficulties breathing because they do not have full control over muscles usually involved while breathing and they usually sit in their wheelchairs bent forward. These aspects exacerbate the SNP control for longer periods. Passive sniff-controlled HMIs do not interfere with the user's breathing but SNP-controlled HMIs do. SNP-controlled HMIs require a significant amount of training since the variation of pneumatic amplitude and sign is usually perceived as counterintuitive by the naive users.

A.4.6 Facial Expression Control

Facial expression controlled HMIs interpret the user's facial expressions that are regarded as input signals. These HMIs utilize common H2H communication as a channel for the H2M interaction. To prevent the system from interpreting the facial expressions permanently and risk misclassifications some systems put a kind of clutch to use. This clutch can be engaged or disengaged by the user to tell the system to take the current facial expressions as input signals or not. For instance, in [139] the system only interprets the facial expression if the user moves the head into the central position. Two major sorts of facial expression HMIs are available, namely the camera-based and the EMG-based systems.

In purely camera-based systems, cameras permanently point at the user's face and specialized image processing software extracts information interpreted as HMI input [90, 139]. [199] developed a purely EMG-based facial expression HMI. Hybrid interfaces make use of both image processing and additional information such as EMG signals from the forehead to improve the overall system's accuracy [31, 77, 222, 223]. In [162] facial expressions acquired with the aid of 14-channel electroencephalography (EEG) and head movements were combined.

Facial expression HMIs are non-invasive and merely necessitate moderate training effort as they make use of a common H2H communication channel. On the downside, by default the system interprets each facial movement. That means unless there is some kind of clutch incorporated the system treats the user's facial expressions as input signals while speaking, laughing and eating. Issues such as face normalization or facial expression intensity need to be addressed [53]. As for the forehead EMG-based systems, there is an aesthetical impairment.

A.4.7 Imagination Control

Brain-computer interfaces (BCIs) refer to a subclass of HMIs that make use of biosignals acquired directly from the brain. That is opposed to the indirect biosignal acquisition from other body parts that are basically controlled by the brain. BCIs are non-muscular interfaces. Common synonyms are mind-machine interfaces (MMIs), direct neural interfaces (DNIs), synthetic telepathy interfaces (STIs) and brain-machine interfaces (BMIs). The fundamental concept of imagination-based HMIs is the detection of electric fields in the brain caused by neuron activity. Profound reviews on BCI technology can be found in [140, 229].

The non-invasive detection of electric potentials on the scalp (pericranium) is termed EEG. Numerous surface electrodes that are held by a bonnet are distributed across the head. There are various EEG subcategories [20]. One subcategory encompasses the steady-state visually evoked potentials (SSVEPs) and visual-evoked potentials (VEPs) [81, 94, 236]. These are natural responses of the brain to a visual stimulation (visual stimulus flickering) and at the same frequency or multiples of the stimulation frequency. Another subcategory contains the event-related synchronization (ERS), event-related desynchronization (ERD) and slow-cortical potentials (SCPs) [148, 149, 151, 195, 201].

These systems make use of the intentional amplitude modulation of the μ-rhythm, also known as sensorimotor rhythm (SMR). The user modulates the amplitude by the imagination of movements. When the user imagines a movement with a certain part of the body the corresponding area in the motor cortex that represents that part of the body shows a changed μ-rhythm. The increase of the μ-rhythm when imagining movements is

termed ERS while the decrease of the μ-rhythm when imagining movements is said to be ERD. Yet another subcategory is the event-related brain potential (ERP), especially the well-studied P300 ERP [51, 103, 135]. The "oddball" evoked potential ERP which is a natural response of the brain to a rare event is elicited in the EEG at a latency of about 300 ms.

Typically band-pass filters are utilized to cope with artifacts from EMG and EOG as these are only present at certain frequency bands. It is estimated that 20-25 % of all subjects are not able to operate EEG-based BCIs at all [68]. For these subjects either no idle SMR is observed over motor areas or this idle rhythm is not modulated during motor imagery [217]. Wheelchairs and mobile robots can be controlled via these interfaces [6, 32, 95, 115, 200]. One of the most advanced BCI is the Berlin-BCI [21]. Spelling devices were developed that enable the users to spell texts [18, 101]. It was found that EEG signals and electrocorticography (ECoG) signals respectively acquired from paralyzed and non-paralyzed subjects differ significantly. The reason for that phenomenon is not yet completely understood [79]. Some hybrid systems rely on a combination of different BCI subcategories. For instance, the hybrid BCI in [110, 150] combines SSVEP and ERD. EEG-based BCIs provide only a low signal-to-noise ratio.

Magnetoencephalography (MEG) is another non-invasive sort of BCIs. It measures the magnetic fields of the brain caused by neuronal activity. As compared to EEG it provides higher spatial and temporal resolution but classification accuracies do not differ significantly [93, 173].

Electrocorticography (ECoG), also known as intracranial EEG (iEEG), is an invasive type of BCI. It makes use of electrodes that are implanted into the brain. Research on rhesus macaque monkeys (Macaca mulatta) demonstrated this method successfully [137]. An intracortical multi-electrode array was implanted into the monkey's brain. The monkey succeeded in using neural control to move the computer cursor which was connected to the BCI [188]. In [227] an intracortical multi-electrode array was implanted in a human subject's left motor cortex.

Another non-invasive HMI based on the user's imagination examines the effects of imagery on salivary pH. Patients could answer to yes-or-no questions by imagery of food [226]. It is not a BCI as it does not analyze signals directly related to the brain activity.

BCIs possess high potential as mind reading assistive devices for severely disabled persons. However, at present time they do not provide sufficient accuracy and therefore further research is necessary. Researchers and society need to further discuss ethical considerations with respect to this cutting-edge technology. For instance, there is a certain risk of misusing BCIs as mind-reading devices. The sleep quality of the user could be effected negatively. Moreover, the invasive BCIs lack user acceptance because of the high injury and infection risk.

A.4.8 Eye Control

Eye movements generate biosignals that can be harnessed for HMI control. Two major types of eye-controlled HMIs can be identified, namely camera-based and EOG-based interfaces.

In camera-based systems the camera points towards the eye and analyzes its exact orientation through tracking the pupil's position [113]. Examples for commercial systems based on cameras and image processing software are iView X HED by SensoMotoric Instruments[2] and Mobile Eye-XG by Applied Science Laboratories[3].

Electrooculography (EOG) bases on the fact that the eye is a dipole. The retina is the negative pole and the cornea is the positive pole. Two pairs of electrodes are adhered to the facial skin. The first pair of electrodes detects the difference of potential between cornea and retina horizontally and therefore infers the horizontal eye movement. The second pair of electrodes infers the vertical eye movement analogously via the potential difference between cornea and retina vertically. In addition, one reference electrode placed somewhere else onto the skin detects the reference potential. Research revealed a partly linear relation between the angle of viewing direction and the electric potential [106]. Application-oriented publications dealt with mobile EOG-based systems with glasses [24, 107]. Also, EOG-controlled electric powered wheelchairs were analyzed [12, 13]. In contrast to camera-based eye-controlled interfaces, EOG-based systems work with closed eyes and total darkness.

[2] `http://www.smivision.com`
[3] `http://www.asleyetracking.com`

Beside the horizontal and vertical eye movements the eye blinking constitutes an additional DOF [46, 159]. It is referred to as eyelid control. Apart from purely camera-based and purely EOG-based systems hybrid solutions such as an EEG-based system enhanced with eye blinking signals [114].

The Midas touch problem addresses that eyes are never inactive but constantly moving as the human looks around. From the HMI perspective this hampers the interpretation of eye movements as a communication channel. The implementation of a clutch – for instance, triggered by the user's head position – solves that problem. If engaged the clutch connects the user to the HMI. On the other side, if the clutch is disengaged the user can look around without the system interpreting the eye movement. The clutch should be able to engage and disengage as quickly as possible. The act of engaging or disengaging should be as intuitive as possible (i.e., not requiring too much of concentration) [63]. In case no clutch is implemented, looking around and HMI operation at the same time is not possible. Also, most of eye-controlled HMIs imply a certain aesthetical impairment. For persons suffering from nystagmus eye-controlled HMIs are not applicable. Nystagmus is a pathological condition of involuntary, mostly horizontal eye movements, also known as "dancing eyes".

A.4.9 Muscle Control

The deliberate activation of muscles serves as a communication channel for HMIs. Muscle activity can be detected with the aid of EMG or acoustic myography (AMG).

Electromyography (EMG) yields MESs (cf. Section 1.2.5). As the signal quality depends on the electrode positioning, automated electrode placement methods were developed [180]. EMG-based HMIs rely on muscle contraction and relaxation for the generation of high-level and low-level signals. A historic overview of the EMG technology is provided in [69]. There are two main classes, namely pattern and non-pattern recognition interfaces [143, 231]. As for pattern recognition, the common steps are data segmentation, feature extraction, classification and performing corresponding actions. The desired classes of functions are discriminated from signal patterns by classifiers and the variety of functions depends

directly on classification performance. As for non-pattern recognition, various schemes are feasible, like proportional control, threshold control or FSMs. Proportional control means that signal strength is proportional to the controlled variable such as speed or force.

Single threshold methods usually perform actions when a predefined threshold is exceeded. Improved single threshold methods like the Marple-Hovart and Gilbey (MHG) algorithm are more advanced. Two adjacent time windows that are equal in length are defined, the first is leading the latter is trailing. These windows slide over a data sequence. In each leading window, the MAV of the signal is calculated and compared with the signal in the trial window. Onset and offset time can be obtained by relying on the hypothesis that the maximum difference between mean values occurs when one window contains a muscle contraction, and the other does not [143]. Double threshold methods with more parameters to tune provide higher detection rates. FSMs require data segmentation, feature extraction and the definition of states and transitions.

Many application-oriented EMG-based HMIs were developed such as arm and hand prostheses [28, 157, 161, 163, 165], robotic arms and hands [19, 34, 124] and EPWs [33, 55, 199, 208, 231]. Robotic exoskeleton systems as well as mobile robots were developed [96, 218]. Some works also deal with the implementation of specialized command languages [146, 157].

Acoustic myography (AMG), also known as phonomyography (PMG), sound myography, vibromyography and surface mechanomyogram, is non-invasive. It detects low frequency sounds (infrasounds, $f < 20$ Hz) caused by contracting muscles with specialized microphones. These are inaudible for humans. Researchers found that AMG exceeds EMG as a technique to monitor muscle fatigue non-invasively as the root mean square (RMS) amplitude of sEMG signals does not correlate well with fatigue [14].

Targeted muscle reinnervation (TMR) is a surgical procedure for upper extremity amputees. Peripheral nerves which normally innervate the arm are reattached to residual, unused muscles; usually the pectoral muscles [104, 105, 184]. EMG of the pectoral muscles is acquired to control arm/hand prostheses. With this method patients control prostheses rather intuitively as the innervation of the pectoral muscles corresponds to the innervation of the amputated extremity. However, it is not applicable for patients with paralyzed limbs, but exclusively applicable for amputees.

Facial muscles such as the forehead or eye-winking muscles are crucial for non-verbal communication. HMIs relying on signals from these muscles do not allow users to express themselves facially without risking system misclassifications. These muscles perform two functions at the same time: Facial expression and HMI control. This problem is solved by the implementation of a virtual clutch to enable and disable the biosignal's interpretation. Distinguishing between facial muscle movements meant for non-verbal communication and the generation of control signals is challenging. Interfaces based on facial muscles also tend to imply certain impairment to esthetics. The system in charge should not stigmatize the users in the social context unduly due to a rather apparatus in their face and due to requiring the users to make funny faces. As for spinal cord injured patients EMG-based interfaces are limited to muscles of above-lesion areas.

A.5 Digital Signal Normalization

A.5.1 Digital Preprocessed Signal

The digital signal normalization aims at producing smooth and normalized signals serving as interpretable activity signals intended for the control of HMIs. Values close to zero represent low activity (e.g., muscle relaxation in case of MESs) and values close to one stand for high activity (e.g., muscle contraction in case of MESs).

Signal normalization algorithms are widely utilized in the context of MESs. An extensive literature review regarding the normalization of sEMG signals was presented in [122]. On the other hand, in [175], a threshold-based algorithm to detect muscle activation without normalization was proposed.

The n-bit digitized signal $x_i[k] \in [0, 2^n - 1]$ represents the preprocessed input modality (cf. Section 3.4) where $i \in \{1, ..., \tilde{I}\}$ denotes the index of input modalities. Any kind of biosignals (e.g., MESs) can be represented by $x_i[k]$. In addition, non-biosignals, these are signals mapping physical quantities, can be represented by $x_i[k]$. Figure A.3 exemplarily depicts a digital preprocessed MES.

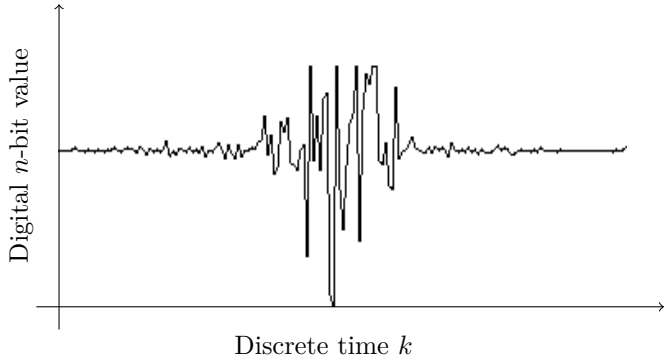

Figure A.3: Digital preprocessed signal

A.5.2 Rectified Signal

The preprocessed signal $x_i[k]$ is not suitable for controlling purposes as it is biased by a specific digital value representing the direct current (DC) offset of the sensor power supply. In order to remove the bias the signal ground level $x_{\mathrm{f,glvl},i}$ is subtracted from $x_i[k]$. This parameter needs to be determined manually or by means of a calibration method. Furthermore, the unbiased signal is rectified (absolute value) and multiplied by a gain constant $g_i \in \mathbb{R}_{>0}$ to get the full range of positive digital values.

The rectified (i.e., unbiased and positive valued) signal $x_{\mathrm{r},i}[k] \in [0, 2^n - 1]$ is calculated in accord with

$$x_{\mathrm{r},i}[k] = g_i \cdot \left| x_i[k] - x_{\mathrm{f,glvl},i} \right|. \tag{A.1}$$

A digital rectified MES is depicted in Figure A.4.

A.5.3 Filtered Signal

The overall characteristics of the control signals need to be smooth in order to apply threshold-based methods. However, the rectified signal $x_{\mathrm{r},i}[k]$ is volatile and therefore needs to be smoothed.

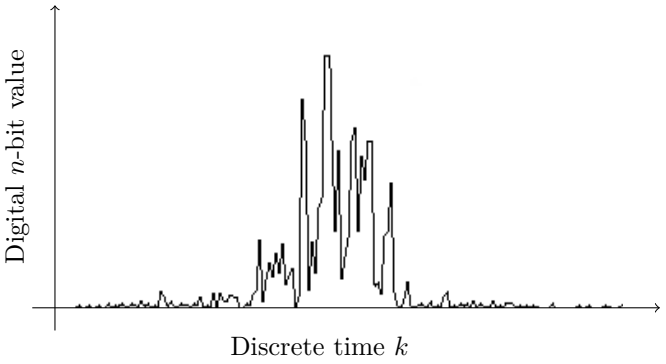

Figure A.4: Digital rectified signal

In order to get a smooth signal the rectified signal $x_{\mathrm{r},i}[k]$ is processed sequentially by the RMS filter and the infinite impulse response (IIR) filter. The RMS filter applies the preset window width parameter $m_i \in \mathbb{N}_{>0}$ which indicates the usage of the previous m_i rectified values (i.e., $x_{\mathrm{r},i}[k]$, $x_{\mathrm{r},i}[k-1]$, ..., $x_{\mathrm{r},i}[k-m_i]$). The IIR filter applies the preset trade-off parameter $a_i \in [0,1)$ which indicates the share between the previously filtered value $x_{\mathrm{f},i}[k-1]$ and the currently RMS-filtered value in order to calculate the newly filtered value $x_{\mathrm{f},i}[k]$. The filtered signal $x_{\mathrm{f},i}[k] \in [0, 2^n - 1]$ is calculated according to

$$x_{\mathrm{f},i}[k] = a_i \cdot x_{\mathrm{f},i}[k-1] + (1-a_i) \cdot \sqrt{\frac{1}{m_i+1} \cdot \sum_{l=0}^{m_i} x_{\mathrm{r},i}^2[k-l]}. \qquad \text{(A.2)}$$

Figure A.5 shows a typical filtered MES.

A.5.4 Normalized Signal

The filtered signal $x_{\mathrm{f},i}[k]$ does not necessarily occupy the full value range $[0, 2^n - 1]$ and hence is not applicable as control signal. The normalization scales the filtered signal $x_{\mathrm{f},i}[k]$ to the range between zero and one.

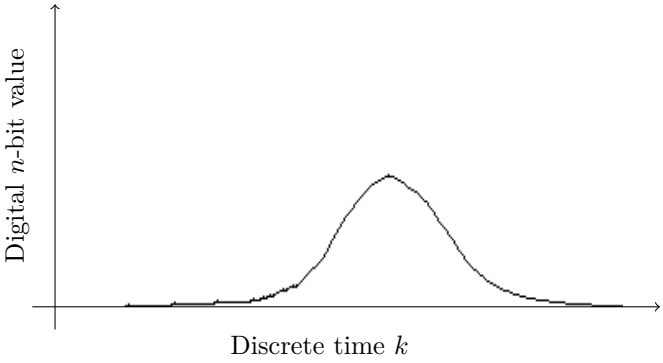

Figure A.5: Digital filtered signal

The normalization is based on the minimum value $x_{\mathrm{f,min},i}$ and maximum value $x_{\mathrm{f,max},i}$ of the filtered signal $x_{\mathrm{f},i}[k]$. These parameters are set manually or with the aid of the calibration method. The normalized signal $x_{\mathrm{n},i}[k] \in [0,1]$ is also called activity signal of the input modality i. It is calculated in accordance with (3.3).

A typical normalized digitized MES is presented in Figure A.6.

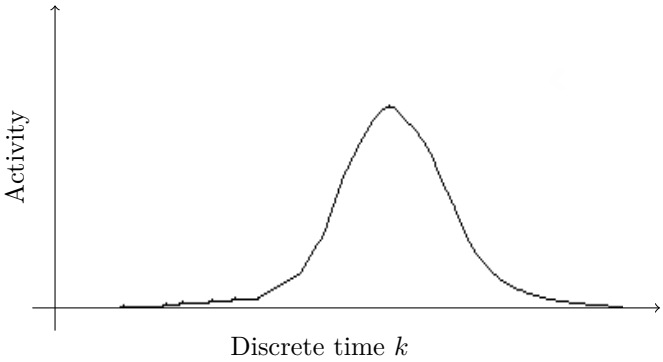

Figure A.6: Digital normalized signal

A.6 Derivation of Model Coefficients for Crosstalk Compensation

The system of linear equations (cf. (3.24)) is defined as

$$\boldsymbol{\omega}_{xT} = \boldsymbol{X}_{xT}\,\boldsymbol{\alpha}_{xT} \tag{A.3}$$

$$\begin{pmatrix} -1 \\ 1 \end{pmatrix} = \begin{pmatrix} 1 & x_{\mathrm{n},1xT2} \\ x_{\mathrm{n},2xT1} & 1 \end{pmatrix} \begin{pmatrix} \alpha_{xT1} \\ \alpha_{xT2} \end{pmatrix}. \tag{A.4}$$

The linear equations are to be solved for $\boldsymbol{\alpha}_{xT}$ following

$$\boldsymbol{\alpha}_{xT} = \boldsymbol{X}_{xT}^{-1}\,\boldsymbol{\omega}_{xT}, \tag{A.5}$$

with the inverse matrix

$$\boldsymbol{X}_{xT}^{-1} = \frac{1}{\det \boldsymbol{X}_{xT}} \begin{pmatrix} 1 & -x_{\mathrm{n},1xT2} \\ -x_{\mathrm{n},2xT1} & 1 \end{pmatrix} \tag{A.6}$$

and the determinant

$$\det \boldsymbol{X}_{xT} = 1 - x_{\mathrm{n},1xT2} \cdot x_{\mathrm{n},2xT1}. \tag{A.7}$$

The multiplication yields the equations for both model coefficients, namely α_{xT1} and α_{xT2}, according to

$$\boldsymbol{\alpha}_{xT} = \begin{pmatrix} \frac{1}{1-x_{\mathrm{n},1xT2}\cdot x_{\mathrm{n},2xT1}} & -\frac{x_{\mathrm{n},1xT2}}{1-x_{\mathrm{n},1xT2}\cdot x_{\mathrm{n},2xT1}} \\ -\frac{x_{\mathrm{n},2xT1}}{1-x_{\mathrm{n},1xT2}\cdot x_{\mathrm{n},2xT1}} & \frac{1}{1-x_{\mathrm{n},1xT2}\cdot x_{\mathrm{n},2xT1}} \end{pmatrix} \begin{pmatrix} -1 \\ 1 \end{pmatrix} \tag{A.8}$$

$$= \begin{pmatrix} -\frac{1+x_{\mathrm{n},1xT2}}{1-x_{\mathrm{n},1xT2}\cdot x_{\mathrm{n},2xT1}} \\ \frac{1+x_{\mathrm{n},2xT1}}{1-x_{\mathrm{n},1xT2}\cdot x_{\mathrm{n},2xT1}} \end{pmatrix}. \tag{A.9}$$

A.7 Control Signal Generators

A.7.1 One-Signal Morse

In case merely one human-generated signal is available this control signal generator, as depicted in Figure A.7, is applicable.

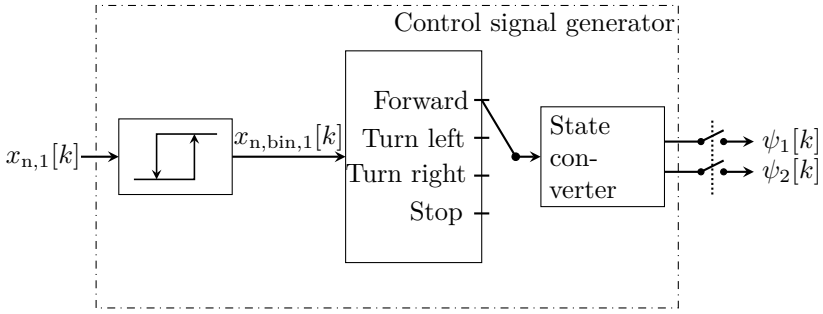

Figure A.7: One-signal Morse control signal generator containing one bang-bang hysteresis controller, a finite state machine and a state converter

The information of the signal is modulated by frequency. Therefore the control signal generator implements a self-devised Morse code comprising four words as presented in Table A.1. This Morse code meets the Fano variety [58] – none of the words is the prefix of another word.

Word	Modulation	Short form
Forward	"long, long"	- -
Turn left	"long, short, short"	- · ·
Turn right	"long, short, long"	- · -
Stop	"short"	·

Table A.1: Patterns of the Morse code alphabet with short activity (·) and long activity (-)

Figure A.8 depicts the finite state machine. Each of the executive states *forward*, *turn left* and *turn right* need to be activated via the idling state *stop*. The turning states are on-the-spot turns, while turning the translational speed equals zero. There are no transitions between the executive states. The translational and rotational speeds are constant and predefined.

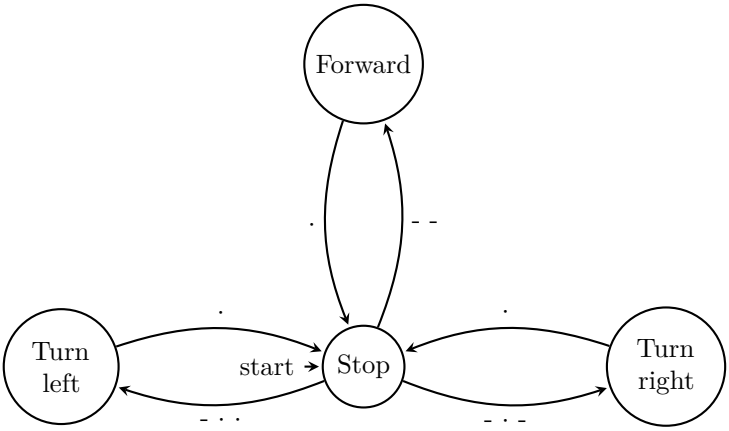

Figure A.8: Finite state machine of the one-signal Morse control signal generator with short activity (·) and long activity (-)

A.7.2 One-Signal Morse Proportional

The previous control signal generator (cf. Appendix A.7.1) enables the user to navigate based on only one biosignal. However, it may become tedious for the user to rely merely on straightforward movements together with left and right on-the-spot turns in order to navigate freely.

The one-signal Morse proportional control signal generator enables the user to perform turns with translational speed. It outputs a rotational signal dependent on the actual biosignal amplitude rather than standing still and turning on-the-spot.

After parsing the complete patterns representing the left resp. right turn (short forms - · · resp. - · -), the amplitude of the biosignal is interpreted as the inverse desired radius. In other words, high biosignal amplitudes stand for small radii and low biosignal amplitudes yield large radii. This special mode of biosignal interpretation is disabled and the pattern parsing is enabled again as soon as the biosignal amplitude falls below a predefined threshold.

A.7.3 Two-Signal Threshold

Figure A.9 illustrates a control signal generator comprising two bang-bang hysteresis controllers, a finite-state machine and a state converter. This control signal generator requires two input signals $x_{\mathrm{n},1}[k]$ and $x_{\mathrm{n},2}[k]$ and, in turn, generates two control signals for both translation velocity $\psi_1[k]$ and rotation velocity $\psi_2[k]$.

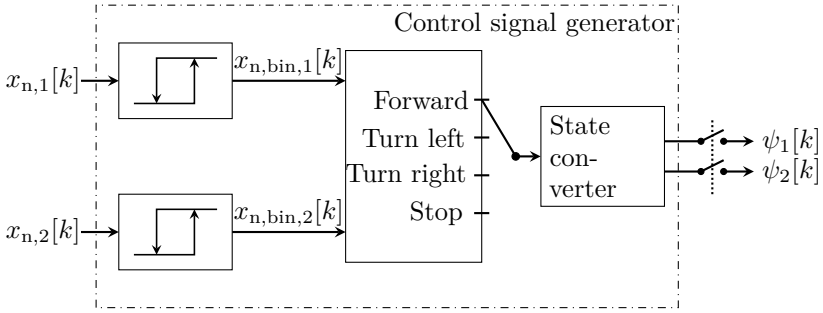

Figure A.9: Two-signal threshold control signal generator containing two bang-bang hysteresis controllers, a finite state machine and a state converter

The bang-bang hysteresis controllers output binary signals $x_{\mathrm{n,bin},1}[k]$ representing the (abstract) presence of activity and the absence of activity, respectively, according to

$$x_{\mathrm{n,bin},i}[k] = \begin{cases} 1 & \text{, if } x_{\mathrm{n},i}[k] \geq \theta_{\mathrm{u}}, \text{ short form } \text{“}x_i = 1\text{”} \\ 0 & \text{, if } x_{\mathrm{n},i}[k] \leq \theta_{\mathrm{l}}, \text{ short form } \text{“}x_i = 0\text{”} \end{cases} . \tag{A.10}$$

The upper threshold θ_{u} and the lower threshold θ_{l} of the hysteresis are set manually with

$$\theta_{\mathrm{u}} > \theta_{\mathrm{l}}. \tag{A.11}$$

The state diagram of the finite-state machine is depicted in Figure A.10. It is based on both the binary signals x_1 and x_2. The initial state is the idling state termed *stop*. The states *turn left* and *turn right* rotate the

vehicle on-the-spot. On the other hand, the state *forward* propels the vehicle straightforward without any rotation. For better intuitiveness, it is not feasible to transition directly from one turning state into the other.

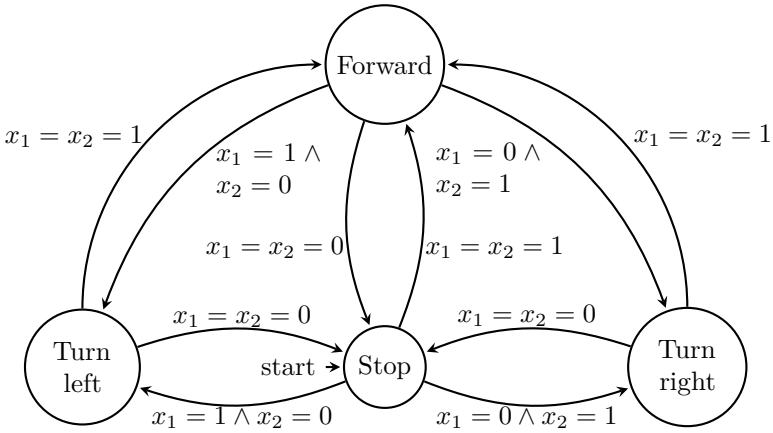

Figure A.10: Finite state machine of the two-signal threshold control signal generator (modified from [183])

A.8 Adaptive HMIs in Assistive Technologies

In the context of assistive technologies and rehabilitation engineering plenty of works dealt with the design of adaptive HMIs to address the need for patient customized solutions.

[174, 175] developed an EMG signal based adaptive HMI that recognize user triggered signal pattern through wavelet decomposition. By means of self-adjustable thresholds it detects different muscle contraction types for different users. [196] presented an EMG pattern classifier for wheelchair control. It was designed to cope with the effects of muscle fatigue.

When controlling a computer mouse or computer pen the presence of tremor is problematic. [170, 171] sought to improve the accuracy of manual input

by canceling involuntary motion with a feedforward neural network. The tremor is modeled by forming a truncated Fourier series estimate. An adaptive filter is implemented which learns the tremor user's frequency and amplitude (tremor estimator) in order to suppress the tremor during HMI control (tremor canceler). [28] presented a tendon driven under-actuated prosthetic hand providing adaptive grasp. [234] proposed the EMG driven meal assistance robotic system. It applies an adapting single-threshold method on EMG power. Two bipolar EMG sensors are attached to the left and the right calf. [96] developed a robotic exoskeleton arm with a neuro-fuzzy controller by means of several surface EMG sensors attached to the user's elbow and shoulder. The controller adapts itself to the individual need of different users. The adaptation is performed by the aid of the backpropagation learning algorithm. The adaptation is carried out offline before operation. It is based on desired muscle activity level of the user.

[146] presented an adaptive threshold method for generating Morse code. [125] presented an adaptive system based on the satisfaction measurement. The key idea was the development of human-oriented interfaces (i.e., the executing device adapts to the human), in contrast to machine-oriented interfaces (i.e., the human adapts to the executing device) based on the assessment of human satisfaction. The user carries out a simple mental task that is the addition of two-digit numbers. The user's satisfaction level is measured by means of extracted EEG signals. The time interval between the presentation of one addition problem and the next is adapted to meet the user's satisfaction. [10] maintained the task difficulty using an adaptive staircase algorithm based on task performance. The task is to play an adaptive version of the multitasking training game NeuroRacer. In order to assess the multitasking costs during playing the game EEG signals are acquired from the user. [30] presented a robotic arm for rehabilitation purposes named GENTLE/A. The user task was 3D point-to-point movements with embedded and VR environment. The deviation between the actual 3D coordinates and the reference 3D coordinates at a given time was used to identify the lead-lag contribution of the participant interacting with the system. The duration for executing one path segment was adjusted between the trials. [35] presented a data glove incorporating 19 resistive sensors to detect the hand posture. The user task is to reach certain positions with the virtual cursor that is representing the hand. The hand posture is mapped to a virtual 2-DOF robotic arm via

mapping matrix. The adaptation mechanism is based on the endpoint error (time-to-target timeout). [59] developed an EMG based master-slave manipulator system for arm amputees. The system works with EMG signal pattern recognition via statistical neural networks. It adapts the pattern recognition depending on the user. The EMG entropy level was utilized as a measure of the classifier input-output pairs' validity. They stated that if the EMG entropy was lower than a predefined threshold, then the reliability of the classified patterns could be high. Thus, the input-output pairs could be added to the neural network's on-line training set, while the oldest pairs were deleted from it.

[168, 169] presented a virtual forearm prosthesis controlled by EMG signals taken from the biceps brachii and triceps brachii muscle. The system incorporates affective measures by acquiring the entropy of the alpha band of the forehead EEG signals taken from a pair of electrodes placed on forehead. Therefore, this HMI can adapt itself to the subject's mental states. [186] examined an object grasping task. The grasping force prediction is designed adaptive depending on the object's image information and the object's sEMG information without actually lifting the object.

[198] utilized two sEMG electrodes and one goniometer to control a virtual hand within a virtual grasping task. The task difficulty level is adaptive and dependent on the task success of the user.

[217] showed how the performance in EEG control could be improved by the developed adaptive calibration. [231] developed an adaptive HMI using incremental SVM with sEMG signals. An EPW was controlled. [124] analyzed an adaptive SVM with sEMG signals to control a robotic arm.

A.9 ASIA

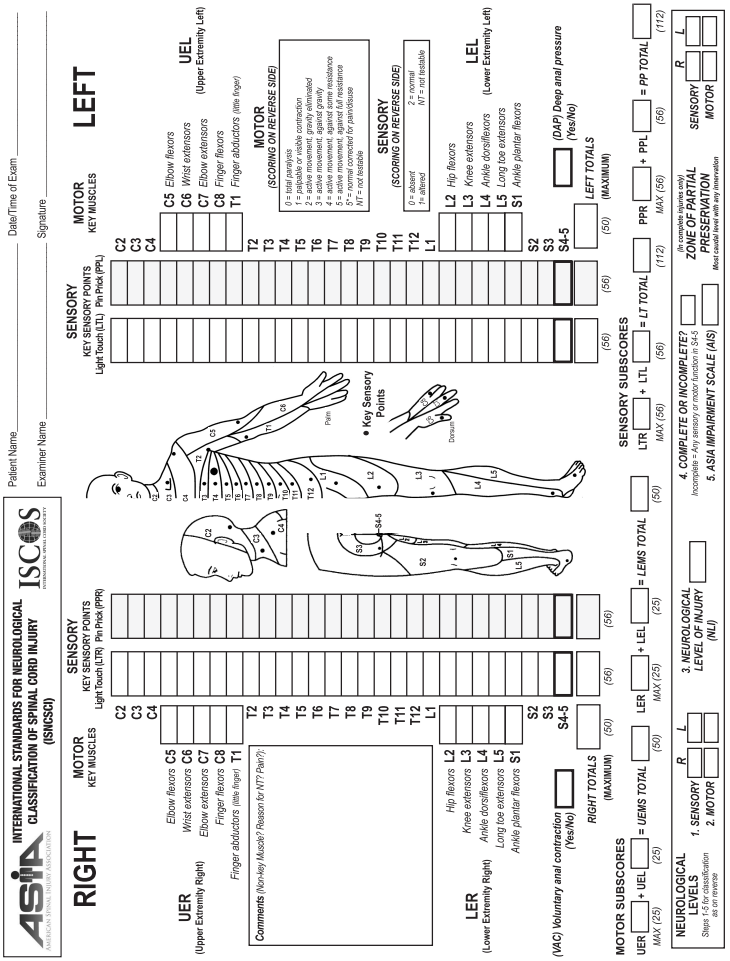

Figure A.11: Page 1 of the ASIA form[4]

[4] http://www.asia-spinalinjury.org/information/downloads

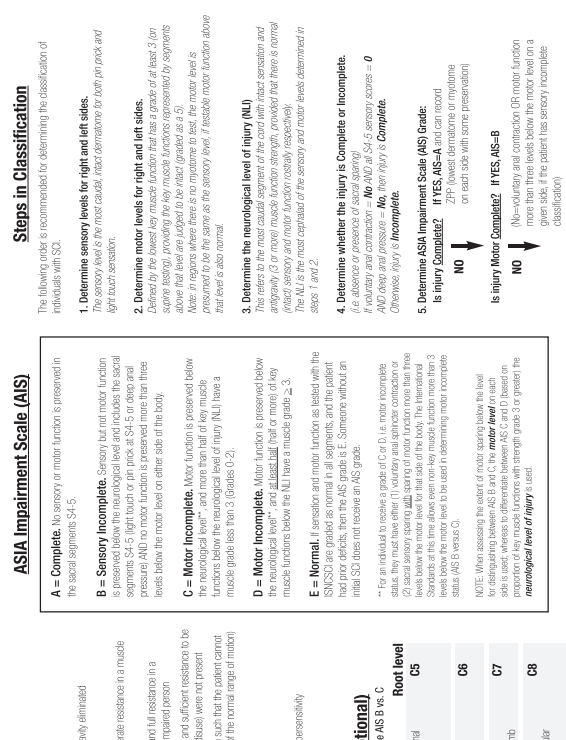

Muscle Function Grading

0 = total paralysis

1 = palpable or visible contraction

2 = active movement, full range of motion (ROM) with gravity eliminated

3 = active movement, full ROM against gravity

4 = active movement, full ROM against gravity and moderate resistance in a muscle specific position

5 = (normal) active movement, full ROM against gravity and full resistance in a functional muscle position expected from an otherwise unimpaired person

5* = (normal) active movement, full ROM against gravity and sufficient resistance to be considered normal if identified inhibiting factors (i.e. pain, disuse) were not present

NT = not testable (i.e. due to immobilization, severe pain such that the patient cannot be graded, amputation of limb, or contracture of > 50% of the normal range of motion)

Sensory Grading

0 = Absent

1 = Altered, either decreased/impaired sensation or hypersensitivity

2 = Normal

NT = Not testable

Non Key Muscle Functions (optional)

May be used to assign a motor level to differentiate AIS B vs. C

Movement	Root level
Shoulder: Flexion, extension, abduction, adduction, internal and external rotation	C5
Elbow: Supination	
Elbow: Pronation	C6
Wrist: Flexion	
Finger: Flexion at proximal joint, extension.	C7
Thumb: Flexion, extension and abduction in plane of thumb	
Finger: Flexion at MCP joint	C8
Thumb: Opposition, adduction and abduction perpendicular to palm	
Finger: Abduction of the index finger	T1
Hip: Adduction	L2
Hip External rotation	L3
Hip: Extension, abduction, internal rotation	L4
Knee: Flexion	
Ankle: Inversion and eversion	
Toe: MP and IP extension	
Hallux and Toe: DIP and PIP Flexion and abduction	L5
Hallux: Adduction	S1

ASIA Impairment Scale (AIS)

A = Complete. No sensory or motor function is preserved in the sacral segments S4-5.

B = Sensory Incomplete. Sensory but not motor function is preserved below the neurological level and includes the sacral segments S4-5 (light touch or pin prick at S4-5 or deep anal pressure) AND no motor function is preserved more than three levels below the motor level on either side of the body.

C = Motor Incomplete. Motor function is preserved below the neurological level** , and more than half of key muscle functions below the neurological level of injury (NLI) have a muscle grade less than 3 (Grades 0-2).

D = Motor Incomplete. Motor function is preserved below the neurological level** , and at least half (half or more) of key muscle functions below the NLI have a muscle grade ≥ 3.

E = Normal. If sensation and motor function as tested with the SCI/SCD are graded as normal in all segments, and the patient had prior deficits, then the AIS grade is E. Someone without an initial SCI does not receive an AIS grade.

** For an individual to receive a grade of C or D, i.e. motor incomplete status, they must have either (1) voluntary anal sphincter contraction or (2) sacral sensory sparing at the lowest sacral segments (S4-5) and more than three levels below the motor level on either side of the body. The International Standards at this time allows even non-key muscle function more than 3 levels below the motor level to be used in determining motor incomplete status (AIS B versus C).

NOTE: When assessing the extent of motor sparing below the level for distinguishing between AIS B and C, the ***motor level*** on each side is defined by the most caudal key muscle that has a grade of at least 3 on proportion of key muscle functions with strength grade 3 or greater) the ***neurological level of injury*** is used.

ASIA
AMERICAN SPINAL INJURY ASSOCIATION

INTERNATIONAL STANDARDS FOR NEUROLOGICAL CLASSIFICATION OF SPINAL CORD INJURY

ISCOS
INTERNATIONAL SPINAL CORD SOCIETY

Steps in Classification

The following order is recommended for determining the classification of individuals with SCI.

1. Determine sensory levels for right and left sides.
The sensory level is the most caudal, intact dermatome for both pin prick and light touch sensation.

2. Determine motor levels for right and left sides.
Defined by the lowest key muscle function that has a grade of at least 3 (on supine testing), providing the key muscle functions represented by segments above that level are judged to be intact (graded as a 5).
Note: in regions where there is no myotome to test, the motor level is presumed to be the same as the sensory level, if testable motor function above that level is also normal.

3. Determine the neurological level of injury (NLI)
This refers to the most caudal segment of the cord with intact sensation and antigravity (3 or more) muscle function strength, provided that there is normal (intact) sensory and motor function rostrally respectively.
The NLI is the most cephalad of the sensory and motor levels determined in steps 1 and 2.

4. Determine whether the injury is Complete or Incomplete.
(i.e. absence or presences of sacral sparing)
*If voluntary anal contraction = **No** AND all S4-5 sensory scores = **0** AND deep anal pressure = **No**, then injury is **Complete**.*
*Otherwise, injury is **Incomplete**.*

5. Determine ASIA Impairment Scale (AIS) Grade:

Is injury Complete? **If YES, AIS=A** and can record ZPP (lowest dermatome or myotome on each side with some preservation)

NO →

Is injury Motor Complete? **If YES, AIS=B**

NO → (No=voluntary anal contraction OR motor function more than three levels below the motor level on a given side, if the patient has sensory incomplete classification)

Are at least half (half or more) of the key muscles below the neurological level of injury graded 3 or better?

NO → **AIS=C**

YES → **AIS=D**

If sensation and motor function is normal in all segments, AIS=E
Note: AIS E is used in follow-up testing when an individual with a documented SCI has recovered normal function. If at initial testing no deficits are found, the individual is neurologically intact, the ASIA Impairment Scale does not apply.

Figure A.12: Page 2 of the ASIA form[5]

[5] `http://www.asia-spinalinjury.org/information/downloads`

A.10 Application for Ethical Approval (German)

Antrag an die Ethikkommission des KIT zur Beurteilung eines Forschungsvorhabens

1. Bezeichnung des Forschungsvorhabens

Wirksamkeitsuntersuchung inkrementeller Parameteradaptionsalgorithmen im Kontext einer myoelektrisch gesteuerten Mensch-Maschine-Schnittstelle

2. Name und Kontaktdaten des Antragstellers

Institut für Angewandte Informatik (IAI)
Hermann-von-Helmholtz-Platz 1
76344 Eggenstein-Leopoldshafen
Dipl.-Ing. Michele René Tuga
michele.tuga@kit.edu
0721-608-26672
24.02.2015
Kein vorheriger Antrag

3. Auftraggeber bzw. Geldgeber des Projekts

Bundesministerium für Bildung und Forschung (BMBF)
TELMYOS – telemetrisches, myoelektrisches Ohrmuskelableitsystem zur Steuerung technischer Rehabilitationsmittel – im Forschungsprogramm „Innovative Hilfen in der Rehabilitation und für Behinderte“
FKZ: 01EZ1122C

4. Angaben zu den Rahmenbedingungen des Vorhabens

Die Probandenstudie beginnt am 16.03.2015 und dauert ca. 2 Wochen.

5. Gegenstand und Verfahren des Vorhabens

Gegenstand: Es werden zwei Adaptionsalgorithmen zur Optimierung der Steuerung eines virtuellen Rollstuhls verglichen. Ziel ist der Nachweis einer signifikanten Verbesserung der Steuerung gegenüber einer Steuerung ohne Adaptionsalgorithmus.

Methoden: Es werden Muskelaktivitätssignale (EMG-Signalen) von der Unterarmmuskulatur der Probanden abgeleitet.

Aufgaben: Den Probanden werden je eine (nicht invasive) Oberflächen-EMG-Elektrode auf dem linken und eine auf dem rechten Unterarm platziert. Die Elektroden werden mit Hilfe von Manschetten an den Unterarmen befestigt und vor Deplatzierung gesichert. Um eine bessere Signalqualität zu gewährleisten, wird die Hautoberfläche unter der Elektrode lokal leicht mit Wasser angefeuchtet.

Figure A.13: Application for ethical approval, Page 1

Über Anspannung (Kontraktion) und Entspannung (Relaxation) der Unterarmmuskulatur (hauptsächlich M. extensor digitorum) kann der Proband in einem Computerspiel ein virtuelles Auto nach links oder rechts steuern. Die Probanden werden gebeten, mittels dieser vereinfachten Steuerung ein Auto auf einer sich ändernden Straße zu halten. Die Muskelaktivität des Probanden wird erfasst und der Echtzeit-Signalverarbeitung zugeführt.

In den ersten Minuten hat der Proband Zeit, die Steuerung des Autos zu üben. Dabei ist dauerhaft eine Aufsichtsperson anwesend, die bei Bedarf Fragen beantworten kann. Nach dieser Übungsphase werden die Daten zur Steuerung des Autos während des Computerspiels aufgezeichnet. Die Performanz der Probanden wird in Form eines quantitativen Gütekriteriums während des Spiels berechnet. Die Probanden werden aufgefordert, 10 Mal hintereinander das Autorennen zu absolvieren. Ein Durchgang dauert ca. 60 Sekunden. Zwischen den Durchgängen wird eine Ruhephase von ca. 30 Sekunden eingehalten, in der den Probanden die Möglichkeit gegeben wird, die Muskulatur zu entspannen. Die Probanden werden in drei Gruppen (A, B, C) eingeteilt.
Gruppe A dient als Kontrollgruppe. Probanden dieser Gruppe absolvieren das Spiel ohne Anwendung eines Adaptionsalgorithmus. Die Gruppe B steuert das Auto unter Hinzunahme des Adaptionsalgorithmus1 und die Gruppe C unter Hinzunahme des Adaptionsalgorithmus2.

Einschätzung der wissenschaftlichen Relevanz: Um Mensch-Maschine-Schnittstellen effektiv einsetzen zu können, ist eine individuelle Anpassung an den Nutzer erforderlich. Diese Studie dient der Untersuchung einer Form der schnittstellenseitigen, automatisierten Anpassung an den Benutzer.

6. Wo sehen Sie mögliche ethische Fragestellungen durch das Projekt aufgeworfen?

Unter Umständen könnten Probanden Frustration erleben, falls das virtuelle Auto sich nicht wie erwartet verhält bzw. sich auf dem Bildschirm darstellt.

7. Wurden die jeweils zuständigen Beauftragten z.B. Datenschutz beteiligt?

Die Datenschutzbeauftragte des KIT, Frau Marina Bitmann, wurde im Vorfeld konsultiert und hat nach Prüfung der vorgelegten Unterlagen keine datenschutzrechtlichen Bedenken hinsichtlich der Studiendurchführung.

8. Projekte unter Einbeziehung von Probandinnen/Probanden

a) Abwägung der wissenschaftlichen Relevanz der Projektergebnisse mit möglichen Auswirkungen auf Probanden/Probandinnen:
Mit der Teilnahme an dieser Studie bietet sich den Probanden die Möglichkeit einen Beitrag zur Verbesserung von automatisierten Schnittstellenanpassungen zu leisten.

b) Gewinnung der Personenstichprobe und Vergütung von Probanden/Probandinnen:
Es werden pro Gruppe 5 Probanden benötigt, insgesamt also 15 Probanden.

Figure A.14: Application for ethical approval, Page 2

Geschäftsfähigkeit: Sämtliche Teilnehmer sind volljährig und geschäftsfähig

Einschlusskriterien

- Menschen (m/w) im Alter zwischen 18 und 70 Jahren ohne signifikante körperliche oder geistige Beeinträchtigungen

Ausschlusskriterien

- Körperliche Beeinträchtigungen, die die Steuerung mittels Unterarmmuskulatur verhindern
- Geistige Beeinträchtigungen
- Psychische Auffälligkeiten
- Epilepsie
- Erfahrungen mit der EMG-Schnittstellen in Bezug auf das Autorennen

Teilnahmevergütung: Die Teilnahme an dieser Studie wird nicht vergütet.

c) Freiwilligkeit der Studienteilnahme ist in der Teilnehmerinformation angegeben.

Die Teilnahme ist absolut freiwillig. Jederzeitige Rücktrittsmöglichkeit ohne Nachteile und mit Recht auf Löschung der eigenen Daten ist sichergestellt.

d) Die Teilnehmerinformation sowie die Einwilligungserklärung sind diesem Antrag beigefügt.

Ich bestätige, dass alle Angaben in diesem Antrag korrekt sind.

Ort, Datum

Unterschrift der Leitung des Forschungsvorhabens

Figure A.15: Application for ethical approval, Page 3

Studienleitung:
Karlsruher Institut für Technologie
Institut für Angewandte Informatik
Hermann-von-Helmholtz-Platz 1
76344 Eggenstein-Leopoldshafen
Dipl.-Ing. Michele René Tuga
T: +49 721 608-26672
F: +49 721 608-22602
E: michele.tuga@kit.edu

Probandeninformation

Wirksamkeitsuntersuchung inkrementeller Parameteradaptionsalgorithmen im Kontext einer myoelektrisch gesteuerten Mensch-Maschine-Schnittstelle

Sehr geehrte Probandin, sehr geehrter Proband,

die Arbeitsgruppe Biosignalanalyse des Instituts für Angewandte Informatik beschäftigt sich mit der Entwicklung innovativer Rehabilitationshilfen für Behinderte. Sogenannte Mensch-Maschine-Schnittstellen nehmen in der Mensch-Maschine-Kommunikation eine Schlüsselrolle ein. Es handelt sich dabei um technische Realisationen, die körpereigene Biosignale, z.B. Muskelaktivität, des Menschen interpretieren und daraus Steuerungssignale für technische Geräte, z.B. Elektrorollstühle, generieren.

In diesem Forschungsvorhaben werden Adaptionsalgorithmen zur Optimierung der Steuerung eines virtuellen Rollstuhls verglichen. Es werden dazu Muskelaktivitätssignale (EMG-Signale) von Ihrer Unterarmmuskulatur beidseitig gemessen. Nicht-invasive Oberflächen-Elektroden werden Ihnen von einer Aufsichtsperson auf den Unterarmen platziert und mit Manschetten vor Deplatzierung gesichert. Die Messung der EMG-Signale ist also schmerzfrei und gefahrlos. Um eine bessere Signalqualität zu gewährleisten, wird die Hautoberfläche unter der Elektrode lokal leicht mit Wasser angefeuchtet.

Über Anspannung (Kontraktion) und Entspannung (Relaxation) Ihrer beidseitigen Unterarmmuskulatur (hauptsächlich M. extensor digitorum) können Sie in einem

Figure A.16: Information sheet regarding the study, Page 1

Computerspiel ein virtuelles Auto horizontal nach links oder rechts steuern. Sie werden gebeten, mittels dieser vereinfachten Steuerung ein Auto auf einer sich ändernden Straße zu halten. Ihre EMG-Signale werden erfasst und der Echtzeit-Signalverarbeitung zugeführt.

In den ersten Minuten einer jeden Sitzung haben Sie Zeit, die Steuerung des Autos zu üben. Sie sitzen bequem mit angeschlossenen Elektroden und blicken auf einen Computermonitor, der das Computerspiel visualisiert. Dabei ist dauerhaft eine Aufsichtsperson anwesend, die Ihnen bei Bedarf Fragen beantworten wird. Nach dieser initialen Übungsphase wird der erste Durchgang gestartet und es werden die Daten zur Steuerung des Autos während des Computerspiels aufgezeichnet, um diese später auszuwerten. Ihre Performanz wird in Form eines quantitativen Gütekriteriums während des Spiels berechnet. Sie werden aufgefordert, in 10 hintereinander folgenden Durchgängen das Autorennen zu absolvieren. Ein Durchgang des Autorennens dauert ca. 60 Sekunden. Zwischen den Durchgängen wird eine Ruhephase von ca. 30 Sekunden eingehalten, in der Sie die Möglichkeit haben, die Muskulatur zu entspannen und sich auf den nächsten Durchgang vorzubereiten. Nach diesen 10 Durchgängen folgt eine Pause von einigen Minuten. In einem abschließenden Test werden Sie gebeten einen virtuellen Rollstuhl durch einen dreidimensionalen Parkour zu steuern. Hierbei können Sie neben der Richtungssteuerung auch die Geschwindigkeit beeinflussen. Diese lässt sich durch die Intensität der Muskelkontraktionen verändern. Je nach Geschwindigkeit kann dieser Durchgang 3-6 Minuten dauern.

Alle Messungen werden an einem Tag durchgeführt. Dies bedeutet für Sie einen Zeitaufwand von ca. 20 Minuten. Ein Termin wird in Absprache mit Ihnen im Voraus vereinbart. Falls der Termin nicht eingehalten werden kann, sind Sie gebeten dies rechtzeitig zu melden.

Sie werden in eine von drei Gruppen (A, B, C) eingeteilt. Gruppe A dient als Kontrollgruppe. Probanden dieser Gruppe absolvieren das Spiel ohne Anwendung eines Adaptionsalgorithmus. Die Gruppe B steuert das Auto unter Hinzunahme des Adaptionsalgorithmus1 und die Gruppe C unter Hinzunahme des Adaptionsalgorithmus2.

Figure A.17: Information sheet regarding the study, Page 2

Es existiert keine gesonderte Versicherung für die Teilnahme an diesem Forschungsvorhaben.

Figure A.18: Information sheet regarding the study, Page 3

Informationen zum Datenschutz

Während der Studie werden keine Kontaktdaten erhoben. Die gemessenen Muskelsignale werden sogleich anonymisiert gespeichert.

Die Teilnahme an der Studie ist freiwillig. Es entstehen für Sie keinerlei Nachteile, falls Sie sich nicht zu einer Teilnahme an der Studie entschließen sollten. Auch wenn Sie die Einverständniserklärung unterschrieben haben, können Sie die Untersuchung während ihrer Durchführung ohne Nennung von Gründen jederzeit abbrechen. Im Falle eines Abbruchs werden sämtliche bis dahin erhobenen Daten gelöscht.

Die anonymisierten Forschungsdaten werden 10 Jahre nach der letzten Publikation gelöscht.

Die Studienergebnisse werden ausschließlich in aggregierter Form veröffentlicht.

Wenn Sie noch weitere Fragen über den Studienablauf haben oder Ihnen noch etwas unklar ist, wenden Sie sich bitte an die Studienleitung. Sollten Sie nach dem Untersuchungstermin noch Fragen haben, können Sie sich jederzeit an den/die VersuchsleiterIn oder den/die StudienleiterIn wenden.

_____

(Studienleiter Dipl.-Ing. Michele René Tuga)

Figure A.19: Information sheet regarding the data privacy

Studienleitung:
Karlsruher Institut für Technologie
Institut für Angewandte Informatik
Hermann-von-Helmholtz-Platz 1
76344 Eggenstein-Leopoldshafen
Dipl.-Ing. Michele René Tuga
T: +49 721 608-26672
F: +49 721 608-22602
E: michele.tuga@kit.edu

Einwilligungserklärung

Wirksamkeitsuntersuchung inkrementeller Parameteradaptionsalgorithmen im Kontext einer myoelektrisch gesteuerten Mensch-Maschine-Schnittstelle

Name der/s ProbandIn

Herr Michele René Tuga hat mit mir heute ein ausführliches Aufklärungsgespräch über Art, Umfang und Bedeutung dieser Studie geführt. Dabei wurden u.a. Studienziel und Studienlänge, studienbedingte Erfordernisse und mögliche Nebenwirkungen der Studie besprochen. Die Probandeninformation sowie ein Exemplar der Einverständniserklärung habe ich erhalten, gelesen und verstanden. In diesem Zusammenhang bestehende Fragen wurden besprochen und beantwortet. Ich hatte ausreichend Zeit, mich für oder gegen eine Teilnahme an dieser Studie zu entscheiden. Ich wurde darüber informiert, dass keine gesonderte Versicherung während der Studienteilnahme existiert.

Ich bin einverstanden, als UntersuchungsteilnehmerIn an dieser Studie teilzunehmen.

Figure A.20: Declaration of consent, Page 1

Mir ist bekannt, dass diese Studie in erster Linie der Wissenserweiterung dient, und gegebenenfalls auch keinen persönlichen Vorteil für mich bringen kann.

Ich bin darüber unterrichtet worden, dass meine Teilnahme vollkommen freiwillig erfolgt und ich meine Einwilligung zur Teilnahme an dieser Studie jederzeit ohne Angabe von Gründen und ohne persönlichen Nachteil widerrufen kann.

Ich habe die Probandeninformationen und insbesondere den Abschnitt **"Informationen zum Datenschutz"** gelesen und meine Fragen wurden ausreichend beantwortet.

Mir ist bekannt, dass bei dieser Studie auch personenbezogene Daten über mich erhoben, gespeichert und ausgewertet werden sollen. Die Verwendung der personenbezogene Daten erfolgt nach gesetzlichen Bestimmungen und setzt vor der Teilnahme an der Studie folgende freiwillig abgegebene Einwilligungserklärung voraus, d.h. ohne die nachfolgende Einwilligung kann ich nicht an der Studie teilnehmen.

Ich bin damit einverstanden, dass im Rahmen der Studie die in den „Informationen zum Datenschutz" beschriebenen Daten erhoben und in anonymisierter Form gespeichert und für die in den „Probandeninformationen" dargestellten Zwecken verarbeitet werden.

Name ProbandIn	Ort, Datum, Unterschrift
Name StudienleiterIn	Ort, Datum, Unterschrift

Figure A.21: Declaration of consent, Page 2

A.11 Paradigms

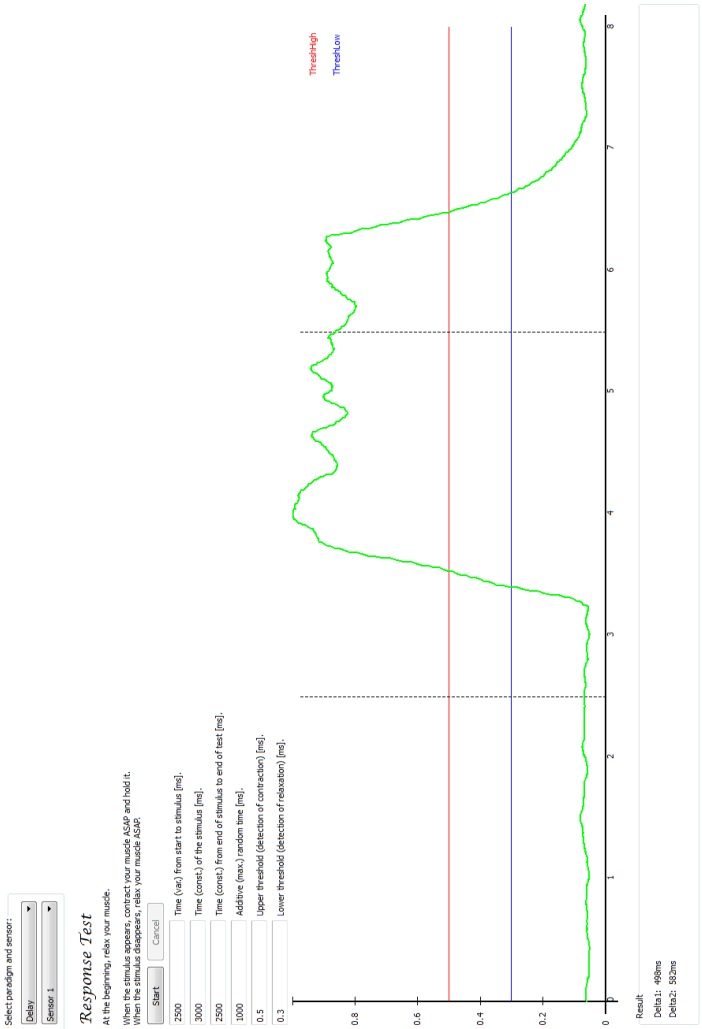

Figure A.22: Response time paradigm

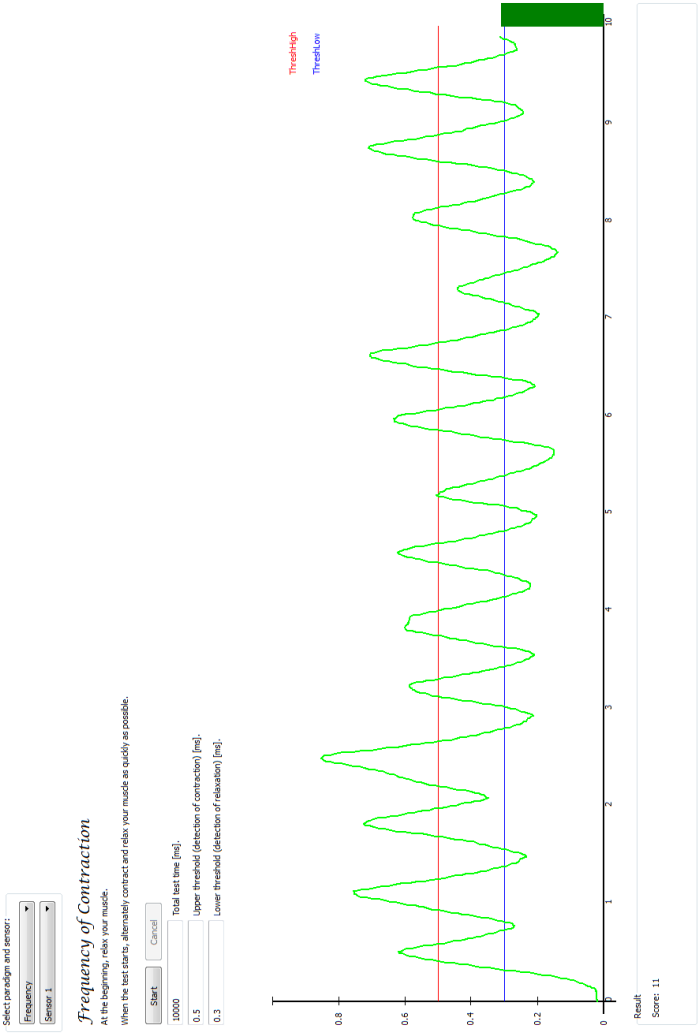

Figure A.23: Frequency paradigm

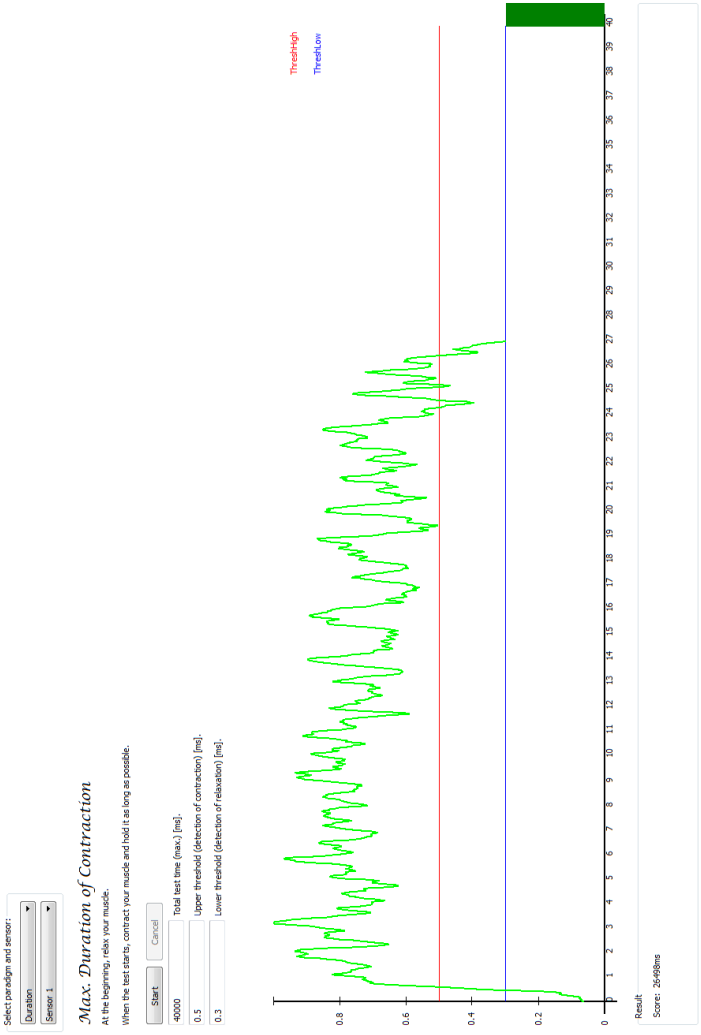

Figure A.24: Duration of maximum activity paradigm

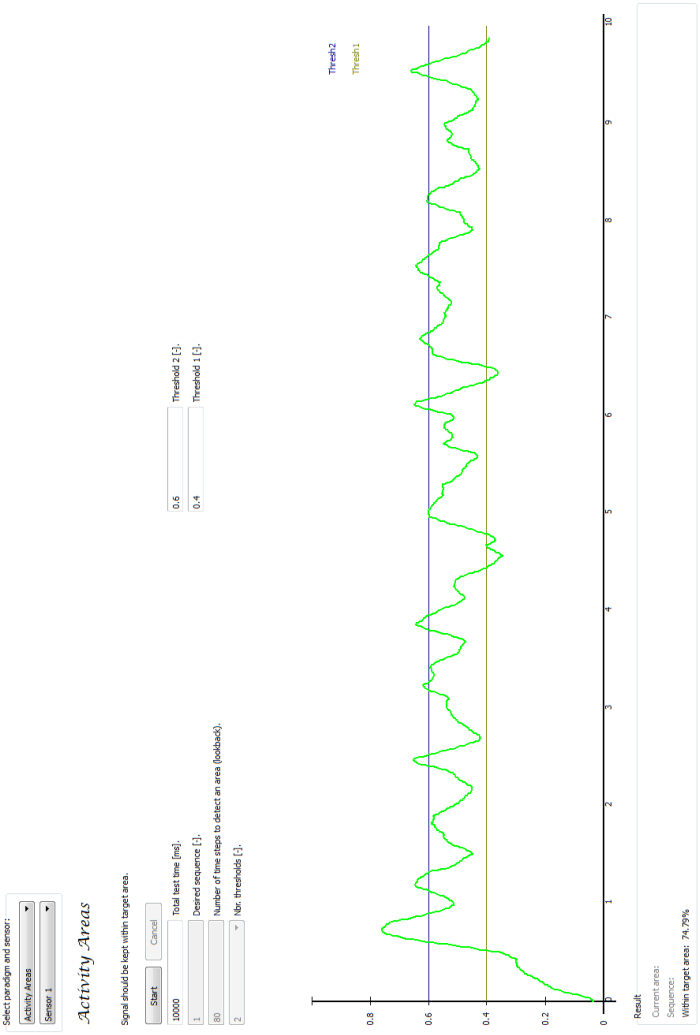

Figure A.25: Duration of range activity paradigm

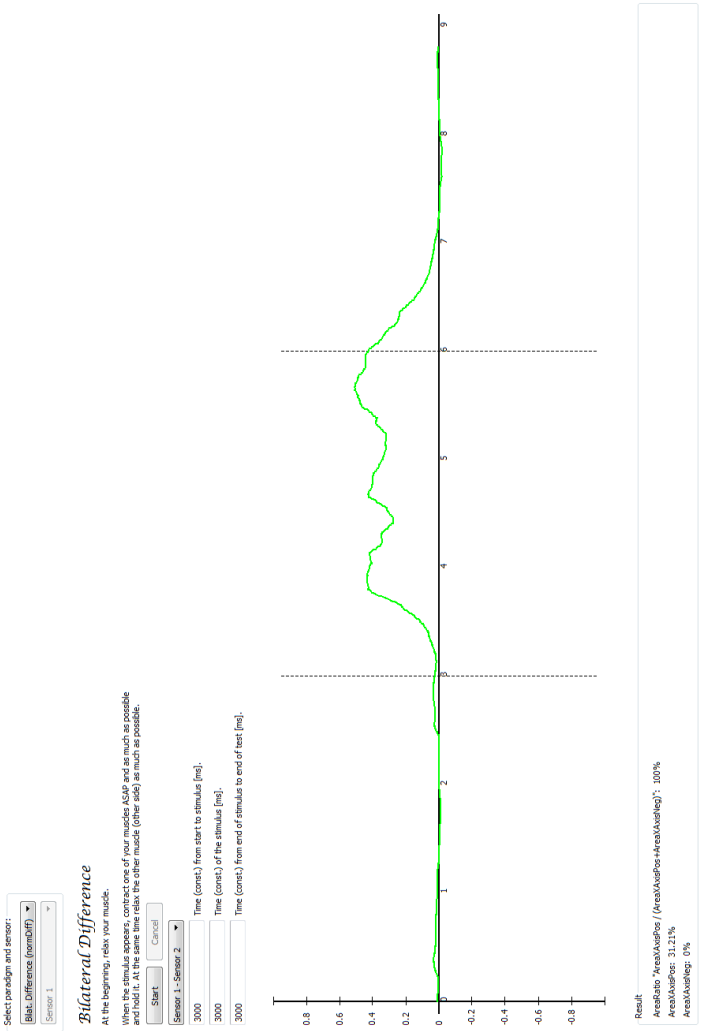

Figure A.26: Bilateral paradigm

A.12 Code Composer Studio

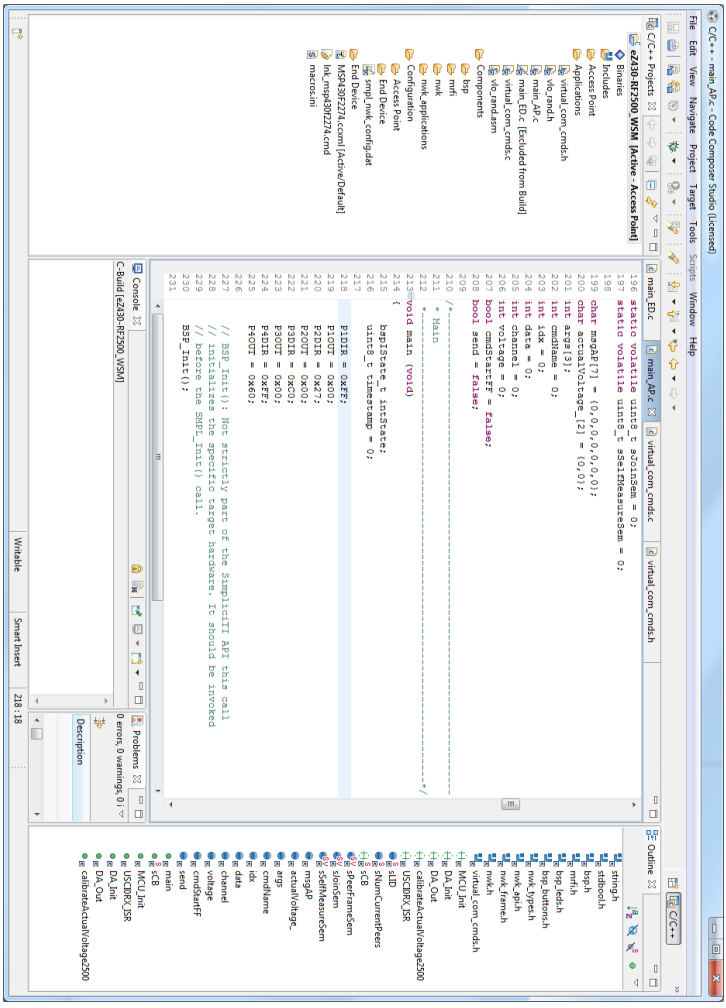

Figure A.27: Code Composer Studio by Texas Instruments

A.13 Commands

ID	Command	Details	Receiver
1	Stand-by	Set MCU's low-power mode and RF transceiver's sleep mode. No data transmission. End stand-by by activating push button.	MCU ED
2	Restart	Non-flash-memory data gets lost.	MCU ED
3	Restart	Non-flash-memory data gets lost.	MCU AP
4	Set sampling rate	< 125 Hz	MCU ED
5	Get sampling rate	Current sampling rate.	MCU ED
6	Set voltage channel 1	[1700 mV, 3300 mV]	MCU AP
7	Get voltage channel 1	Current voltage	MCU AP
8	Set voltage channel 2	[1700 mV, 3300 mV]	MCU AP
9	Get voltage channel 2	Current voltage	MCU AP
10	n/a	n/a	n/a
11	Set receiving rate	[1, 1000]	MCU ED
12	Get receiving rate	Current receiving rate	MCU ED
13	n/a	n/a	n/a
14	n/a	n/a	n/a
15	n/a	n/a	n/a
16	Amend voltage channel 1	[1700 mV, 3300 mV]	MCU AP
17	Amend voltage channel 2	[1700 mV, 3300 mV]	MCU AP
18	Set voltage channel 4	[1700 mV, 3300 mV]	MCU AP
19	Set voltage channel 5	[1700 mV, 3300 mV]	MCU AP
20	Set voltage channel 6	[1700 mV, 3300 mV]	MCU AP

Table A.2: GUI commands intended for ED and AP (modified from [42])

B Bibliography

[1] A. L. M. Abeloos, M. Mulder, and M. M. R. van Paassen. "The Applicability of an Adaptive Human-Machine Interface in the Cockpit". *EAM 2000 - 19th European Annual Conference on Human Decision Making and Manual Control* (2000), pp. 193–8.

[2] S. J. Aiken, J. N. Andrus, M. Bance, and D. P. Phillips. "Acoustic Stapedius Reflex Function in Man Revisited". *Ear and Hearing* 34.4 (2013), e38–e51.

[3] E. Alberg. *Dokumentation zur TELMYOS 3D-Simulation*. German. Tech. rep. Institute for Applied Computer Science, 2014.

[4] L. Alexander. *Microsoft: Kinect Hits 10 Million Units, 10 Million Games*. `http://www.gamasutra.com/view/news/33430/Microsoft_Kinect_Hits_10_Million_Units_10_Million_Games.php`. Retrieved: March 10 2011; Accessed: January 26 2015. Mar. 2011.

[5] G. Allison, P. Godfrey, and G. Robinson. "EMG Signal Amplitude Assessment During Abdominal Bracing and Hollowing". *Journal of Electromyography and Kinesiology* 8.1 (1998), pp. 51–57.

[6] W. Amai, J. Fahrenholtz, and C. Leger. "Hands-Free Operation of a Small Mobile Robot". *Autonomous Robots* 11.1 (2001), pp. 69–76.

[7] A. Amditis, L. Andreone, A. Polychronopoulos, and J. Engström. "Design and Development of an Adaptive Integrated Driver-Vehicle Interface: Overview of the AIDE Project". *IFAQ Conference* 3 (2005).

[8] A. Amditis, H. Kußmann, A. Polychronopoulos, J. Engström, and L. Andreone. "System Architecture for Integrated Adaptive HMI Solutions". *Intelligent Vehicles* (2006), pp. 388–93.

[9] R. D. Amori. “Vocomotion - An Intelligent Voicecontrol System for Powered Wheelchairs”. *Proceedings of the Rehabilitation Engineering Society of North America (RESNA)* (1992), pp. 421–423.

[10] J. Anguera, J. Boccanfuso, J. Rintoul, O. Al-Hashimi, F. Faraji, J. Janowich, E. Kong, Y. Larraburo, C. Rolle, E. Johnston, et al. “Video Game Training Enhances Cognitive Control in Older Adults”. *Nature* 501.7465 (2013), pp. 97–101.

[11] P. Bach-y-Rita and S. W. Kercel. “Sensory Substitution and the Human-Machine Interface”. *Trends in Cognitive Sciences* 7 (2003), pp. 541–6.

[12] R. Barea, L. Boquete, M. Mazo, and E. López. “System for Assisted Mobility Using Eye Movements Based on Electrooculography”. *IEEE Transactions on Neural Systems and Rehabilitation Engineering: A publication of the IEEE Engineering in Medicine and Biology Society* 10.4 (Dec. 2002), pp. 209–18.

[13] R. Barea, L. Boquete, M. Mazo, E. López, and L. M. Bergasa. “EOG Guidance of a Wheelchair Using Neural Networks”. *International Conference on Pattern Recognition* 4 (2000), pp. 668–71.

[14] D. T. Barry, S. R. Geiringer, and R. D. Ball. “Acoustic Myography: A Noninvasive Monitor of Motor Unit Fatigue”. *Muscle & Nerve* 8.3 (1985), pp. 189–94.

[15] J.-D. Bauby. *The Diving Bell and the Butterfly*. Éditions Robert Laffont, 1997.

[16] F. Berzin and C. Fortinguerra. “EMG Study of the Anterior, Superior and Posterior Auricular Muscles in Man”. *Annals of Anatomy-Anatomischer Anzeiger* 175.2 (1993), pp. 195–197.

[17] E. A. Biddiss and T. T. Chau. “Upper Limb Prosthesis Use and Abandonment: A Survey of the Last 25 Years”. *Prosthetics and Orthotics International* 31.3 (2007), pp. 236–57.

[18] N. Birbaumer, N. Ghanayim, T. Hinterberger, I. Iversen, B. Kotchoubey, A. Kübler, J. Perelmouter, E. Taub, and H. Flor. “A Spelling Device for the Paralysed”. *Nature* 398 (1999), pp. 297–298.

[19] S. Bitzer and P. van der Smagt. “Learning EMG Control of a Robotic Hand: Towards Active Prostheses”. *Robotics and Automation, 2006. ICRA 2006. Proceedings 2006 IEEE International Conference on*. May. 2006, pp. 2819–23.

[20] B. Blankertz, K.-R. Müller, G. Curio, T. M. Vaughan, G. Schalk, J. R. Wolpaw, A. Schlögl, C. Neuper, G. Pfurtscheller, T. Hinterberger, M. Schröder, and N. Birbaumer. “The BCI Competition 2003: Progress and Perspectives in Detection and Discrimination of EEG Single Trials”. *IEEE Transactions on Biomedical Engineering* 51(6) (2004), pp. 1044–1051.

[21] B. Blankertz, G. Dornhege, M. Krauledat, K.-R. Müller, and G. Curio. “The Non-Invasive Berlin Brain-Computer Interface: Fast Acquisition of Effective Performance in Untrained Subjects”. *NeuroImage* 37.2 (Aug. 2007), pp. 539–50.

[22] R. Boostani and M. H. Moradi. “Evaluation of the Forearm EMG Signal Features for the Control of a Prosthetic Hand”. *Physiological Measurement* 24 (2003), pp. 309–319.

[23] W. Bradley. *Neurology in Clinical Practice: Principles of Diagnosis and Management*. Neurology in Clinical Practice. Butterworth-Heinemann, 2004.

[24] A. Bulling, D. Roggen, and G. Tröster. “Wearable EOG Goggles: Seamless Sensing and Context-Awareness in Everyday Environments”. *Journal of Ambient Intelligence and Smart Environments* 1.2 (2009), pp. 157–171.

[25] M. B. Bunge. “Book Review: Bridging Areas of Injury in the Spinal Cord”. *The Neuroscientist* 7.4 (2001), pp. 325–339.

[26] J. Cai and R. Liu. “An Improved Online SVM Algorithm for Overcoming the Influence of Muscle Fatigue in sEMG Based Human Machine Interaction”. *Applied Mechanics and Materials* 536 (2014), pp. 1026–1031.

[27] J. Cannan and H. Hu. “Human-Machine Interaction (HMI): A Survey”. *University of* (2011).

[28] M. Carozza and G. Cappiello. "On the Development of a Novel Adaptive Prosthetic Hand with Compliant Joints: Experimental Platform and EMG Control". *IEEE/RSJ International Conference on Intelligent Robots and Systems*. 2005, pp. 1271–6.

[29] J. M. Carroll. *Designing Interaction: Psychology at the Human-Computer Interface*. Vol. 4. CUP Archive, 1991.

[30] R. Chemuturi, F. Amirabdollahian, and K. Dautenhahn. "Adaptive Training Algorithm for Robot-Assisted Upper-Arm Rehabilitation, Applicable to Individualised and Therapeutic Human-Robot Interaction". *Journal of NeuroEngineering and Rehabilitation* 10.1 (2013), e102.

[31] C. A. Chin, A. Barreto, J. G. Cremades, and M. Adjouadi. "Integrated Electromyogram and Eye-Gaze Tracking Cursor Control System for Computer Users with Motor Disabilities". *Journal of Rehabilitation Research and Development* 45.1 (2008), p. 161.

[32] S.-Y. Cho, A. P. Winod, and K. W. E. Cheng. "Towards a Brain-Computer Interface based control for next generation electric wheelchairs". *Power Electronics Systems and Applications (PESA)* (2009), pp. 1–5.

[33] K. Choi, M. Sato, and Y. Koike. "A New, Human-Centered Wheelchair System Controlled by the EMG Signal". *International Joint Conference on Neural Networks*. IEEE. 2006, pp. 4664–4671.

[34] B. Crawford, K. Miller, P. Shenoy, and R. Rao. "Real-time classification of electromyographic signals for robotic control". *AAAI*. 2005, pp. 523–528.

[35] Z. Danziger, A. Fishbach, and F. A. Mussa-Ivaldi. "Learning Algorithms for Human-Machine Interfaces". *IEEE Transactions on Biomedical Engineering* 56 (2009), pp. 1502–11.

[36] C. R. Darwin. "On the Origin of Species by Means of Natural Selection, or the Preservation of Favoured Races in the Struggle for Life (London, 1859)". 1963, p. 117.

[37] M. R. Dawson, F. Fahimi, and J. P. Carey. "The Development of a Myoelectric Training Tool for Above-Elbow Amputees". *The Open Biomedical Engineering Journal* 6 (2012), p. 5.

[38] C. J. De Luca. “Use of the Surface EMG Signal for Performance Evaluation of Back Muscles”. *Muscle & Nerve* 16.2 (1993), pp. 210–216.

[39] B. Denby, T. Schultz, K. Honda, T. Hueber, J. Gilbert, and J. Brumberg. “Silent Speech Interfaces”. *Speech Communication* 52.4 (2010), pp. 270–287.

[40] S. Deterding, D. Dixon, R. Khaled, and L. Nacke. “From Game Design Elements to Gamefulness: Defining Gamification”. *Proceedings of the 15th International Academic MindTrek Conference: Envisioning Future Media Environments*. ACM. 2011, pp. 9–15.

[41] S. Deterding, M. Sicart, L. Nacke, K. O’Hara, and D. Dixon. “Gamification. Using Game-Design Elements in Non-Gaming Contexts”. *CHI’11 Extended Abstracts on Human Factors in Computing Systems*. ACM. 2011, pp. 2425–2428.

[42] W. Doneit. “Entwicklung und Implementierung einer bidirektionalen Kommunikation im Wireless Sensor Network”. German. MA thesis. Karlsruhe Institute of Technology, 2013.

[43] W. Doneit, M. R. Tuga, R. Mikut, D. Liebetanz, R. Rupp, and M. Reischl. “Strategies for Calibration and Training to Individualize Signal Generation in Myoelectric Control of Assistive Devices”. German. *Technisches Messen* 82.9 (Sept. 2015), pp. 411–421.

[44] R. Drake. *Gray’s Atlas of Anatomy*. Churchill Livingstone. Churchill Livingstone/Elsevier, 2008.

[45] D. Drotar. *Measuring Health-Related Quality of Life in Children and Adolescents: Implications for Research and Practice*. Psychology Press, 2014.

[46] M. Duguleana and G. Mogan. “Using Eye Blinking for EOG-Based Robot Control”. *Emerging Trends in Technological Innovation* (2010), pp. 343–50.

[47] *European Disability Strategy 2010-2020: A Renewed Commitment to a Barrier-Free Europe*. European Commission, 2010.

[48] G. Exner. “The Working Group "Paraplegy" of the Federation of Commercial Professional Associations in Germany”. *Trauma und Berufskrankheit* 6.2 (2004), p. 147.

[49] *eZ430-RF2500 Development Tool User's Guide (SLAU227E)*. Texas Instruments Inc. 2009.

[50] *Fact Sheet No. 384: Spinal Cord Injury*. World Health Organization (WHO), 2013.

[51] L. A. Farwell and E. Donchin. "Talking Off the Top of Your Head: Toward a Mental Prosthesis Utilizing Event-Related Brain Potentials". *Electroencephalography and Clinical Neurophysiology* 70.6 (1988), pp. 510–23.

[52] R. Farzan, J. M. DiMicco, D. R. Millen, B. Brownholtz, W. Geyer, and C. Dugan. "When the Experiment is Over: Deploying an Incentive System to all the Users". *Proceedings of the Symposium on Persuasive Technology, In conjunction with the AISB*. 2008, pp. 1–6.

[53] B. Fasel and J. Luettin. "Automatic Facial Expression Analysis: A Survey". *Pattern Recognition* 36.1 (2003), pp. 259–275.

[54] P. Felleiter, S. Reinbott, F. Michel, and M. Baumberger. "Das traumatische Querschnittssyndrom". German. *Schweiz Med Forum 2004; 4: 1166*. Vol. 1172.

[55] T. Felzer and B. Freisleben. "HaWCoS: The Hands-Free Wheelchair Control System". *Proceedings of the Fifth International ACM Conference on Assistive Technologies*. ACM. 2002, pp. 127–134.

[56] J. Fitzpatrick and M. Wallace. *Encyclopedia of Nursing Research*. Springer Publishing Company, 2005.

[57] S. Frantz. "Embryonic Stem Cell Pioneer Geron Exits Field, Cuts Losses". *Nature Biotechnology* 30.1 (2012), pp. 12–13.

[58] K. Fujita et al. "Simple Normal Crossing Fano Varieties and Log Fano Manifolds". *Nagoya Mathematical Journal* 214 (2014), pp. 95–123.

[59] O. Fukuda, T. Tsuji, M. Kaneko, and A. Otsuka. "A Human-Assisting Manipulator Teleoperated by EMG Signals and Arm Motions". *IEEE Robotics and Automation* 19 (2003), pp. 210–22.

[60] G. J. Gage, K. A. Ludwig, K. J. Otto, E. L. Ionides, and D. R. Kipke. "Naive Coadaptive Cortical Control". *Journal of Neural Engineering* 2.2 (2005), p. 52.

[61] C. Gerdtman and M. Lindén. “Six-Button Click Interface for a Disabled User by an Adjustable Multi-level Sip-and-Puff Switch”. *Proceedings of: Content Aggregation and Visualization* (2010), pp. 25–26.

[62] J. Giuffrida and P. Crago. “Reciprocal EMG Control of Elbow Extension by FES”. *IEEE Transactions on Neural Systems and Rehabilitation Engineering* 9, No.4 (2001), pp. 338–346.

[63] A. J. Glenstrup and T. Engell-Nielsen. “Eye Controlled Media: Present and Future State”. PhD thesis. University of Copenhagen, 1995.

[64] N. Gómara-Toldrà, M. Sliwinski, and M. P. Dijkers. “Physical Therapy After Spinal Cord Injury: A Systematic Review of Treatments Focused on Participation”. *The Journal of Spinal Cord Medicine* (2014).

[65] H. Gray. *Anatomy of the Human Body*. Lea & Febiger, 1918.

[66] S. Greenberg and I. H. Witten. “Adaptive Personalized Interfaces - A Question of Viability”. *Behaviour & Information Technology* 4 (1985), pp. 31–45.

[67] J. Grizou, I. Iturrate, L. Montesano, M. Lopes, P.-Y. Oudeyer, et al. “Zero-Calibration BMIs for Sequential Tasks Using Error-Related Potentials”. *IROS 2013 Workshop on Neuroscience and Robotics*. 2013.

[68] C. Guger, G. Edlinger, W. Harkam, I. Niedermayer, and G. Pfurtscheller. “How Many People are Able to Operate an EEG-Based Brain-Computer Interface (BCI)?” *IEEE Transactions on Neural Systems and Rehabilitation Engineering* 11.2 (2003), 145–7.

[69] S. D. Gupta, S. Al Yusuf, J. K. Ammar, and K. Hasan. “An Analysis to Generate EMG Signal and its Perspective: A Panoramic Approach”. *Advances in Power Conversion and Energy Technologies (APCET), 2012 International Conference on*. IEEE. 2012, pp. 1–5.

[70] G. H. Guyatt, D. H. Feeny, and D. L. Patrick. “Measuring Health-Related Quality of Life”. *Annals of Internal Medicine* 118.8 (1993), pp. 622–629.

[71] M. L. Hackett, C. Yapa, V. Parag, and C. S. Anderson. “Frequency of Depression After Stroke: A Systematic Review of Observational Studies”. *Stroke* 36.6 (2005), pp. 1330–1340.

[72] Y. Haik and T. Shahin. *Engineering Design Process*. Cengage Learning, 2010.

[73] R. Hainisch and M. Platz. “Phonetic Control: A New Approach for Continuous, Non-Invasive Device Control Using the Vocal Tract”. *Rehabilitation Robotics, 2007. ICORR 2007. IEEE 10th International Conference on*. IEEE. 2007, pp. 688–692.

[74] J. Hamari. “Transforming Homo Economicus Into Homo Ludens: A Field Experiment on Gamification in a Utilitarian Peer-to-Peer Trading Service”. *Electronic Commerce Research and Applications* 12.4 (2013), pp. 236–245.

[75] J. Hamari, J. Koivisto, and H. Sarsa. “Does Gamification Work? A Literature Review of Empirical Studies on Gamification”. *System Sciences (HICSS), 2014 47th Hawaii International Conference on*. IEEE. 2014, pp. 3025–3034.

[76] S. G. Hart. “NASA-Task Load Index (NASA-TLX); 20 Years Later”. *Proceedings of the Human Factors and Ergonomics Society Annual Meeting*. Vol. 50. 9. Sage Publications. 2006, pp. 904–908.

[77] M. Hashimoto, K. Takahashi, and M. Shimada. “Wheelchair Control Using an EOG- and EMG-Based Gesture Interface”. *IEEE/ASME International Conference on Advanced Intelligent Mechatronics* (2009), pp. 1212–7.

[78] P. Hekkert, D. Snelders, and P. C. Wieringen. “’Most Advanced, Yet Acceptable’: Typicality and Novelty as Joint Predictors of Aesthetic Preference in Industrial Design”. *British Journal of Psychology* 94.1 (2003), pp. 111–124.

[79] N. J. Hill, T. N. Lal, M. Schröder, T. Hinterberger, B. Wilhelm, F. Nijboer, U. Mochty, G. Widman, C. Elger, B. Schölkopf, A. Kübler, and N. Birbaumer. “Classifying EEG and ECoG Signals Without Subject Training for Fast BCI Implementation: Comparison of Nonparalyzed and Completely Paralyzed Subjects”. *IEEE Transactions on Neural Systems and Rehabilitation Engineering* 14.2 (2006), pp. 183–6.

[80] A. Holtz and R. Levi. *Spinal Cord Injury.* Oxford University Press, USA, 2010.

[81] P. Horki, T. Solis-Escalante, C. Neuper, and G. Müller-Putz. "Combined Motor Imagery and SSVEP Based BCI Control of a 2 DoF Artificial Upper Limb". *Medical & Biological Engineering & Computing* 49.5 (2011), pp. 567–77.

[82] X. Huo and M. Ghovanloo. "Using Unconstrained Tongue Motion as an Alternative Control Mechanism for Wheeled Mobility". *IEEE Transactions on Biomedical Engineering* 56.6 (2009), pp. 1719–26.

[83] X. Huo and M. Ghovanloo. "Evaluation of a Wireless Wearable Tongue-Computer Interface by Individuals with High-Level Spinal Cord Injuries". *J. Neural Eng.* 7.2 (2010), p. 26008.

[84] A. F. Huxley and R. Niedergerke. "Structural Changes in Muscle During Contraction". *Nature* 173.4412 (1954), pp. 971–973.

[85] H. Huxley and J. Hanson. "Changes in the Cross-Striations of Muscle During Contraction and Stretch and their Structural Interpretation". *Nature* 173.4412 (1954), pp. 973–976.

[86] *Instructions for Use | B600.* Otto Bock Mobility Solutions GmbH. 2010.

[87] K. Iwatsuki, T. Yoshimine, H. Kishima, M. Aoki, K. Yoshimura, M. Ishihara, Y. Ohnishi, and C. Lima. "Transplantation of Olfactory Mucosa Following Spinal Cord Injury Promotes Recovery in Rats". *Neuroreport* 19.13 (2008), pp. 1249–1252.

[88] M. Jones, K. Grogg, J. Anschutz, and R. Fierman. "A Sip-and-Puff Wireless Remote Control for the Apple iPod". *Assistive Technology* 20.2 (2008), pp. 107–10.

[89] P. J. Jongen, D. Lehnick, E. Sanders, P. Seeldrayers, S. Fredrikson, M. Andersson, and J. Speck. "Health-Related Quality of Life in Relapsing Remitting Multiple Sclerosis Patients During Treatment with Glatiramer Acetate: A Prospective, Observational, International, Multi-Centre Study". *Health and Quality of Life Outcomes* 8 (2010), p. 133.

[90] J. S. Ju, Y. Shin, and E. Y. Kim. "Intelligent Wheelchair (IW) Interface Using Face and Mouth Recognition". *Proceedings of the 14th international conference on Intelligent user interfaces* (2009), pp. 307–14.

[91] S. Kar, M. Bhagat, and A. Routray. "EEG Signal Analysis for the Assessment and Quantification of Driver's Fatigue". *Transportation Research Part F: Traffic Psychology and Behaviour* 13.5 (2010), pp. 297–306.

[92] R. Kato, T. Fujita, H. Yokoi, and T. Arai. "Adaptable EMG Prosthetic Hand using On-line Learning Method". *15th IEEE International Symposium on Robot and Human Interactive Communication* (2006), pp. 599–604.

[93] L. Kauhanen, T. Nykopp, J. Lehtonen, P. Jylanki, J. Heikkonen, P. Rantanen, H. Alaranta, and M. Sams. "EEG and MEG Brain-Computer Interface for Tetraplegic Patients". *Neural Systems and Rehabilitation Engineering* 14.2 (2006), pp. 190–3.

[94] S. P. Kelly, E. C. Lalor, C. Finucane, G. McDarby, and R. B. Reilly. "Visual Spatial Attention Control in an Independent Brain-Computer Interface". *IEEE Transactions on Biomedical Engineering* 52.9 (2005), pp. 1589–1596.

[95] V. Khare, J. Santhosh, S. Anand, and M. Bhatia. "Brain Computer Interface Based Real Time Control of Wheelchair Using Electroencephalogram". *International Journal of Soft Computing and Engineering* 1.5 (2011).

[96] K. Kiguchi, T. Tanaka, and T. Fukuda. "Neuro-Fuzzy Control of a Robotic Exoskeleton With EMG Signals". *IEEE Transactions on Fuzzy Systems* 12.4 (Aug. 2004), pp. 481–490.

[97] J. Kim, H. Park, J. Bruce, E. Sutton, D. Rowles, D. Pucci, J. Holbrook, J. Minocha, B. Nardone, D. West, A. Laumann, E. Roth, M. Jones, E. Veledar, and M. Ghovanloo. "The Tongue Enables Computer and Wheelchair Control for People with Spinal Cord Injury". *Science Translational Medicine* 5.213 (2013), 213ra166–213ra166.

[98] P.-J. Kindermans, H. Verschore, D. Verstraeten, and B. Schrauwen. "A P300 BCI for the Masses: Prior Information Enables Instant Unsupervised Spelling." *NIPS*. 2012, pp. 719–727.

[99] S. C. Kirshblum, S. P. Burns, F. Biering-Sorensen, W. Donovan, D. E. Graves, A. Jha, M. Johansen, L. Jones, A. Krassioukov, M. J. Mulcahey, M. Schmidt-Read, and W. Waring. "International Standards for Neurological Classification of Spinal Cord Injury". *The Journal of Spinal Cord Medicine* 34.6 (2011), pp. 535–46.

[100] N. Knoller, G. Auerbach, V. Fulga, G. Zelig, J. Attias, R. Bakimer, J. B. Marder, E. Yoles, M. Belkin, M. Schwartz, et al. "Clinical Experience Using Incubated Autologous Macrophages as a Treatment for Complete Spinal Cord Injury: Phase I Study Results". *Journal of Neurosurgery: Spine* 3.3 (2005), pp. 173–181.

[101] J. V. Kokswijk and M. V. Hulle. "Self Adaptive BCI as Service-Oriented Information System for Patients with Communication Disabilities". *International Conference on New Trends in Information Science and Service Science*. 2010.

[102] K. Komiya, K. Morita, K. Kagekawa, and K. Kurosu. "Guidance of a Wheelchair by Voice". *Conference of the IEEE Industrial Electronics Society (IECON)* 1 (2000), pp. 102–7.

[103] D. J. Krusienski, E. W. Sellers, D. J. McFarland, T. M. Vaughan, and J. R. Wolpaw. "Toward Enhanced P300 Speller Performance". *Journal of Neuroscience Methods* 167.1 (2008), pp. 15–21.

[104] T. Kuiken. "Targeted Reinnervation for Improved Prosthetic Function". *Physical Medicine and Rehabilitation Clinics of North America* 17(1) (2006), pp. 1–13.

[105] T. A. Kuiken, G. Li, B. A. Lock, R. D. Lipschutz, L. A. Miller, K. A. Stubblefield, and K. B. Englehart. "Targeted Muscle Reinnervation for Real-Time Myoelectric Control of Multifunction Artificial Arms". *The Journal of the American Medical Association (JAMA)* 301.6 (2009), pp. 619–628.

[106] D. Kumar and E. Poole. "Classification of EOG for Human Computer Interface". *Proceedings of the Second Joint 24th Annual Conference and the Annual Fall Meeting of the Biomedical Engineering Society* 1 (2002), pp. 64–67.

[107] C.-H. Kuo, Y.-C. Chan, H.-C. Chou, and J.-W. Siao. "Eyeglasses Based Electrooculography Human-Wheelchair Interface". *IEEE International Conference on Systems, Man and Cybernetics* (2009), pp. 4746–51.

[108] *Kurzbericht - Statistik der schwerbehinderten Menschen 2011*. German. Federal Statistical Office of Germany (DESTATIS), 2013.

[109] B. Laurel and S. J. Mountford. *The Art of Human-Computer Interface Design*. Addison-Wesley Longman Publishing Co., Inc., 1990.

[110] R. Leeb, H. Sagha, R. Chavarriaga, and J. Del R Millan. "Multimodal Fusion of Muscle and Brain Signals for a Hybrid-BCI". *Engineering in Medicine and Biology Society (EMBC), 2010 Annual International Conference of the IEEE*. Vol. 2010. Jan. 2010, pp. 4343–6.

[111] L. Li, D. Weng, Nan-Ning, and L.-C. Shen. "Cognitive Cars: A New Frontier for ADAS Research". *IEEE Transactions on Intelligent Transportation Systems* 13.1 (2012), pp. 395–407.

[112] C. Lima, P. Escada, J. Pratas-Vital, C. Branco, C. A. Arcangeli, G. Lazzeri, C. A. S. Maia, C. Capucho, A. Hasse-Ferreira, and J. D. Peduzzi. "Olfactory Mucosal Autografts and Rehabilitation for Chronic Traumatic Spinal Cord Injury". *Neurorehabilitation and Neural Repair* 24 (2009), pp. 10–22.

[113] C.-S. Lin, C.-W. Ho, W.-C. Chen, C.-C. Chiu, and M.-S. Yeh. "Powered Wheelchair Controlled by Eye-Tracking System". *Optica Applicata* 36.2-3 (2006), pp. 401–12.

[114] J.-S. Lin, K.-C. Chen, and W.-C. Yang. "EEG and Eye-Blinking Signals Through a Brain-Computer Interface Based Control for Electric Wheelchairs with Wireless Scheme". *International Conference on New Trends in Information Science and Service Science (NISS)* (2010), pp. 731–4.

[115] A. C. Lopes, G. Pires, and U. Nunes. "RobChair: Experiments Evaluating Brain-Computer Interface to Steer a Semi-Autonomous Wheelchair". *Intelligent Robots and Systems (IROS), 2012 IEEE/RSJ International Conference on*. IEEE. 2012, pp. 5135–5136.

[116] J. H. Loveless and W. Seamone. "Chin Controller System for Powered Wheelchair". 4,260,035. 1981.

[117] M. E. Lund, H. V. Christiensen, H. A. Caltenco, E. R. Lontis, B. Bentsen, and L. N. S. Andreasen Struijk. "Inductive Tongue Control of Powered Wheelchairs". *Annual International Conference of the IEEE Engineering in Medicine and Biology Society (EMBC)* (2010), pp. 3361–4.

[118] M. Mace, K. Abdullah-Al-Mamun, R. Vaidyanathan, and L. Gupta. "Real-Time Implementation of a Non-Invasive Tongue-Based Human-Robot Interface". *2010 IEEE/RSJ International Conference on Intelligent Robots and Systems* (Oct. 2010), pp. 5486–5491.

[119] M. Mace, R. Vaidyanathan, S. Wang, and L. Gupta. "Tongue in Cheek: A Novel Concept in Assistive Human-Machine Interface". *Journal of Assistive Technologies* 3.3 (2009), pp. 14–26.

[120] T. W. Malone. "Heuristics for Designing Enjoyable User Interfaces: Lessons from Computer Games". *Proceedings of the 1982 Conference on Human Factors in Computing Systems*. ACM. 1982, pp. 63–68.

[121] E. Marieb, K. Hoehn, and M. Hutchinson. *Human Anatomy and Physiology*. Pearson Education, Limited, 2014.

[122] S. Mathiassen, J. Winkel, and G. Hägg. "Normalization of Surface EMG Amplitude from the Upper Trapezius Muscle in Ergonomic Studies - A Review". *Journal of Electromyography and Kinesiology* 5.4 (1995), pp. 197–226.

[123] A. Maton. *Human Biology and Health*. Prentice Hall, 1997.

[124] T. Matsubara and J. Morimoto. "Bilinear Modeling of EMG Signals to Extract User-Independent Features for Multi-User Myoelectric Interface". *IEEE Transactions on Biomedical Engineering* 60.8 (2013), pp. 2205–13.

[125] H. Matsunaga and H. Nakazawa. "Design Method Considering Human Satisfaction: Development of Adaptive Human-Machine Interface Based on Satisfaction Measures". *Human Factors and Ergonomics in Manufacturing* 9 (1999), pp. 253–66.

[126] M. Mazo, F. J. Rodríguez, J. L. Lázaro, J. Ureña, J. C. García, E. Santiso, and P. A. Revenga. "Electronic Control of a Wheelchair Guided by Voice Commands". *Control Engineering Practice* 3.5 (1995), pp. 665–74.

[127] M. McTear. “Spoken Dialogue Technology: Enabling the Conversational User Interface”. *ACM Computing Surveys (CSUR)* 34.1 (2002), pp. 90–169.

[128] L. Meister. “Conception and Evaluation of a Volunteer Study to Validate Parameter Adaptation Methods for EMG-Controlled Human-Machine Interfaces”. BA thesis. Karlsruhe Institute of Technology, 2015.

[129] L. Meister. “Development, Implementation and Evaluation of a Novel Adaption Algorithm for a Co-Adaptive EMG-Controlled Human-Machine Interface”. BA thesis. Karlsruhe Institute of Technology, 2015.

[130] M. Mend and W. H. Kullmann. “Human Computer Interface with Online Brute Force Feature Selection”. *Biomedical Engineering* 57 (2012), pp. 659–62.

[131] L. Mertz. “The Next Generation of Exoskeletons: Lighter, Cheaper Devices are in the Works”. *Pulse, IEEE* 3.4 (2012), pp. 56–61.

[132] R. Mikut, O. Burmeister, S. Braun, and M. Reischl. “The Open Source Matlab Toolbox Gait-CAD and its Application to Bioelectric Signal Processing”. *Proc., DGBMT-Workshop Biosignalverarbeitung, Potsdam.* 2008, pp. 109–111.

[133] R. Mikut, T. Krüger, M. Reischl, O. Burmeister, R. Rupp, and T. Stieglitz. “Regelungs- und Steuerungskonzepte für Neuroprothesen am Beispiel der oberen Extremitäten”. German. *at - Automatisierungstechnik* 54(11) (2006), pp. 523–536.

[134] G. E. Miller, T. E. Brown, and W. R. Randolph. “Voice Controller for Wheelchairs”. *Medical and Biological Engineering and Computing* 23 (1985), pp. 597–600.

[135] G. R. Müller, C. Neuper, R. Rupp, C. Keinrath, H. J. Gerner, and G. Pfurtscheller. “Event-Related Beta EEG Changes During Wrist Movements Induced by Functional Electrical Stimulation of Forearm Muscles in Man”. *Neuroscience Letters* 340.2 (2003), pp. 143–7.

[136] R. Murphy. *The Body Silent: The Different World of the Disabled.* Henry Holt and Company, Inc., 1987.

[137] S. Musallam, B. Corneil, B. Greger, H. Scherberger, and R. Andersen. “Cognitive Control Signals for Neural Prosthetics”. *Science* 305.5681 (2004), pp. 258–262.

[138] A. Muzumdar. *Powered Upper Limb Prostheses: Control, Implementation and Clinical Application ; 11 Tables*. Springer, 2004.

[139] Y. Nam, Q. Zhao, A. Cichocki, and S. Choi. “A Tongue-Machine Interface: Detection of Tongue Positions by Glossokinetic Potentials”. *Neural Information Processing. Models and Applications* (2010), pp. 34–41.

[140] L. F. Nicolas-Alonso and J. Gomez-Gil. “Brain-Computer Interfaces - A Review”. *Sensors* 12.2 (2012), pp. 1211–1279.

[141] J. Niparko. *Cochlear Implants: Principles & Practices*. Lippincott Williams & Wilkins, 2009.

[142] A. Norcio and J. Stanley. “Adaptive Human-Computer Interfaces: A Literature Survey and Perspective”. *IEEE Transactions on Systems, Man, and Cybernetics* 19 (1989), pp. 399–408.

[143] M. A. Oskoei and H. Hu. “Myoelectric Control Systems – A Survey”. *Biomedical Signal Processing and Control* 2.4 (2007), pp. 275–294.

[144] M. A. Oskoei and H. Hu. “Adaptive Myoelectric Human-Machine Interface for Video Games”. *Mechatronics and Automation* (2009), pp. 1015–20.

[145] G. Pahl, K. Wallace, and L. Blessing. *Engineering Design: A Systematic Approach*. Solid Mechanics and its Applications. Springer, 2007.

[146] H. Park and S. Kwon. “Adaptive EMG-Driven Communication for the Disabled”. *Engineering in Medicine and Biology* 41 (1999).

[147] H. Peng, A. Bria, Z. Zhou, G. Iannello, and F. Long. “Extensible Visualization and Analysis for Multidimensional Images using Vaa3D”. *Nature Protocols* 9.1 (2014), pp. 193–208.

[148] G. Pfurtscheller and F. H. Lopes Da Silva. “Event-Related EEG/MEG Synchronization and Desynchronization: Basic Principles”. *Clinical Neurophysiology* 110 (1999), pp. 1842–1857.

[149] G. Pfurtscheller. “Event-related synchronization (ERS): an electrophysiological correlate of cortical areas at rest”. *Electroencephalography and clinical neurophysiology* 83.1 (1992), pp. 62–9.

[150] G. Pfurtscheller, B. Z. Allison, G. Bauernfeind, C. Brunner, T. S. Escalante, R. Scherer, T. O. Zander, G. Mueller-Putz, C. Neuper, and N. Birbaumer. "The Hybrid BCI". *Frontiers in Neuroscience* 4 (2010), p. 3.

[151] G. Pfurtscheller, C. Neuper, and W. Mohl. "Event-Related Desynchronization (ERD) During Visual Processing". *International Journal of Psychophysiology* 16.2 (1994), pp. 147–53.

[152] R. Picard and J. Healey. "Affective Wearables". *Personal and Ubiquitous Computing* (1997), pp. 231–240.

[153] W. Piechulla, C. Mayser, H. Gehrke, and W. König. "Reducing Drivers' Mental Workload by means of an Adaptive Man-Machine Interface". *Transportation Research Part F: Traffic Psychology and Behaviour* 6 (2003), pp. 233–48.

[154] P. M. Pilarski, M. R. Dawson, T. Degris, F. Fahimi, J. P. Carey, and R. S. Sutton. "Online Human Training of a Myoelectric Prosthesis Controller via Actor-Critic Reinforcement Learning". *IEEE International Conference on Rehabilitation Robotics (ICORR)*. IEEE. 2011, pp. 1–7.

[155] G. Pires and U. Nunes. "A Wheelchair Steered through Voice Commands and Assisted by a Reactive Fuzzy-Logic Controller". *Journal of Intelligent and Robotic Systems* 34.3 (2002), pp. 301–14.

[156] A. Plotkin, L. Sela, A. Weissbrod, R. Kahana, L. Haviv, Y. Yeshurun, N. Soroker, and N. Sobel. "Sniffing Enables Communication and Environmental Control for Severely Disabled". *Proceedings of the National Academy of Science of the United States (PNAS)* 107.32 (2010), pp. 14413–18.

[157] J. L. Pons, R. Ceres, E. Rocon, S. Levin, I. Markovitz, B. Saro, D. Reynaerts, W. Van Moorleghem, and L. Bueno. "Virtual Reality Training and EMG Control of the MANUS Hand Prosthesis". *Robotica* 23 (2005), pp. 311–7.

[158] L. C. Populin and T. C. T. Yin. "Pinna Movements of the Cat during Sound Localization". *The Journal of Neuroscience* 18.11 (1998), pp. 4233–43.

[159] D. Purwanto, R. Mardiyanto, and K. Arai. “Electric Wheelchair Control with Gaze Direction and Eye Blinking”. *Artificial Life and Robotics* 14.3 (2009), pp. 397–400.

[160] S. Raskin. *Neuroplasticity and Rehabilitation*. Guilford Publications, 2011.

[161] S. Raspopovic, M. Capogrosso, F. M. Petrini, M. Bonizzato, J. Rigosa, G. D. Pino, J. Carpaneto, M. Controzzi, T. Boretius, E. Fernandez, G. Granata, C. M. Oddo, L. Citi, A. L. Ciancio, C. Cipriani, M. C. Carrozza, W. Jensen, E. Guglielmelli, T. Stieglitz, P. M. Rossini, and S. Micera. “Restoring Natural Sensory Feedback in Real-Time Bidirectional Hand Prostheses”. *Science Translational Medicine* 6 (2014), 222ra19.

[162] E. J. Rechy-Ramirez and H. Hu. “Flexible Bi-modal Control Modes for Hands-Free Operation of a Wheelchair by Head Movements and Facial Expressions”. *New Trends in Medical and Service Robots*. Springer, 2014, pp. 109–123.

[163] M. Reischl, R. Mikut, C. Pylatiuk, and S. Schulz. “Control and Signal Processing Concepts for a Multifunctional Hand Prosthesis”. *Proc., Myoelectric Controls/Powered Prosthetics Symposium*. Fredericton, Canada: University of New Brunswick, 2002, pp. 116–119.

[164] M. Reischl. “Ein Verfahren zum automatischen Entwurf von Mensch-Maschine-Schnittstellen am Beispiel myoelektrischer Handprothesen”. German. PhD thesis. Universität Karlsruhe, Universitätsverlag Karlsruhe, 2006.

[165] M. Reischl, L. Gröll, and R. Mikut. “Evaluation of Data Mining Approaches for the Control of Multifunctional Arm Prostheses”. *Integrated Computer-Aided Engineering* 18 (2011), pp. 235–249.

[166] M. Reischl, M. R. Tuga, L. Meister, E. Alberg, W. Doneit, D. Liebetanz, R. Rupp, and R. Mikut. “Effects of training on the parameter adaptation in man-machine-interfaces in medical engineering”. German. *at - Automatisierungstechnik* 64.10 (2016), pp. 816–826.

[167] C. Remondini and F. Rotondi. *Sony Sees 'Strong' Europe Christmas Sales on PS3 Rise*. `http://www.bloomberg.com/news/2010-10-14/sony-sees-strong-europe-christmas-sales-says-ps3-may-beat-its-targets.html`. Retrieved: October 15 2010; Accessed: January 26 2015. Oct. 2010.

[168] I. M. Rezazadeh, S. M. P. Firoozabadi, S. M. R. H. Golpayegani, and H. Hu. "Controlling a Virtual Forehand Prosthesis Using an Adaptive and Affective Human-Machine Interface". *Annual International Conference of the IEEE Engineering in Medicine and Biology Society* (2011), pp. 4128–31.

[169] I. M. Rezazadeh and M. Firoozabadi. "Co-Adaptive and Affective Human-Machine Interface for Improving Training Performances of Virtual Myoelectric Forearm Prosthesis". *IEEE Trans. Affective Computing* 3.3 (2012), pp. 285–97.

[170] C. N. Riviere and P. K. Khosla. "Augmenting the Human-Machine Interface: Improving Manual Accuracy". *Robotics and Automation* (1997), pp. 3546–50.

[171] C. Riviere and N. Thakor. "Adaptive Human-Machine Interface for Persons with Tremor". *Engineering in Medicine and Biology Society* 2 (1995), pp. 1193–4.

[172] R. Rupp, L. Schmalfuß, M. R. Tuga, A. Kogut, M. Hewitt, J. Meincke, W. Duttenhöfer, U. Eck, R. Mikut, M. Reischl, and D. Liebetanz. "TELMYOS - A Telemetric Wheelchair Control Interface based on the Bilateral Recording of Myoelectric Signals from Ear Muscles". *Abstractband der Technically Assisted Rehabilitation (TAR) Conference*. 2015.

[173] N. I. Sabra and M. Wahed. "The Use of MEG-based Brain-Computer Interface for Classification of Wrist Movements in Four Different Directions". *Radio Science Conference (NRSC)* (2011), pp. 1–7.

[174] A. Salazar, R. Bravo, and D. Ponticelli. "An Hybrid Multi-Source, Multi-Function Patient Adaptable System for Assistive Technology Control Applications". *3rd European Medical & Biological Engineering Conference/IFMBE European Conference on Biomedical Engineering*. 2005.

[175] A. J. Salazar and R. J. Bravo. “Multi-Functional Interface for Patients with Severe Motor Disabilities: Managing EMG signals for control strategies”. *Information Technology Applications in Biomedicine, IEEE International Conference on* (2006).

[176] C. Salem and S. Zhai. “An Isometric Tongue Pointing Device”. *Proceedings of the SIGCHI conference on Human factors in computing systems CHI 97* (1997), pp. 538–539.

[177] M. Schablowski-Trautmann, M. Kögel, R. Rupp, R. Mikut, and H. Gerner. “From Diagnostics to Therapy - Conceptional Basis for Realtime Movement Feedback in Rehabilitation Medicine”. *Biomedizinische Technik* 51(5/6) (2006), pp. 299–304.

[178] M. J. Scherer and L. A. Cushman. “Measuring Subjective Quality of Life Following Spinal Cord Injury: A Validation Study of the Assistive Technology Device Predisposition Assessment”. *Disability and Rehabilitation* 23.9 (2001), pp. 387–393.

[179] F. Schettini, F. Aloise, P. Aricò, S. Salinari, D. Mattia, and F. Cincotti. “Self-Calibration Algorithm in an Asynchronous P300-based Brain-Computer Interface”. *Journal of Neural Engineering* 11.3 (2014), p. 035004.

[180] O. Schill. “Konzept zur automatisierten Anpassung der neuronalen Schnittstellen bei nichtinvasiven Neuroprothesen”. German. PhD thesis. Karlsruher Institut für Technologie, KIT Scientific Publishing, 2014.

[181] L. Schmalfuß, W. Duttenhoefer, J. Meincke, F. Klinker, M. Hewitt, M. R. Tuga, A. Kogut, M. Reischl, R. Rupp, and D. Liebetanz. “Myoelectric Control by Auricular Muscles - An Alternative Human-Machine Interface”. *Clinical Neurophysiology* 125 (2014), p. 116.

[182] L. Schmalfuß, R. Rupp, M. R. Tuga, A. Kogut, M. Hewitt, J. Meincke, F. Klinker, W. Duttenhoefer, U. Eck, R. Mikut, M. Reischl, and D. Liebetanz. “Steer by Ear: Myoelectric Auricular Control of Powered Wheelchairs for Individuals with Spinal Cord Injury”. *Restorative Neurology and Neuroscience* 34 (2015), pp. 79–95.

[183] B. Schott. “Entwicklung, Simulation und Validierung von Steuerkonzepten auf der Basis von myoelektrischen Signalen”. German. BA thesis. Karlsruhe Institute of Technology, 2012.

[184] A. E. Schultz and T. A. Kuiken. "Neural Interfaces for Control of Upper Limb Prostheses: The State of the Art and Future Possibilities". *PM&R: the Journal of Injury, Function, and Rehabilitation* 3.1 (2011), pp. 55–67.

[185] S. Schulz, C. Pylatiuk, M. Reischl, J. Martin, R. Mikut, and G. Bretthauer. "A Lightweight Multifunctional Prosthetic Hand". *Robotica* 23(3) (2005), pp. 293–299.

[186] K. Sekiyama, M. Ito, T. Fukuda, T. Suzuki, and K. Yamashita. "An Adaptive Muscular Force Generation Mechanism based on Prior Information of Handling Object". *SCIS & ISIS* 2008 (2008), pp. 311–316.

[187] G. Serra, V. Tugnoli, M. Cristofori, R. Eleopra, and D. De Grandis. "The Electromyographic Examination of the Posterior Auricular Muscle". *Electromyography and Clinical Neurophysiology* 26.8 (1986), pp. 661–665.

[188] M. Serruya, N. Hatsopoulos, L. Paninski, M. Fellows, and J. Donoghue. "Instant Neural Control of a Movement Signal". *Nature* 416 (2002), pp. 141–142.

[189] R. Sharma, V. Pavlovic, and T. Huang. "Toward Multimodal Human-Computer Interface". *Proceedings of the IEEE* 86.5 (May 1998).

[190] L. Sherwood. *Human Physiology: From Cells to Systems*. Thomson Books/Cole, 2007.

[191] B. Shneiderman. *Designing the User Interface: Strategies for Effective Human-Computer Interaction*. Vol. 3. Addison-Wesley Reading, MA, 1992.

[192] H. Siebner and J. Rothwell. "Transcranial Magnetic Stimulation: New Insights into Representational Cortical Plasticity". *Experimental Brain Research* 148.1 (2003), pp. 1–16.

[193] S. Sircar. *Principles of Medical Physiology*. Thieme, 2008.

[194] P. J. Snyder and H. A. Whitaker. "Neurologic Heuristics and Artistic Whimsy: The Cerebral Cartography of Wilder Penfield". *Journal of the History of the Neurosciences* 22.3 (2013), pp. 277–291.

[195] S. R. Soekadar, M. Witkowski, J. Mellinger, A. Ramos, N. Birbaumer, and L. G. Cohen. "ERD-Based Online Brain-Machine Interfaces (BMI) in the Context of Neurorehabilitation: Optimizing BMI Learning and Performance". *Neural Systems and Rehabilitation Engineering, IEEE Transactions on* 19.5 (2011), pp. 542–549.

[196] J.-H. Song, J.-W. Jung, S.-W. Lee, and Z. Bien. "Robust EMG Pattern Recognition to Muscular Fatigue Effect for Powered Wheelchair Control". *Journal of Intelligent and Fuzzy Systems* 20.1 (2009), pp. 3–12.

[197] E. Strickland. "Good-bye, Wheelchair". *Spectrum, IEEE* 49.1 (2012), pp. 30–32.

[198] T. Takeuchi, T. Wada, M. Mukobaru, and S. Doi. "A Training System for Myoelectric Prosthetic Hand in Virtual Environment". *IEEE/ICME International Conference on Complex Medical Engineering*. 2007.

[199] H. Tamura, T. Manabe, T. Goto, Y. Yamashita, and K. Tanno. "A Study of the Electric Wheelchair Hands-Free Safety Control System Using the Surface-Electromyogram of Facial Muscles". *Intelligent Robotics and Applications* (2010). Ed. by H. Liu, H. Ding, Z. Xiong, and X. Zhu, pp. 97–104.

[200] K. Tanaka, K. Matsunaga, and H. O. Wang. "Electroencephalogram-based Control of an Electric Wheelchair". *Robotics, IEEE Transactions on* 21.4 (2005), pp. 762–766.

[201] M. Tangermann, M. Krauledat, K. Grzeska, M. Sagebaum, B. Blankertz, C. Vidaurre, and K.-R. Müller. "Playing Pinball with Non-Invasive BCI". *NIPS* (2008), pp. 1641–8.

[202] K. Tervo and H. N. Koivo. "Adaptation of the Human-Machine Interface to the Human Skill and Dynamic Characteristics". *World Congress*. Vol. 19. 1. 2014, pp. 3539–3544.

[203] *The 2014 Annual Statistical Report for the Spinal Cord Injury Model Systems - Complete Public Version*. National Spinal Cord Injury Statistical Center, 2013.

[204] *The International Classification of Functioning, Disability and Health*. World Health Organization (WHO), 2001.

[205] R. Thietje. *Die operative Versorgung bei Querschnittlähmung*. German. `http://www.der-querschnitt.de/archive/17878`. Retrieved: February 9 2015; Accessed: March 12 2015. Feb. 2015.

[206] J. Thom, D. Millen, and J. DiMicco. "Removing Gamification from an Enterprise SNS". *Proceedings of the ACM 2012 conference on Computer Supported Cooperative Work*. ACM. 2012, pp. 1067–1070.

[207] A. Troiano, F. Naddeo, E. Sosso, G. Camarota, R. Merletti, and L. Mesin. "Assessment of Force and Fatigue in Isometric Contractions of the Upper Trapezius Muscle by Surface EMG Signal and Perceived Exertion Scale". *Gait & Posture* 28.2 (2008), pp. 179–186.

[208] C. S. L. Tsui, P. Jia, J. Q. Gan, H. Hu, and K. Yuan. "EMG-Based Hands-Free Wheelchair Control with EOG Attention Shift Detection". *Robotics and Biomimetics, 2007. ROBIO 2007. IEEE International Conference on*. IEEE. 2007, pp. 1266–1271.

[209] M. R. Tuga, R. Rupp, A. Kogut, D. Liebetanz, L. Schmalfuß, R. Mikut, and M. Reischl. "Incremental Parameter Adaptation Scheme for Myoelectric-Controlled Human-Machine Interfaces". *Biomedical Engineering* 59 (2014), pp. 148–51.

[210] M. R. Tuga, R. Rupp, D. Liebetanz, R. Mikut, and M. Reischl. "Concept of a Co-Adaptive Training Environment for Human-Machine Interfaces Based on EMG-Control". *Biomedical Engineering* 58 (2013), pp. 233–4.

[211] M. R. Tuga, R. Rupp, D. Liebetanz, L. Schmalfuß, E. Hübner, W. Doneit, R. Mikut, and M. Reischl. "Co-Adaptives Lernen: Untersuchungen einer Mensch-Maschine-Schnittstelle mit anpassungsfähigem Systemverhalten". German. *Proc., 23. Workshop Computational Intelligence, Dortmund*. KIT Scientific Publishing, 2013, pp. 247–264.

[212] M. R. Tuga, L. Meister, and M. Reischl. *Efficacy Test of Incremental Parameter Adaptation in the Context of Myoelectric-Controlled Human-Machine Interfaces*. Tech. rep. Institute for Applied Computer Science and Automation, 2015.

[213] M. R. Tuga, R. Rupp, D. Liebetanz, L. Meister, E. Alberg, R. Mikut, and M. Reischl. "The Human in the Loop: Co-Adaptive Learning in Myoelectric Human-Machine Interfaces" (submitted).

[214] V. M. Tysseling-Mattiace, V. Sahni, K. L. Niece, D. Birch, C. Czeisler, M. G. Fehlings, S. I. Stupp, and J. A. Kessler. "Self-Assembling Nanofibers Inhibit Glial Scar Formation and Promote Axon Elongation after Spinal Cord Injury". *The Journal of Neuroscience* 28.14 (2008), pp. 3814–3823.

[215] A. Tzekou and M. G. Fehlings. "Treatment of Spinal Cord Injury with Intravenous Immunoglobulin G: Preliminary Evidence and Future Perspectives". *Journal of clinical immunology* (2014), pp. 1–7.

[216] R. Vaidyanathan, B. Chung, L. Gupta, H. Kook, S. Kota, and J. D. West. "Tongue-Movement Communication and Control Concept for Hands-Free Human-Machine Interfaces". *IEEE Transactions on Systems Man and Cybernetics* 37.4 (2007), pp. 533–46.

[217] C. Vidaurre, C. Sannelli, K.-R. Müller, and B. Blankertz. "Co-Adaptive Calibration to Improve BCI Efficiency". *Journal of Neural Engineering* 8.2 (2011).

[218] N. Vitiello, U. Olcese, C. M. Oddo, J. Carpaneto, S. Micera, M. C. Carrozza, and P. Dario. "A Simple Highly Efficient Non-Invasive EMG-Based HMI". *IEEE Engineering in Medicine and Biology Society* 1 (2006), p. 3403.

[219] F. Vogt, G. McCaig, A. Ali, and S. Fels. "Tongue'n'Groove: An Ultrasound Based Music Controller". *Proceedings of the 2002 Conference on New Interfaces for Musical Expression.* 2002, pp. 24–27.

[220] W. Wahlster and A. Kobsa. "Dialogue-Based User Models". *Proceedings of the IEEE* 74 (1986), pp. 948–60.

[221] E. M. Wassermann and S. H. Lisanby. "Therapeutic Application of Repetitive Transcranial Magnetic Stimulation: A Review". *Clinical Neurophysiology* 112.8 (2001), pp. 1367–1377.

[222] L. Wei and H. Hu. "EMG and Visual Based HMI for Hands-Free Control of an Intelligent Wheelchair". *Intelligent Control and Automation (WCICA), IEEE 8th World Congress on* (2010), pp. 1027–1032.

[223] L. Wei, H. Hu, T. Lu, and K. Yuan. "Evaluating the Performance of a Face Movement Based Wheelchair Control Interface in an Indoor Environment". *IEEE International Conference on Robotics and Biomimetics (ROBIO)* (2010), pp. 387–92.

[224] T. Whitehead. *Wii Balance Board Enters Record Books*. `http://www.nintendolife.com/news/2012/01/wii_balance_board_enters_record_books`. Retrieved: July 12 2013; Accessed: January 26 2015. Jan. 2012.

[225] WHO. *Disability - Report by the Secretariat*. Tech. rep. World Health Organization, 2013.

[226] B. Wilhelm, M. Jordan, and N. Birbaumer. "Communication in Locked-In Syndrome: Effects of Imagery on Salivary pH". *Neurology* 67 (2006), pp. 534–5.

[227] B. Wodlinger, J. Downey, E. Tyler-Kabara, A. Schwartz, M. Boninger, and J. Collinger. "Ten-Dimensional Anthropomorphic Arm Control in a Human Brain-Machine Interface: Difficulties, Solutions, and Limitations". *Journal of Neural Engineering* 12.1 (2015), p. 016011.

[228] A. Wolczowski, M. Kurzynski, and P. Zaplotny. "Concept of a System for Training of Bioprosthetic Hand Control in One Side Handless Humans using Virtual Reality and Visual and Sensory Biofeedback". *Medical Informatics and Technologies* 18 (2011), pp. 85–91.

[229] J. R. Wolpaw, N. Birbaumer, D. J. McFarland, G. Pfurtscheller, and T. M. Vaughan. "Brain-Computer Interfaces for Communication and Control". *Clinical Neurophysiology* 113 (2002), pp. 767–791.

[230] *World Report on Disability*. World Health Organization (WHO), 2012.

[231] X. Xu, Y. Zhang, Y. Luo, and D. Chen. "Robust Bio-Signal Based Control of an Intelligent Wheelchair". *Robotics* 2.4 (2013), pp. 187–197.

[232] C. C. Ying. "Learning by Doing - An Adaptive Approach to Multiperiod Decisions". *Operations Research* 15.5 (1967), pp. 797–812.

[233] E. D. Young, J. J. Rice, and S. C. Tong. “Effects of Pinna Position on Head-Related Transfer Functions in the Cat”. *The Journal of the Acoustical Society of America* 99.5 (1996), pp. 3064–3076.

[234] X. Zhang, X. Wang, B. Wang, T. Sugi, and M. Nakamura. “Real-Time Control Strategy for EMG-Drive Meal Assistance Robot - My Spoon”. *2008 International Conference on Control, Automation and Systems* 1 (Oct. 2008), pp. 800–803.

[235] X. Z. Zheng and K. Tsuchiya. “Development of Human-Machine Interface in Disaster-Purposed Search Robot Systems that Serve as Surrogates for Human”. *Robotics and Automation* (2004), pp. 225–230.

[236] D. Zhu, J. Bieger, G. G. Molina, and R. M. Aarts. “A Survey of Stimulation Methods Used in SSVEP-Based BCIs”. *Computational Intelligence and Neuroscience* (2010), p. 702357.

[237] G. Zichermann and C. Cunningham. *Gamification by Design: Implementing Game Mechanics in Web and Mobile Apps*. O’Reilly Media, 2011.

C Index